UNIVERSIDAD COMPLUTENSE DE MADRID

FACULTAD DE CIENCIAS MATEMÁTICAS

Departamento de Matemática Aplicada

Mathematical Modeling and Optimization of Bioreactors and Liquid Crystals

Modelización Matemática y Optimización de Biorreactores y Cristales Líquidos

Tesis doctoral realizada por:

María Crespo Moya

Bajo la dirección de:

Ángel Manuel Ramos del Olmo

y Benjamin Ivorra

Madrid 2016

A mis padres

Agradecimientos

Esta tesis ha sido realizada gracias al apoyo económico del "Ministerio de Economía y Competitividad", a través del proyecto MTM2011-22658, el grupo de investigación MOMAT y la Universidad Complutense de Madrid.

En primer lugar quiero dar las gracias a mis directores de tesis Ángel Manuel Ramos y Benjamin Ivorra, por toda la ayuda recibida durante estos cuatro años. Sobre todo por vuestra paciencia, vuestra dedicación y por haberos preocupado por mí no sólo a nivel académico sino también a nivel personal. Gracias por animarme a ir cursos, congresos y a realizar estancias en otras universidades, ya que creo que me han ayudado a crecer un poco más como matemática y como persona.

También quiero agradecer a otros profesores e investigadores que han hecho valiosas aportaciones a este trabajo: a Alain Rapaport por todas las veces que durante estos años me ha ayudado e iluminado con su gran conocimiento sobre biorreactores; a Ian Griffiths y Apala Majumdar por su gran implicación profesional y personal durante mis estancias en Oxford; a Juan Antonio Infante por darme aliento en los momentos más difíciles y en general a todo el Departamento de Matemática Aplicada por haber hecho de mi lugar de trabajo un hogar donde sentirme a gusto.

A mis compañeros de doctorado Carlos, Carely, Javi, Silvia, Edu, Marcos, Luis y Edwin con los que he pasado tanto tiempo estos años y que han hecho este camino más llevadero. A mis amigos de Madrid Joan, Vicky, Tere, Jolu, Edu, Alfonso y Maripaz por haber formado parte de mi vida, por vuestra vitalidad y vuestras ganas aprovechar el tiempo, que harán que recuerde Madrid siempre con una sonrisa.

Me gustaría enviar un agradecimiento especial a mis amigas Sandri, Elena, Ade, Laura, Amanda y Judith que han aprendido a vivir sin mí todo este tiempo pero siempre han abierto sus brazos cuando he vuelto a Vall de Uxó. Gracias también a Carlos, Clara, Lucas y Javi, que han estado animándome desde la distancia.

Quiero dejar estas últimas lineas para agradecer a mi familia su gran apoyo, ahora y siempre. Por vuestro cariño, vuestra preocupación y por haber creído incondicionalmente en mí.

Contents

Agradecimientos **i**

Resumen **iv**

Preface **xi**

Part I Bioreactors **1**

1 Introduction **3**
1.1 Mathematical Modeling 4
1.1.1 Well-mixed bioreactors 5
1.1.2 Unmixed bioreactors 5
1.2 Optimization problems in water treatment 7
1.2.1 Hybrid Genetic Algorithms 7
1.2.2 Bioremediation of natural water resources 7
1.2.3 Optimal shape of the continuous bioreactor 8

2 Mathematical Modeling **11**
2.1 Well-mixed bioreactors 11
2.1.1 Description of the model 11
2.1.2 Existence, uniqueness, nonnegativity and boundedness 12
2.1.3 Nondimensional analysis 16
2.1.4 Asymptotic behavior. 17
2.2 Unmixed bioreactors 22
2.2.1 Description of the model 22
2.2.2 Existence, uniqueness, positivity and boundedness 25
2.2.3 Nondimensional analysis 40
2.2.4 Asymptotic behavior 41

3 Optimization problems in Water Treatment **59**
3.1 Description and validation of the considered optimization method 59
3.1.1 Description of the algorithm 60
3.1.2 Implementation of HGA 63
3.1.3 Validation 64
3.2 Bioremediation of natural water resources 66
3.2.1 Mathematical modeling 67
3.2.2 Optimization problem 72
3.2.3 Numerical experiments 78
3.2.4 Conclusions 85
3.3 Optimal shape of the continuous bioreactor 86
3.3.1 Optimization Problem 86

3.3.2 Numerical Experiments . . . 90
3.3.3 Conclusions . . . 96

4 Conclusions and future work **103**

Part II Liquid Crystals **105**

5 Introduction **107**
5.1 Mathematical Modeling . . . 109
5.2 Flow induced behavior of nematic liquid crystals . . . 110

6 Mathematical Modeling **113**
6.1 General Leslie–Ericksen model . . . 113
6.2 Simplified model . . . 115
6.2.1 Non-dimensional analysis . . . 119

7 Asymptotic Behavior **121**
7.1 Equilibrium Solutions . . . 121
7.1.1 No fluid flow ($\mathcal{G} = 0$) . . . 121
7.1.2 Fluid flow ($\mathcal{G} > 0$) . . . 128
7.2 Time-dependent solutions . . . 133

8 Conclusions and future work **137**

Appendix A **139**
A.1 Elementary inequalities . . . 139
A.2 Ordinary differential equations . . . 139
A.3 Partial differential equations . . . 143

Resumen

Con mucha frecuencia, se desea describir el comportamiento de algún sistema o fenómeno de la vida real en términos matemáticos; dicho sistema puede ser físico, sociológico, económico, etc. La descripción matemática de un sistema o fenómeno se llama modelo matemático y se formula con ciertos objetivos en mente: por ejemplo, podríamos tratar de predecir el movimiento de un cuerpo celeste estudiando las fuerzas gravitatorias a las que está sometido. El proceso de desarrollo de un modelo matemático se llama modelización matemática, y consiste en identificar las variables principales del sistema, formular hipótesis razonables y obtener ecuaciones matemáticas, cuya solución concuerde con los datos experimentales. Para algunos fines puede ser suficiente el uso de modelos simples: por ejemplo, en los cursos básicos de física, al estudiar el movimiento del planeta Tierra se tiene únicamente en cuenta la fuerza gravitatoria ejercida por el Sol. Sin embargo, si el objetivo de un científico es predecir con mucha exactitud la trayectoria de un satélite enviado al espacio, puede que necesite tener en cuenta las fuerzas gravitatorias ejercidas por otros cuerpos celestes, como por ejemplo, la Luna. Una vez aceptado el modelo matemático como descripción válida del sistema real, el análisis matemático de las ecuaciones resultantes (idealmente, encontrar sus soluciones, obtener propiedades de dichas soluciones, etc.) puede proporcionar información nueva que no se había derivado previamente de la mera observación del sistema real. Además, en muchas ocasiones se pueden aplicar técnicas de optimización para mejorar el comportamiento de algunas características del sistema: por ejemplo, se pueden elegir las maniobras que realizará un satélite espacial, para desplazarse desde el punto de partida hasta el punto de destino, de manera que se minimice el consumo de combustible de la nave.

En el contexto de la modelización, análisis y optimización arriba mencionados, en esta tesis se han aplicado diversas herramientas matemáticas con el objetivo de estudiar dos fenómenos diferentes en el ámbito de los fluidos, por lo que la tesis se ha dividido en dos grandes partes: *Biorreactores* y *Cristales Líquidos*.

Biorreactores

Introducción y objetivos

Esta parte se modelizan y analizan matemáticamente los procesos que tienen lugar en biorreactores utilizados para el tratamiento de agua contaminada. Un biorreactor es un tanque en el que tienen lugar reacciones biológicas y se utiliza con el fin de producir o degradar cierta sustancia. Se compone de dos elementos: sustratos (sustancias requeridas para el crecimiento de microorganismos) y microorganismos (bacterias que crecen al consumir sustrato). Los biorreactores se han utilizado desde la antigüedad, por ejemplo, como herramienta para la producción de vino o de mantequilla. La comercialización de biorreactores experimentó su máximo auge en los años 20 con el descubrimiento de la penicilina, ya que éstos se empleaban para la producción antibióticos [**?**, **?**]. En los años 70, empezaron a utilizarse para la producción de bioetanol [**?**, **?**, **?**]. Por último, la aplicación de biorreactores para el tratamiento de aguas ha sido tema de estudio durante los últimos 40 anõs, debido a la escasez, cada vez más preocupante, de agua potable en la Tierra [**?**, **?**, **?**].

Existen tres modos principales de funcionamiento del biorreactor: discontinuo, semicontinuo y continuo: en el modo discontinuo se añade sustrato al inicio y no se recoge el efluente hasta el final del proceso; en el modo semicontinuo se añade sustrato constantemente y el efluente no se recoge hasta el final; en el modo continuo, tanto la inyección de sustrato como la recogida del efluente se lleva a cabo ininterrumpidamente. De entre

esos tres tipos de biorreactores, en esta tesis trabajaremos con biorreactores continuos, que se ha demostrado que son los más eficientes para el tratamiento de aguas en la mayoría de casos [**?**, **?**, **?**, **?**]. La evolución de las concentraciones de sustrato y biomasa en un biorreactor continuo depende de varios factores, como por ejemplo las propiedades físicas de las sustancias (su tasa de difusión en agua ó el tipo de reacción entre ambas), la cantidad de sustrato que se añade a la mezcla por unidad de tiempo (así como la velocidad a la que se añade), las dimensiones del reactor o la concentración inicial de sustrato y biomasa. La modelización matemática es una herramienta muy útil para describir algunos de los procesos que ocurren en el biorreactor y puede ser una manera rápida y económica de hacerlo, ya que minimiza el número de experimentos que hay que llevar a cabo. Dependiendo de las características del proceso (las dimensiones del reactor, la tasa de difusión de las sustancias, etc.) el modelo matemático usado será distinto. Por ejemplo, cuando la velocidad de difusión del sustrato y la biomasa sea muy grande (en comparación con las velocidades del fluido y de la reacción química) es suficiente considerar un modelo, basado en ecuaciones diferenciales ordinarias, que describa la evolución de las concentraciones en función del tiempo [**?**, **?**]. En otros casos, es necesario incluir también los efectos de la difusión de las sustancias y de la advección debida al movimiento del fluido, utilizando modelos basados en ecuaciones en derivadas parciales, que describen la evolución de las concentraciones no sólo en función del tiempo sino también del espacio [**?**, **?**, **?**]. Hasta la fecha, la mayoría de trabajos realizados en torno a la modelización de biorreactores continuos consideran modelos basados en ecuaciones diferenciales ordinarias, o en todo caso, modelos basados en ecuaciones en derivadas parciales con una única dimensión espacial [**?**, **?**, **?**, **?**].

El objetivo de esta parte de la tesis ha sido entender el funcionamiento de un biorreactor continuo (incluyendo los efectos de reacción, difusión y advección), para lo que hemos considerado un modelo cilíndrico en dos dimensiones. Una vez entendida la dinámica en el biorreactor, se han abordado problemas de optimización que tienen como objetivo mejorar el tratamiento de aguas mediante biorreactores.

En el Capítulo 2 se presenta, en primer lugar, un modelo propuesto en [**?**, **?**], que describe la dinámica en el biorreactor bajo la hipótesis de distribución homogénea de sustancias en el tanque. En segundo lugar, se desarrolla un modelo que tiene en cuenta la posible heterogeneidad espacial en el biorreactor. Los modelos presentados en este capítulo son utilizados en el Capítulo 3 para caracterizar el comportamiento en el biorreactor al resolver los problemas de optimización que allí se abordan.

En el Capítulo 3 se abordan dos problemas de optimización en los que un biorreactor continuo es utilizado para el tratamiento de agua. El primer problema pretende minimizar el tiempo necesario para descontaminar un recurso hídrico natural (por ejemplo, un lago). El segundo problema tiene como objetivo encontrar la forma geométrica óptima del biorreactor para minimizar su volumen, asegurando que la concentración de contaminante se reduce por debajo de un nivel deseado. Este capítulo contiene, además, información detallada sobre el algoritmo de minimización utilizado para resolver ambos problemas.

Aportaciones fundamentales

El primer modelo presentado en el Capítulo 2 es válido bajo la hipótesis de que las sustancias se distribuyen de manera uniforme en el biorreactor. El modelo está basado en un sistema no lineal de ecuaciones diferenciales ordinarias, que describe la evolución de las concentraciones del sustrato y biomasa en función del tiempo. Hemos revisado resultados consabidos de no-negatividad y acotación de la solución, los cuales han sido empleados posteriormente para probar la existencia y unicidad de solución del modelo. Mediante técnicas de análisis dimensional, hemos obtenido una escala temporal característica del modelo. Hemos explorado propiedades conocidas sobre el comportamiento asintótico del modelo, calculando sus puntos de equilibrio y estudiando su estabilidad asintótica mediante técnicas de linealización.

El segundo modelo presentado en el Capítulo 2 tiene en cuenta que las sustancias pueden distribuirse de forma heterogénea en el biorreactor. El modelo está basado en un sistema acoplado de ecuaciones de Advección-Difusión-Reacción, no-lineal debido al término reactivo, completado con condiciones de contorno mixtas. En algunos casos, se considerará que el fluido en el biorreactor se mueve verticalmente hacia abajo, y en otros casos, se describirán movimientos más complejos del fluido utilizando ecuaciones de Navier–Stokes. Hemos probado que el sistema tiene una única solución, que es no negativa y está acotada. Para demostrar estas

propiedades se han utilizado métodos variacionales, resultados de Análisis Funcional y el Teorema de punto fijo de Schauder. Mediante técnicas de análisis dimensional hemos conseguido reducir el número de parámetros del modelo, así como calcular una escala temporal característica del proceso. Utilizando técnicas de linealización, hemos obtenido condiciones suficientes para la estabilidad asintótica de las soluciones estacionarias del sistema. Estos resultados se han validado numéricamente y han sido comparados con los resultados obtenidos para el primer modelo. Se concluye que, a medida que las velocidades de difusión del sustrato y de la biomasa disminuyen, la velocidad del fluido debe disminuir para favorecer la reacción (ya que se aumenta el tiempo en el que las sustancias están en contacto) y los resultados de estabilidad obtenidos para ambos modelos difieren. Sin embargo, cuando las velocidades de difusión son muy grandes (de forma que la distribución de sustancias es prácticamente homogénea en el biorreactor) los resultados de estabilidad obtenidos para ambos modelos son similares.

En el Capítulo 3 se presentan dos problemas de optimización relacionados con biorreactores. Ambos problemas de optimización se han abordado utilizando un algoritmo de minimización global llamado Algoritmo Genético Híbrido. Este algoritmo combina algoritmos genéticos (con los que se realiza una búsqueda global en el espacio de posibles soluciones) con un método de gradiente (con el que se realiza una búsqueda local de la solución).

El primer problema tiene como objetivo descontaminar un recurso natural hídrico (por ejemplo, un lago) mediante la utilización de un biorreactor que opera de manera continua. El agua es bombeada, a una cierta velocidad, desde el lago hasta el biorreactor. Allí, se limpia gracias a la reacción entre el sustrato y la biomasa y se devuelve al lago con la misma velocidad. Este proceso se detiene cuando la concentración de contaminante en el lago ha sido reducida hasta alcanzar el nivel deseado. El problema de optimización pretende minimizar el tiempo de limpieza del lago mediante una elección óptima de la velocidad de bombeo del agua. Este problema fue abordado en [**?**] bajo la hipótesis de distribución homogénea de sustancias en el biorreactor. En este trabajo se comparan dichos resultados con los que se obtienen al considerar biorreactores donde las sustancias se distribuyen de manera no-uniforme en el tanque. Se observa que, cuando hay heterogeneidad espacial en el biorreactor (por ejemplo, si el flujo del fluido exhibe un perfil no homogéneo o si las velocidades de difusión de las sustancias son muy pequeñas) los resultados obtenidos en [**?**] no son válidos, dado que, con ellos, la concentración de contaminante en el lago no puede alcanzar el nivel deseado. En esos casos, es posible obtener velocidades de bombeo óptimas utilizando la metodología propuesta en este trabajo.

El segundo problema abordado en este capítulo tiene como objetivo minimizar el volumen del biorreactor (con la restricción de que éste asegure que la concentración de contaminante se ha reducido hasta alcanzar un nivel deseado), optimizando su forma. De entre las formas más conocidas de biorreactores, destacamos los biorreactores planos, tubulares y toroidales (véase Figura 1.4). Se ha utilizado un biorreactor tubular en el que el sustrato y el flujo de entrada son constantes, y se han considerado dos tipos distintos de reacción entre especies para estudiar el efecto de la reacción en los resultados de optimización. Se concluye que, en general, el biorreactor óptimo es más alto que ancho (en la dirección del flujo), en línea con los resultados presentados en [**?**, **?**], donde los autores llevaron a acabo estudios experimentales y concluyeron que el biorreactor más eficiente era tubular y su altura era mucho más grande que su radio. Además, se observa que, generalmente, la pared lateral del biorreactor óptimo es cóncava: este tipo de curvatura favorece la reacción dado que ralentiza la velocidad vertical del fluido y crea zonas de almacenamiento de biomasa. Además, se observa que la anchura de la parte superior del biorreactor es más o menos pronunciada según sea el tipo de reacción considerada. Estos resultados pueden guiar a empresas del sector industrial para construir biorreactores más pequeños, no sólo reduciendo así el coste de producción del tanque, sino también el espacio destinado al tratamiento de agua.

Perspectivas futuras

En esta parte de la tesis se ha modelizado, analizado y optimizado el comportamiento de un biorreactor continuo. En particular, nos hemos centrado en modelizar los fenómenos de difusión, advección y reacción en el interior del biorreactor. Este modelo podría extenderse en el futuro añadiendo efectos, observados a nivel experimental, como la reinyección de biomasa, el suministro de oxígeno, etc.
Se ha estudiado la influencia de la heterogeneidad en el biorreactor cuando éste se emplea para descontaminar

un lago. Esta aproximación supone un paso al frente con respecto a estudios previos (en los que los biorreactores se asumían perfectamente mezclados). Sin embargo, se obtendrían resultados más precisos si se añadiera la disparidad espacial también en el lago. Por último, la optimización de la forma del biorreactor se ha realizado para un conjunto determinado de parámetros del modelo. Nótese que la misma metodología puede ser utilizada con otros parámetros si así se requiere.

Cristales Líquidos

Introducción y objetivos

La segunda parte de la tesis tiene como objetivo entender el comportamiento de cristales líquidos confinados en un microcanal y sometidos al flujo de un fluido. El cristal líquido es un tipo especial de estado de agregación de la materia que tiene propiedades tanto de la fase líquida como de la fase sólida. El descubrimiento de los cristales líquidos se remonta a 1888 [**?**, **?**], cuando se observó que un compuesto derivado del colesterol (sólido a temperatura ambiente) parecía tener dos puntos de fusión: a 145.5°C los cristales se fundían generando un fluido denso y opaco, mientras que a 178.5°C, este compuesto se convertía en un líquido transparente parecido al agua. Los cristales líquidos revolucionaron la industria de las pantallas de visualización, mercado valorado en 75 millones de dólares en 2008 [**?**, **?**]. Las pantallas de cristal líquido, compuestas por millones de capas de este material, explotan la propiedad de doble refracción de los cristales para obtener diferentes propiedades ópticas (por ejemplo, la cantidad de luz que pasa a través de la pantalla). En su descripción más simple, se puede pensar que un cristal líquido está formado por moléculas alargadas que siguen un cierto orden posicional y direccional.

En esta parte de la tesis, nos centramos en el estudio de los cristales líquidos de tipo nemático, en los que las moléculas no exhiben orden posicional pero sí direccional. Hasta la fecha, se han realizado numerosos estudios en los que las moléculas se reorientan mediante la aplicación de campos de flujo, magnéticos o eléctricos, con el objetivo de obtener diferentes propiedades del material [**?**, **?**]. En particular, la manipulación del cristal líquido mediante campos de flujo es un área en creciente expansión, ya que ha dado lugar a nuevos métodos de transporte y mezclado en fluidos, con aplicaciones en medicina y farmacología [**?**, **?**, **?**]. Además, cuando un cristal líquido está limitado por una superficie, creada por contacto con otra fase (sólida, líquida o gaseosa), la orientación de sus moléculas puede cambiar drásticamente. El fenómeno de orientación de las moléculas cerca de la superficie se conoce como *anclaje*. Hay dos tipos principales de anclaje: fuerte (la orientación cerca de la superficie está predefinida) o débil (la orientación cerca de la superficie depende de un nuevo parámetro que describirá la fuerza anclaje: si dicha fuerza es muy pequeña, el anclaje no intervendrá de manera importante en la orientación de las moléculas). Así, cuando un cristal líquido se coloca en un microcanal y es sometido a un flujo, hay dos causas que influyen en el orden direccional de sus moléculas: la magnitud del flujo y el tipo de anclaje de las moléculas a la superficie de dicho canal.

La modelización matemática es una herramienta muy útil para describir y predecir el comportamiento del cristal líquido en este contexto. Debe acoplar dos procesos: la orientación de las moléculas y la descripción del fluido en el canal.

En el Capítulo 6 introducimos la teoría de Leslie–Ericksen, que caracteriza la evolución de la orientación de las moléculas del cristal líquido bajo la influencia de campos de flujo. Se presenta una simplificación del modelo de Leslie–Ericksen, propuesta en [**?**], donde la magnitud del flujo y la fuerza de anclaje de los cristales a la superficie del canal pueden variar con el tiempo.

En el Capítulo 7 estudiamos el comportamiento asintótico del modelo. En primer lugar, se obtienen las soluciones estacionarias dependiendo de los parámetros del modelo. En segundo lugar, se realizan pruebas numéricas para estudiar el comportamiento dinámico del modelo a medida que sus soluciones se aproximan a dichos estados estacionarios.

Aportaciones fundamentales

El Capítulo 6 presenta el modelo general de Leslie–Ericksen, el cual describe la orientación de las moléculas de un cristal líquido, y que puede ser simplificado bajo ciertas hipótesis. En nuestro caso, se asume que el cristal líquido es de tipo nemático monoaxial, es decir, las moléculas no presentan orden posicional pero tienden a alinearse de manera que su eje largo sigue una dirección preferida. Se considera que, tanto dicho vector director como el campo de flujo del fluido, dependen únicamente de la coordenada vertical (es decir, de la altura en el canal). Se supone que el flujo del fluido exhibe un perfil simétrico con respecto al centro del canal. Bajo estas hipótesis, el modelo simplificado resultante consta de un sistema acoplado de dos ecuaciones en derivadas parciales (dependientes del tiempo y de la coordenada vertical), describiendo el movimiento instantáneo del fluido y la evolución de la orientación de las moléculas. Además, la ecuación que caracteriza la orientación molecular puede desacoplarse y capturar la dinámica del fluido a través de una sola variable: el gradiente de presión a lo largo del canal. El sistema se completa mediante condiciones de frontera mixtas, las cuales describen el anclaje débil de las moléculas a la superficie del canal (añadiendo así un nuevo parámetro al modelo para caracterizar la fuerza de anclaje a la superficie). A diferencia del trabajo realizado en [**?**], aquí se considera anclaje débil en ambas superficies del canal, de forma que el modelo resultante es capaz de capturar también el anclaje de tipo fuerte cuando se consideran valores grandes del parámetro que describe la fuerza de anclaje.

El comportamiento asintótico del modelo simplificado se estudia en el Capítulo 7. Las soluciones estacionarias del modelo dependen del gradiente de presión y de la fuerza de anclaje. Cuando dicho gradiente es nulo, las soluciones estacionarias se obtienen de manera analítica. Para valores muy pequeños (o muy grandes) de gradiente se han empleado técnicas de análisis asintótico para aproximar el valor de la solución estacionaria, lo que ha proporcionado información sobre las capas límite (observadas experimentalmente en [**?**]) cerca de la superficie del canal. Para valores generales de gradiente de presión, se han aproximado numéricamente las soluciones estacionarias del modelo empleando métodos de continuación. Hemos utilizado técnicas de linealización y hemos concluido que, dependiendo de los parámetros, el sistema puede ser multi-estable. Además, se observa que las soluciones estacionarias asintóticamente estables son aquellas que exhiben anclaje homeotrópico a la superficie del canal (es decir, las moléculas se alinean perpendiculares a la superficie) mientras que las soluciones inestables muestran anclaje plano a la superficie del canal (es decir, las moléculas se alinean paralelas a la superficie). Los experimentos realizados en [**?**] señalan que, a medida que aumenta el gradiente de presión en el canal, se pueden observar transiciones en la orientación de las moléculas del cristal líquido. En [**?**] los autores tratan de explicar estas transiciones basándose en la energía asociada a las diferentes soluciones estacionarias del sistema, y conjeturan que existe un valor crítico de gradiente de presión donde la estabilidad de las soluciones estacionarias cambia (de inestable a estable o vicecersa). Sin embargo, nuestro análisis de estabilidad sugiere que las soluciones estacionarias del modelo presentado en [**?**] no pierden estabilidad a medida que aumenta el gradiente de presión.

Finalmente, se ha estudiado la sensibilidad del modelo con respecto a la condición inicial. Trabajando con condiciones iniciales de tipo constante, se observa que el estado final del sistema no depende de la condición inicial considerada. Sin embargo, trabajando con condiciones iniciales de tipo lineal, se han encontrado valores críticos que separan cuencas de atracción de los diferentes estados estacionarios. Además, también se han estudiado los efectos de cambiar el gradiente de presión y la fuerza de anclaje con el tiempo y cómo esta tasa de cambio puede afectar a las condiciones iniciales que llevan a la selección de un estado estacionario particular. Estos resultados pueden servir de guía para futuros experimentos si uno es capaz de controlar el flujo del fluido y el tipo de anclaje de los cristales, obteniendo así orientaciones moleculares próximas al estado estacionario deseado.

Perspectivas futuras

En esta parte de la tesis hemos llevado a cabo un análisis exhaustivo del comportamiento asintótico de los cristales líquidos nemáticos sometidos a un campo de flujo, utilizando una gran variedad de técnicas matemáticas. Sin embargo, todavía hay muchas mejoras que se pueden llevar a cabo para capturar las propiedades nemáticas observadas en los experimentos reales. Por ejemplo, el modelo dinámico propuesto

en el Capítulo 6 podría ser remplazado por un modelo Leslie–Ericksen completo, eliminando la hipótesis de simetría en el perfil del flujo y permitiendo transiciones entre estados estacionarios (no capturadas por nuestro modelo). Por otro lado, se podría utilizar la teoría de Beris–Edwards (en lugar de utilizar la teoría de Leslie–Ericksen), que utiliza modelos matemáticos más complejos que permiten capturar variaciones en el orden direccional y defectos topológicos (regiones donde la dirección de las moléculas no está definida).

Preface

Frequently, one may want to describe a real world system or problem (that can be physical, sociological, economic, etc.) in mathematical terms. A mathematical description of a system is called a mathematical model. The activity we do to get it is the mathematical modeling, which consists in identifying the main variables of the system, stating reasonable hypothesis and obtaining mathematical equations whose solution is consistent with the experimental data. Once the mathematical model has been accepted to describe the real problem, a mathematical analysis of the resulting equations may provide new information that could not have been derived from real observations, offering different points of view and new lines of study. Moreover, in many scenarios one can apply mathematical optimization methods with a view in to improve the system dynamics.

Through this thesis, we have applied various mathematical techniques in order to study two different real world

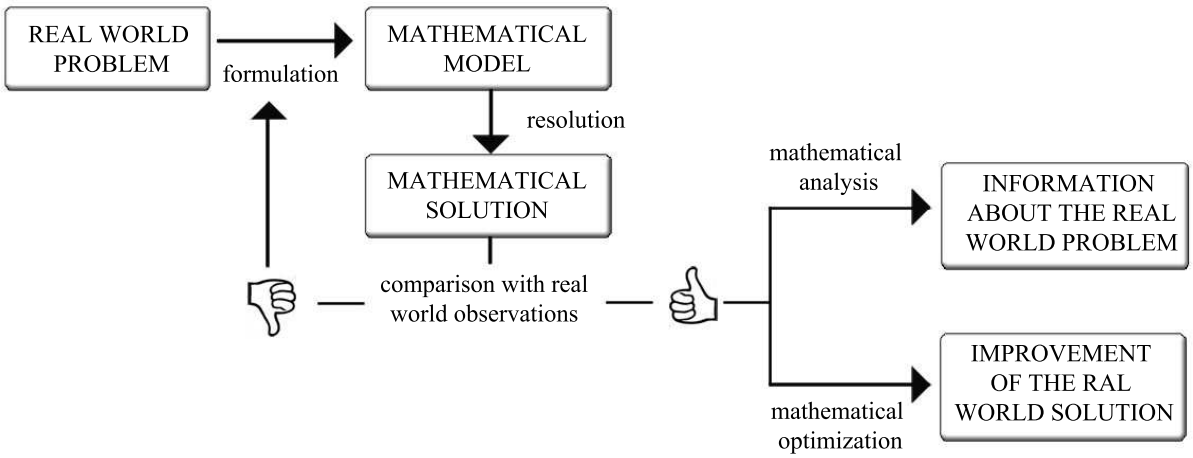

problems. The mathematical models, proposed for both problems, are mainly based on Ordinary Differential Equations (ODE) and Partial Differential Equations (PDE). When performing the mathematical analysis of the proposed models, we have studied the existence and uniqueness of solution, together with results about its nonnegativity and boundedness, using (among others) the Schauder Fixed Point Theorem and variational techniques. We have tackled the dimensional analysis of the resulting models, which has given us a clue on the characteristic time scales of the process dynamics and has led to a reduction in the number of model parameters. We obtained approximate solutions, in cases where the resulting systems were affected by the presence of small or large parameters, by applying asymptotic analysis techniques. We also studied the asymptotic behavior of the models, performing a stability analysis of the equilibria via linearization methods. Finally, we have come up with some optimization problems and addressed them by using a Hybrid Genetic Algorithm, which is a global optimization method that combines metaheuristic and gradient descent methods.

• Water treatment using biological reactors

The study of this industrial problem was one of the objectives of this thesis and its formulation was the result of a collaboration with professors Alain Rapaport and Jérôme Harmand, from the INRA Institute in Montpellier.

In order to properly tackle the water treatment problem, we were first interested in understanding the dynamics in a continuous bioreactor (a tank where biological interactions take place) which can be used to treat

polluted water. Chapter 1 gives an introduction to some basic descriptions in bioreactor theory and review previous results regarding the use of bioreactors in water treatment processes. Having in mind that most of the works in the literature consider well-mixed bioreactors, we focused on studying the influence of spatial inhomogeneities in the bioreactor performance. Thus, in Chapter 2 we propose two different mathematical models, which describe the behavior of perfectly mixed and unmixed bioreactors, respectively. We have performed a mathematical analysis of both models, which has provided useful information about the bioreactor dynamics, for instance, regarding the stability of the different equilibria that the system may approach. Once understood the bioreactor behavior, in Chapter 3 we have studied two optimization problems in which a bioreactor is used to decontaminate waste water. The first problem aims to minimize the time needed to clean a polluted water resource, which is connected with a continuous bioreactor. The second problem aims to reduce the reactor volume by optimizing the reactor shape. The main conclusions derived from this study are outlined in Chapter 4.

The work developed in this part of the thesis has lead us to write the following papers:

- Crespo, M. and Ivorra, B. and Ramos, A.M. "*Existence and uniqueness of solution of a continuous flow bioreactor model with two species*". RACSAM. Serie A. Matemáticas, 110(2):357–377, 2016. [**?**]
- Crespo, M. and Ivorra, B. and Ramos, A.M. and Rapaport, A. "*Modeling and optimization of activated sludge bioreactors for wastewater treatment taking into account spatial inhomogeneities*". Submitted. [**?**]
- Crespo, M. and Ivorra, B. and Ramos, A.M. "*Asymptotic stability of a coupled Advection-Diffusion-Reaction system arising in bioreactor processes*". Submitted. [**?**]
- Crespo, M. and Ivorra, B. and Ramos, A.M. and Rapaport, A. "*Modeling and optimization applied to the design of a continuous bioreactor*". Submitted. [**?**]

• Flow induced behavior of nematic liquid crystals

This problem was introduced by the researchers Ian Griffiths, from the Mathematical Institute in the University of Oxford, and Apala Majumdar, from the Department of Mathematical Sciences in the University of Bath. This collaboration was the result of two scientific stays (with a total duration of 5 months), supported by the Spanish Government scholarship *Predoctoral mobility for the realization of short academic stays in I+D Researching Centers in Spain and abroad - 2015 / 2016*, with references EEBB-I-15-09969 and EEBB-I-16-11180.

We aimed to comprehend the behavior of nematic liquid crystals (states of matter that are observed to occur between the solid crystal state and the conventional liquid state) confined in a microfluidic channel. Chapter 5 gives a brief introduction to the liquid crystal theory and reviews previous works studying the influence of the flow field on the molecular alignment of the liquid crystal. In Chapter 6 we propose a mathematical model, based on the well-known Leslie–Ericksen theory, which allows us to capture the competition between the pressure gradient (related to the flow dynamics) and the anchoring strength (which describes the alignment of the crystal molecules on the boundary surfaces of the channel). Then, in Chapter 7 we perform an extensive study of the asymptotic behavior of the model. Particularly, we build on a solution landscape of equilibrium solutions as a function of the pressure gradient and the anchoring strength, and perform a preliminary investigation of the numerical solution of the dynamic model. The main conclusions obtained from this study are presented in Chapter 8.

The work developed in this part of the thesis has lead us to write the following paper:

- Crespo, M. and Griffiths, I and Majumdar, A. and Ramos, A.M. "*Solution landscapes in nematic microfluidics*". Submitted. [**?**]

Finally, the Appendix presents well-known results, useful for the mathematical analysis of ordinary and partial differential equations, which have been used in the proofs presented throughout both parts of the thesis.

Part I

Bioreactors

Chapter 1

Introduction

A bioreactor is a vessel in which biological interactions take place. It can be used to perform chemical processes for either producing or degrading biochemical substances. It is composed of two elements:

1. The substrates required for the growth of microorganisms. Examples of substrate are sources of carbon (glucose, ethanol, etc.) and sources of nitrogen (nitrites, nitrates, etc.).

2. The microorganisms that develop by substrate consumption. These microorganisms are called biomass and they can be of different nature. Examples of biomass are bacteria, enzymes, yeasts and moulds.

History

Biological reactors have been used since ancient times, for instance, as a tool for wine production (due to the conversion of the sugar into alcohol) or for butter production (due to the fermentation of milk). The rise of the bioreactor market occurred with the development of pharmaceutical and biotechnology industries. After the discovery of penicillin in 1920 and monoclonal antibodies in 1970, the biological reactors played a key role in the large production of antibiotics and immunoglobulin, with product revenues of several billions of dollars (see [**?**, **?**]). Also during the early 1970s, the application of bioreactors was introduced for the production of bioethanol. Brazil was a pioneer country in developing bioreactors for ethanol production from its huge sugarcane industry and along side it an expanding industry for production of ethanol-utilizing cars (see [**?**]). Recent reviews (see [**?**, **?**]) report certain group of microalgae (which grow rapidly in bioreactors), appeared to be a source of renewable biodiesel capable of meeting the global demand for transport fuels. In summer 2016, the company *Airbus* set as a goal to turn algae into biofuel for planes, with the plan maker saying that, by 2050, five percent of jet fuel could be provided by algaculture. Last but not least, the application of bioreactors for waste water treatment has been a subject of study over the past 40 years (see, e.g., [**?**, **?**, **?**]). Due to the availability of drinking water becoming scarce in the earth, efforts have to be made to re-use water and to preserve aquatic environments. Therefore, in this work we focus on bioreactors used for water treatment. These bioreactors are commonly cylindrical, ranging in size from liters to cubic meters, and are often made of stainless steel. An example can be seen in Figure 1.1.

Basic descriptions

The operating mode of a bioreactor can be characterized by the type of liquid exchange, i.e., by the type of substrate supply of the reactor. We can distinguish three main operating modes: batch, fed-batch and continuous (a schematic representation of the three operating modes is depicted in Figure 1.2).

- Batch (also called discontinuous): substrate is added only at the beginning of the process and the product is not removed until the end of.

Figure 1.1: An example of bioreactor used for water treatment. This picture is courtesy of the *Laboratoire de Biotechnologie de l'Environnement*, placed in Narbonne (France).

- Fed-batch (also called semi-continuous): substrate is added continuously with a particular feed rate that may be changed during the process, but no product is removed until the end.
- Continuous (also called chemostat): substrate is continually added and product continually removed.

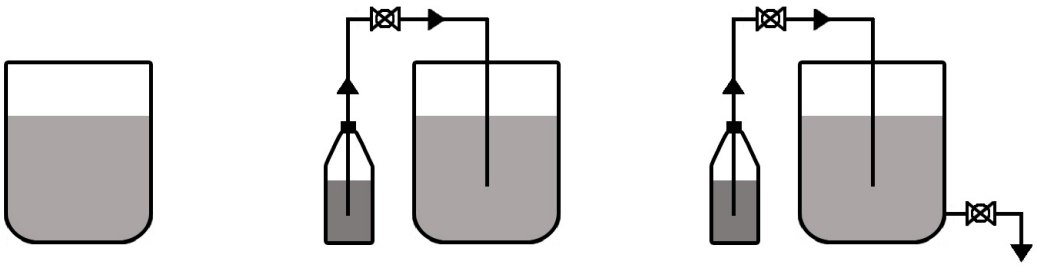

(a) Batch (b) Fed-batch (c) Continuous

Figure 1.2: A schematic representation of the three main bioreactor operating modes.

Among the three modes of operation, the continuous operation is the most widely and a better choice over other options in many scenarios (see, e.g., [**?**, **?**, **?**, **?**]). In line with these works, in this part of the thesis we consider bioreactors operating continuously (i.e., chemostats).

In order to increase the productivity and profitability of bioprocesses, many research efforts have been devoted to their improvement. Particularly, mathematical modeling and optimization have become fundamental tools to optimally design and operate production facilities using bioreactor processes. The state of art of these two areas of research is detailed in Sections 1.1 and 1.2, respectively.

1.1 Mathematical Modeling

Mathematical modeling is a very useful tool for understanding, characterizing and optimizing the interaction between substrate and biomass inside a bioreactor. In the simplest description, the mass balance

equations for the substrate and biomass in the bioreactor can be described as follows:

$$\begin{bmatrix}\text{Accumulation}\\ \text{of substrate}\\ \text{in the reactor}\end{bmatrix} = \begin{bmatrix}\text{Substrate}\\ \text{entering}\\ \text{the reactor}\end{bmatrix} - \begin{bmatrix}\text{Substrate}\\ \text{leaving}\\ \text{the reactor}\end{bmatrix} - \begin{bmatrix}\text{Substrate}\\ \text{consumed in}\\ \text{the reaction}\end{bmatrix},$$

$$\begin{bmatrix}\text{Accumulation}\\ \text{of biomass}\\ \text{in the reactor}\end{bmatrix} = \begin{bmatrix}\text{Biomass}\\ \text{entering}\\ \text{the reactor}\end{bmatrix} - \begin{bmatrix}\text{Biomass}\\ \text{leaving}\\ \text{the reactor}\end{bmatrix} + \begin{bmatrix}\text{Biomass}\\ \text{generated in}\\ \text{the reaction}\end{bmatrix}.$$

From the view point of mathematical modeling, biological reactors can be divided into two major classes:

- Well-mixed bioreactors (also called stirred tank reactors (STR)): substances are uniformly distributed in the reacting medium and the dynamics is described by ordinary differential equations.
- Unmixed bioreactors: substances are spatially distributed in the reacting medium and the dynamics is described by partial differential equations.

1.1.1 Well-mixed bioreactors

Most theoretical works studying the competition between biomass and substrate in bioreactors consider a well-mixed environment, i.e., the concentrations of substrate and biomass are assumed constant throughout the tank. The first model describing a well-mixed continuous bioreactor was proposed in 1950 by Jacques Monod, Aaron Novick and Leo Szilard [**?**, **?**, **?**] and it is usually called *chemostat* model. The chemostat model includes a growth rate function, referring to the growth rate of the biomass in function of the substrate concentration. The growth rate function originally proposed by Monod [**?**] was monotonic, i.e., he assumed that the growth rate increased with the substrate concentration. Nevertheless, when the substrate concentration reaches a high level, an inhibitory effect on the growth rate may occur; in such cases the Monod model is not suitable. In 1968, Andrews [**?**] suggested a model, which is similar to that of Monod [**?**] for low concentrations, but which includes the inhibitory effect at high concentrations. The chemostat model has been also modified, by introducing more than one microorganism, in order to allow the competition of substances inside the reactor (see, e.g., [**?**, **?**, **?**, **?**, **?**, **?**, **?**]).

The mathematical analysis of the chemostat is mainly devoted to the study of its asymptotic behavior. Focusing on monotonic growth rate functions, the computation of the steady-states and their stability analysis were tackled either with linearization techniques [**?**, **?**, **?**, **?**] or by finding an appropriate Liapunov function [**?**, **?**, **?**]. Similar works were performed in [**?**, **?**] for non-monotonic growth rate functions. Other properties, as the nonnegativity and boundedness of the solution, were proven in [**?**, **?**, **?**, **?**]. One can find an exhaustive analysis of the existence and uniqueness of solution of the chemostat model in [**?**].

In Section 2.1.1 we present a modified chemostat model, originally proposed by Rapaport et al. [**?**], which allows the entering substrate and the flow rate to vary with time. Our model accounts for both monotonic and non-monotonic growth rate functions. Then, in Section 2.1.2 we prove the existence and uniqueness of solution, together with results about the nonnegativity and boundedness of the solution. The underlying ideas in our proofs are taken from [**?**, **?**, **?**], although the proofs differ from previous results, where the entering substrate and the flow rate were assumed constant. In Section 2.1.3 we perform the dimensional analysis of the system and finally, in Section 2.1.4, we review some well-known results on the asymptotic behavior of the chemostat [**?**, **?**, **?**].

1.1.2 Unmixed bioreactors

It is of interest to study the influence of spatial inhomogeneities in the bioreactor. While the chemostat model is valid for small sized systems, it does not describe the diffusion phenomena or the impact of fluid

motions that may occur in larger tanks. Some of the first explorations of bacterial growth in spatially distributed environments were carried out by McGowin and Perlmutter [**?**] and Lauffenburger, Aris and Keller [**?**]. Particularly, Kung and Baltzis [**?**] considered a tubular bioreactor (assumed to be a thin tube), through which a liquid charged with a substrate at constant concentration enters the bioreactor with a constant flow rate, and the outflow leaves the bioreactor with the same flow rate. These considerations lead to a coupled system of two Advection-Diffusion-Reaction equations with Danckwerts boundary conditions (see Section 2.2.1 for more details), typically used for continuous flows bioreactors (see, e.g., [**?**, **?**, **?**]). The one-dimensional version of this nonlinear parabolic system can be found in most theoretical works studying the dynamics in the tubular reactor (see for instance [**?**, **?**, **?**, **?**, **?**, **?**]). Later, Dochain and Vanrolleghem [**?**] modified this model by introducing the radial coordinate r and studied the effect of the axial dispersion of the substrate in the tubular reactor.

There exist many works on the existence and uniqueness of solution of linear parabolic equations [**?**, **?**, **?**, **?**], particularly, for general bounded domains (see, e.g., [**?**, **?**, **?**, **?**]). For the existence, uniqueness, positivity and boundedness of solution of nonlinear parabolic systems in $\mathcal{C}^{1+\alpha}$ domains with mixed boundary conditions one can see the work developed by Pao [**?**, **?**]. The existence and uniqueness for a predator-prey type model with nonlinear reaction term is proved in [**?**] for Neumann boundary conditions.

Far more studied is the asymptotic behavior and stability analysis of bioreactor models. Most theoretical studies consider Diffusion-Reaction systems, i.e., they assume that the advection effect is negligible (see, e.g. [**?**, **?**, **?**, **?**]). For instance, in Morita and Ogawa [**?**], the authors showed the existence of two different steady-states (one constant, and another one spatially distributed) and developed bifurcation diagrams of the equilibrium solutions for specific model parameters. Nevertheless, such Diffusion-Reaction systems describe the behavior of batch type bioreactors, which are different to continuous flow type bioreactors, for which the addition of an advective term in the system is required. The asymptotic behavior and stability analysis of Advection-Diffusion-Reaction systems is mainly dedicated to the one-dimensional case [**?**, **?**, **?**, **?**, **?**, **?**, **?**, **?**]. In [**?**, **?**, **?**, **?**], the authors studied the asymptotic behavior of coupled systems of Advection-Diffusion-Reaction equations together with Danckwerts boundary conditions. Presuming that the substrate and the biomass diffuse throughout the water in the reactor with the same diffusion coefficient, the authors discussed the asymptotic stability of the different steady states of the system. In [**?**, **?**, **?**], the authors dropped the assumption that substrate and biomass diffusivity coefficients are identical and analyze the influence of the model parameters on the stability of the different equilibrium configurations of the system.

In Section 2.2.1, we describe the interaction of a substrate and the biomass with a three-dimensional coupled system of Advection-Diffusion-Reaction equations completed with Danckwerts boundary conditions. In contrast to previous models, we combine the following features

- We consider cylindrical reactors.
- We allow the diffusion rates of substrate and biomass to be distinct.
- We allow the entering substrate and the flow rate to vary with time and space.

Then, in Section 2.2.2 we prove the existence and uniqueness of solution, together with results about the nonnegativity and boundedness of the solution. In Section 2.2.3 we perform the dimensional analysis of the coupled system, to highlight the dominant terms in the model. Finally, in Section 2.2.4 we present the steady-states of the system and analyze their asymptotic stability using linearization methods.

1.2 Optimization problems in water treatment

The optimization of biological reactors has received a great attention in the literature (see, e.g., [?] and [?] for reviews of the different optimization techniques that have been used in bioprocesses). Usually the objective of the process is either to maximize the biomass production (see, e.g., [?, ?, ?, ?, ?, ?, ?]), or to remove the substrate in polluted water (see, e.g., [?, ?, ?, ?, ?]). Different optimization techniques have been used, as the Pontryagin Maximum Principle (see [?, ?, ?, ?, ?, ?]), Genetic Algorithms (see [?, ?, ?, ?, ?]) or Hybrid Stochastic-Deterministic Methods (see [?, ?]). In Section 1.2.1, we introduce a Hybrid Genetic Algorithm, used in Section 3 to solve two optimization problems for water treatment. In the first problem, we aim to decrease the substrate concentration in a water natural resource by using a continuous reactor; in the second problem, we aim to find an optimal design for the bioreactor device. The state of art of these two problems is reviewed in Sections 1.2.2 and 1.2.3, respectively.

1.2.1 Hybrid Genetic Algorithms

A Hybrid Genetic Algorithm (HGA) (see [?]) is a global optimization method based on a combination between a Genetic Algorithm (GA) (which performs a first coarse global search of the solution) with a Steepest Descent method (SD) (which performs a fine local search of the solution).

A GA is an optimization method for solving both constrained and unconstrained optimization problems based on a natural selection process that mimics biological evolution. One of the advantages of genetic algorithms is that they can solve a large range of optimization problems, including problems in which the fitness function is discontinuous, nondifferentiable, stochastic, or highly nonlinear. The algorithm repeatedly modifies a population of individuals (i.e., a set of points in the set of admissible solutions) in such a way that at each step, GA randomly selects individuals from the current population (called *parents*) and uses them to produce new individuals (called *children*) for the next generation. Over successive generations (i.e., iterations), the population may evolve toward an optimal solution. A brief description of the genetic algorithm used here is given in Section 3.1; for a general description one can see [?, ?, ?, ?, ?].

A SD method is an iterative minimization algorithm which finds a local minimum by taking steps in the opposite direction of the gradient of the objective function. A brief description of the steepest descent method used here is given in Section 3.1; for a general description one can see [?, ?].

1.2.2 Bioremediation of natural water resources

The decontamination of water resources and reservoirs in natural environments (lakes, lagoons, etc.) is a major environmental issue in the areas of prevention of eutrophication and wastewater treatment. Eutrophication is a process whereby water resources become too rich in organic material and mineral nutrients. Household products (phosphorus detergents) and products used in agriculture (nitrate fertilizers) are the main causes of pollution of water resources. As a result, some plants (in particular planktonic algae) can grow rapidly and reduce the available oxygen of the aquatic ecosystem resulting, for instance, in the death of local bio-organisms (such as fishes). Such an ecological question has given rise to many studies over the last 40 years (see, for instance, [?, ?]).

The bioremediation of natural resources is an example of application of continuous bioreactors (see the work of Rapaport et al. [?, ?, ?]). One can consider a bioreactor that continuously treats the water pumped from the reservoir and that injects it back (see Figure 1.3). A settler separates biomass from the water at the output of the bioreactor, since introducing biomass in the resource enhance the risk of having bacteria growing in competition with other populations that also need oxygen. The usual optimization problem aims to minimize the time needed to reach a prescribed minimal value of contamination in the resource by choosing the input flow rate. In [?] the authors tackled this problem under the assumption

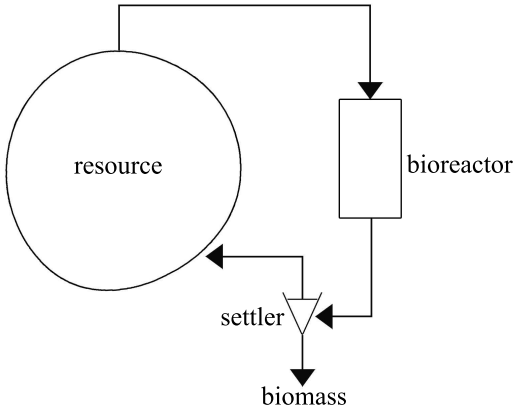

Figure 1.3: Connection of the bioreactor with the resource

of uniform concentration of substances in the water resource and the bioreactor. They characterized the optimal policies among constant and state-feedback controls and used Pontryagin Maximum Principle to solve the problem. The influence of inhomogeneity was studied in [?, ?, ?], where the problem of water treatment was addressed by dropping the assumption of uniform substrate concentration in the water resource. In all these works, the authors described the process dynamics by using a coupled system based on ordinary differential equations.

In Section 3.2.2 we solve the water treatment problem under the assumption of uniform distribution of substances in the water resource but with possible inhomogeneities of concentrations in the bioreactor. The process dynamics is described by using a coupled system based on both ordinary differential equations (describing the dynamics in the water resource) and partial differential equations (describing the dynamics in the bioreactor). Following [?], we characterize the optimal policies as open-loops (time-dependent controls) or feedbacks (state-dependent controls). Then, we solve the problem of water treatment by using a Hybrid Genetic Algorithm and discuss the impact of inhomogeneities in the optimization results.

1.2.3 Optimal shape of the continuous bioreactor

The shape optimization has been extensively exploited in design engineering [?, ?]. Traditionally, finding the optimal geometry of a particular device is based on a trial and error approach, in which, a number of prospective configurations is simulated and the results are compared. An alternative strategy relays in performing the mathematical modeling of the process, carrying out numerical simulations and solving the desired optimization problem with an appropriate optimization algorithm. Looking at the exponential growth of the available computing power, this second approach provides a powerful computational tool able to simulate and analyze the efficiency of different geometry configurations. Particularly, fluid flow simulations are needed for many design optimization problems. Computational fluid dynamics (CFD) has proven to be quite useful in predicting the flow pattern for a given set of design parameters. CFD coupled with optimization techniques were applied in many engineering problems (see [?, ?, ?]), and extensively used in aeronautical [?, ?, ?] and automotive areas [?]. In many of these works [?, ?, ?, ?, ?] the authors used Genetic Algorithms to solve their design optimization problems.

The influence of the bioreactor design into the process efficiency was studied mainly by experimentalists (see, e.g., [?, ?]). Among the different reactor geometry configurations reviewed in literature, the most popular are flat-plate reactors [?, ?], torus-shaped reactors [?], and tubular reactors [?, ?] (see Figure 1.4 for a schematic representation of these three reactor designs). Flow conditions (regarding mass transfer, shear stress, mixing, etc.) are strongly influenced by the reactor geometry [?], particularly at large scales.

Nevertheless, CFD has not been commonly used to its full capacity to optimize reactor performance. Of particular interest are the works developed by Ansoni et al. [**?**] and Coenen et al. [**?**]. In [**?**], the authors consider a tubular reactor and model its hydrodynamics with 3D Navier-Stokes equations. They look for the optimal design (configuration of the inlet and the outlet pipes) of a given bioreactor, so that the dispersion of the residence time and the shear flow of the associated CFD are minimized. These two concepts, related to fluid dynamics, are linked to the reactor effectiveness. In [**?**], the authors consider a cylindrical photobioreactor (a bioreactor that utilizes a light source to cultivate phototrophic microorganism) and model the dynamics of the organic compound with an Advection-Reaction equation. They look for the optimal geometry (radius and height) so that the substrate concentration at the outlet of the bioreactor is minimized.

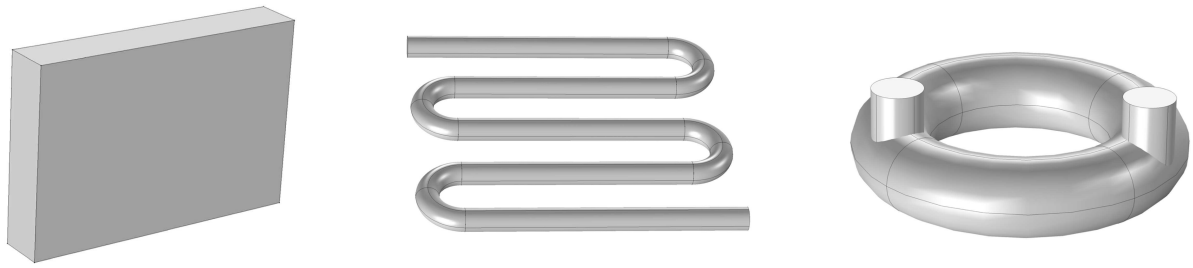

(a) Flat-plate reactor (b) Tubular reactor (c) Torus-shaped reactor

Figure 1.4: Schematic representation of three typical reactor device geometries.

In Section 3.3 we aim to solve the following design optimization problem: given the input reactant concentrations and the flow rate to be processed, what is the minimal reactor volume so that a desired output reactant concentration is attained? This problem has been modeled using ordinary differential equations (see, e.g., [**?**, **?**, **?**, **?**, **?**]) by approximating the behavior of a tubular device with a bioreactor composed by N tanks in series. Then, the aim of the optimization becomes to find what are the volumes of the N tanks such that the total volume of the whole process is minimal. However, these studies suffer of two important drawbacks:

- While the proposed results are valid for small and medium sized systems, the diffusion phenomena that occur in larger tanks were not studied;
- The dimensioning parameters were not considered; only the total volume of the systems were optimized. However, in a real case, design parameters such as the diameter or the height of any biological or chemical system will influence its performance.

In order to overcome these drawbacks, in Section 3.3 we propose to couple hydrodynamics with biological phenomena occurring in a diffusive bioreactor. We optimize the main design parameters (reactor shape and total volume) with respect to the output concentration. To do so, we use a particular spatial modeling based on the Navier Stokes equations (describing the fluid dynamics) together with a Advection-Diffusion-Reaction system (describing the behavior of the reactants in the bioreactor). The optimization problem is solved for monotonic and non-monotonic growth rate functions, in order to analyze the influence of the reaction into the optimal reactor configuration. Compared to the works developed in [**?**, **?**], we couple the fluid flow with the biological phenomena, while in [**?**, **?**] the authors only model one of the two physics. Furthermore, in this case, the reactor geometry is parametrized with five variables (compared to the two-dimensional parametrization performed in [**?**, **?**]) to be able to obtain a broader range of possible bioreactor shapes.

Chapter 2

Mathematical Modeling

This chapter is devoted to the mathematical modeling of the bioreactor. Particularly, in Section 2.1 we present a model, based on ordinary differential equations, which describes the dynamics in a well-mixed reactor. Then, in Section 2.2, we propose a model, based on partial differential equations, which describes the dynamics in an unmixed reactor.

2.1 Well-mixed bioreactors

In this section we model the behavior of a continuous bioreactor under the assumption of uniform concentration of substances through the tank. The mathematical model is presented in Section 2.1.1. Then, in Section 2.1.2 we prove the existence and uniqueness of solution, together with results about its nonnegativity and boundedness. In Section 2.1.3 we perform the dimensional analysis of the system and finally, in Section 2.1.4, we review some well-known results on the asymptotic behavior of this model.

2.1.1 Description of the model

We consider the following chemostat model, presented in [**?**], to describe the behavior of the bioreactor

$$\begin{cases} \dfrac{\mathrm{d}S}{\mathrm{d}t}(t) = -\dfrac{\mu(S(t))B(t)}{Y} + \dfrac{Q(t)}{V}(S_{\mathrm{e}}(t) - S(t)) & \forall t \in (0,T), \\ \dfrac{\mathrm{d}B}{\mathrm{d}t}(t) = \mu(S(t))B(t) - \dfrac{Q(t)}{V}B(t) & \forall t \in (0,T), \\ S(0) = S_0, \qquad B(0) = B_0, \end{cases} \tag{2.1}$$

where $T > 0$ (s) is the length of the time interval for which we want to model the process, S (kg/m^3) and B (kg/m^3) indicate the concentration (inside the bioreactor) of substrate and biomass respectively, S_{e} (kg/m^3) is the value of concentration of substrate that enters into the reactor, Q (m^3/s) is the volumetric flow rate, V (m^3) is the volume of the reactor and Y is a yield coefficient reflecting the conversion of substrate to biomass, which can be set to 1 without loss of generality; it suffices to make the change of variables $\tilde{S} = \frac{S}{Y}$ and $\tilde{B} = \frac{B}{Y}$ (see, e.g., [**?**]). Finally, μ (1/s) refers to the growth rate of the biomass in function of the substrate concentration. From a general point of view, due to experimental observations, we consider growth rate functions that satisfy the following hypothesis (see [**?**, **?**, **?**]):

Hypothesis. Function $\mu : \mathbb{R} \to \mathbb{R}$ is such that $\mu(z) = 0$ for $z \leq 0$, $\mu(z) > 0$ for $z > 0$ and fulfills one of the following properties:

- μ is increasing, bounded and concave in $[0, +\infty)$. (H1)
- There exists $s > 0$ such that μ is increasing on $(0, s)$ and decreasing on $(s, +\infty)$. (H2)

Notice that $\mathbb{R}$ is the domain of function μ only for general purposes. As we will see in Lemma 2.1.2, if $S_0 \geq 0$ and $Q(t), S_e(t) \geq 0$ for all $t \geq 0$, then $S(t) \geq 0$ for all $t > 0$, and so, it would be sufficient to define μ in $[0, +\infty)$. Through this part of the thesis, we work with the following growth rate functions, which are extensively used in literature: the Monod function [**?**], defined in $[0, +\infty)$ by

$$\mu(S) = \mu_{\max} \frac{S}{K_S + S}, \tag{2.2}$$

and the Haldane function [**?**], defined in $[0, +\infty)$ by

$$\mu(S) = \mu^* \frac{S}{K_S + S + S^2/K_I}, \tag{2.3}$$

where $\mu_{\max}$ (1/s) is the maximum specific growth rate, μ^* (1/s) is the maximum specific growth rate in the absence of inhibition, K_S (kg/m^3) is the half-saturation constant and K_I (kg/m^3) is the inhibition constant. Notice that the Monod function satisfies (H1) while the Haldane function satisfies (H2).

2.1.2 Existence, uniqueness, nonnegativity and boundedness

Nonnegativity

Lemma 2.1.1 (Nonnegativity of B)**.** *Assuming the existence of solution of* (2.1)*, if the initial condition* $B(0) = B_0 > 0$ *(respectively,* $B_0 = 0$*) then* $B(t) > 0$ *(respectively,* $B(t) = 0$*) for all* $t \in (0, T)$*.*

Proof. The second equation of system (2.1) can be seen as a separable differential equation

$$\frac{\mathrm{d}B(t)}{B(t)} = (\mu(S(t)) - \frac{Q(t)}{V})\mathrm{d}t,$$

and integrating one obtains

$$B(t) = B_0 \mathrm{e}^{\int_0^t (\mu(S(\tau)) - \frac{Q(\tau)}{V})\mathrm{d}\tau},$$

which proves the statement of the lemma. □

Lemma 2.1.2 (Nonnegativity of S)**.** *Assuming the existence of solution of* (2.1)*, if* $S(0) = S_0 \geq 0$*, the following situations hold:*

(a) If $Q(t)$*,* $S_e(t)$ *are positive functions on* $[0, T]$*, then* $S(t) > 0$ *for all* $t \in (0, T]$*.*

(b) If $Q(t)$*,* $S_e(t)$ *are nonnegative functions on* $[0, T]$*, then* $S(t) \geq 0$ *for all* $t \in [0, T]$*.*

Proof. (a):

1. $S(0) = 0$: Since we assume that $\mu(0) = 0$, it follows that

$$\frac{\mathrm{d}S}{\mathrm{d}t}(0) = \frac{Q(0)}{V} S_e(0) > 0,$$

   and so we can conclude that, for t small enough, one has $S(t) > 0$. Then, we can apply the case (a)-2 changing the starting time.

2. $S(0) > 0$: We use a reductio ad absurdum proof. Let us assume that there exists $t_1 > 0$ such that $S(t_1) = 0$ and that t_1 is the first time for which S is zero. Thus:

$$\frac{\mathrm{d}S}{\mathrm{d}t}(t_1) = \frac{Q(t_1)}{V} S_e(t_1) > 0.$$

But in the other hand, by definition one has:

$$\frac{\mathrm{d}S}{\mathrm{d}t}(t_1) = \lim_{t\to t_1^-} \frac{S(t_1)-S(t)}{t_1-t} \leq 0,$$

which is a contradiction with the previous inequality. We can conclude that it does not exist $t_1 > 0$ such that $S(t_1) = 0$.

Proof. (b):

1. $S(0) = 0$: If $Q(0) = 0$ or $S_\mathrm{e}(0) = 0$, since we assume that $\mu(0) = 0$, it follows that $\frac{\mathrm{d}S}{\mathrm{d}t}(0) = 0$ and S will remain null until $Q(t_1)$, $S_\mathrm{e}(t_1) > 0$ for some $t_1 > 0$. In this case $\frac{\mathrm{d}S}{\mathrm{d}t}(t_1) > 0$ and thus, we can conclude that, for $t > t_1$ small enough, it follows that $S(t) > 0$. Then we can apply the following case (b)-2 changing the starting time.

2. $S(0) > 0$: We distinguish two different subcases

   (i) If $Q(0) = 0$ or $S_\mathrm{e}(0) = 0$, one has that $\frac{\mathrm{d}S}{\mathrm{d}t}(0) < 0$, and thus, we can conclude that, for t small enough, $S(t)$ decreases. If there exists $t_1 > 0$ such that $S(t_1) = 0$, we can apply the case (b)-(1) changing the starting time.

   (ii) If $Q(0) > 0$ and $S_\mathrm{e}(0) > 0$, we can not deduce the sign of $\frac{\mathrm{d}S}{\mathrm{d}t}$ but, if $S(t)$ decreases and there exists $t_1 > 0$ such that $S(t_1) = 0$, we can apply the case (b)-1 changing the starting time.

□

Boundedness

Lemma 2.1.3 (Boundedness of the solution)**.** *Let us assume that Q and S_e are nonnegative functions in $[0,T]$, $S_0, B_0 \geq 0$ and $\mu \in L^\infty(\mathbb{R})$. Let us also assume the existence of solution of (2.1). Then it follows that*

$$B(t) \leq B_0 e^{\|\mu\|_{L^\infty(\mathbb{R})} t} \qquad \text{and} \qquad S(t) \leq S_0 + \int_0^t \frac{Q(\tau)}{V} S_\mathrm{e}(\tau)\mathrm{d}\tau \qquad \forall t \in (0,T].$$

Furthermore, if $Q, S_\mathrm{e} \in L^\infty(0,T)$ one has that

$$S(t) \leq S_0 + \frac{\|Q\|_{L^\infty(0,T)}\|S_\mathrm{e}\|_{L^\infty(0,T)}}{V} t \qquad \forall t \in (0,T].$$

Proof. If we integrate the second equation in (2.1) in time we obtain:

$$\int_0^t \tfrac{\mathrm{d}B}{\mathrm{d}\tau}\mathrm{d}\tau = \int_0^t \mu(S(\tau))B(\tau)\mathrm{d}\tau - \underbrace{\int_0^t \frac{Q(\tau)}{V} B(\tau)\mathrm{d}\tau}_{\geq 0 \text{ Lemma 2.1.1}} \leq \|\mu\|_{L^\infty(\mathbb{R})} \int_0^t B(\tau)\mathrm{d}\tau.$$

Then, it follows that

$$B(t) \leq B_0 + \|\mu\|_{L^\infty(\mathbb{R})} \int_0^t B(\tau)\mathrm{d}\tau$$

Now, applying Gronwall's inequality (see (A.2)) it follows

$$B(t) \leq B_0 \mathrm{e}^{\|\mu\|_{L^\infty(\mathbb{R})} t}.$$

Similarly, if we integrate the first equation in (2.1) in time we obtain:

$$\int_0^t \frac{\mathrm{d}S}{\mathrm{d}\tau}\mathrm{d}\tau = -\int_0^t \underbrace{\mu(S(\tau))B(\tau)}_{\geq 0 \text{ (Lemmas 2.1.1 and 2.1.2)}} \mathrm{d}\tau + \int_0^t \frac{Q(\tau)}{V} S_\mathrm{e}(\tau)\mathrm{d}\tau - \int_0^t \underbrace{\frac{Q(\tau)}{V} S(\tau)}_{\geq 0 \text{ (Lemma 2.1.2)}} \mathrm{d}\tau,$$

and so

$$S(t) \leq S_0 + \int_0^t \frac{Q(\tau)}{V} S_{\mathrm{e}}(\tau) \mathrm{d}\tau.$$

Moreover, if $Q, S_{\mathrm{e}} \in L^\infty(0,T)$ it is straightforward to see that

$$S(t) \leq S_0 + \frac{\|Q\|_{L^\infty(0,T)} \|S_{\mathrm{e}}\|_{L^\infty(0,T)}}{V} t \qquad \forall t \in (0,T].$$

□

Existence and Uniqueness

Theorem 2.1.4 (Existence and Uniqueness Theorem)**.** *Let us assume that Q, $S_{\mathrm{e}} \in L^\infty(0,T)$ are nonnegative measurable functions, $\mu \in L^\infty(\mathbb{R})$ is Lipschitz continuous and $S_0, B_0 \geq 0$, then there exists a unique solution $(S,B) \in AC([0,\bar{T}])^2$ (see Definition A.2.1) for the initial value problem (2.1), with $\bar{T} \in (0,T]$.*

Proof of Theorem 2.1.4. Since in $\mathbb{R}^n$ all norms are equivalent, we will use $\|\cdot\| = \|\cdot\|_1$. We recall that $\|x\|_1 = \sum_{i=1}^n |x_i|$.
System (2.1) can be rewritten as

$$\begin{pmatrix} x(t) \\ y(t) \end{pmatrix}' = F(t, x(t), y(t)) = \begin{pmatrix} F_1(t, x(t), y(t)) \\ F_2(t, x(t), y(t)) \end{pmatrix}, \tag{2.4}$$

where $F_1(t,x,y) = \frac{Q(t)}{V}(S_{\mathrm{e}}(t) - x) - \mu(x)y$ and $F_2(t,x,y) = -\frac{Q(t)}{V}y + \mu(x)y$. In order to prove Theorem 2.1.4 we apply Theorem A.2.3 with $G = [0,T] \times R$, where $R = [0, S_0 + \frac{\|Q\|_{L^\infty(0,T)} \|S_{\mathrm{e}}\|_{L^\infty(0,T)}}{V} T] \times [0, B_0 \mathrm{e}^{\|\mu\|_{L^\infty(\mathbb{R})} T}]$ (the set R has been taken following Lemmas 2.1.1, 2.1.2 and 2.1.3).

Step 1: Existence.
Let us prove that $F : G \to \mathbb{R}^2$ satisfies the Carathéodory conditions (see Definition A.2.2).

- Given $t \in [0,T]$, $F(t,\cdot,\cdot)$ is continuous in R because μ is continuous.
- For a given pair (x,y), $F(\cdot,x,y)$ is measurable in $[0,T]$ because Q and S_{e} are measurable in $[0,T]$.
- There exists a Lebesgue integrable function $m : [0,T] \to \mathbb{R}$ such that $\|F(t,x,y)\| \leq m(t)$ in G:

$$\|F(t,x,y)\| = |F_1(t,x,y)| + |F_2(t,x,y)| \leq |\frac{Q(t)}{V} S_{\mathrm{e}}(t)| + |\frac{Q(t)}{V} x| + |\frac{Q(t)}{V} y| + 2|\mu(x)y|.$$

  Taking into account the definition of the set R, it follows that

$$\|F(t,x,t)\| \leq \frac{Q(t)}{V}\big(S_{\mathrm{e}}(t) + S_0 + \frac{\|Q\|_{L^\infty(0,T)} \|S_{\mathrm{e}}\|_{L^\infty(0,T)}}{V} T\big) + \big(\frac{Q(t)}{V} + 2\|\mu\|_{L^\infty(\mathbb{R})}\big) B_0 \mathrm{e}^{\|\mu\|_{L^\infty(\mathbb{R})} T} := m(t).$$

  It is obvious that m is Lebesgue integrable in $[0,T]$.

Step 2: Uniqueness.
Let us prove that there is a Lebesgue integrable function $k : [0,T] \to \mathbb{R}$ such that

$$\|F(t,x_1,y_1) - F(t,x_2,y_2)\| \leq k(t) \|(x_1,y_1) - (x_2,y_2)\| \text{ for any } (t,x_1,y_1), (t,x_2,y_2) \in G.$$

In the one hand,

$$|F_1(t,x_1,y_1) - F_1(t,x_2,y_2)| = |-\mu(x_1)y_1 + \frac{Q(t)}{V}(S_{\mathrm{e}}(t) - x_1) + \mu(x_2)y_2 - \frac{Q(t)}{V}(S_{\mathrm{e}}(t) - x_2)|.$$

Since μ is Lipschitz, there exists a constant $C_{\mathrm{L}} > 0$ such that

$$|F_1(t, x_1, y_1) - F_1(t, x_2, y_2)| \leq |\mu(x_2)||y_2 - y_1| + \frac{Q(t)}{V}|x_2 - x_1| + C_{\mathrm{L}}|y_1||x_2 - x_1|.$$

Again taking into account the definition of R, one has that

$$|F_1(t, x_1, y_1) - F_1(t, x_2, y_2)| \leq \big(\|\mu\|_{L^\infty(\mathbb{R})} + \frac{Q(t)}{V} + C_{\mathrm{L}} B_0 \mathrm{e}^{\|\mu\|_{L^\infty(\mathbb{R})} T}\big)\|(x_1, y_1) - (x_2, y_2)\|.$$

On the other hand, one has:

$$\begin{aligned} |F_2(t, x_1, y_1) - F_2(t, x_2, y_2)| = \; & |\mu(x_1)y_1 - \tfrac{Q(t)}{V} y_1 - \mu(x_2)y_2 + \tfrac{Q(t)}{V} y_2| \\ \leq \; & \|\mu\|_{L^\infty(\mathbb{R})}|y_2 - y_1| + \tfrac{Q(t)}{V}|y_2 - y_1| + C_{\mathrm{L}} B_0 \mathrm{e}^{\|\mu\|_{L^\infty(\mathbb{R})} T}|x_2 - x_1|. \end{aligned}$$

Thus, the Lebesgue integrable function k can be taken as

$$k(t) = 2\big(\|\mu\|_{L^\infty(\mathbb{R})} + \frac{Q(t)}{V} + C_{\mathrm{L}} B_0 \mathrm{e}^{\|\mu\|_{L^\infty(\mathbb{R})} T}\big),$$

and the statement of the theorem is proved. □

Lemma 2.1.5. *Under the assumptions of Theorem 2.1.4, if $\mu \in C^1(\mathbb{R})$ and Q, S_{e} are constants (as in Section 2.1.4), then there exists a unique solution $(S, B) \in \mathcal{C}^1([0, +\infty))^2$ for the initial value problem* (2.1).

Proof. As in the proof of Theorem 2.1.4, we use $\|\cdot\| = \|\cdot\|_1$ and rewrite system (2.1) as in (2.4). In order to prove Lemma 2.1.5 we apply Theorem A.2.4 (with $G = [0, T] \times R$, where $R = [0, S_0 + \frac{QS_{\mathrm{e}}}{V} T] \times [0, B_0 \mathrm{e}^{\|\mu\|_{L^\infty(\mathbb{R})} T}]$) and Theorem A.2.5.

Step 1: Existence and Uniqueness.
Let us prove that $F : G \to \mathbb{R}^2$ satisfies the conditions in Theorem A.2.4.

- F is continuous in G because μ is continuous.
- Proceeding as in the proof of Theorem 2.1.4, it follows that

  $$\|F(t, x_1, y_1) - F(t, x_2, y_2)\| \leq k\|(x_1, y_1) - (x_2, y_2)\|,$$

  with $k = 2\big(\|\mu\|_{L^\infty(\mathbb{R})} + \frac{Q}{V} + C_{\mathrm{L}} B_0 \mathrm{e}^{\|\mu\|_{L^\infty(\mathbb{R})} T}\big)$.

From Theorem A.2.4 one has that there exists a unique solution $(S, B) \in \mathcal{C}^1([0, \bar{T}])^2$ for the initial value problem (2.1), with $\bar{T} \in (0, T]$.

Step 2: Continuation of the solution.
Let us prove that $F : G \to \mathbb{R}^2$ satisfies the conditions in Theorem A.2.5.

- F and $\frac{\partial F}{\partial x}$, $\frac{\partial F}{\partial y}$ are continuous functions in $\mathbb{R}^2$ because $\mu \in \mathcal{C}^1(\mathbb{R})$.
- Taking into account the definition of R, one has that

  $$\|(x(t), y(t))\| \leq \frac{Q}{V}\big(S_{\mathrm{e}} + S_0 + \frac{Q}{V} S_{\mathrm{e}} T\big) + \big(2\|\mu\|_{L^\infty(\mathbb{R})} + \frac{Q}{V}\big) B_0 e^{\|\mu\|_{L^\infty(\mathbb{R})} T} := M.$$

From Theorem A.2.5, it follows that the solution (S, B) for the initial value problem (2.1) is defined in $[0, +\infty)$. □

Remark 2.1.6. *Notice that the Monod and Haldane functions (see* (2.2) *and* (2.3)*, respectively) satisfy the Lipschitz continuity property needed in Theorem 2.1.4 and the continuous differentiability property needed in Lemma 2.1.5.*

Remark 2.1.7. *Notice that we assume that Q and S_{e} are nonnegative and essentially bounded because of their physical meaning. The assumption $\mu(0) = 0$ is due to the fact that, if there is no substrate concentration, no reaction is produced; the assumption of considering that function μ is essentially bounded is caused by the fact that the microorganisms have a maximum specific growth rate (see equations* (2.2) *and* (2.3)*).*

2.1.3 Nondimensional analysis

System (2.1) is non-dimensionalised by setting

$$\hat{B} = \frac{B}{b} \qquad \hat{S} = \frac{S}{s}, \qquad \hat{t} = \frac{t}{\tau}, \qquad \hat{Q} = \frac{Q}{\gamma}, \qquad \hat{S}_{\mathrm{e}} = \frac{S_{\mathrm{e}}}{e}, \qquad \text{and} \qquad \hat{\mu}(\hat{S}) = \frac{\mu(s\hat{S})}{\nu},$$

where b, s, τ, γ, e, and ν are suitable scales. Thus, for $0 < \hat{t} < \frac{T}{\tau}$, system (2.1) becomes

$$\begin{cases} \frac{\mathrm{d}\hat{S}}{\mathrm{d}\hat{t}}(\hat{t}) = -\dfrac{\tau\nu\hat{\mu}(\hat{S}(\hat{t}))b\hat{B}(\hat{t})}{s} + \dfrac{\tau\hat{Q}(\hat{t})\gamma}{V}\dfrac{(e\hat{S}_{\mathrm{e}}(\hat{t}) - s\hat{S}(\hat{t}))}{s}, \\ \frac{\mathrm{d}\hat{B}}{\mathrm{d}\hat{t}}(\hat{t}) = \tau\nu\hat{\mu}(\hat{S}(\hat{t}))\hat{B}(\hat{t}) - \dfrac{\tau\hat{Q}(\hat{t})\gamma\hat{B}(\hat{t})}{V}, \\ \hat{S}(0) = \dfrac{S_0}{s}, \qquad \hat{B}(0) = \dfrac{B_0}{b}. \end{cases} \tag{2.5}$$

For ease of notation we drop the $\hat{}$ notation, and so S, B, S_{e}, Q and t are now the non-dimensional variables. The dimensionless groups of parameters in system (2.5) are

$$\alpha_1 = \frac{S_0}{s}, \quad \alpha_2 = \frac{B_0}{b}, \quad \alpha_3 = \tau\nu, \quad \alpha_4 = \frac{\tau\nu b}{s}, \quad \alpha_5 = \frac{\tau\gamma}{V} \quad \text{and} \quad \alpha_6 = \frac{\tau\gamma e}{Vs}.$$

We set $\nu = \|\mu\|_{L^\infty(\mathbb{R})}$ and $e = \|S_{\mathrm{e}}\|_{L^\infty(0,T)}$ for the reaction and the entering substrate scales, respectively. In order to choose the scale γ we take into account that we are interested in the case in which $Q(t) < V \max_{S\in[0,S_{\mathrm{e}}(t)]} \mu(S)$ for all $t > 0$ (see Remark 2.1.12), so that $\gamma = V\|\mu\|_{L^\infty(\mathbb{R})}$ is chosen. We also set $s = b = \|S_{\mathrm{e}}\|_{L^\infty(0,T)}$ in order to simplify the system. This leads to

$$\tau = \frac{1}{\|\mu\|_{L^\infty(\mathbb{R})}}.$$

Particularly, if S_{e} and Q are constants, the system in its non-dimensional form is therefore given by:

$$\begin{cases} \frac{\mathrm{d}S}{\mathrm{d}t}(t) = -\mu(S(t))B(t) + D(1 - S(t)) & \forall t \in (0,T), \\ \frac{\mathrm{d}B}{\mathrm{d}t}(t) = \mu(S(t))B(t) - DB(t) & \forall t \in (0,T), \end{cases} \tag{2.6}$$

completed with the initial conditions

$$S(0) = \alpha_1, \qquad B(0) = \alpha_2, \tag{2.7}$$

where $D = \dfrac{Q}{V\|\mu\|_{L^\infty(\mathbb{R})}}$, $\alpha_1 = \dfrac{S_0}{S_{\mathrm{e}}}$, $\alpha_2 = \dfrac{B_0}{S_{\mathrm{e}}}$ and $\dfrac{T}{\tau}$ has been redefined as T for convenience.

2.1.4 Asymptotic behavior.

The equilibria of (2.6) are the points (S^*, B^*) satisfying

$$\begin{cases} -\mu(S^*)B^* + D(1 - S^*) = 0, \\ \\ \mu(S^*)B^* - DB^* = 0. \end{cases}$$

From the second equation one gets $B^*\big(\mu(S^*) - D\big) = 0$, so either $B^* = 0$ or $\mu(S^*) = D$. In the first case, from the first equation one gets $S^* = 1$. In the second case, from the first equation it follows that $B^* = 1 - S^*$. Since we are interested in the equilibria with nonnegative components, we focus on the case $S^* \in [0, 1]$.

Theorem 2.1.8. *If μ fulfills* (H1) *(or fulfills* (H2) *and $\mu(1) = \max\limits_{S\in[0,1]} \mu(S)$), it follows that:*

1. *If $D \geq \mu(1)$, the equilibrium point $(S_1^*, B_1^*) = (1, 0)$, usually called washout, is the unique equilibrium with nonnegative components of system* (2.6) *and it is asymptotically stable.*

2. *If $D < \mu(1)$, system* (2.6) *has two equilibria with nonnegative components* $(1, 0)$ *and* $(S_2^*, 1 - S_2^*)$, *where $\mu(S_2^*) = D$. Furthermore, the equilibrium point $(S_2^*, 1 - S_2^*)$ is asymptotically stable and the equilibrium point* $(1, 0)$ *is unstable.*

A schematic representation of the two situations considered in Theorem 2.1.8 can be observed in Figures 2.1-(a) and 2.1-(b), respectively.

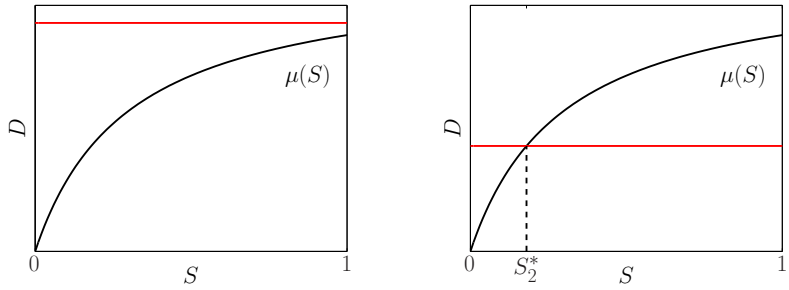

(a) $D \geq \mu(1)$ (b) $D < \mu(1)$

Figure 2.1: Graphical interpretation of the two situations considered in Theorem 2.1.8.

Remark 2.1.9. *In terms of the variables with dimensions appearing in system* (2.1), *Theorem 2.1.8 can be rewritten as follows. If μ fulfills* (H1) *(or fulfills* (H2) *and $\mu(S_e) = \max_{S\in[0,S_e]} \mu(S)$), one has that:*

1. *If $Q \geq V\mu(S_e)$, the equilibrium point $(S_1^*, B_1^*) = (S_e, 0)$, usually called washout, is the unique equilibrium with nonnegative components of system* (2.1) *and it is asymptotically stable.*

2. *If $Q < V\mu(S_e)$, system* (2.1) *has two equilibria with nonnegative components* $(S_e, 0)$ *and* $(S_2^*, S_e - S_2^*)$, *where $V\mu(S_2^*) = Q$. Furthermore, the equilibrium point $(S_2^*, S_e - S_2^*)$ is asymptotically stable and the equilibrium point* $(S_e, 0)$ *is unstable.*

Proof of Theorem 2.1.8.
Case 1. We divide the proof of the first statement in Theorem 2.1.8 in two steps:
Step 1. Let us prove that $(1, 0)$ is the unique equilibrium of system (2.6) with nonnegative components. We distinguish between the different hypothesis that function μ can fulfill.

- μ fulfills (H1): since μ is increasing, one can conclude that, if $D = \mu(1)$, then $(1, 0)$ is the unique equilibrium of system (2.6). If $1 > D > \mu(1)$, there exist an equilibrium $(S^*, 1 - S^*)$ (different from $(1, 0)$) with $\mu(S^*) = D$, but since μ is increasing and $D > \mu(1)$, it follows that $S^* > 1$ and so the second component of the equilibrium is negative. Finally, if $D \geq 1$, it does not exist S^* such that $\mu(S^*) = D$, and thus, $(1, 0)$ is the unique equilibrium of system (2.6).
- μ fulfills (H2) and $\mu(1) = 1$: If $D \geq 1$, then $(1, 0)$ is the unique equilibrium of system (2.6).
- μ fulfills (H2) and $\mu(1) < 1$: Let us denote $s := \arg \max_{S \in [0, +\infty)} \mu(S)$ (i.e., $\mu(s) = 1$). If $D = \mu(1)$ and if there would exist a solution $S^* > s$ of the equation $D = \mu(S^*)$, then the second component of $(S^*, 1 - S^*)$ would be negative. If $\mu(1) < D < 1$, there exist one (or two) solution(s) of the equation $D = \mu(S^*)$ (depending if $\mu\big|_{(s,+\infty)} > D$ or not) satisfying $S^* > 1$, and so the second component of the associated equilibrium $(S^*, 1 - S^*)$ is negative. If $D = 1$, the point $(s, 1 - s)$ is an equilibrium of the system (different from $(1, 0)$) with negative second component. Finally, If $D > 1$, then $(1, 0)$ is the unique equilibrium of system (2.6).

Step 2. Let us study the asymptotic stability of the equilibrium $(1, 0)$.
In order to investigate the stability of $(1, 0)$, we linearize system (2.6) and use *Hartman-Grobman Theorem* (see Theorem A.2.11). The Jacobian matrix associated to the equilibrium (S^*, B^*) is

$$J(S^*, B^*) = \begin{bmatrix} -\mu'(S)B - D & -\mu(S) \\ \mu'(S)B & \mu(S) - D \end{bmatrix} \Big|_{(S,B)=(S^*,B^*)}.$$

Particularly, $J(1, 0) = \begin{bmatrix} -D & -\mu(1) \\ 0 & \mu(1) - D \end{bmatrix}$ and thus, the associated eigenvalues are the ones which fulfill the following second order equation:

$$|\lambda I - J(1, 0)| = \begin{vmatrix} \lambda + D & \mu(1) \\ 0 & \lambda - \mu(1) + D \end{vmatrix} = 0 \Leftrightarrow \big(\lambda + D\big)\big(\lambda - \mu(1) + D\big) = 0,$$

i.e.,

$$\lambda_1 = -D \qquad \text{and} \qquad \lambda_2 = \mu(1) - D.$$

Case 1.1: $D > \mu(1)$

In this case, both λ_1 and λ_2 are negative and so the equilibrium point $(1, 0)$ is asymptotically stable.

Case 1.2: $D = \mu(1)$

In this case, $\lambda_1 = -D$ and $\lambda_2 = 0$, and according to the *Hartman-Grobman Theorem* (see Theorem A.2.11) we cannot conclude the stability of the equilibrium with the linear test. In order to study the stability, we use *Poincaré-Bendixson Theorem* and *Dulac's Criterion* (see Theorems A.2.15 and A.2.16, respectively) to see that $(1, 0)$ is asymptotically stable. We consider the sets $K = \{(S, B) | S + B \leq \max\{1, \alpha_1 + \alpha_2\}\}$ and $E = \{(S, B) | S + B \leq 1\}$, as is depicted in Figure 2.2. First of all, we would like to see that any trajectory of (2.6) relays in the compact set K. In order to see this, we consider the function $M(t) = S(t) + B(t) - 1$. From system (2.6), one has that

$$\frac{\mathrm{d}M}{\mathrm{d}t}(t) = \frac{\mathrm{d}S}{\mathrm{d}t}(t) + \frac{\mathrm{d}B}{\mathrm{d}t}(t) = D(-S(t) - B(t) + 1) = -DM(t).$$

One can conclude that $M(t) = M(0)e^{-Dt}$, with $M(0) = S(0) + B(0) - 1 = \alpha_1 + \alpha_2 - 1$. Consequently $\lim_{t \to \infty} M(t) = 0$, and moreover, $\lim_{t \to \infty} S(t) + B(t) = 1$.

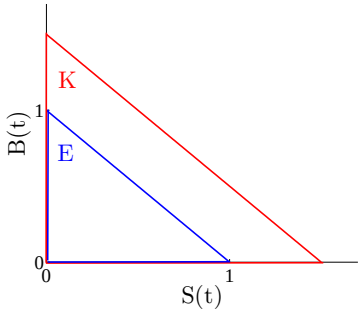

Figure 2.2: A schematic representation of the sets K and E, defined in the proof of Theorem 2.1.8.

Now using *Poincaré-Bendixson Theorem* (see Theorem A.2.15), one has that the trajectories approach either an equilibrium point or either a closed orbit of K. Taking into account that the only equilibrium point in K is the point $(1,0)$, it is sufficient to show that there are no closed orbits in K in order to conclude that the equilibrium point $(1,0)$ is asymptotically stable. In this direction, we are able to use the *Dulac's Criterion* (see Theorem A.2.16).
In this case, E is the simply connected set considered in *Dulac's Criterion*, and $\psi(S,B)=1$. It is necessary to check that $\mathrm{div}(F)$ has constant sign in E, where $F:\mathbb{R}^2\to\mathbb{R}^2$ fulfills $\begin{bmatrix} \frac{\mathrm{d}S}{\mathrm{d}t} \\ \\ \frac{\mathrm{d}B}{\mathrm{d}t} \end{bmatrix} = F(S,B)$ in system (2.6). In this case,

$$\mathrm{div}(F) = \frac{\mathrm{d}}{\mathrm{d}S}\left(\frac{\mathrm{d}S}{\mathrm{d}t}\right) + \frac{\mathrm{d}}{\mathrm{d}B}\left(\frac{\mathrm{d}B}{\mathrm{d}t}\right) = \underbrace{-\mu'(S)B}_{\leq 0 \text{ (H1) and Lemma 2.1.1}} \underbrace{-D+\mu(S)-D}_{(*)}$$

Let us recall that, from the hypothesis (H1), the function μ is increasing and moreover $S\in[0,1]$, since we are considering $(S,B)\in E$. Consequently $\mu(S)\leq\mu(1)$ for any $S\in[0,1]$, and thus $(*)\leq 0$. Therefore, $\mathrm{div}(F)\leq -D<0$ for all $(S,B)\in E$, and there are no closed orbits in E. In order to conclude that there are no closed orbits in K we take into account that any trajectory starting in $K\setminus E$ is approaching E exponentially, so the fact that there are no closed orbits in E implies that there are not closed orbits in K either.

Case 2: We also divide the proof of the second statement in Theorem 2.1.8 in two steps:
Step 1. Let us prove that system (2.6) has two equilibria with nonnegative components.
As in the case 1, we distinguish between the different hypothesis that function μ can fulfill.

- μ fulfills (H1): Since μ is increasing, one can conclude that, if $D<\mu(1)$, then there exist an equilibrium (different from $(1,0)$ and denoted by $(S_2^*,1-S_2^*)$) satisfying $\mu(S_2^*)=D$ with $S_2^*<1$.
- μ fulfills (H2): Since μ is increasing in $[0,1]$, we can conclude that there exist an equilibrium (different from $(1,0)$ and denoted by $(S_2^*,1-S_2^*)$) satisfying $\mu(S_2^*)=D$ with $S_2^*<1$. If there would exist another solution $S^*>1$ of the equation $D=\mu(S^*)$, then the second component of the equilibrium $(S^*,1-S^*)$ would be negative.

Step 2. Let us study the stability properties of the equilibria $(1,0)$ and $(S_2^*,1-S_2^*)$.
As seen in the proof of case 1, the eigenvalues associated to $(1,0)$ are $\lambda_1=-D$ and $\lambda_2=\mu(1)-D$. In this case $\lambda_2>0$ and so the equilibrium point $(1,0)$ is unstable.
The Jacobian matrix associated to $(S_2^*,1-S_2^*)$ is $J(S_2^*,B_2^*)=\begin{bmatrix} -\mu'(S_2^*)(1-S^*)-D & -D \\ \\ \mu'(S_2^*)(1-S_2^*) & 0 \end{bmatrix}$ and thus,

the associated eigenvalues are the ones which fulfill the following second order equation:

$$|\lambda I - J(S_2^*, B_2^*)| = \begin{vmatrix} \lambda + \mu'(S_2^*)(1-S_2^*) + D & +D \\ -\mu'(S_2^*)(1-S_2^*) & \lambda \end{vmatrix} = 0$$

$$\Leftrightarrow \lambda^2 + (\mu'(S_2^*)(1-S_2^*) + D)\lambda + D\mu'(S_2^*)(1-S_2^*) = 0.$$

Thus,

$$\begin{aligned} \lambda_{1,2} &= \frac{-(\mu'(S_2^*)(1-S_2^*)+D) \pm \sqrt{(\mu'(S_2^*)(1-S_2^*)+D)^2 - 4D\mu'(S_2^*)(1-S_2^*)}}{2} \\ &= \frac{-(\mu'(S_2^*)(1-S_2^*)+D) \pm \sqrt{(\mu'(S_2^*)(1-S_2^*)-D)^2}}{2} \\ &= \frac{-(\mu'(S_2^*)(1-S_2^*)+D) \pm |\mu'(S_2^*)(1-S_2^*)-D|}{2}. \end{aligned}$$

We are left in the task of determining the sign of the real part of the eigenvalues. In this direction, we recall that $1 - S_2^* > 0$ and $\mu'(S_2^*) > 0$. Denoting by $\Delta = \mu'(S_2^*)(1-S_2^*) - D$, two different cases arise:

- If $\Delta \neq 0$, then $\lambda_1 = -D$ and $\lambda_2 = -\mu'(S_2^*)(1-S_2^*)$ and both eigenvalues are negative
- If $\Delta = 0$, then there is just one eigenvalue $\lambda_1 = -\frac{\mu'(S_2^*)(1-S_2^*)+D}{2} < 0$

Thus, we conclude that $(S_2^*, 1-S_2^*)$ is asymptotically stable. □

Theorem 2.1.10. *If μ fulfills* (H2) *and $\mu(1) < \max_{S\in[0,1]} \mu(S)$ ($= 1$ in this case), then it follows that:*

1. *If $D > 1$, the equilibrium point $(S_1^*, B_1^*) = (1, 0)$ is the unique equilibrium of system* (2.6) *and it is asymptotically stable.*
2. *If $D = 1$, system* (2.6) *has two equilibria with nonnegative components $(1, 0)$ and $(S_2^*, 1 - S_2^*)$ where $\mu(S_2^*) = D$. The equilibrium point $(1, 0)$ is asymptotically stable.*
3. *If $\mu(1) < D < 1$, system* (2.6) *has three equilibria with nonnegative components $(1, 0)$, $(S_2^*, 1 - S_2^*)$ and $(S_3^*, 1 - S_3^*)$ where $\mu(S_2^*) = \mu(S_3^*) = D$ and $S_2^* < S_3^*$. The equilibrium point $(S_3^*, 1 - S_3^*)$ is unstable and both equilibria $(1, 0)$ and $(S_2^*, 1 - S_2^*)$ are asymptotically stable.*
4. *If $D = \mu(1)$, system* (2.6) *has two equilibria with nonnegative components $(1, 0)$ and $(S_2^*, 1 - S_2^*)$, where $\mu(S_2^*) = D$. The equilibrium point $(S_2^*, 1 - S_2^*)$ is asymptotically stable.*
5. *If $D < \mu(1)$, system* (2.6) *has two equilibria with nonnegative components $(1, 0)$ and $(S_2^*, 1 - S_2^*)$, where $\mu(S_2^*) = D$. Furthermore, the equilibrium point $(S_2^*, 1 - S_2^*)$ is asymptotically stable and the equilibrium point $(1, 0)$ is unstable.*

A schematic representation of the situations considered in Theorem 2.1.8 is shown in Figures 2.3-(a), 2.3-(b), 2.3-(c), 2.3-(d) and 2.3-(e), respectively.

Remark 2.1.11. *In terms of the variables with dimensions appearing in system* (2.1)*, Theorem 2.1.10 can be rewritten as follows. If μ fulfills* (H2) *and $\mu(S_e) < \max_{S\in[0,S_e]} \mu(S)$ ($= \|\mu\|_{L^\infty(\mathbb{R})}$ in this case), then it follows that:*

1. *If $Q > V\|\mu\|_{L^\infty(\mathbb{R})}$, the equilibrium point $(S_1^*, B_1^*) = (S_e, 0)$ is the unique equilibrium of system* (2.1) *and it is asymptotically stable.*
2. *If $Q = V\|\mu\|_{L^\infty(\mathbb{R})}$, system* (2.1) *has two equilibria with nonnegative components $(S_e, 0)$ and $(S_2^*, S_e - S_2^*)$ where $V\mu(S_2^*) = Q$. The equilibrium point $(S_e, 0)$ is asymptotically stable.*

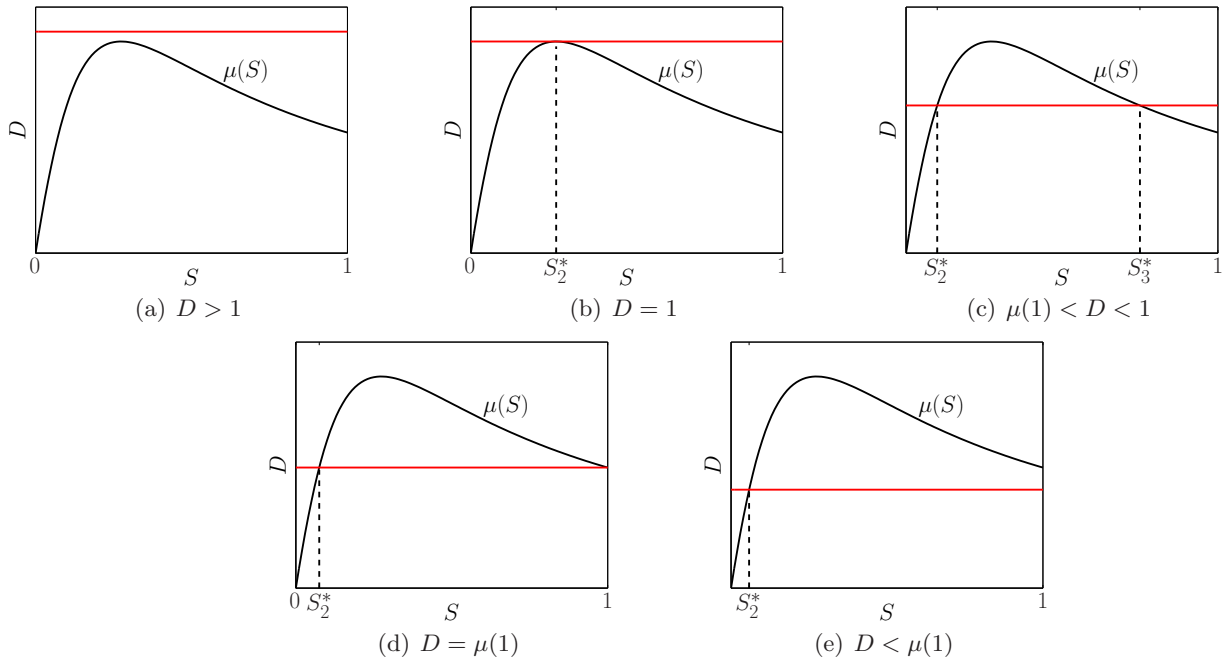

(a) $D > 1$ (b) $D = 1$ (c) $\mu(1) < D < 1$

(d) $D = \mu(1)$ (e) $D < \mu(1)$

Figure 2.3: Graphical interpretation of the situations considered in Theorem 2.1.10.

3. *If* $V\mu(S_e) < Q < V\|\mu\|_{L^\infty(\mathbb{R})}$, *system* (2.1) *has three equilibria with nonnegative components* $(S_e, 0)$, $(S_2^*, S_e - S_2^*)$ *and* $(S_3^*, S_e - S_3^*)$ *where* $V\mu(S_2^*) = V\mu(S_3^*) = Q$ *and* $S_2^* < S_3^*$. *The equilibrium point* $(S_3^*, S_e - S_3^*)$ *is unstable and both equilibria* $(S_e, 0)$ *and* $(S_2^*, S_e - S_2^*)$ *are asymptotically stable.*

4. *If* $Q = V\mu(S_e)$, *system* (2.1) *has two equilibria with nonnegative components* $(S_e, 0)$ *and* $(S_2^*, S_e - S_2^*)$, *where* $V\mu(S_2^*) = Q$. *The equilibrium point* $(S_2^*, S_e - S_2^*)$ *is asymptotically stable.*

5. *If* $Q < V\mu(S_e)$, *system* (2.1) *has two equilibria with nonnegative components* $(S_e, 0)$ *and* $(S_2^*, S_e - S_2^*)$, *where* $V\mu(S_2^*) = Q$. *Furthermore, the equilibrium point* $(S_2^*, S_e - S_2^*)$ *is asymptotically stable and the equilibrium point* $(S_e, 0)$ *is unstable.*

Proof of Theorem 2.1.10.
Case 1: In this case, equation $\mu(S^*) = D$ has no solution and $(1, 0)$ is the unique equilibrium of system (2.6). The proof for the asymptotic stability of $(1, 0)$ is analogous to the one presented in Theorem 2.1.8.

Case 2: One has that $S_2^* = \arg\max_{S\in[0,1]} \mu(S)$ is the unique solution of equation $D = \mu(S^*)$ and $S_2^* > 1$. The proof for the asymptotic stability of $(1, 0)$ is analogous to the one presented in Theorem 2.1.8.

Case 3: It is straightforward to see that there exist two solutions of equation $D = \mu(S^*)$, which we denote by S_2^* and S_3^*, satisfying that $(S_2^*, 1 - S_2^*)$ and $(S_3^*, 1 - S_3^*)$ have nonnegative components. Moreover, one can see that $\mu'(S_2^*) > 0$ and $\mu'(S_3^*) < 0$. As shown in the proof of Theorem 2.1.8, the eigenvalues associated to the equilibria $(S^*, 1 - S^*)$ (where $S^* = S_2^*$ or S_3^*) are

$$\lambda_{1,2} = \begin{cases} \lambda_1 = -D,\ \lambda_2 = -\mu'(S^*)(1 - S^*) & \text{if } \mu'(S^*)(1 - S^*) = D, \\ \lambda_{1,2} = -\frac{\mu'(S^*)(1-S^*)+D}{2} & \text{in other case.} \end{cases}$$

Since $\mu'(S_2^*) > 0$, the eigenvalues associated to the equilibrium point $(S_2^*, 1 - S_2^*)$ are negative and so it is asymptotically stable. Similarly, since $\mu'(S_3^*) < 0$, the eigenvalues associated to the equilibrium point $(S_3^*, 1 - S_3^*)$ are positive and it is unstable. The proof for the asymptotic stability of $(1, 0)$ is analogous to

the one presented in Theorem 2.1.8.

Case 4: We denote by S_2^* the unique solution (different to 1) of equation $\mu(S^*) = D$. The stability of the equilibrium $(S_2^*, 1 - S_2^*)$ is proven as in case 3.

Case 5: We denote by S_2^* the unique solution of equation $\mu(S^*) = D$ such that $S_2^* < 1$. If there would exist another solution S^* of the equation $D = \mu(S^*)$, then the second component of $(S^*, 1 - S^*)$ would be negative. □

Remark 2.1.12. *The equilibrium point* $(1, 0)$*, called washout, corresponds to the extinction of the biomass in the bioreactor, which stops any further reaction with the substrate. As we will see in Chapter 3, the aim for using a bioreactor is the decontamination, i.e., the elimination of substrate supposed to be in excess. Consequently, in real scenarios it is of interest to be in a case where the equilibrium point* $(S_2^*, 1 - S_2^*)$ *is asymptotically stable. In that context, we will study the case* $D < \max_{S\in[0,1]} \mu(S)$*. In terms of dimensional variables, this case corresponds to the case in which* $Q < V \max_{S\in[0,S_e]} \mu(S)$*.*

2.2 Unmixed bioreactors

In this section we model the behavior of a continuous reactor under the assumption of spatially distributed concentration of substances throughout the tank. The mathematical model is presented in Section 2.2.1. Then, in Section 2.2.2 we prove the existence and uniqueness of solution, together with results about its nonnegativity and boundedness. In Section 2.2.3 we perform the dimensional analysis of the system and finally, in Section 2.2.4, we study the asymptotic behavior of the system.

2.2.1 Description of the model

The bioreactor in consideration is a cylinder Ω^* as that depicted in Figure **??**. As in Section 2.1, at the beginning of the process, there is a certain amount of biomass inside Ω^* that is reacting with the polluted water entering the device through the inlet Γ_{in}^* (i.e., the upper boundary of the cylinder). Treated water leaves the reactor through the outlet Γ_{out}^* (i.e., the lower boundary of the cylinder). We denote $\Gamma_{\text{wall}}^* = \delta\Omega^* \setminus (\Gamma_{\text{in}}^* \cup \Gamma_{\text{out}}^*)$, where null flux is considered.

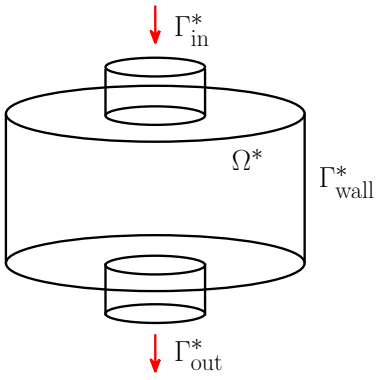

Figure 2.4: 3D reactor

.

We consider the following Advection-Diffusion-Reaction system with Danckwerts boundary conditions, to

describe the behavior of this particular bioreactor:

$$\begin{cases} S_t = \operatorname{div}(D_{\mathrm{S}}\nabla S - \boldsymbol{u}S) - \mu(S)B & \text{in } \Omega^* \times (0,T), \\ B_t = \operatorname{div}(D_{\mathrm{B}}\nabla B - \boldsymbol{u}B) + \mu(S)B & \text{in } \Omega^* \times (0,T), \\ S(x,0) = S_0(x) & \forall x \in \Omega^*, \\ B(x,0) = B_0(x) & \forall x \in \Omega^*, \\ \boldsymbol{n}\cdot(D_{\mathrm{S}}\nabla S - \boldsymbol{u}S) = -\boldsymbol{n}\cdot\boldsymbol{u}\ S_{\mathrm{e}} & \text{in } \Gamma^*_{\mathrm{in}} \times (0,T), \\ \boldsymbol{n}\cdot(D_{\mathrm{B}}\nabla B - \boldsymbol{u}B) = 0 & \text{in } \left(\Gamma^*_{\mathrm{in}} \cup \Gamma^*_{\mathrm{wall}}\right) \times (0,T), \\ \boldsymbol{n}\cdot(D_{\mathrm{S}}\nabla S - \boldsymbol{u}S) = 0 & \text{in } \Gamma^*_{\mathrm{wall}} \times (0,T), \\ \boldsymbol{n}\cdot(D_{\mathrm{S}}\nabla S) = 0 & \text{in } \Gamma^*_{\mathrm{out}} \times (0,T), \\ \boldsymbol{n}\cdot(D_{\mathrm{B}}\nabla B) = 0 & \text{in } \Gamma^*_{\mathrm{out}} \times (0,T), \end{cases} \tag{2.8}$$

where $T > 0$ (s) is the length of the time interval for which we want to model the process, S (kg/m^3) and B (kg/m^3) are the substrate and biomass concentration inside the bioreactor, which diffuse throughout the water in the vessel with diffusion coefficients D_{S} (m^2/s) and D_{B} (m^2/s), respectively. Vector $\boldsymbol{u}$ (m/s) is the fluid velocity (to be described afterward), S_{e} (kg/m^3) is the concentration of substrate that enters into the bioreactor, S_0 (kg/m^3) and B_0 (kg/m^3) are the concentrations of substrate and biomass inside the bioreactor at the beginning of the process, respectively, and $\boldsymbol{n}$ is the outward unit normal vector on the boundary of the domain Ω^*. Notice that besides the Advection-Diffusion terms, we also have a term corresponding to the reaction of biomass and substrate, governed by the growth rate function μ (1/s), which we assume that fulfills either hypothesis (H1) or hypothesis (H2) (see Section 2.1.1). Notice that some physical effects have been disregarded in system (2.8) (e.g., oxygen supply, bubbling...) in order to focus in the differences between homogeneous and inhomogeneous environments without using a more complex model.

Danckwerts boundary conditions

In order to obtain the boundary conditions in (2.8), we follow the reasoning below. Taking into account diffusion and advection, if we denote J the flux, it follows that

$$J = -D\nabla c + \boldsymbol{u}c,$$

where c is the variable of interest, D is the diffusion coefficient and $\boldsymbol{u}$ is the fluid flow. Second, we recall that the flux J that enters the bioreactor is the same that the flux that leaves it.
Applying these two premises, for instance, to the substrate concentration in the boundary Γ^*_{in}, one has $-D_{\mathrm{S}}\nabla S_{\mathrm{e}} + \boldsymbol{u}S_{\mathrm{e}} = -D_{\mathrm{S}}\nabla S + \boldsymbol{u}S$. Since we are considering that S_{e} only depends on the time variable, it follows the boundary condition

$$\boldsymbol{n}\cdot(-D_{\mathrm{S}}\cdot\nabla S + \boldsymbol{u}S) = \boldsymbol{n}\cdot\boldsymbol{u}\ S_{\mathrm{e}} \qquad \text{in } \Gamma^*_{\mathrm{in}}.$$

Similarly, since we assume that there is no biomass entering through the inlet, the boundary condition in Γ^*_{in} for the biomass is

$$\boldsymbol{n}\cdot(-D_{\mathrm{B}}\cdot\nabla B + \boldsymbol{u}B) = 0 \qquad \text{in } \Gamma^*_{\mathrm{in}}.$$

Since the substance cannot leave or enter the bioreactor through the wall Γ^*_{wall}, the normal component of the flux must be zero:

$$\boldsymbol{n} \cdot (-D \cdot \nabla c + \boldsymbol{u}c) = 0 \qquad \text{in } \Gamma^*_{\text{wall}}, \text{ with } (D, c) \in \{(D_{\text{S}}, S), (D_{\text{B}}, B)\}.$$

Finally, for Γ^*_{out} we assume that there is no diffusion for the two concentrations after leaving the reactor. Consequently, one has the equation $-D\nabla c + \boldsymbol{u}c = \boldsymbol{u}c$ and the corresponding boundary condition is

$$\boldsymbol{n} \cdot (-D \cdot \nabla c) = 0 \qquad \text{in } \Gamma^*_{\text{out}}, \text{ with } (D, c) \in \{(D_{\text{S}}, S), (D_{\text{B}}, B)\}.$$

Fluid Flow

In all this part of the thesis (except in Section 3.3) we consider that the fluid flow is described by

$$\boldsymbol{u} = (0, 0, -u(x, t)), \tag{2.9}$$

where u (m/s) is the vertical flow rate. In Section 3.3, we will consider that the flow velocity $\boldsymbol{u} = (u_1, u_2, u_3)$ (m/s) is described by using the stationary Navier–Stokes equations for Newtonian incompressible viscous fluids (see, e.g., [**?**])

$$\begin{cases} -\eta\Delta\boldsymbol{u} + \rho(\boldsymbol{u} \cdot \nabla)\boldsymbol{u} + \nabla p = 0 & \text{in } \Omega^*, \\ \nabla \cdot \boldsymbol{u} = 0 & \text{in } \Omega^*, \\ \boldsymbol{u} = 0 & \text{in } \Gamma^*_{\text{wall}}, \\ \boldsymbol{u} = -u_{\text{in}}\ E(x)\ \boldsymbol{n} & \forall x \in \Gamma^*_{\text{in}}, \\ \boldsymbol{n} \cdot (\eta\nabla\boldsymbol{u}) = 0 & \text{in } \Gamma^*_{\text{out}}, \\ p(x) = p_{\text{atm}} & \forall x \in \Gamma^*_{\text{out}}, \end{cases} \tag{2.10}$$

where p is the pressure field (Pa); p_{atm} is the atmospheric pressure (Pa); η is the fluid dynamic viscosity (kg/m s); ρ is the fluid density (kg/ m^3); u_{in} (m/s) is the maximum injection velocity; E is the laminar flow inlet profile (an ellipsoid of revolution) equal to 0 in the inlet border and unity in the inlet center, and $\boldsymbol{n}$ is the outward-pointing normal vector along the boundary.

Domain Simplification

A typical representation of a bioreactor is a tank as depicted in Figure 2.5-(a), with a small inlet aperture at its top (through which polluted water enters the reactor) and a small outlet aperture at its bottom (through which the treated water leaves the reactor). In Sections 2.2.3, 2.2.4 and 3.2, following the model developed in [**?**] for fluidic mixers, we neglect, for the sake of model simplification, the possible effects coming from the size and collocation of these apertures. To do that, we only model an intermediate part of the bioreactor, denoted by Ω^* (dark part of Figure 2.5-(a)), assuming that the volume of the removed part is negligible compared to the total bioreactor volume. Taking into account that the device's geometry (see Figure (2.5)-(b)) is an empty solid of revolution, it can be simplified and described by using a 2D domain Ω (see Figure (2.5)-(c)) using cylindrical coordinates (r, z) where r is the distance to the cylinder

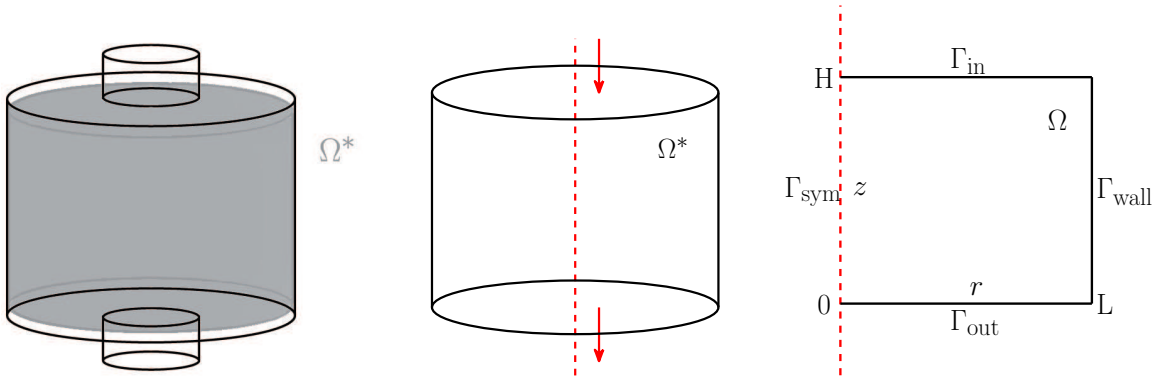

(a) 3D Reactor (b) 3D Reactor simplification (c) 2D Reactor simplification

Figure 2.5: Typical domain representation of the bioreactor geometry.

axis. Then, system (2.8),(2.9) can be rewritten as

$$
\begin{cases}
\frac{\partial S}{\partial t} = \frac{1}{r}\frac{\partial}{\partial r}(rD_{\mathrm{S}}\frac{\partial S}{\partial r}) + \frac{\partial}{\partial z}(D_{\mathrm{S}}\frac{\partial S}{\partial z}) + u\frac{\partial S}{\partial z} - \mu(S)B & \text{in } \Omega \times (0,T), \\
\frac{\partial B}{\partial t} = \frac{1}{r}\frac{\partial}{\partial r}(rD_{\mathrm{B}}\frac{\partial B}{\partial r}) + \frac{\partial}{\partial z}(D_{\mathrm{B}}\frac{\partial B}{\partial z}) + u\frac{\partial B}{\partial z} + \mu(S)B & \text{in } \Omega \times (0,T) \\
S(r,z,0) = S_0(r,z) & \forall (r,z) \in \Omega, \\
B(r,z,0) = B_0(r,z) & \forall (r,z) \in \Omega, \\
D_{\mathrm{S}}\frac{\partial S}{\partial z} + uS = uS_{\mathrm{e}} & \text{in } \Gamma_{\mathrm{in}} \times (0,T), \\
D_{\mathrm{B}}\frac{\partial B}{\partial z} + uB = 0 & \text{in } \Gamma_{\mathrm{in}} \times (0,T), \\
\frac{\partial S}{\partial r} = 0 & \text{in } \left(\Gamma_{\mathrm{wall}} \cup \Gamma_{\mathrm{sym}}\right) \times (0,T), \\
\frac{\partial B}{\partial r} = 0 & \text{in } \left(\Gamma_{\mathrm{wall}} \cup \Gamma_{\mathrm{sym}}\right) \times (0,T), \\
\frac{\partial S}{\partial z} = 0 & \text{in } \Gamma_{\mathrm{out}} \times (0,T), \\
\frac{\partial B}{\partial z} = 0 & \text{in } \Gamma_{\mathrm{out}} \times (0,T),
\end{cases}
\tag{2.11}
$$

where in the simplified model the domain is the rectangle $\Omega = [0,L] \times [0,H]$, $\Gamma_{\mathrm{sym}} = \{0\} \times (0,H)$ is the axis of symmetry, $\Gamma_{\mathrm{in}} = (0,L) \times \{H\}$ is the bioreactor inlet and $\Gamma_{\mathrm{out}} = (0,L) \times \{0\}$ is the bioreactor outlet. We denote $\Gamma_{\mathrm{wall}} = \delta\Omega \setminus \left(\Gamma_{\mathrm{in}} \cup \Gamma_{\mathrm{out}} \cup \Gamma_{\mathrm{sym}}\right)$, where null flux is assumed.

2.2.2 Existence, uniqueness, positivity and boundedness

Definition of weak solution

Assuming $S, B \in W(0,T,H^1(\Omega^*),(H^1(\Omega^*))')$ (see Definition A.3.5 for more details of this functional space), $u \in L^\infty(0,T,\mathcal{C}(\bar{\Omega}^*))$, $S_{\mathrm{e}} \in L^2(0,T)$ and $\mu \in L^\infty(\mathbb{R})$, if we multiply (duality pairing between $H^1(\Omega^*)$ and its dual space) the first equation of (2.8) by $v \in H^1(\Omega^*)$, it follows that

$$< S_t, v >_{(H^1(\Omega^*))'\times H^1(\Omega^*)} - < \operatorname{div}(D_{\mathrm{S}}\nabla S - \boldsymbol{u}S), v >_{(H^1(\Omega^*))'\times H^1(\Omega^*)} + \int_{\Omega^*} \mu(S(x,t))B(x,t)v(x)\mathrm{d}x = 0.$$

Then, applying the Green's Formula and taking into account the boundary conditions, we obtain

$$< S_t, v >_{(H^1(\Omega^*))'\times H^1(\Omega^*)} + \int_{\Omega^*} \mu(S(x,t))B(x,t)v(x)\mathrm{d}x - \int_{\Gamma^*_{\mathrm{in}}} u(x,t)S_{\mathrm{e}}(t)v(x)\mathrm{d}\Gamma^*_{\mathrm{in}}$$

$$+ \int_{\Omega^*}(D_{\mathrm{S}}\nabla S(x,t) - \boldsymbol{u}(x,t)S(x,t))\nabla v(x)\mathrm{d}x + \int_{\Gamma^*_{\mathrm{out}}} u(x,t)S(x,t)v(x)\mathrm{d}\Gamma^*_{\mathrm{out}} = 0.$$

Similarly, multiplying the second equation of (2.8) by $w \in H^1(\Omega^*)$, applying the Green's Formula and taking into account the boundary conditions, one has that

$$< B_t, w >_{(H^1(\Omega^*))'\times H^1(\Omega^*)} + \int_{\Omega^*}(D_{\mathrm{B}}\nabla B(x,t) - \boldsymbol{u}(x,t)B(x,t))\nabla w(x)\mathrm{d}x + \int_{\Gamma^*_{\mathrm{out}}} u(x,t)B(x,t)w(x)\mathrm{d}\Gamma^*_{\mathrm{out}}$$

$$- \int_{\Omega^*} \mu(S(x,t))B(x,t)w(x)\mathrm{d}x = 0.$$

Let us denote $\boldsymbol{\psi} = \begin{pmatrix} p \\ q \end{pmatrix}$, $\boldsymbol{\phi} = \begin{pmatrix} v \\ w \end{pmatrix}$, $\mathbf{H}^1(\Omega^*) = H^1(\Omega^*) \times H^1(\Omega^*)$ and $(\mathbf{H}^1(\Omega^*))' = (H^1(\Omega^*))' \times (H^1(\Omega^*))'$ and consider the bilinear form $A(t,\cdot,\cdot) : \mathbf{H}^1 \times \mathbf{H}^1 \to \mathbb{R}$ defined by:

$$\begin{aligned} A(t,\boldsymbol{\psi},\boldsymbol{\phi}) = \; & \int_{\Omega^*}(D_{\mathrm{S}}\nabla p(x) - \boldsymbol{u}(x,t)p(x))\nabla v(x)\mathrm{d}x + \int_{\Omega^*}(D_{\mathrm{B}}\nabla q(x) - \boldsymbol{u}(x,t)q(x))\nabla w(x)\mathrm{d}x \\ & + \int_{\Gamma^*_{\mathrm{out}}} u(x,t)\big(p(x)v(x) + q(x)w(x)\big)\mathrm{d}\Gamma^*_{\mathrm{out}}. \end{aligned}$$

Definition 2.2.1. *A weak solution of problem (2.8) is a function $\boldsymbol{\xi} = (S,B)$ such that $S, B \in W(0,T,H^1(\Omega^*),(H^1(\Omega^*))')$ and satisfy*

$$\begin{cases} < \boldsymbol{\xi}_t(\cdot), \boldsymbol{\phi} >_{(\mathbf{H}^1(\Omega^*))'\times\mathbf{H}^1(\Omega^*)} + A(\cdot,\boldsymbol{\xi}(\cdot),\boldsymbol{\phi}) = \\ \quad \int_{\Gamma^*_{\mathrm{in}}} u(x,\cdot)S_{\mathrm{e}}(\cdot)v(x)\mathrm{d}\Gamma^*_{\mathrm{in}} + \int_{\Omega^*} \mu(S(x,\cdot))B(x,\cdot)(w(x)-v(x))\mathrm{d}x \\ \qquad\qquad \text{for all } \boldsymbol{\phi} = (v,w) \in \mathbf{H}^1(\Omega^*) \end{cases} \tag{2.12}$$

in the sense of $\mathcal{D}'(0,T)$ (see, e.g., [?]), i.e., all the terms above are considered as distributions in t. Notice that

$$\begin{aligned} < \boldsymbol{\xi}_t(\cdot), \boldsymbol{\phi} >_{(\mathbf{H}^1(\Omega^*))'\times\mathbf{H}^1(\Omega^*)} &=< S_t(\cdot), v >_{(H^1(\Omega^*))'\times H^1(\Omega^*)} + < B_t(\cdot), w >_{(H^1(\Omega^*))'\times H^1(\Omega^*)} \\ &= \tfrac{\mathrm{d}}{\mathrm{d}t}\Big(\int_{\Omega^*} S(\cdot,x)v(x)\mathrm{d}x + \int_{\Omega^*} B(\cdot,x)w(x)\mathrm{d}x\Big) \end{aligned}$$

in the sense of $\mathcal{D}'(0,T)$.

Existence

The existence of solution of system (2.8) (stated in Theorem 2.2.2) is proved as follows. First, in Theorem 2.2.5, we prove the existence and uniqueness of solution of a simplified linear system. Then, in Proposition 2.2.6, we prove that the solution of the simplified linear system is bounded. Finally, in Theorem 2.2.2, we prove the existence of solution of system (2.8) by using Theorem 2.2.5, Proposition 2.2.6 and the Schauder Fixed Point Theorem (see Theorem A.3.1).

Theorem 2.2.2 (Existence of solution)**.** *Let us assume $\boldsymbol{u}$ is as in (2.9) with $u \in L^\infty(0,T,\mathcal{C}(\bar{\Omega}^*))$ is nonnegative, $S_{\mathrm{e}} \in L^2(0,T)$, $S_0, B_0 \in L^2(\Omega^*)$, $D_{\mathrm{S}}, D_{\mathrm{B}} > 0$ and $\mu \in L^\infty(\mathbb{R})$ is continuous. Then, system (2.8) has at least one weak solution (S,B).*

Remark 2.2.3. *Notice that we assume that u is nonnegative because of its physical meaning. However, in order to prove Theorem 2.2.2 it suffices to consider u with negative part u^- such that $\|u^-\|_{L^\infty(\bar\Omega^*\times(0,T))} < \frac{\min(D_{\rm S},D_{\rm B})}{C_{\rm T}^2}$ a.e. $t\in(0,T)$, where $C_{\rm T}$ is a constant coming from the Trace inequality (see* (A.4)*) .*

In order to prove Theorem 2.2.2, we first investigate the existence and uniqueness of solution of the following linear parabolic system:

$$\begin{cases} S_t - \operatorname{div}(D_{\rm S}\nabla S - \boldsymbol{u}S) + cB = 0 & \text{in } \Omega^*\times(0,T),\\ B_t - \operatorname{div}(D_{\rm B}\nabla B - \boldsymbol{u}B) - cB = 0 & \text{in } \Omega^*\times(0,T),\\ S(x,0) = S_0(x) & \forall x\in\Omega^*,\\ B(x,0) = B_0(x) & \forall x\in\Omega^*,\\ \boldsymbol{n}\cdot(D_{\rm S}\nabla S - \boldsymbol{u}S) = uS_{\rm e} & \text{in } \Gamma^*_{\rm in}\times(0,T),\\ \boldsymbol{n}\cdot(D_{\rm B}\nabla B - \boldsymbol{u}B) = 0 & \text{in } \big(\Gamma^*_{\rm in}\cup\Gamma^*_{\rm wall}\big)\times(0,T),\\ \boldsymbol{n}\cdot(D_{\rm S}\nabla S - \boldsymbol{u}S) = 0 & \text{in } \Gamma^*_{\rm wall}\times(0,T),\\ \boldsymbol{n}\cdot(D_{\rm S}\nabla S) = 0 & \text{in } \Gamma^*_{\rm out}\times(0,T),\\ \boldsymbol{n}\cdot(D_{\rm B}\nabla B) = 0 & \text{in } \Gamma^*_{\rm out}\times(0,T), \end{cases} \tag{2.13}$$

where $c\in L^\infty(\Omega^*\times(0,T))$. Proceeding analogously to the nonlinear case, we first define the concept of weak solution for this system.

Definition 2.2.4. *A weak solution of problem (2.13) is a function $\boldsymbol{\xi}=(S,B)$ such that $S,B\in W(0,T,H^1(\Omega^*),(H^1(\Omega^*))')$ and satisfy*

$$\begin{cases} <\boldsymbol{\xi}_t(\cdot),\boldsymbol{\phi}>_{(\mathbf{H}^1(\Omega^*))'\times\mathbf{H}^1(\Omega^*)} + \bar A(\cdot,\boldsymbol{\xi}(\cdot),\boldsymbol{\phi}) = \int_{\Gamma^*_{\rm in}} u(x,\cdot)S_{\rm e}(\cdot)v(x)\mathrm{d}\Gamma^*_{\rm in}\\ \qquad\qquad\qquad\qquad\qquad\qquad \text{for all } \phi=(v,w)\in\mathbf{H}^1(\Omega^*)) \end{cases} \tag{2.14}$$

in the sense of $\mathcal{D}'(0,T)$. Here, $\boldsymbol{\psi}=\begin{pmatrix}p\\q\end{pmatrix}$, $\boldsymbol{\phi}=\begin{pmatrix}v\\w\end{pmatrix}$ and the bilinear form $\bar A(t,\cdot,\cdot):\mathbf{H}^1\times\mathbf{H}^1\to\mathbb{R}$ is defined by

$$\begin{aligned}\bar A(t,\boldsymbol{\psi},\boldsymbol{\phi}) = {}& \int_{\Omega^*}(D_{\rm S}\nabla p(x) - \boldsymbol{u}(x,t)p(x))\nabla v(x)\mathrm{d}x + \int_{\Omega^*}(D_{\rm B}\nabla q(x) - \boldsymbol{u}(x,t)q(x))\nabla w(x)\mathrm{d}x\\ &+ \int_{\Omega^*} c(x,t)q(x)\big(v(x)-w(x)\big)\mathrm{d}x + \int_{\Gamma^*_{\rm out}} u(x,t)\big(p(x)v(x)+q(x)w(x)\big)\mathrm{d}\Gamma^*_{\rm out}.\end{aligned}$$

We now focus on proving the existence and uniqueness of solution of the linear system (2.13).

Theorem 2.2.5. *Under the assumptions of Theorem 2.2.2, problem (2.13) has a unique weak solution (S,B).*

Proof of Theorem 2.2.5. Since equation for B in system (2.13) does not depend on S, Theorem 2.2.5 can be proved by applying Theorem A.3.7 twice (taking $V=H^1(\Omega^*)$ and $H=L^2(\Omega^*)$) to a single equation,

namely

$$\begin{cases} R_t = \mathrm{div}(D_r\nabla R - \boldsymbol{u}R) + \gamma R - f & \text{in } \Omega^* \times (0,T), \\ R(x,0) = R_0(x) & \forall x \in \Omega^*, \\ \boldsymbol{n}\cdot(D_r\nabla R - \boldsymbol{u}R) = G & \text{in } \Gamma^*_{\text{in}} \times (0,T), \\ \boldsymbol{n}\cdot(D_r\nabla R - \boldsymbol{u}R) = 0 & \text{in } \Gamma^*_{\text{wall}} \times (0,T), \\ \boldsymbol{n}\cdot(D_r\nabla R) = 0 & \text{in } \Gamma^*_{\text{out}} \times (0,T), \end{cases} \tag{2.15}$$

with $(D_r, \gamma, f, R_0, G) = (D_{\text{B}}, c, 0, B_0, 0)$, and then with $(D_r, \gamma, f, R_0, G) = (D_{\text{S}}, 0, cB, S_0, S_e u)$.

Notice that the application of Theorem A.3.7 is analogous in both cases. In order to shorten the length of this work we only present a detailed proof for the second one, assuming that $B \in L^2(\Omega^* \times (0,T))$. We define the bilinear operator $\bar{a}(t,\cdot,\cdot) : H^1(\Omega^*) \times H^1(\Omega^*) \to \mathbb{R}$ as

$$\bar{a}(t,p,v) = \int_{\Omega^*}(D_{\text{S}}\nabla p(x) - \boldsymbol{u}(x,t)p(x))\nabla v(x)\mathrm{d}x + \int_{\Gamma^*_{\text{out}}} u(x,t)p(x)v(x)\mathrm{d}\Gamma^*_{\text{out}}$$

so that a weak solution of equation (2.15) is a function $S \in W(0,T,H^1(\Omega^*),(H^1(\Omega^*))')$ satisfying

$$\begin{cases} < S_t(\cdot), \boldsymbol{\phi} >_{(H^1(\Omega^*))'\times H^1(\Omega^*)} + \bar{a}(\cdot, S(\cdot), v) = \int_{\Gamma^*_{\text{in}}} u(x,\cdot)S_{\text{e}}(\cdot)v(x)\mathrm{d}\Gamma^*_{\text{in}} - \int_{\Omega^*} c(x,\cdot)B(x,\cdot)v(x)\mathrm{d}x \\ \qquad\qquad \text{for all } v \in H^1(\Omega^*) \end{cases} \tag{2.16}$$

in the sense of $\mathcal{D}'(0,T)$.

Step 1: Let us see that $\bar{a}$ satisfies the condition (A.11).
For all $p, v \in H^1(\Omega^*)$, function $t \to \bar{a}(t,p,v)$ is Lebesgue measurable. This follows from the fact that u is assumed to be Lebesgue measurable function.

To be able to apply Theorem A.3.7, we need to find $k \in \mathbb{R}$ such that $|\bar{a}(t,p,v)| \le k\|p\|_{H^1(\Omega^*)}\|v\|_{H^1(\Omega^*)}$ for all $p, v \in H^1(\Omega^*)$, a.e. $t \in (0,T)$. Now,

$$\begin{aligned} |\bar{a}(t,p,v)| \le \; & D_{\text{S}} \int_{\Omega^*} |\nabla p(x)||\nabla v(x)|\mathrm{d}x + \|u\|_{L^\infty(\bar{\Omega}^*\times(0,T))} \int_{\Omega^*} |p(x)||\nabla v(x)|\mathrm{d}x \\ & + \|u\|_{L^\infty(\bar{\Omega}^*\times(0,T))}\|p\|_{L^2(\Gamma^*_{\text{out}})}\|v\|_{L^2(\Gamma^*_{\text{out}})}. \end{aligned}$$

Then, using the Trace inequality (see (A.4)), we can conclude that there exist a constant $C_{\text{T}} > 0$ such that

$$|\bar{a}(t,p,v)| \le (D_{\text{S}} + (1 + C_{\text{T}}^2)\|u\|_{L^\infty(\bar{\Omega}^*\times(0,T))}\|p\|_{H^1(\Omega^*)}\|v\|_{H^1(\Omega^*)}.$$

Step 2: Let us see that $\bar{a}$ satisfies the condition (A.12).
We need to find $\alpha, \lambda > 0$ such that $\bar{a}(t,p,p) + \lambda\|p\|^2_{L^2(\Omega^*)} \ge \alpha\|p\|^2_{H^1(\Omega^*)}$ for all $p \in H^1(\Omega^*)$, a.e. $t \in (0,T)$. We have that

$$\bar{a}(t,p,p) = D_{\text{S}}\|\nabla p\|^2_{L^2(\Omega^*)} - \int_{\Omega^*} \boldsymbol{u}(x,t)p(x)\nabla p(x)\mathrm{d}x + \int_{\Gamma^*_{\text{out}}} u(x,t)p(x)^2\mathrm{d}x.$$

Applying Young's inequality (see (A.1)) with $\epsilon > 0$, to be chosen later, the following inequality holds:

$$-\int_{\Omega^*} \boldsymbol{u}(x,t)p(x)\nabla p(x)\mathrm{d}x \ge -(\epsilon\|p\|^2_{L^2(\Omega^*)} + \tfrac{1}{4\epsilon}\|\nabla p\|^2_{L^2(\Omega^*)})\|u\|_{L^\infty(\bar{\Omega}^*\times(0,T))}.$$

Furthermore,

$\int_{\Gamma^*_{\text{out}}} u(x,t)p(x)^2 \mathrm{d}\Gamma^*_{\text{out}} \geq 0$, since u is nonnegative by assumption.

Consequently,

$$\bar{a}(t,p,p) \geq (D_{\text{S}} - \tfrac{1}{4\epsilon}\|u\|_{L^\infty(\bar{\Omega}^*\times(0,T))})\|\nabla p\|^2_{L^2(\Omega^*)} - \epsilon\|u\|_{L^\infty(\bar{\Omega}^*\times(0,T))})\|p\|^2_{L^2(\Omega^*)}.$$

We choose $\epsilon > 0$ such that

$$\alpha_1 = D_{\text{S}} - \frac{1}{4\epsilon}\|u\|_{L^\infty(\bar{\Omega}^*\times(0,T))} > 0,$$

and then, we choose $\lambda > 0$ such that

$$\alpha_2 = \lambda - \epsilon\|u\|_{L^\infty(\bar{\Omega}^*\times(0,T))} > 0.$$

Therefore, choosing $\alpha = \min\{\alpha_1, \alpha_2\}$, one has that

$$|\bar{a}(t,p,p)| + \lambda\|p\|^2_{L^2(\Omega^*)} \geq \alpha\|p\|^2_{H^1(\Omega^*)}.$$

Step 3: Let us see that the function $f : (0,T) \longrightarrow (H^1(\Omega^*))'$, with $f(t) : H^1(\Omega^*) \longrightarrow \mathbb{R}$ defined by

$$v \to \int_{\Gamma^*_{\text{in}}} u(x,t)S_{\text{e}}(t)v(x)\mathrm{d}\Gamma^*_{\text{in}} + \int_{\Omega^*} c(x,t)B(x,t)v(x)\mathrm{d}x,$$

is in $L^2(0,T,H^1(\Omega^*)')$.
Firstly, we must see that $f(t)$ is linear and continuous a.e. $t \in (0,T)$. The linearity of $f(t)$ follows from the linearity of the integral. Because of this linearity, the continuity property is equivalent to the existence of $k(t) > 0$ such that $|f(t)(v)| \leq k(t)\|v\|_{H^1(\Omega^*)}$, $\forall v \in H^1(\Omega^*)$. But one has

$$\begin{aligned} |f(t)(v)| = & \ |\textstyle\int_{\Gamma^*_{\text{in}}} u(x,t)S_{\text{e}}(t)v(x)\mathrm{d}\Gamma^*_{\text{in}} + \int_{\Omega^*} c(x,t)B(x,t)v(x)\mathrm{d}x| \\ \leq & \ \|u(\cdot,t)\|_{L^\infty(\bar{\Omega}^*)}|S_{\text{e}}(t)||\Gamma^*_{\text{in}}|^{\frac{1}{2}}\|v\|_{L^2(\Gamma^*_{\text{in}})} + \|c(\cdot,t)\|_{L^\infty(\Omega^*)}\|B(\cdot,t)\|_{L^2(\Omega^*)}\|v\|_{L^2(\Omega^*)} \end{aligned}$$

a.e. $t \in (0,T)$, where $|\Gamma^*_{\text{in}}|$ is the Lebesgue measure of Γ^*_{in}. Using the Trace inequality (see (A.4)), we conclude that there exists a constant $C_{\text{T}} > 0$ such that:

$$\begin{aligned} |f(t)(v)| \leq & \ C_{\text{T}}|\Gamma^*_{\text{in}}|^{\frac{1}{2}}\|u(\cdot,t)\|_{L^\infty(\bar{\Omega}^*)}|S_{\text{e}}(t)|\|v\|_{H^1(\Omega^*)} + \|c(\cdot,t)\|_{L^\infty(\Omega^*)}\|B(\cdot,t)\|_{L^2(\Omega^*)}\|v\|_{L^2(\Omega^*)} \\ = & \ k(t)\|v\|_{H^1(\Omega^*)}, \end{aligned}$$

with $k(t) = C_{\text{T}}|\Gamma^*_{\text{in}}|^{\frac{1}{2}}\|u(\cdot,t)\|_{L^\infty(\bar{\Omega}^*)}|S_{\text{e}}(t)| + \|c(\cdot,t)\|_{L^\infty(\Omega^*)}\|B(\cdot,t)\|_{L^2(\Omega^*)}$.
Secondly, we must see that $\int_0^T \|f(t)\|^2_{(H^1(\Omega^*))'}\mathrm{d}t < \infty$. We use that

$$\|G\|_{(H^1(\Omega^*))'} = \sup_{\substack{v\in H^1(\Omega^*)\\ \|v\|\leq 1}} |< G, v >|,$$

and thus, by the hypothesis on u, S_{e}, c and B we have that

$$\begin{aligned} \textstyle\int_0^T \|f(t)\|^2_{(H^1(\Omega^*))'}\mathrm{d}t & \leq \textstyle\int_0^T \left(|\Gamma^*_{\text{in}}|^{\frac{1}{2}}C_{\text{T}}|S_{\text{e}}(t)|\|u(\cdot,t)\|_{L^\infty(\bar{\Omega}^*)} + \|c(\cdot,t)\|_{L^\infty(\Omega^*)}\|B(\cdot,t)\|_{L^2(\Omega^*)}\right)^2\mathrm{d}t \\ & \leq |\Gamma^*_{\text{in}}|C^2_{\text{T}}\|u\|^2_{L^\infty(\bar{\Omega}^*\times(0,T))}\|S_{\text{e}}\|^2_{L^2(0,T)} + \|c\|^2_{L^\infty(\Omega^*\times(0,T))}\|B\|^2_{L^2(\Omega^*\times(0,T))} \\ & \quad +2|\Gamma^*_{\text{in}}|^{\frac{1}{2}}C_{\text{T}}\|u\|_{L^\infty(\bar{\Omega}^*\times(0,T))}\|c\|_{L^\infty(\Omega^*\times(0,T))}\|S_{\text{e}}\|_{L^2(0,T)}\|B\|_{L^2(\Omega^*\times(0,T))} < \infty. \end{aligned}$$

Since we have proved that all the assumptions of Theorem A.3.7 are satisfied, the proof of Theorem 2.2.5 is finished. □

Before proving Theorem 2.2.2, we prove the following result:

Proposition 2.2.6. *If (S, B) is the weak solution of system (2.13), then*

$$\|S\|_{W(0,T,H^1(\Omega^*),(H^1(\Omega^*))')} \leq C \text{ and } \|B\|_{W(0,T,H^1(\Omega^*),(H^1(\Omega^*))')} \leq C,$$

where C depends on D_{S}, D_{B}, $\|S_0\|_{L^2(\Omega^*)}$, $\|B_0\|_{L^2(\Omega^*)}$, $\|u\|_{L^\infty(\bar{\Omega}^*\times(0,T))}$, $\|S_{\mathrm{e}}\|_{L^2(0,T)}$, $|\Gamma^*_{\mathrm{in}}|$, T, $\|c\|_{L^\infty(\Omega^*\times(0,T))}$ and C_{T} (i.e., the constant coming from the Trace inequality (see (A.4)).

Proof of Proposition 2.2.6. From the first equation in system (2.13), it follows that

$$\begin{aligned}\|\tfrac{\mathrm{d}S}{\mathrm{d}t}\|_{L^2(0,T,(H^1(\Omega^*))')} &= \sup_{\substack{\phi\in L^2(0,T,H^1(\Omega^*)),\\ \|\phi\|\leq 1}} |<\tfrac{\mathrm{d}S}{\mathrm{d}t},\phi>| \\ &= \sup_{\substack{\phi\in L^2(0,T,H^1(\Omega^*)),\\ \|\phi\|\leq 1}} |<\mathrm{div}(D_{\mathrm{S}}\nabla S - \boldsymbol{u}S) - cB,\phi>|.\end{aligned}$$

If C_{T} is the constant coming from the Trace inequality (see (A.4)), one has that

$$\begin{aligned}\|\tfrac{\mathrm{d}S}{\mathrm{d}t}\|_{L^2(0,T,(H^1(\Omega^*))')} \leq\ & C_{\mathrm{T}}\|u\|_{L^\infty(\bar{\Omega}^*\times(0,T))}\|S_{\mathrm{e}}\|_{L^2(0,T)}|\Gamma^*_{\mathrm{in}}|^{\frac{1}{2}} + \|c\|_{L^\infty(\Omega^*\times(0,T))}\|B\|_{L^2(0,T,L^2(\Omega^*))} \\ & +(D_{\mathrm{S}} + (1+C_{\mathrm{T}}^2)\|u\|_{L^\infty(\bar{\Omega}^*\times(0,T))})\|S\|_{L^2(0,T,H^1(\Omega^*))}.\end{aligned} \tag{2.17}$$

Similarly, from the second equation in system (2.13), it follows that

$$\|\tfrac{\mathrm{d}B}{\mathrm{d}t}\|_{L^2(0,T,(H^1(\Omega^*))')} \leq (D_{\mathrm{B}} + (1+C_{\mathrm{T}}^2)\|u\|_{L^\infty(\bar{\Omega}^*\times(0,T))} + \|c\|_{L^\infty(\Omega^*\times(0,T))})\|B\|_{L^2(0,T,H^1(\Omega^*))}. \tag{2.18}$$

Now, in order to obtain an estimate for $\|S\|_{L^2(0,T,H^1(\Omega^*))}$, we consider $\lambda \geq 0$ and the variable $\bar{S} = \mathrm{e}^{-\lambda t}S$, that fulfill

$$\bar{S}_t + \lambda\bar{S} - \mathrm{div}(D_{\mathrm{S}}\nabla\bar{S} - \boldsymbol{u}\bar{S}) + c\bar{B} = 0 \tag{2.19}$$

Multiplying (2.19) by $\bar{S}$ (here, this multiplication is in the sense of the duality product $<\cdot,\cdot>_{(H^1(\Omega^*))'\times H^1(\Omega^*)}$) and integrating, one obtains

$$\begin{aligned}&\tfrac{1}{2}\|\bar{S}(T)\|^2_{L^2(\Omega^*)} + \lambda\textstyle\int_0^T \|\bar{S}(\tau)\|^2_{L^2(\Omega^*)}\mathrm{d}\tau + \int_0^T\int_{\Gamma^*_{\mathrm{out}}} u(x,\tau)\bar{S}^2(x,\tau)\mathrm{d}x\mathrm{d}\tau \\ &+D_{\mathrm{S}}\textstyle\int_0^T \|\nabla\bar{S}(\tau)\|^2_{L^2(\Omega^*)}\mathrm{d}\tau = \tfrac{1}{2}\|S_0\|^2_{L^2(\Omega^*)} + \underbrace{\int_0^T \mathrm{e}^{-\lambda\tau}\int_{\Gamma^*_{\mathrm{in}}} u(x,\tau)S_{\mathrm{e}}(\tau)\bar{S}(x,\tau)\mathrm{d}x\mathrm{d}\tau}_{(*)} \\ &+\underbrace{\int_0^T\int_{\Omega^*}\boldsymbol{u}(x,\tau)\bar{S}(x,\tau)\nabla\bar{S}(x,\tau)\mathrm{d}x\mathrm{d}\tau}_{(**)} - \underbrace{\int_0^T\int_{\Omega^*} c(x,\tau)\bar{S}(x,\tau)\bar{B}(x,\tau)\mathrm{d}x\mathrm{d}\tau}_{(***)}.\end{aligned} \tag{2.20}$$

Applying Young's inequality (see (A.1)) in $(*)$, $(**)$ and $(***)$ (with $\epsilon_1 > 0$, $\epsilon_2 > 0$ and $\epsilon = \frac{1}{2}$, respectively) and the Trace inequality (see (A.4)) in $(*)$, it follows

$$\begin{aligned}&\tfrac{1}{2}\|\bar{S}(T)\|^2_{L^2(\Omega^*)} + (D_{\mathrm{S}} - \|u\|_{L^\infty(\bar{\Omega}^*\times(0,T))}(\tfrac{1}{4\epsilon_2} + \tfrac{|\Gamma^*_{\mathrm{in}}|^{\frac{1}{2}}C_{\mathrm{T}}^2}{4\epsilon_1}))\|\nabla\bar{S}(\tau)\|^2_{L^2(0,T,L^2(\Omega^*))} \\ &+(\lambda - \|u\|_{L^\infty(\bar{\Omega}^*\times(0,T))}(\epsilon_2 + \tfrac{|\Gamma^*_{\mathrm{in}}|^{\frac{1}{2}}C_{\mathrm{T}}^2}{4\epsilon_1}) - \tfrac{\|c\|_{L^\infty(\Omega^*\times(0,T))}}{2})\|\bar{S}\|^2_{L^2(0,T,L^2(\Omega^*))} \\ &\leq \tfrac{1}{2}\|S_0\|^2_{L^2(\Omega^*)} + \epsilon_1\|u\|_{L^\infty(\bar{\Omega}^*\times(0,T))}\|S_{\mathrm{e}}\|^2_{L^2(0,T)}|\Gamma^*_{\mathrm{in}}|^{\frac{1}{2}} + \tfrac{\|c\|_{L^\infty(\Omega^*\times(0,T))}\|\bar{B}\|^2_{L^2(0,T,L^2(\Omega^*))}}{2}.\end{aligned} \tag{2.21}$$

Considering the variable $\bar{B} = \mathrm{e}^{-\lambda t}B$ and using the same reasoning as the one followed above, one has that

$$\begin{aligned}\tfrac{1}{2}\|\bar{B}(T)\|^2_{L^2(\Omega^*)} + (\lambda - \epsilon_3\|u\|_{L^\infty(\bar{\Omega}^*\times(0,T))} - \|c\|_{L^\infty(\Omega^*\times(0,T))})\|\bar{B}\|^2_{L^2(0,T,L^2(\Omega^*))}\\ +(D_{\mathrm{B}} - \tfrac{\|u\|_{L^\infty(\bar{\Omega}^*\times(0,T))}}{4\epsilon_3})\|\nabla\bar{B}(\tau)\|^2_{L^2(0,T,L^2(\Omega^*))} \leq \tfrac{1}{2}\|B_0\|^2_{L^2(\Omega^*)}.\end{aligned} \tag{2.22}$$

Choosing ϵ_1, ϵ_2 and ϵ_3 such that $D_{\mathrm{S}} \geq \|u\|_{L^\infty(\bar{\Omega}^*\times(0,T))}(\frac{1}{4\epsilon_2} + \frac{|\Gamma^*_{\mathrm{in}}|^{\frac{1}{2}}C^2_{\mathrm{T}}}{4\epsilon_1})$, $\epsilon_3 \geq \frac{\|u\|_{L^\infty(\bar{\Omega}^*\times(0,T))}}{4D_{\mathrm{B}}}$ and $\lambda > \|u\|_{L^\infty(\bar{\Omega}^*\times(0,T))}\max(\epsilon_3, \epsilon_2 + \frac{C^2_{\mathrm{T}}|\Gamma^*_{\mathrm{in}}|^{\frac{1}{2}}}{4\epsilon_1}) + \|c\|_{L^\infty(\Omega^*\times(0,T))}$, it follows that

$$\begin{aligned}\|\bar{B}\|^2_{L^2(0,T,H^1(\Omega^*))} \leq\ & \alpha_1\|B_0\|^2_{L^2(\Omega^*)},\\ \|\bar{S}\|^2_{L^2(0,T,H^1(\Omega^*))} \leq\ & \alpha_2(\tfrac{1}{2}\|S_0\|^2_{L^2(\Omega^*)} + \epsilon_1\|u\|_{L^\infty(\bar{\Omega}^*\times(0,T))}\|S_{\mathrm{e}}\|^2_{L^2(0,T)}|\Gamma^*_{\mathrm{in}}|^{\frac{1}{2}})\\ & +\alpha_1\alpha_2\tfrac{\|c\|_{L^\infty(\Omega^*\times(0,T))}}{2}\|B_0\|^2_{L^2(\Omega^*)},\end{aligned} \tag{2.23}$$

where $\alpha_1, \alpha_2 > 0$ depend on $|\Gamma^*_{\mathrm{in}}|, \|c\|_{L^\infty(\Omega^*\times(0,T))}, \|u\|_{L^\infty(\bar{\Omega}^*\times(0,T))}, C_{\mathrm{T}}, D_{\mathrm{S}}$ and D_{B}.

Furthermore, it is straight forward to see that

$$\begin{aligned}\|B\|^2_{L^2(0,T,L^2(\Omega^*))} &\leq \mathrm{e}^{2\lambda T}\|\bar{B}\|^2_{L^2(0,T,L^2(\Omega^*))},\\ \|S\|^2_{L^2(0,T,H^1(\Omega^*))} &\leq \mathrm{e}^{2\lambda T}\|\bar{S}\|^2_{L^2(0,T,H^1(\Omega^*))}.\end{aligned} \tag{2.24}$$

From (2.17), (2.23) and (2.24), it follows that

$$\|S\|_{W(0,T,H^1(\Omega^*),(H^1(\Omega^*))')}, \|B\|_{W(0,T,H^1(\Omega^*),(H^1(\Omega^*))')} \leq C,$$

where C depends on $T, \|S_0\|_{L^2(\Omega^*)}, \|B_0\|_{L^2(\Omega^*)}, D_{\mathrm{S}}, D_{\mathrm{B}}, \|u\|_{L^\infty(\bar{\Omega}^*\times(0,T))}, \|S_{\mathrm{e}}\|_{L^2(0,T)}, \|c\|_{L^\infty(\Omega^*\times(0,T))}, |\Gamma^*_{\mathrm{in}}|$ and C_{T}. □

Proof of Theorem 2.2.2. In order to prove the existence of solution, we apply Schauder Fixed Point Theorem (see Theorem A.3.1). We have to choose a Banach space X and a compact and convex subset $K \subset X$. We consider the Banach Space $W(0,T,H^1(\Omega^*),(H^1(\Omega^*))')$, which is compactly embedded in $L^2(0,T,L^2(\Omega^*))$ (see Lemma A.3.8).

If $Z \in W(0,T,H^1(\Omega^*),(H^1(\Omega^*))')$ and we solve the linear system (2.13) with $c(x,t) = \mu(Z(x,t))$, Theorem 2.2.5 proves that there exists a unique weak solution $(S_{\mathrm{Z}}, B_{\mathrm{Z}})$ with $S_{\mathrm{Z}}, B_{\mathrm{Z}} \in W(0,T,H^1(\Omega^*),(H^1(\Omega^*))')$. Furthermore, Proposition 2.2.6 shows that

$$\|B_Z\|_{W(0,T,H^1(\Omega^*),(H^1(\Omega^*))')} \leq C \text{ and } \|S_Z\|_{W(0,T,H^1(\Omega^*),(H^1(0,T))')} \leq C,$$

where C depends (among others) on the norm of $\mu(Z(x,t))$. Since $\mu \in L^\infty(\mathbb{R})$ it follows that, for all $Z \in W(0,T,H^1(\Omega^*),(H^1(\Omega^*))')$, we have

$$\|B_Z\|_{W(0,T,H^1(\Omega^*),(H^1(\Omega^*))')} \leq \bar{C} \text{ and } \|S_Z\|_{W(0,T,H^1(\Omega^*),(H^1(\Omega^*))')} \leq \bar{C},$$

where $\bar{C}$ is a constant depending (among others) on $\|\mu\|_{L^\infty(\mathbb{R})}$.

If we define the set

$$K := \{z \in W(0,T,H^1(\Omega^*),(H^1(\Omega^*))') : \|z\|_{W(0,T,H^1(\Omega^*),(H^1(\Omega^*))')} \leq \bar{C}\}, \tag{2.25}$$

from Lemma A.3.8 and the definition of compact operator, K is a compact set of the Banach Space $X := L^2(0,T,L^2(\Omega^*))$.

Let us define the application $A : K \to K$ by $A(Z) = S_{\mathrm{Z}}$. We prove Theorem 2.2.2 by showing that A has a fixed point. In order to apply Schauder Fixed Point Theorem, it is enough to prove that A is continuous.

In this direction, if $\{Z_n\}_n \subset K$, $Z \in K$ are such that $\|Z_n - Z\|_X \overset{n\to\infty}{\longrightarrow} 0$, we must prove that

$$\|A(Z_n) - A(Z)\|_X = \|S_{\mathrm{Z}_n} - S_{\mathrm{Z}}\|_{L^2(0,T,L^2(\Omega^*))} \overset{n\to\infty}{\longrightarrow} 0.$$

Let $(S_{\mathrm{Z}_n}, B_{\mathrm{Z}_n})$ and $(S_{\mathrm{Z}}, B_{\mathrm{Z}})$ be the weak solutions of the linear system (2.13) when $c(x,t) = \mu(Z_n(x,t))$ and $c(x,t) = \mu(Z(x,t))$, respectively. We denote $V_n = S_{\mathrm{Z}_n} - S_{\mathrm{Z}}$ and $W_n = B_{\mathrm{Z}_n} - B_{\mathrm{Z}}$. Then (V_n, W_n) is a weak solution of:

$$\begin{cases} (V_n)_t - \operatorname{div}(D_{\mathrm{S}}\nabla V_n - \boldsymbol{u}V_n) + \mu(Z)B_{\mathrm{Z}} - \mu(Z_n)B_{\mathrm{Z}_n} = 0 & \text{in } \Omega^* \times (0,T), \\ (W_n)_t - \operatorname{div}(D_{\mathrm{B}}\nabla W_n - \boldsymbol{u}W_n) - \mu(Z)B_{\mathrm{Z}} + \mu(Z_n)B_{\mathrm{Z}_n} = 0 & \text{in } \Omega^* \times (0,T), \end{cases}$$

with the initial and boundary conditions

$$\begin{cases} V_n(x,0) = 0 & \forall x \in \Omega^*, \\ W_n(x,0) = 0 & \forall x \in \Omega^*, \\ \boldsymbol{n}\cdot(D_{\mathrm{S}}\nabla V_n - \boldsymbol{u}V_n) = 0 & \text{in } \left(\Gamma^*_{\mathrm{in}} \cup \Gamma^*_{\mathrm{wall}}\right) \times (0,T), \\ \boldsymbol{n}\cdot(D_{\mathrm{B}}\nabla W_n - \boldsymbol{u}W_n) = 0 & \text{in } \left(\Gamma^*_{\mathrm{in}} \cup \Gamma^*_{\mathrm{wall}}\right) \times (0,T), \\ \boldsymbol{n}\cdot(D_{\mathrm{S}}\nabla V_n) = 0 & \text{in } \Gamma^*_{\mathrm{out}} \times (0,T), \\ \boldsymbol{n}\cdot(D_{\mathrm{B}}\nabla W_n) = 0 & \text{in } \Gamma^*_{\mathrm{out}} \times (0,T). \end{cases}$$

Given $\lambda > 0$, then $\bar{V}_n = \mathrm{e}^{-\lambda t}V_n$ and $\bar{W}_n = \mathrm{e}^{-\lambda t}W_n$ fulfill:

$$\begin{aligned} &(\bar{V}_n)_{\mathrm{t}} + \lambda\bar{V}_n - \operatorname{div}(D_{\mathrm{S}}\nabla\bar{V}_n - \boldsymbol{u}\bar{V}_n) + \mathrm{e}^{-\lambda t}\Big(\mu(Z)B_{\mathrm{Z}} - \mu(Z_n)B_{\mathrm{Z}_n}\Big) = 0, \\ &(\bar{W}_n)_{\mathrm{t}} + \lambda\bar{W}_n - \operatorname{div}(D_{\mathrm{B}}\nabla\bar{W}_n - \boldsymbol{u}\bar{W}_n) - \mathrm{e}^{-\lambda t}\Big(\mu(Z)B_{\mathrm{Z}} - \mu(Z_n)B_{\mathrm{Z}_n}\Big) = 0. \end{aligned} \tag{2.26}$$

Multiplying the first equation of (2.26) by $\bar{V}_n$ and integrating, one obtains:

$$\begin{aligned} &\tfrac{1}{2}\|\bar{V}_n(T)\|^2_{L^2(\Omega^*)} + \lambda\int_0^T \|\bar{V}_n(\tau)\|^2_{L^2(\Omega^*)}\mathrm{d}\tau + \int_0^T\int_{\Gamma^*_{\mathrm{out}}} u(x,\tau)\bar{V}_n^2(x,\tau)\mathrm{d}x\mathrm{d}\tau \\ &+D_{\mathrm{S}}\int_0^T \|\nabla\bar{V}_n(\tau)\|^2_{L^2(\Omega^*)}\mathrm{d}\tau = \int_0^T\int_{\Omega^*} \boldsymbol{u}(x,\tau)\bar{V}_n(x,\tau)\nabla\bar{V}_n(x,\tau)\mathrm{d}x\mathrm{d}\tau \\ &+\int_0^T \mathrm{e}^{-\lambda\tau}\int_{\Omega^*}\Big(\mu(Z_n(x,\tau))B_{\mathrm{Z}_n}(x,\tau) - \mu(Z(x,\tau))B_{\mathrm{Z}}(x,\tau)\Big)\bar{V}_n(x,\tau)\mathrm{d}x\mathrm{d}\tau. \end{aligned} \tag{2.27}$$

Similarly, if we multiply the second equation in (2.26) by $\bar{W}_n$, we have

$$\begin{aligned} &\tfrac{1}{2}\|\bar{W}_n(T)\|^2_{L^2(\Omega^*)} + \lambda\int_0^T \|\bar{W}_n(\tau)\|^2_{L^2(\Omega^*)}\mathrm{d}\tau + \int_0^T\int_{\Gamma^*_{\mathrm{out}}} u(x,\tau)\bar{W}_n^2(x,\tau)\mathrm{d}x\mathrm{d}\tau \\ &+D_{\mathrm{B}}\int_0^T \|\nabla\bar{W}_n(\tau)\|^2_{L^2(\Omega^*)}\mathrm{d}\tau = \int_0^T\int_{\Omega^*} \boldsymbol{u}(x,\tau)\bar{W}_n(x,\tau)\nabla\bar{W}_n(x,\tau)\mathrm{d}x\mathrm{d}\tau \\ &+\int_0^T \mathrm{e}^{-\lambda\tau}\int_{\Omega^*}\Big(\mu(Z(x,\tau))B_{\mathrm{Z}}(x,\tau) - \mu(Z_n(x,\tau))B_{\mathrm{Z}_n}(x,\tau)\Big)\bar{W}_n(x,\tau)\mathrm{d}x\mathrm{d}\tau. \end{aligned} \tag{2.28}$$

Summing equations (2.27) and (2.28) it follows:

$$\begin{aligned}
&\tfrac{1}{2}\Big(\|\bar{V}_n(T)\|^2_{L^2(\Omega^*)} + \|\bar{W}_n(T)\|^2_{L^2(\Omega^*)}\Big) + \lambda\int_0^T (\|\bar{V}_n(\tau)\|^2_{L^2(\Omega^*)} + \|\bar{W}_n(\tau)\|^2_{L^2(\Omega^*)})\mathrm{d}\tau \\
&+ \int_0^T \int_{\Gamma^*_{\text{out}}} u(x,\tau)\big(\bar{V}_n^2(x,\tau) + \bar{W}_n^2(x,\tau)\big)\mathrm{d}x\mathrm{d}\tau \\
&+ \int_0^T (D_{\mathrm{S}}\|\nabla\bar{V}_n(\tau)\|^2_{L^2(\Omega^*)} + D_{\mathrm{B}}\|\nabla\bar{W}_n(\tau)\|^2_{L^2(\Omega^*)})\mathrm{d}\tau \qquad (2.29)\\
&= \int_0^T \int_{\Omega^*} \boldsymbol{u}(x,\tau)\Big(\bar{V}_n(x,\tau)\nabla\bar{V}_n(x,\tau) + \bar{W}_n(x,\tau)\nabla\bar{W}_n(x,\tau)\Big)\mathrm{d}x\mathrm{d}\tau \\
&+ \int_0^T \mathrm{e}^{-\lambda\tau}\int_{\Omega^*}\Big(\mu(Z(x,\tau))B_{\mathrm{Z}}(x,\tau) - \mu(Z_n(x,\tau))B_{\mathrm{Z}_n}(x,\tau)\Big)\Big(\bar{W}_n(x,\tau) - \bar{V}_n(x,\tau)\Big)\mathrm{d}x\mathrm{d}\tau
\end{aligned}$$

For the last term in (2.29) we have that

$$\begin{aligned}
&\int_0^T \mathrm{e}^{-\lambda\tau}\int_{\Omega^*}\Big(\mu(Z(x,\tau))B_{\mathrm{Z}}(x,\tau) - \mu(Z_n(x,\tau))B_{\mathrm{Z}_n}(x,\tau)\Big)\Big(\bar{W}_n(x,\tau) - \bar{V}_n(x,\tau)\Big)\mathrm{d}x\mathrm{d}\tau \\
&= \int_0^T \mathrm{e}^{-\lambda\tau}\int_{\Omega^*}\mu(Z(x,\tau))\Big(B_{\mathrm{Z}}(x,\tau) - B_{\mathrm{Z}_n}(x,\tau)\Big)\Big(\bar{W}_n(x,\tau) - \bar{V}_n(x,\tau)\Big)\mathrm{d}x\mathrm{d}\tau \\
&+ \int_0^T \mathrm{e}^{-\lambda\tau}\int_{\Omega^*} B_{\mathrm{Z}_n}(x,\tau)\Big(\mu(Z(x,\tau)) - \mu(Z_n(x,\tau))\Big)\Big(\bar{W}_n(x,\tau) - \bar{V}_n(x,\tau)\Big)\mathrm{d}x\mathrm{d}\tau \\
&\le \tfrac{3}{2}\|\mu\|_{L^\infty(\mathbb{R})}\int_0^T \|\bar{W}_n(\tau)\|^2_{L^2(\Omega^*)}\mathrm{d}\tau + \tfrac{1}{2}\|\mu\|_{L^\infty(\mathbb{R})}\int_0^T \|\bar{V}_n(\tau)\|^2_{L^2(\Omega^*)}\mathrm{d}\tau \\
&+ \int_0^T |\mu(Z(x,\tau)) - \mu(Z_n(x,\tau))||B_{\mathrm{Z}_n}(x,\tau)||\bar{W}_n(x,\tau) - \bar{V}_n(x,\tau)|\mathrm{d}x\mathrm{d}\tau.
\end{aligned}$$

Moreover, by applying Young's inequality (see (A.1)) with $\epsilon_1 > 0$, which will be chosen below, it follows

$$\begin{aligned}
&\int_0^T \int_{\Omega^*} \boldsymbol{u}(x,\tau)\bar{V}_n(x,\tau)\nabla\bar{V}_n(x,\tau)\mathrm{d}x\mathrm{d}\tau \\
&\qquad \le \|u\|_{L^\infty(\bar{\Omega}^*\times(0,T))}\int_0^T (\epsilon_1\|\bar{V}_n(\tau)\|^2_{L^2(\Omega^*)} + \tfrac{1}{4\epsilon_1}\|\nabla\bar{V}_n(\tau)\|^2_{L^2(\Omega^*)})\mathrm{d}\tau.
\end{aligned}$$

We apply the same reasoning for $\bar{W}_n$ with some positive constant $\epsilon_2 > 0$.

Coming back to (2.29) it follows that

$$\begin{aligned}
&\tfrac{1}{2}\Big(\|\bar{V}_n(T)\|^2_{L^2(\Omega^*)} + \|\bar{W}_n(T)\|^2_{L^2(\Omega^*)}\Big) + \int_0^T \int_{\Gamma^*_{\text{out}}} u(x,\tau)\big(\bar{V}_n^2(x,\tau) + \bar{W}_n^2(x,\tau)\big)\mathrm{d}x\mathrm{d}\tau \\
&+(D_{\mathrm{S}} - \tfrac{\|u\|_{L^\infty(\bar{\Omega}^*\times(0,T))}}{4\epsilon_1})\int_0^T \|\nabla\bar{V}_n(\tau)\|^2_{L^2(\Omega^*)}\mathrm{d}\tau + (D_{\mathrm{B}} - \tfrac{\|u\|_{L^\infty(\bar{\Omega}^*\times(0,T))}}{4\epsilon_2})\int_0^T \|\nabla\bar{W}_n(\tau)\|^2_{L^2(\Omega^*)})\mathrm{d}\tau \\
&+ \underbrace{\Big(\lambda - \epsilon_1\|u\|_{L^\infty(\bar{\Omega}^*\times(0,T))} - \frac{\|\mu\|_{L^\infty(\mathbb{R})}}{2}\Big)}_{:=C}\int_0^T \|\bar{V}_n(\tau)\|^2_{L^2(\Omega^*)}\mathrm{d}\tau \qquad (2.30)\\
&+(\lambda - \epsilon_2\|u\|_{L^\infty(\bar{\Omega}^*\times(0,T))} - \tfrac{3}{2}\|\mu\|_{L^\infty(\mathbb{R})})\int_0^T \|\bar{W}_n(\tau)\|^2_{L^2(\Omega^*)}\mathrm{d}\tau \\
&\le \int_0^T \int_{\Omega^*} |\mu(Z(x,\tau)) - \mu(Z_n(x,\tau))||B_{\mathrm{Z}_n}(x,\tau)||(\bar{W}_n(x,\tau) - \bar{V}_n(x,\tau))|\mathrm{d}x\mathrm{d}\tau.
\end{aligned}$$

If ϵ_1, ϵ_2 and λ are chosen such that $\epsilon_1 \ge \frac{\|u\|_{L^\infty(\bar{\Omega}^*\times(0,T))}}{4D_{\mathrm{S}}}$, $\epsilon_2 \ge \frac{\|u\|_{L^\infty(\bar{\Omega}^*\times(0,T))}}{4D_{\mathrm{B}}}$ and

$$\lambda > \|u\|_{L^\infty(\bar{\Omega}^*\times(0,T))}\max(\epsilon_1,\epsilon_2) + \frac{3}{2}\|\mu\|_{L^\infty(\mathbb{R})},$$

one has

$$\begin{aligned}&\int_0^T \|\bar{V}_n(\tau)\|^2_{L^2(\Omega^*)}\mathrm{d}\tau\\ &\quad\le 2\int_0^T\int_{\Omega^*}|\mu(Z(x,\tau))-\mu(Z_n(x,\tau))||B_{\mathrm{Z}_n}(x,\tau)||(\bar{W}_n(x,\tau)-\bar{V}_n(x,\tau))|\mathrm{d}x\mathrm{d}\tau.\end{aligned}\tag{2.31}$$

To prove that the right hand side of (2.31) converges to 0 as $n\to\infty$, we use the following steps:

1. Since $\|Z_n - Z\|_{L^2(\Omega^*\times(0,T))} \overset{n\to\infty}{\longrightarrow} 0$, using Theorem A.3.3, there exists a subsequence $\{Z_{n_k}\}_k \subset \{Z_n\}_n$ such that $Z_{n_k}\to Z$ a.e. in $\Omega^*\times(0,T)$. Then, since μ is continuous, $\mu(Z_{n_k})\to\mu(Z)$ a.e. in $\Omega^*\times(0,T)$. For simplicity, we denote $\{Z_{n_k}\}_k = \{Z_k\}_k$.

2. Since $\|\mu(Z_k)\|_{L^\infty(\mathbb{R})}\le\|\mu\|_{L^\infty(\mathbb{R})}<+\infty$, by applying Theorem A.3.2 using that $L^1(\Omega^*\times(0,T))$ is separable and $(L^1(\Omega^*\times(0,T)))' = L^\infty(\Omega^*\times(0,T))$, there exists a subsequence $\{\mu(Z_{k_j})\}_j$ weak-$*$ convergent to some $\omega\in L^\infty(\Omega^*\times(0,T))$. For simplicity, we denote $\{Z_{k_j}\}_j = \{Z_j\}_j$.

Due to steps 1 and 2, we conclude that $\{\mu(Z_j)\}_j$ is weak-$*$ convergent to $\mu(Z)$.

3. $B_{\mathrm{Z}_j}\in K$, since $(S_{\mathrm{Z}_j}, B_{\mathrm{Z}_j})$ is solution of (2.13) with $c=\mu(Z_j)$. Moreover, since $K\subset X$ is compact, there exists a subsequence $\{B_{Z_{j_i}}\}_i\subset\{B_{\mathrm{Z}_j}\}_j$ such that there exist some $B\in X$ fulfilling $\|B_{\mathrm{Z}_{j_i}} - B\|_X \overset{i\to\infty}{\longrightarrow} 0$. For simplicity, we denote $\{Z_{j_i}\}_i = \{Z_i\}_i$.

4. We define

$$\bar{K} = \{z\in W(0,T,H^1(\Omega^*),(H^1(\Omega^*))') \;:\; \|z\|_{W(0,T,H^1(\Omega^*),(H^1(\Omega^*))')}\le 4\bar{C}\},$$

where $\bar{C}$ is the constant appearing in the definition of K in (2.25). Notice that $\bar{K}$ is a compact set of X (see Lemma A.3.8). Since $W_i - V_i = B_{\mathrm{Z}_i} - S_{\mathrm{Z}_i} - B_{\mathrm{Z}} + S_{\mathrm{Z}}\in\bar{K}$, using the same reasoning as the one followed above, one obtains that there exists a subsequence $\{W_{i_r}-V_{i_r}\}_r\subset\{W_i-V_i\}_i$ and $P\in X$ such that $\|(W_{i_r}-V_{i_r})-P\|_X\overset{r\to\infty}{\longrightarrow}0$. For simplicity, we denote $\{Z_{i_r}\}_r=\{Z_r\}_r$.

By steps 3 and 4, we conclude that $B_r(W_r-V_r)\subset L^1(\Omega^*\times(0,T))$ and $\|B_r(W_r-V_r)-BP\|_{L^1(\Omega^*\times(0,T))}\overset{r\to\infty}{\longrightarrow}0$.

Furthermore, since $\{Z_r\}_r\subset\{Z_j\}_j$, it also follows that $\{\mu(Z_r)\}_r$ is weak-$*$ convergent to $\mu(Z)$. Using Theorem A.3.4, if follows that

$$\begin{aligned}&\int_0^T\int_{\Omega^*}\underbrace{|\mu(Z(x,\tau))-\mu(Z_r(x,\tau))|}_{L^\infty(\Omega^*\times(0,T))}\underbrace{|B_{\mathrm{Z}_r}(x,\tau)||(\bar{W}_r(x,\tau)-\bar{V}_r(x,\tau))|}_{L^1(\Omega^*\times(0,T))}\mathrm{d}x\mathrm{d}\tau\\ &\qquad\overset{r\to\infty}{\longrightarrow}\int_0^T\int_{\Omega^*}0\cdot B(x,\tau)\cdot P(x,\tau)\mathrm{d}x\mathrm{d}\tau.\end{aligned}\tag{2.32}$$

From (2.31), this implies that

$$\int_0^T\int_{\Omega^*}\mathrm{e}^{-2\lambda\tau}|S_{\mathrm{Z}_r}(x,\tau)-S_{\mathrm{Z}}(x,\tau)|^2\mathrm{d}x\mathrm{d}\tau\overset{r\to\infty}{\longrightarrow}0,$$

but since $\min_{\tau\in[0,T]}\mathrm{e}^{-2\lambda\tau}=\mathrm{e}^{-2\lambda T}$, one has that

$$\|S_{\mathrm{Z}_r}-S_Z\|_{L^2(\Omega^*\times(0,T))}\overset{r\to\infty}{\longrightarrow}0.$$

Finally, we prove that $\|S_{\mathrm{Z}_n}-S_Z\|_{L^2(\Omega^*\times(0,T))}\overset{n\to\infty}{\longrightarrow}0$ (convergence of the whole sequence instead of subsequence) by reduction to absurdum. Let us assume that this is not true. Then, there exists $\epsilon>0$ and a subsequence $\{S_{\mathrm{Z}_{n_l}}\}_l\subset\{S_{\mathrm{Z}_n}\}_n$ such that

$$\|S_{\mathrm{Z}_{n_l}}-S_Z\|_{L^2(\Omega^*\times(0,T))}>\epsilon,\qquad\forall l\in\mathbb{N}.\tag{2.33}$$

If we now proceed as above, we can find a subsection $\{S_{\mathrm{Z}_{n_m}}\}_m \subset \{S_{\mathrm{Z}_{n_l}}\}_l$ such that

$$\|S_{\mathrm{Z}_{n_m}} - S_Z\|_{L^2(\Omega^*\times(0,T))} \overset{m\to\infty}{\longrightarrow} 0,$$

which contradicts (2.33). □

Nonnegativity and boundedness

Theorem 2.2.7 (Nonnegativity and boundedness of B)**.** *Under assumptions of Theorem 2.2.2:*

(i) If $B_0 \geq 0$ in Ω^*, then $B \geq 0$ in $\Omega^* \times (0,T)$.

(ii) If $B_0 \in L^\infty(\Omega^*)$, then $B(x,t) \leq \|B_0\|_{L^\infty(\Omega^*)} \mathrm{e}^{\|\mu\|_{L^\infty(\mathbb{R})}t}$ a.e. $(x,t) \in \Omega^* \times (0,T)$.

Proof. We define the new variables $B^+ = \max(B,0)$ and $B^- = -\min(B,0)$, then $B = B^+ - B^-$ and the first statement of Theorem 2.2.7 can be reformulated as

$$B^-(x,0) = 0 \text{ in } \Omega^* \qquad \Rightarrow \qquad B^-(x,t) = 0 \text{ in } \Omega^* \times (0,T).$$

Multiplying the second equation of (2.8) by B^- and integrating, one obtains

$$\begin{aligned} \tfrac{1}{2}\int_0^t \tfrac{\mathrm{d}}{\mathrm{d}\tau}\|B^-(\tau)\|^2_{\mathrm{L}^2(\Omega^*)}\mathrm{d}\tau &= \int_0^t\int_{\Omega^*} \boldsymbol{u}(x,\tau)B^-(x,\tau)\nabla B^-(x,\tau)\mathrm{d}x\mathrm{d}\tau \\ &\quad - \int_0^t\int_{\Gamma^*_{\mathrm{out}}} u(x,\tau)(B^-(x,\tau))^2\mathrm{d}x\mathrm{d}\tau - \int_0^t\int_{\Omega^*} D_{\mathrm{B}}(\nabla B^-(x,\tau))^2\mathrm{d}x\mathrm{d}\tau \\ &\quad + \int_0^t\int_{\Omega^*} \mu(S(x,\tau))B^-(x,\tau)^2\mathrm{d}x\mathrm{d}\tau. \end{aligned}$$

Applying Young's inequality (see (A.1)) with $\epsilon > 0$ (that will be specified below), one has:

$$\begin{aligned} \tfrac{1}{2}\int_0^t \tfrac{\mathrm{d}}{\mathrm{d}\tau}\|B^-(\tau)\|^2_{\mathrm{L}^2(\Omega^*)}\mathrm{d}\tau \leq\ & (\epsilon\|u\|_{L^\infty(\bar\Omega^*\times(0,T))} - D_{\mathrm{B}})\int_0^t \|\nabla B^-(\tau)\|^2_{L^2(\Omega^*)}\mathrm{d}\tau \\ & + (\tfrac{\|u\|_{L^\infty(\bar\Omega^*\times(0,T))}}{4\epsilon} + \|\mu\|_{L^\infty(\mathbb{R})})\int_0^t \|B^-(\tau)\|^2_{L^2(\Omega^*)}\mathrm{d}\tau. \end{aligned}$$

Choosing ϵ such that $\epsilon\|u\|_{L^\infty(\bar\Omega^*\times(0,T))} - D_{\mathrm{B}} \leq 0$ and applying Gronwall's inequality in its integral form (see (A.2)), one has:

$$\|B^-(t)\|^2_{\mathrm{L}^2(\Omega^*)} \leq \underbrace{\|B^-(0)\|^2_{\mathrm{L}^2(\Omega^*)}}_{=0 \text{ by hypothesis}} \underbrace{\mathrm{e}^{2(\frac{\|u\|_{L^\infty(\bar\Omega^*\times(0,T))}}{4\epsilon} + \|\mu\|_{L^\infty(\mathbb{R})})t}}_{\geq 0} = 0.$$

Consequently $B^- = 0$ in $\Omega^* \times (0,T)$ and the statement (i) of the theorem is proved.

Now, we denote $U(x,t) = \|B_0\|_{L^\infty(\Omega^*)}\mathrm{e}^{\|\mu\|_{L^\infty(\mathbb{R})}t} - B(x,t)$. We want to prove that $U(x,t) \geq 0$ in $\Omega^* \times (0,T)$. It fulfills

$$\begin{cases} U_{\mathrm{t}} = \mathrm{div}(D_{\mathrm{B}}\nabla U - \boldsymbol{u}U) + \mu(S)U + \alpha\mathrm{e}^{\|\mu\|_{L^\infty(\mathbb{R})}t} & \forall x \in \Omega^*,\ t \in (0,T), \\ U(x,0) = \|B_0\|_{L^\infty(\Omega^*)} - B_0(x) & \forall x \in \Omega^*, \\ \boldsymbol{n}\cdot(D_{\mathrm{B}}\nabla U - \boldsymbol{u}U) = u\|B_0\|_{L^\infty(\Omega^*)}\mathrm{e}^{\|\mu\|_{L^\infty(\mathbb{R})}t} & \forall x \in \Gamma^*_{\mathrm{in}},\ t \in (0,T), \\ \boldsymbol{n}\cdot(D_{\mathrm{B}}\nabla U - \boldsymbol{u}U) = 0 & \forall x \in \Gamma^*_{\mathrm{wall}},\ t \in (0,T), \\ \boldsymbol{n}\cdot(D_{\mathrm{B}}\nabla U) = 0 & \forall x \in \Gamma^*_{\mathrm{out}},\ t \in (0,T), \end{cases} \tag{2.34}$$

where $\alpha = (\|\mu\|_{L^\infty(\mathbb{R})} - \mu(S))\|B_0\|_{L^\infty(\Omega^*)}$. We define the new variables $U^+ = \max(U,0)$ and $U^- = -\min(U,0)$, and proceeding as we did previously with B, it follows that

$$\|U^-(t)\|^2_{\mathrm{L}^2(\Omega^*)} \leq \|U^-(0)\|^2_{L^2(\Omega^*)} \mathrm{e}^{2(\|\mu\|_{L^\infty(\Omega^*)} + \frac{\|u\|_{L^\infty(\bar{\Omega}^*\times(0,T))}}{4\epsilon})t},$$

where ϵ is such that $\epsilon\|u\|_{L^\infty(\bar{\Omega}^*\times(0,T))} - D_{\mathrm{B}} \leq 0$. Since $U(x,0) \geq 0$, then $\|U^-(0)\|^2_{\mathrm{L}^2(\Omega^*)} = 0$ and, consequently, $U^- = 0$ in $\Omega^* \times (0,T)$ and the statement (ii) of the theorem is proved. □

Theorem 2.2.8 (Nonnegativity and boundedness of S)**.** *Under assumptions of Theorem 2.2.2 and Theorem 2.2.7-(ii), if $S_{\mathrm{e}} \geq 0$ and $S_0 \geq 0$ in Ω^*, μ is Lipschitz and $\mu(0) = 0$, then $S \geq 0$ in $\Omega^* \times (0,T)$. Furthermore, if $S_0 \in L^\infty(\Omega^*)$, $S_{\mathrm{e}} \in L^\infty(0,T)$ and $\mu(z) > 0$ for $z > 0$, then $S \leq \max(\|S_0\|_{\mathrm{L}^\infty(\Omega^*)}, \|S_{\mathrm{e}}\|_{\mathrm{L}^\infty(0,\mathrm{T})})$ in $\Omega^* \times (0,T)$.*

Proof. We define the new variables $S^+ = \max(S,0)$ and $S^- = -\min(S,0)$. Then, multiplying the first equation of (2.8) by S^- and integrating it follows

$$\begin{aligned}
&\tfrac{1}{2}\int_0^t \tfrac{\mathrm{d}}{\mathrm{d}\tau}\|S^-(\tau)\|^2_{\mathrm{L}^2(\Omega^*)}\mathrm{d}\tau = \int_0^t\int_{\Omega^*} \boldsymbol{u}(x,\tau)S^-(x,\tau)\nabla S^-(x,\tau)\mathrm{d}x\mathrm{d}\tau \\
&- \int_0^t\int_{\Omega^*} D_{\mathrm{S}}(\nabla S^-(x,\tau))^2\mathrm{d}x\mathrm{d}\tau + \int_0^t\int_{\Omega^*}\mu(S(x,\tau))B(x,\tau)S^-(x,\tau)\mathrm{d}x\mathrm{d}\tau \\
&- \int_0^t\int_{\Gamma^*_{\mathrm{in}}} u(x,\tau)S_{\mathrm{e}}(\tau)S^-(x,\tau)\mathrm{d}x\mathrm{d}\tau - \int_0^t\int_{\Gamma^*_{\mathrm{out}}} u(x,\tau)(S^-(x,\tau))^2\mathrm{d}x\mathrm{d}\tau.
\end{aligned} \tag{2.35}$$

Under the hypothesis formulated on μ, there exists a constant C_{L} such that

$$\begin{aligned}
|\int_0^t\int_{\Omega^*}\mu(S(x,\tau))B(x,\tau)S^-(x,\tau)\mathrm{d}x\mathrm{d}\tau| &\leq C_{\mathrm{L}}\int_0^t\int_{\Omega^*}|S(x,\tau)||B(x,\tau)|S^-(x,\tau)\mathrm{d}x\mathrm{d}\tau \\
&\leq C_{\mathrm{L}}\|B\|_{L^\infty(\Omega^*\times(0,T))}\int_0^t\int_{\Omega^*}(S^-(x,\tau))^2\mathrm{d}x\mathrm{d}\tau.
\end{aligned}$$

Furthermore, since S_{e}, u and S^- are nonnegative, from equation (2.35) one obtains

$$\begin{aligned}
&\tfrac{1}{2}\int_0^t \tfrac{\mathrm{d}}{\mathrm{d}\tau}\|S^-(\tau)\|^2_{\mathrm{L}^2(\Omega^*)}\mathrm{d}\tau \leq C_{\mathrm{L}}\|B\|_{L^\infty(\Omega^*\times(0,T))}\int_0^t\int_{\Omega^*}(S^-(x,\tau))^2\mathrm{d}x\mathrm{d}\tau \\
&- \int_0^t\int_{\Omega^*} D_{\mathrm{S}}(\nabla S^-(x,\tau))^2\mathrm{d}x\mathrm{d}\tau + \int_0^t\int_{\Omega^*}\boldsymbol{u}(x,\tau)S^-(x,\tau)\nabla S^-(x,\tau)\mathrm{d}x\mathrm{d}\tau.
\end{aligned} \tag{2.36}$$

Moreover, applying Young's inequality (see (A.1)) with $\epsilon > 0$ (that will be specified below), one has:

$$\begin{aligned}
\tfrac{1}{2}\int_0^t \tfrac{\mathrm{d}}{\mathrm{d}\tau}\|S^-(\tau)\|^2_{\mathrm{L}^2(\Omega^*)}\mathrm{d}\tau &\leq (\epsilon\|u\|_{L^\infty(\bar{\Omega}^*\times(0,T))} - D_{\mathrm{S}})\int_0^T\|\nabla S^-(\tau)\|^2_{L^2(\Omega^*)}\mathrm{d}\tau \\
&+ (\tfrac{\|u\|_{L^\infty(\bar{\Omega}^*\times(0,T))}}{4\epsilon} + C_{\mathrm{L}}\|B\|_{L^\infty(\Omega^*\times(0,T))})\int_0^T\|S^-(\tau)\|^2_{L^2(\Omega^*)}\mathrm{d}\tau.
\end{aligned}$$

Choosing ϵ such that $\epsilon\|u\|_{L^\infty(\bar{\Omega}^*\times(0,T))} - D_{\mathrm{S}} \leq 0$ and applying Gronwall's inequality in its integral form (see (A.2)), one has:

$$\|S^-(t)\|^2_{\mathrm{L}^2(\Omega^*)} \leq \underbrace{\|S^-(0)\|^2_{\mathrm{L}^2(\Omega^*)}}_{=0 \text{ by hypothesis}} \mathrm{e}^{2(\frac{\|u\|_{L^\infty(\bar{\Omega}^*\times(0,T))}}{4\epsilon} + C_{\mathrm{L}}\|B\|_{L^\infty(\Omega^*\times(0,T))})t} = 0.$$

Consequently $S^- = 0$ in $\Omega^* \times (0,T)$ and the first statement of the theorem is proved.

Now, we denote $\beta = \max(\|S_0\|_{L^\infty(\Omega^*)}, \|S_{\mathrm{e}}\|_{L^\infty(0,T)})$ and $U(x,t) = \beta - S(x,t)$. We want to prove that

$U(x,t) \geq 0$ in $\Omega^* \times (0,T)$. It fulfills

$$\begin{cases} U_{\rm t} = \operatorname{div}(D_{\rm S}\nabla U - \boldsymbol{u}U) + \mu(S)B & \text{in } \Omega^* \times (0,T), \\ U(x,0) = \beta - S_0(x) & \forall x \in \Omega^*, \\ \boldsymbol{n}\cdot(D_{\rm S}\nabla U - \boldsymbol{u}U) = u(\beta - S_{\rm e}) & \text{in } \Gamma^*_{\rm in} \times (0,T), \\ \boldsymbol{n}\cdot(D_{\rm S}\nabla U - \boldsymbol{u}U) = 0 & \text{in } \Gamma^*_{\rm wall} \times (0,T), \\ \boldsymbol{n}\cdot(D_{\rm S}\nabla U) = 0 & \text{in } \Gamma^*_{\rm out} \times (0,T). \end{cases} \tag{2.37}$$

We define the new variables $U^+ = \max(U,0)$ and $U^- = -\min(U,0)$, and using the same reasoning as the one followed in Theorem 2.2.7 one has

$$\|U^-(t)\|^2_{\mathrm{L}^2(\Omega^*)} \leq \|U^-(0)\|^2_{L^2(\Omega^*)} \mathrm{e}^{\frac{\|u\|_{L^\infty(\bar\Omega^*\times(0,T))}}{2\epsilon}t},$$

where ϵ is such that $\epsilon\|u\|_{L^\infty(\bar\Omega^*\times(0,T))} - D_{\rm S} \leq 0$.
Since $U(x,0) \geq 0$, then $\|U^-(0)\|^2_{\mathrm{L}^2(\Omega^*)} = 0$ and, consequently, $U^- = 0$ in $\Omega^* \times (0,T)$ and the second statement of the theorem is proved. □

Remark 2.2.9. *As in Remark 2.1.7, we assume that u, $S_{\rm e}$, B_0 and S_0 are nonnegative and essentially bounded because of their physical meaning. The assumption $\mu(0) = 0$ is due to the fact that if there is no substrate concentration, no reaction is produced; the assumption $\mu(z) > 0$ if $z > 0$ follows from the fact that if there is substrate, the reaction makes the substrate concentration decrease and the biomass concentration increase (see system (2.8)). Furthermore, the assumption of considering that function μ is essentially bounded is caused by the fact that microorganisms have a maximum specific growth rate.*

Theorem 2.2.10. *Under assumptions of Theorem 2.2.8, if $D_{\rm S} = D_{\rm B}$ then*

$$B(x,t) \in [0, \max\{\|S_{\rm e}\|_{L^\infty(0,T)}, \|S_0 + B_0\|_{L^\infty(\Omega^*)}\}] \qquad \text{a.e. } (x,t) \in \Omega^* \times (0,T).$$

Proof. We set $\beta = \max\{\|S_{\rm e}\|_{L^\infty(0,T)}, \|S_0 + B_0\|_{L^\infty(\Omega^*)}\}$ and define $M = S + B - \beta$, which fulfills

$$\begin{cases} \frac{\mathrm{d}M}{\mathrm{d}t} = \operatorname{div}(D_{\rm S}\nabla M - \boldsymbol{u}M) & \text{in } \Omega^* \times (0,T), \\ M(x,0) = S_0(x) + B_0(x) - \beta & \forall x \in \Omega^*, \\ \boldsymbol{n}\cdot(D_{\rm S}\nabla M - \boldsymbol{u}M) = u(S_{\rm e} - \beta) & \text{in } \Gamma^*_{\rm in} \times (0,T), \\ \boldsymbol{n}\cdot(D_{\rm S}\nabla M - \boldsymbol{u}M) = 0 & \text{in } \Gamma^*_{\rm wall} \times (0,T), \\ \boldsymbol{n}\cdot(D_{\rm S}\nabla M) = 0 & \text{in } \Gamma^*_{\rm out} \times (0,T). \end{cases} \tag{2.38}$$

Multiplying the first equation in (2.38) by $M^+ = \max(M,0)$ it follows that

$$\begin{aligned} \tfrac{1}{2}\textstyle\int_0^t \frac{\mathrm{d}}{\mathrm{d}\tau}\|M^+(\tau)\|^2_{L^2(\Omega^*)}\mathrm{d}\tau &= -D_{\rm S}\textstyle\int_0^t\int_{\Omega^*}(\nabla M^+(x,\tau))^2\mathrm{d}x\mathrm{d}\tau - \int_0^t\int_{\Gamma^*_{\rm out}} u(x,\tau)(M^+(x,\tau))^2\mathrm{d}x\mathrm{d}\tau \\ &+ \textstyle\int_0^t\int_{\Gamma^*_{\rm in}} u(x,\tau)(S_{\rm e}(\tau) - \beta)M^+(x,\tau)\mathrm{d}x\mathrm{d}\tau - \int_0^t\int_{\Omega^*}\boldsymbol{u}(x,\tau)M^+(x,\tau)\nabla M^+(x,\tau)\mathrm{d}x\mathrm{d}\tau. \end{aligned} \tag{2.39}$$

Moreover, taking into account that, by definition, $S_{\mathrm{e}}(\tau) \leq \beta$ for all $\tau > 0$ and applying Young's inequality (see (A.1)) with $\epsilon > 0$ (to be fixed afterward) one has

$$\begin{aligned}&\tfrac{1}{2}\int_0^t \tfrac{\mathrm{d}}{\mathrm{d}\tau}\|M^+(\tau)\|^2_{L^2(\Omega^*)}\mathrm{d}\tau + (D_{\mathrm{S}} - \epsilon\|u\|_{L^\infty(\bar{\Omega}^*\times(0,T))})\int_0^t \|\nabla M^+(\tau)\|^2_{L^2(\Omega^*)}\\ &\qquad \leq \tfrac{\|u\|_{L^\infty(\bar{\Omega}^*\times(0,T))}}{4\epsilon}\int_0^t \|M^+(\tau)\|^2_{L^2(\Omega^*)}\mathrm{d}\tau.\end{aligned}$$

Taking $\epsilon < \frac{D_{\mathrm{S}}}{\|u\|_{L^\infty(\bar{\Omega}^*\times(0,T))}}$ and applying Gronwall's inequality in its integral form (see (A.2)) one concludes that

$$\|M^+(t)\|^2_{L^2(\Omega^*)} \leq \|M^+(0)\|^2_{L^2(\Omega^*)}\mathrm{e}^{\frac{\|u\|_{L^\infty(\bar{\Omega}^*\times(0,T))}}{4\epsilon}t}.$$

By definition $M(x,0) \leq 0$ and thus $M^+(0) = 0$. Consequently, one has that $M^+ = 0$ and so

$$S(x,t) + B(x,t) \leq \max\{\|S_{\mathrm{e}}\|_{L^\infty(0,T)}, \|S_0 + B_0\|_{L^\infty(\Omega^*)}\}.$$

Since $S(x,t)$ and $B(x,t)$ are positive functions (see Theorems 2.2.7 and 2.2.8), this implies that

$$B(x,t) \leq \max\{\|S_{\mathrm{e}}\|_{L^\infty(0,T)}, \|S_0 + B_0\|_{L^\infty(\Omega^*)}\} \text{ for all } (x,t) \in \Omega^* \times (0,T),$$

and so the proof of the theorem is completed. □

Uniqueness

Theorem 2.2.11 (Uniqueness of solution)**.** *Under the hypothesis of Theorem 2.2.7 and if μ is Lipschitz, then system (2.8) has a unique weak solution (S,B).*

Proof. Let us assume that (S_1,B_1) and (S_2,B_2) are two different weak solutions of system (2.8). We denote $V = S_1 - S_2$, $W = B_1 - B_2$ and $\bar{V} = \mathrm{e}^{-\lambda t}V$, $\bar{W} = \mathrm{e}^{-\lambda t}W$, where $\lambda > 0$ will be chosen later. Proceeding as in previous theorems, we can obtain the following energy estimate:

$$\begin{aligned}&\tfrac{1}{2}\|\bar{V}(T)\|^2_{L^2(\Omega^*)} + \lambda\int_0^T \|\bar{V}(\tau)\|^2_{L^2(\Omega^*)}\mathrm{d}\tau + \int_0^T\int_{\Gamma^*_{\mathrm{out}}} u(x,\tau)\bar{V}(x,\tau)^2\mathrm{d}x\mathrm{d}\tau\\ &+D_{\mathrm{S}}\int_0^T \|\nabla\bar{V}(\tau)\|^2_{L^2(\Omega^*)}\mathrm{d}\tau = \int_0^T\int_{\Omega^*}\boldsymbol{u}(x,\tau)\bar{V}(x,\tau)\nabla\bar{V}(x,\tau)\mathrm{d}x\mathrm{d}\tau\\ &+\underbrace{\int_0^T \mathrm{e}^{-\lambda\tau}\int_{\Omega^*}\Big(\mu(S_2(x,\tau))B_2(x,\tau) - \mu(S_1(x,\tau))B_1(x,\tau)\Big)\bar{V}(x,\tau)\mathrm{d}x\mathrm{d}\tau}_{(I)}.\end{aligned} \tag{2.40}$$

Now,

$$\begin{aligned}(I) = &\int_0^T \mathrm{e}^{-\lambda\tau}\int_{\Omega^*}\mu(S_1(x,\tau))\Big(B_2(x,\tau) - B_1(x,\tau)\Big)\bar{V}(x,\tau)\mathrm{d}x\mathrm{d}\tau\\ &+\int_0^T \mathrm{e}^{-\lambda\tau}\int_{\Omega^*}\Big(\mu(S_2(x,\tau)) - \mu(S_1(x,\tau))\Big)B_2(x,\tau)\bar{V}(x,\tau)\mathrm{d}x\mathrm{d}\tau.\end{aligned}$$

Moreover, since $B_2 \in L^\infty(\Omega^*\times(0,T))$ (see Theorem 2.2.7), and using the fact that μ is Lipschitz, there exists a constant $C_{\mathrm{L}} > 0$ such that

$$\begin{aligned}(I) &\leq \|\mu\|_{L^\infty(\mathbb{R})}\int_0^T\int_{\Omega^*}|\bar{V}(x,\tau)||\bar{W}(x,\tau)|\mathrm{d}x\mathrm{d}\tau\\ &+C_{\mathrm{L}}\int_0^T \mathrm{e}^{-\lambda\tau}\int_{\Omega^*}|S_2(x,\tau) - S_1(x,\tau)||B_2(x,\tau)||\bar{V}(x,\tau)|\mathrm{d}x\mathrm{d}\tau\\ &\leq \tfrac{\|\mu\|_{L^\infty(\mathbb{R})}}{2}\int_0^T(\|\bar{V}(\tau)\|^2_{L^2(\Omega^*)} + \|\bar{W}(\tau)\|^2_{L^2(\Omega^*)})\mathrm{d}\tau + C_{\mathrm{L}}\|B_2\|_{L^\infty(\Omega^*\times(0,T))}\int_0^T \|\bar{V}(\tau)\|^2_{L^2(\Omega^*)}\mathrm{d}\tau\\ &= \tfrac{\|\mu\|_{L^\infty(\mathbb{R})}}{2}\int_0^T \|\bar{W}(\tau)\|^2_{L^2(\Omega^*)}\mathrm{d}\tau + (\tfrac{\|\mu\|_{L^\infty(\mathbb{R})}}{2} + C_{\mathrm{L}}\|B_2\|_{L^\infty(\Omega^*\times(0,T))})\int_0^T \|\bar{V}(\tau)\|^2_{L^2(\Omega^*)}\mathrm{d}\tau.\end{aligned}$$

Coming back to (2.40) and applying Young's inequality (see (A.1)) with $\epsilon_1 > 0$ (that will be chosen later), one has:

$$\begin{aligned}
&\tfrac{1}{2}\|\bar{V}(T)\|^2_{L^2(\Omega^*)} + \Big(\lambda - \epsilon_1\|u\|_{L^\infty(\bar{\Omega}^*\times(0,T))} - \tfrac{\|\mu\|_{L^\infty(\mathbb{R})}}{2} - C_{\mathrm{L}}\|B_2\|_{L^\infty(\Omega^*\times(0,T))}\Big)\int_0^T \|\bar{V}(\tau)\|^2_{L^2(\Omega^*)}\mathrm{d}\tau \\
&+ \int_0^T\int_{\Gamma^*_{\mathrm{out}}} u(x,\tau)\bar{V}(x,\tau)^2\mathrm{d}x\mathrm{d}\tau + \Big(D_{\mathrm{S}} - \tfrac{\|u\|_{L^\infty(\bar{\Omega}^*\times(0,T))}}{4\epsilon_1}\Big)\int_0^T \|\nabla\bar{V}(\tau)\|^2_{L^2(\Omega^*)}\mathrm{d}\tau \qquad (2.41)\\
&\leq \tfrac{\|\mu\|_{L^\infty(\mathbb{R})}}{2}\int_0^T \|\bar{W}(\tau)\|^2_{L^2(\Omega^*)}\mathrm{d}\tau.
\end{aligned}$$

Proceeding analogously, we obtain the following energy estimate

$$\begin{aligned}
&\tfrac{1}{2}\|\bar{W}(T)\|^2_{L^2(\Omega^*)} + \lambda\int_0^T \|\bar{W}(\tau)\|^2_{L^2(\Omega^*)}\mathrm{d}\tau + \int_0^T\int_{\Gamma^*_{\mathrm{out}}} u(x,\tau)\bar{W}(x,\tau)^2\mathrm{d}x\mathrm{d}\tau \\
&+D_{\mathrm{B}}\int_0^T \|\nabla\bar{W}(\tau)\|^2_{L^2(\Omega^*)}\mathrm{d}\tau = \int_0^T\int_{\Omega^*} \boldsymbol{u}(x,\tau)\bar{W}(x,\tau)\nabla\bar{W}(x,\tau)\mathrm{d}x\mathrm{d}\tau \\
&+ \underbrace{\int_0^T \mathrm{e}^{-\lambda\tau}\int_{\Omega^*}(\mu(S_1(x,\tau))B_1(x,\tau) - \mu(S_2(x,\tau))B_2(x,\tau))\bar{W}(x,\tau)\mathrm{d}x\mathrm{d}\tau}_{(II)}.
\end{aligned} \qquad (2.42)$$

Now,

$$(II) = \int_0^T\int_{\Omega^*}\mu(S_1(x,\tau))\bar{W}(x,\tau)^2\mathrm{d}x\mathrm{d}\tau + \int_0^T \mathrm{e}^{-\lambda\tau}\int_{\Omega^*}\Big(\mu(S_1(x,\tau)) - \mu(S_2(x,\tau))\Big)B_2(x,\tau)\bar{W}(x,\tau)\mathrm{d}x\mathrm{d}\tau.$$

Since μ is Lipschitz and $B_2 \in L^\infty(\Omega^*\times(0,T))$ (see Theorem 2.2.7) one has

$$(II) \leq \|\mu\|_{L^\infty(\mathbb{R})}\int_0^T \|\bar{W}(\tau)\|^2_{L^2(\Omega^*)}\mathrm{d}\tau + C_{\mathrm{L}}\|B_2\|_{L^\infty(\Omega^*\times(0,T))}\int_0^T\int_{\Omega^*}|\bar{W}(x,\tau)\bar{V}(x,\tau)|\mathrm{d}x\mathrm{d}\tau.$$

Applying Young's inequality (see (A.1)) with $\epsilon = \frac{1}{2}$, one obtains

$$(II) \leq \|\mu\|_{L^\infty(\mathbb{R})}\int_0^T \|\bar{W}(\tau)\|^2_{L^2(\Omega^*)}\mathrm{d}\tau + C_{\mathrm{L}}\|B_2(\tau)\|_{L^\infty(\Omega^*\times(0,T))}\int_0^T(\tfrac{\|\bar{W}(\tau)\|^2_{L^2(\Omega^*)}}{2} + \tfrac{\|\bar{V}(\tau)\|^2_{L^2(\Omega^*)}}{2})\mathrm{d}\tau.$$

Coming back to equation (2.42), it follows that

$$\begin{aligned}
&\tfrac{1}{2}\|\bar{W}(T)\|^2_{L^2(\Omega^*)} + \int_0^T\int_{\Gamma^*_{\mathrm{out}}} u(x,\tau)\bar{W}(x,\tau)^2\mathrm{d}x\mathrm{d}\tau + \Big(D_{\mathrm{B}} - \tfrac{\|u\|_{L^\infty(\bar{\Omega}^*\times(0,T))}}{4\epsilon_2}\Big)\int_0^T \|\nabla\bar{W}(\tau)\|^2_{L^2(\Omega^*)}\mathrm{d}\tau \\
&+\Big(\lambda - \epsilon_2\|u\|_{L^\infty(\bar{\Omega}^*\times(0,T))} - \|\mu\|_{L^\infty(\mathbb{R})} - \tfrac{C_{\mathrm{L}}\|B_2\|_{L^\infty(\Omega^*\times(0,T))}}{2}\Big)\int_0^T \|\bar{W}(\tau)\|^2_{L^2(\Omega^*)}\mathrm{d}\tau \qquad (2.43)\\
&\leq \tfrac{C_{\mathrm{L}}\|B_2\|_{L^\infty(\Omega^*\times(0,T))}}{2}\int_0^T \|\bar{V}(\tau)\|^2_{L^2(\Omega^*)}\mathrm{d}\tau.
\end{aligned}$$

Finally, adding equations (2.41) and (2.43), we obtain

$$\begin{aligned}
&\tfrac{1}{2}(\|\bar{V}(t)\|^2_{L^2(\Omega^*)} + \|\bar{W}(t)\|^2_{L^2(\Omega^*)}) \\
&+(\lambda - \epsilon_1\|u\|_{L^\infty(\bar{\Omega}^*\times(0,T))} - \tfrac{\|\mu\|_{L^\infty(\mathbb{R})}}{2} - \tfrac{3C_{\mathrm{L}}\|B_2\|_{L^\infty(\Omega^*\times(0,T))}}{2})\int_0^T \|\bar{V}(\tau)\|^2_{L^2(\Omega^*)}\mathrm{d}\tau \\
&+(\lambda - \epsilon_2\|u\|_{L^\infty(\bar{\Omega}^*\times(0,T))} - \tfrac{3}{2}\|\mu\|_{L^\infty(\mathbb{R})} - \tfrac{C_{\mathrm{L}}\|B_2\|_{L^\infty(\Omega^*\times(0,T))}}{2})\int_0^T \|\bar{W}(\tau)\|^2_{L^2(\Omega^*)}\mathrm{d}\tau \qquad (2.44)\\
&+(D_{\mathrm{B}} - \tfrac{\|u\|_{L^\infty(\bar{\Omega}^*\times(0,T))}}{4\epsilon_2})\int_0^T \|\nabla\bar{W}(\tau)\|^2_{L^2(\Omega^*)}\mathrm{d}\tau \\
&+(D_{\mathrm{S}} - \tfrac{\|u\|_{L^\infty(\bar{\Omega}^*\times(0,T))}}{4\epsilon_1})\int_0^T \|\nabla\bar{V}(\tau)\|^2_{L^2(\Omega^*)}\mathrm{d}\tau \leq 0.
\end{aligned}$$

Choosing $\epsilon_1 > \frac{\|u\|_{L^\infty(\bar\Omega^*\times(0,T))}}{4D_{\rm S}}$, $\epsilon_2 > \frac{\|u\|_{L^\infty(\bar\Omega^*\times(0,T))}}{4D_{\rm B}}$ and

$$\lambda > \frac{3C_{\rm L}\|B_2\|_{L^\infty(\Omega^*\times(0,T))}}{2} + \max\{\epsilon_1,\epsilon_2\}\|u\|_{L^\infty(\bar\Omega^*\times(0,T))} + \frac{3}{2}\|\mu\|_{L^\infty(\mathbb{R})},$$

it follows that $\|\bar W\|_{L^2(0,T,H^1(\Omega^*))} + \|\bar V\|_{L^2(0,T,H^1(\Omega^*))} = 0$, which implies that $\bar W = \bar V = 0$ in $\Omega^*\times(0,T)$. Consequently $S_1 = S_2$ and $B_1 = B_2$ in $\Omega^*\times(0,T)$ and we have proved the statement of Theorem 2.2.11. □

2.2.3 Nondimensional analysis

System (2.11) is non-dimensionalized by setting:

$$\hat B = \frac{B}{b},\quad \hat S = \frac{S}{s},\quad \hat t = \frac{t}{\tau},\quad \hat u = \frac{u}{\gamma},\quad \hat S_{\rm e} = \frac{S_{\rm e}}{e},\quad \hat\mu(\hat S) = \frac{\mu(s\hat S)}{\nu},\quad \hat z = \frac{z}{Z} \text{ and } \hat r = \frac{r}{R},$$

where b, s, τ, γ, e, ν, Z and R are suitable scales. Thus, for $0 \le \hat t \le \hat T = \frac{T}{\tau}$ and $(\hat r,\hat z) \in \hat\Omega$ (the nondimensional domain obtained from Ω with the change of variables $(\hat r,\hat z) = (\frac{r}{R},\frac{z}{Z})$) the first and second equations in system (2.11) become

$$\frac{\partial \hat S}{\partial \hat t} = \frac{\tau D_{\rm S}}{R^2\hat r}\frac{\partial}{\partial \hat r}(\hat r\frac{\partial \hat S}{\partial \hat r}) + \frac{\tau D_{\rm S}}{Z^2}\frac{\partial^2 \hat S}{\partial \hat z^2} + \frac{\gamma\tau}{Z}\hat u\frac{\partial \hat S}{\partial \hat z} - \frac{b\tau\nu}{s}\hat\mu(\hat S)\hat B \tag{2.45}$$

and

$$\frac{\partial \hat B}{\partial \hat t} = \frac{\tau D_{\rm B}}{R^2\hat r}\frac{\partial}{\partial \hat r}(\hat r\frac{\partial \hat B}{\partial \hat r}) + \frac{\tau D_{\rm B}}{Z^2}\frac{\partial^2 \hat B}{\partial \hat z^2} + \frac{\gamma\tau}{Z}\hat u\frac{\partial \hat B}{\partial \hat z} + \tau\nu\hat\mu(\hat S)\hat B. \tag{2.46}$$

The dimensionless groups of parameters in equations (2.45) and (2.46) are

$$\alpha_1 = \frac{\tau D_{\rm S}}{R^2},\quad \alpha_2 = \frac{\tau D_{\rm S}}{Z^2},\quad \alpha_3 = \frac{\tau D_{\rm B}}{R^2},\quad \alpha_4 = \frac{\tau D_{\rm B}}{Z^2},\quad \alpha_5 = \frac{\tau\gamma}{Z},\quad \alpha_6 = \tau\nu \text{ and } \alpha_7 = \frac{\tau\nu b}{s}.$$

The radius and the height scales proposed here come from the dimensions of the bioreactor, giving $R = L$ and $Z = H$. We set $\nu = \|\mu\|_{L^\infty(\mathbb{R})}$ and $\gamma = \|u\|_{L^\infty(\bar\Omega\times(0,T))}$ for the reaction and velocity scales, respectively. Finally, for the entering substrate scale we set $e = \|S_{\rm e}\|_{L^\infty(0,T)}$ and, for the sake of simplicity, we choose $s = b = \|S_{\rm e}\|_{L^\infty(0,T)}$. The time scale τ is chosen from equations (2.45) and (2.46) depending on the process (diffusion, advection or reaction) we want to focus on. In particular, we can choose

$$\tau \in \{\frac{L^2}{D_{\rm S}},\frac{L^2}{D_{\rm B}},\frac{H^2}{D_{\rm S}},\frac{H^2}{D_{\rm B}},\frac{H}{\|u\|_{L^\infty(\bar\Omega\times(0,T))}},\frac{1}{\|\mu\|_{L^\infty(\mathbb{R})}}\},$$

where $\tau = \frac{L^2}{D_{\rm S}}$ (resp., $\tau = \frac{H^2}{D_{\rm S}}$) corresponds to the case focusing on the substrate diffusion rate on the horizontal (resp., vertical) axis; $\tau = \frac{L^2}{D_{\rm B}}$ (resp., $\tau = \frac{H^2}{D_{\rm B}}$) focuses on the biomass diffusion rate on the horizontal (resp., vertical) axis; $\tau = \frac{H}{\|u\|_{L^\infty(\bar\Omega\times(0,T))}}$ focuses on the advection transport rate; and $\tau = \frac{1}{\|\mu\|_{L^\infty(\mathbb{R})}}$ focuses on the reaction rate.

Since in this section we perform a comparison with system (2.6), we center our study on the reaction process and take $\tau = \frac{1}{\|\mu\|_{L^\infty(\mathbb{R})}}$. Two well-known dimensionless numbers (see [**?**]) appear now in the non-dimensional form of system (2.11):

- Damkhöler Number: $\mathrm{Da} = \frac{\text{reaction rate}}{\text{advective transport rate}} = \frac{\tau_{\rm a}}{\tau_{\rm r}}$,
- Thiele Modulus: $\mathrm{Th} = \frac{\text{reaction rate}}{\text{diffusive transport rate}} = \frac{\tau_{\rm d}}{\tau_{\rm r}}$,

where $\tau_{\rm d}$, $\tau_{\rm a}$ and $\tau_{\rm r}$ are diffusion, advection and reaction times scales, respectively. For ease of notation, we drop the $\hat{}$ symbol, and so B, S, t, u, $S_{\rm e}$, μ, z, r and T denote now the non-dimensional variables. Particularly, if $S_{\rm e}$ and u are constants, system (2.11) in its non-dimensional form is given by

$$\begin{cases} \frac{\partial S}{\partial t} = \sigma^2 (\mathrm{Th_S})^{-1} \frac{1}{r} \frac{\partial}{\partial r}(r \frac{\partial S}{\partial r}) + (\mathrm{Th_S})^{-1} \frac{\partial^2 S}{\partial z^2} + (\mathrm{Da})^{-1} \frac{\partial S}{\partial z} - \mu(S) B & \text{in } \Omega \times (0,T), \\ \frac{\partial B}{\partial t} = \sigma^2 (\mathrm{Th_B})^{-1} \frac{1}{r} \frac{\partial}{\partial r}(r \frac{\partial B}{\partial r}) + (\mathrm{Th_B})^{-1} \frac{\partial^2 B}{\partial z^2} + (\mathrm{Da})^{-1} \frac{\partial B}{\partial z} + \mu(S) B & \text{in } \Omega \times (0,T), \\ (\mathrm{Th_S})^{-1} \frac{\partial S}{\partial z} + (\mathrm{Da})^{-1} S = (\mathrm{Da})^{-1} & \text{in } \Gamma_{\rm in} \times (0,T), \\ (\mathrm{Th_B})^{-1} \frac{\partial B}{\partial z} + (\mathrm{Da})^{-1} B = 0 & \text{in } \Gamma_{\rm in} \times (0,T), \\ \frac{\partial S}{\partial r} = 0 & \text{in } \left(\Gamma_{\rm wall} \cup \Gamma_{\rm sym}\right) \times (0,T), \\ \frac{\partial B}{\partial r} = 0 & \text{in } \left(\Gamma_{\rm wall} \cup \Gamma_{\rm sym}\right) \times (0,T), \\ \frac{\partial S}{\partial z} = 0 & \text{in } \Gamma_{\rm out} \times (0,T), \\ \frac{\partial B}{\partial z} = 0 & \text{in } \Gamma_{\rm out} \times (0,T), \end{cases} \tag{2.47}$$

completed by the following initial conditions

$$S(r,z,0) = S_{\rm init} \quad \text{and} \quad B(r,z,0) = B_{\rm init} \qquad \forall (r,z) \in \Omega, \tag{2.48}$$

where $\Omega = (0,1) \times (0,1)$ is the nondimensional domain, $\Gamma_{\rm in} = (0,1) \times \{1\}$, $\Gamma_{\rm out} = (0,1) \times \{0\}$, $\Gamma_{\rm wall} = \{1\} \times (0,1)$ and $\Gamma_{\rm sym} = \{0\} \times (0,1)$ are the non-dimensional boundary edges. The final dimensionless parameters are

$$\mathrm{Da} = \frac{H \|\mu\|_{L^\infty(\mathbb{R})}}{u}, \ \mathrm{Th_S} = \frac{H^2 \|\mu\|_{L^\infty(\mathbb{R})}}{D_{\rm S}}, \ \mathrm{Th_B} = \frac{D_{\rm S}}{D_{\rm B}}(\mathrm{Th_S}) \text{ and } \sigma = \frac{H}{L},$$

and the dimensionless initial conditions are $S_{\rm init}(r,z) = \dfrac{S_0(r,z)}{S_{\rm e}}$ and $B_{\rm init}(r,z) = \dfrac{B_0(r,z)}{S_{\rm e}}$ $\forall (r,z) \in \Omega$.

Remark 2.2.12. *Since the bioreactor into consideration is a cylinder of height H and radius L, the reactor volume is $\pi H L^2$ and the volumetric flow rate in system* (2.1) *can be written as $Q = \pi L^2 u$, where u (m/s) is the vertical inflow. Thus, the nondimensional dilution rate D in system* (2.6) *corresponds to the nondimensional flow rate $\frac{1}{\mathrm{Da}}$ in system* (2.47)*.*

2.2.4 Asymptotic behavior

In this section, we study the asymptotic behavior of system (2.47)-(2.48). Firstly, we study the particular case for which diffusion terms in system (2.47) are neglected. Then, we perform the stability analysis of system (2.47) for the general case.

The asymptotic stability of an equilibrium solution of system (2.47) is defined as follows (see Definition A.3.10).

Definition 2.2.13 (Asymptotically Stable Equilibrium)**.** *An equilibrium solution (S^*, B^*) of system* (2.47) *is said to be asymptotically stable if there exists $\delta > 0$ such that*

$$\text{if } \|(S_{\rm init}, B_{\rm init}) - (S^*, B^*)\|_{(L^2(\Omega))^2} < \delta, \text{ then } \lim_{t \to \infty} \|(S(t), B(t)) - (S^*, B^*))\|_{(L^2(\Omega))^2} = 0, \tag{2.49}$$

where (S, B) is the solution of system (2.47)-(2.48)*.*

Case $\frac{1}{\mathrm{Th_S}}, \frac{1}{\mathrm{Th_B}}, \frac{\sigma^2}{\mathrm{Th_S}}, \frac{\sigma^2}{\mathrm{Th_B}} \ll 1$

We consider the particular case where the nondimensional diffusion coefficients are negligible with respect to the advection and reaction coefficients in system (2.47). For each fixed value of $r \in (0,1)$, the solution $S(r,\cdot)$, $B(r,\cdot)$ can be approximated by the solution of the following 1-dimensional Advection-Reaction system:

$$\begin{cases} \frac{\partial S}{\partial t} = (\mathrm{Da})^{-1}\frac{\partial S}{\partial z} - \mu(S)B, & \text{in } (0,1)\times(0,T), \\ \frac{\partial B}{\partial t} = (\mathrm{Da})^{-1}\frac{\partial B}{\partial z} + \mu(S)B & \text{in } (0,1)\times(0,T), \\ S(r,1,t) = 1 & \forall t \in (0,T), \\ B(r,1,t) = 0 & \forall t \in (0,T), \\ S(r,z,0) = S_{\mathrm{init}}(r,z) & \forall z \in (0,1), \\ B(r,z,0) = B_{\mathrm{init}}(r,z) & \forall z \in (0,1). \end{cases} \tag{2.50}$$

Let us prove that $(1,0)$ (which is called the *washout* state), is an asymptotically stable equilibrium. The following theorem shows, in fact, a property for $(1,0)$ stronger than asymptotic stability.

Theorem 2.2.14. *For any arbitrary initial condition $(S_{\mathrm{init}}, B_{\mathrm{init}}) \in (L^\infty(\Omega))^2$, the solution of* (2.50) *satisfies that $S(r,z,t)= 1$ and $B(r,z,t) = 0$, for all $(r,z) \in \Omega$ and $t \geq \mathrm{Da}$.*

Proof. For any fixed value of $r \in (0,1)$, we apply the Euler-Lagrange transformation from (r,z,t) to $(r,\tilde{z}(t,z),t)$, where $\tilde{z}(t,z) = z - \frac{1}{\mathrm{Da}}t$, so that for every fixed value of $(r,z) \in \Omega$, the second equation of system (2.50) is rewritten as

$$\frac{\mathrm{d}B}{\mathrm{d}t}(r,\tilde{z}(t,z),t) = \frac{\partial B}{\partial t}(r,\tilde{z}(t,z),t) - \frac{1}{\mathrm{Da}}\frac{\partial B}{\partial \tilde{z}}(r,\tilde{z}(t,z),t) = \mu(S(r,\tilde{z}(t,z),t))B(r,\tilde{z}(t,z),t).$$

Thus, for any $(r,z) \in \Omega$, one has that

$$B(r,\tilde{z}(t,z),t) = B(r,\tilde{z}(0,z),0) + \int_0^t \mu(S(r,\tilde{z}(\tau,z),\tau))B(\tilde{z}(\tau,z),\tau)\mathrm{d}\tau.$$

Particularly, for $z = 1$, we obtain

$$B(r,\tilde{z}(t,1),t) = \int_0^t \mu(S(r,\tilde{z}(\tau,1),\tau))B(r,\tilde{z}(\tau,1),\tau)\mathrm{d}\tau$$

and, by applying the Gronwall's inequality, we have that $B(r,\tilde{z}(t,1),t) = 0$ for all $t > 0$.

Using the same reasoning for the first equation of system (2.50), it follows that for $z = 1$

$$S(r,\tilde{z}(t,1),t) = 1 + \int_0^t \mu(S(r,\tilde{z}(\tau,1),\tau))B(r,\tilde{z}(\tau,1),\tau)\mathrm{d}\tau.$$

Since $B(r,\tilde{z}(t,1),t) = 0$ for all $t > 0$, we deduce that $S(r,\tilde{z}(t,1),t) = 1$ for all $t > 0$.
Coming back to Eulerian coordinates, one has that

$$B(r,1-\frac{1}{\mathrm{Da}}t,t) = 0 \text{ and } S(r,1-\frac{1}{\mathrm{Da}}t,t) = 1 \text{ for all } t > 0.$$

Consequently, if $t \geq \mathrm{Da}$, $B(r,z,t) = 0$ and $S(r,z,t) = 1$ for all $(r,z) \in \Omega$. □

General Case

In order to obtain a parallelism with the asymptotic analysis of system (2.6), shown in Section 2.1.4, we assume that μ fulfills properties (H1) or (H2). In both cases, the constant (washout) solution $(S_1^*, B_1^*) = (1, 0)$ is a steady state of system (2.47). By analogy with system (2.6), we conjecture, supported by numerical experiments, that system (2.47) has, under suitable conditions, another asymptotically stable steady state (different from the washout) denoted by (S_2^*, B_2^*). First, we use the method of linearization to give a sufficient condition for the asymptotic stability of the washout equilibrium. Then, we use this result to infer a sufficient condition for the asymptotic stability of the other equilibrium solution.

Remark 2.2.15. *We did not find any work studying the multiplicity of steady state solutions of a two dimensional coupled system of advection-diffusion-reaction equations together with boundary conditions of mixed type in a domain with Lipschitz boundary, comparable to (2.47). Similar problems, but with other hypothesis, have been tackled for instance in [**?**, **?**, **?**].*

We first define the following functions, which will be used throughout the rest of this section.

Definition 2.2.16.

- *In terms of the dimensionless variables appearing in system* (2.47)*, we define* $\beta_1(\mathrm{Da}, \mathrm{Th_B})$ *as the smallest positive solution of the transcendental equation* $\tan(\beta) = \dfrac{\mathrm{Th_B}\beta}{\mathrm{Da}\left(\beta^2 - \left(\frac{\mathrm{Th_B}}{2\mathrm{Da}}\right)^2\right)}$ *if* $\mathrm{Th_B} \neq \pi\mathrm{Da}$*. If* $\mathrm{Th_B} = \pi\mathrm{Da}$*, we define* $\beta_1(\mathrm{Da}, \mathrm{Th_B}) = \pi/2$*.*
- *In terms of the variables with dimensions appearing in system* (2.11)*, we define* $\tilde{\beta}_1(H, u, D_\mathrm{B})$ *as the smallest positive solution of the transcendental equation* $\tan(\beta) = \dfrac{Hu\beta}{D_\mathrm{B}\left(\beta^2 - \left(\frac{Hu}{2D_\mathrm{B}}\right)^2\right)}$ *if* $Hu \neq \pi D_\mathrm{B}$*. If* $Hu = \pi D_\mathrm{B}$ *we define* $\tilde{\beta}_1(H, u, D_\mathrm{B}) = \pi/2$*.*

Theorem 2.2.17. *A sufficient condition for* $(S_1^*, B_1^*) = (1, 0)$ *to be an asymptotically stable steady state of system* (2.47) *is that*

$$\mu(1) < \frac{\mathrm{Th_B}}{(2\mathrm{Da})^2} + \frac{(\beta_1(\mathrm{Da}, \mathrm{Th_B}))^2}{\mathrm{Th_B}}. \tag{2.51}$$

Remark 2.2.18. *In terms of the variables with dimensions appearing in system* (2.11)*, the steady state is* $(S_\mathrm{e}, 0)$ *and inequality* (2.51) *is reformulated as*

$$\mu(S_\mathrm{e}) < \frac{u^2}{4D_\mathrm{B}} + \frac{D_\mathrm{B}}{H^2}(\tilde{\beta}_1(H, u, D_\mathrm{B}))^2.$$

Proof of Theorem 2.2.17. In order to check the stability of the equilibrium solution $(S_1^*, B_1^*) = (1, 0)$ we choose initial conditions close to it given by $S(r, z, 0) = 1 + \delta S_\mathrm{init} \geq 0$, $B(r, z, 0) = \delta B_\mathrm{init} \geq 0$, with $\|\delta S_\mathrm{init}\|_{L^2(\Omega)} \ll 1$ and $\|\delta B_\mathrm{init}\|_{L^2(\Omega)} \ll 1$. Linearizing around $(1, 0)$, we obtain

$$\begin{pmatrix} S(r, z, t) \\ B(r, z, t) \end{pmatrix} \approx \begin{pmatrix} 1 \\ 0 \end{pmatrix} + \begin{pmatrix} \bar{S}(r, z, t) \\ \bar{B}(r, z, t) \end{pmatrix}, \tag{2.52}$$

with

$$\begin{cases} \frac{\mathrm{d}\bar{S}}{\mathrm{d}t} = \sigma^2(\mathrm{Th_S})^{-1}\frac{1}{r}\frac{\mathrm{d}}{\mathrm{d}r}(r\frac{\mathrm{d}\bar{S}}{\mathrm{d}r}) + (\mathrm{Th_S})^{-1}\frac{\mathrm{d}^2\bar{S}}{\mathrm{d}z^2} + (\mathrm{Da})^{-1}\frac{\mathrm{d}\bar{S}}{\mathrm{d}z} - \mu(1)\bar{B} & \text{in } \Omega\times(0,T), \\ \frac{\mathrm{d}\bar{B}}{\mathrm{d}t} = \sigma^2(\mathrm{Th_B})^{-1}\frac{1}{r}\frac{\mathrm{d}}{\mathrm{d}r}(r\frac{\mathrm{d}\bar{B}}{\mathrm{d}r}) + (\mathrm{Th_B})^{-1}\frac{\mathrm{d}^2\bar{B}}{\mathrm{d}z^2} + (\mathrm{Da})^{-1}\frac{\mathrm{d}\bar{B}}{\mathrm{d}z} + \mu(1)\bar{B} & \text{in } \Omega\times(0,T), \\ (\mathrm{Th_S})^{-1}\frac{\mathrm{d}\bar{S}}{\mathrm{d}z} + (\mathrm{Da})^{-1}\bar{S} = 0 & \text{in } \Gamma_{\mathrm{in}}\times(0,T), \\ (\mathrm{Th_B})^{-1}\frac{\mathrm{d}\bar{B}}{\mathrm{d}z} + (\mathrm{Da})^{-1}\bar{B} = 0 & \text{in } \Gamma_{\mathrm{in}}\times(0,T), \\ \frac{\mathrm{d}\bar{S}}{\mathrm{d}r} = 0 & \text{in } \big(\Gamma_{\mathrm{wall}}\cup\Gamma_{\mathrm{sym}}\big)\times(0,T), \\ \frac{\mathrm{d}\bar{B}}{\mathrm{d}r} = 0 & \text{in } \big(\Gamma_{\mathrm{wall}}\cup\Gamma_{\mathrm{sym}}\big)\times(0,T), \\ \frac{\mathrm{d}\bar{S}}{\mathrm{d}z} = 0 & \text{in } \Gamma_{\mathrm{out}}\times(0,T), \\ \frac{\mathrm{d}\bar{B}}{\mathrm{d}z} = 0 & \text{in } \Gamma_{\mathrm{out}}\times(0,T), \\ \bar{S}(r,z,0) = \delta S_{\mathrm{init}}(r,z) & \forall (r,z)\in\Omega, \\ \bar{B}(r,z,0) = \delta B_{\mathrm{init}}(r,z) & \forall (r,z)\in\Omega. \end{cases} \tag{2.53}$$

We are going to prove that the steady state $(S_1^*, B_1^*) = (1,0)$ is asymptotically stable by showing that (see Definition A.3.10)

$$\|\bar{S}(t)\|_{L^2(\Omega)} \longrightarrow 0 \quad \text{and} \quad \|\bar{B}(t)\|_{L^2(\Omega)} \longrightarrow 0 \text{ as } t\to\infty.$$

Step 1. Let us prove that $\|\bar{B}(t)\|_{L^2(\Omega)} \longrightarrow 0$ as $t\to\infty$:
Notice that the equations involving the biomass in system (2.53) are decoupled from those involving the substrate, and may be solved by separation of variables by imposing

$$\bar{B}(r,z,t) = R(r)Z(z)T(t).$$

Step 1.1. Separation of variables.
From the second equation in system (2.53) one has that

$$\frac{T'(t)}{T(t)} = \frac{\sigma^2}{\mathrm{Th_B}}\Big(\frac{R''(r)}{R(r)} + \frac{1}{r}\frac{R'(r)}{R(r)}\Big) + \frac{1}{\mathrm{Th_B}}\frac{Z''(z)}{Z(z)} + \frac{1}{\mathrm{Da}}\frac{Z'(z)}{Z(z)} + \mu(1).$$

If we equate this expression to a constant λ, it follows that

$$T'(t) - \lambda T(t) = 0 \text{ and}$$

$$\tfrac{\sigma^2}{\mathrm{Th_B}}\Big(\tfrac{R''(r)}{R(r)} + \tfrac{1}{r}\tfrac{R'(r)}{R(r)}\Big) = -\tfrac{1}{\mathrm{Th_B}}\tfrac{Z''(z)}{Z(z)} - \tfrac{1}{\mathrm{Da}}\tfrac{Z'(z)}{Z(z)} + \lambda - \mu(1).$$

Equating this expression to an arbitrary constant η, one obtains

$$R''(r) + \tfrac{1}{r}R'(r) - \tfrac{\mathrm{Th_B}}{\sigma^2}\eta R(r) = 0 \text{ and}$$

$$\tfrac{1}{\mathrm{Th_B}}Z''(z) + \tfrac{1}{\mathrm{Da}}Z'(z) - \big(\lambda - \mu(1) - \eta\big)Z(z) = 0.$$

Proceeding as in the proof of Theorem 2.2.7 in Section 2.2.2, it is easy to see that

$$\bar{B}(r,z,t) = |\bar{B}(r,z,t)| \le \|\delta B_{\mathrm{init}}\|_{L^\infty(\Omega)}\mathrm{e}^{\mu(1)t} \qquad \forall (r,z,t)\in\Omega\times(0,T).$$

Particularly, the function $R : [0,1] \to \mathbb{R}$ must be bounded in $(0,1)$ (this fact will be used in the step 1.2 of this proof).

Step 1.2. Calculation of $R(r)$.
Using the boundary conditions of system (2.53) on Γ_{wall} and Γ_{sym}, it is clear that $R(r)$ is a solution of system

$$\begin{cases} R''(r) + \frac{1}{r}R'(r) - \frac{\text{Th}_\text{B}}{\sigma^2}\eta R(r) = 0 \quad r \in (0,1), \\ R'(0) = R'(1) = 0. \end{cases} \tag{2.54}$$

Taking the change of variables $s = ar$, with $a = \sqrt{|\eta|\frac{\text{Th}_\text{B}}{\sigma^2}}$, the differential equation for R can be rewritten in one of the following forms

1. $s^2R''(s) + sR'(s) + s^2R(s) = 0$ if $\eta < 0$,
2. $s^2R''(s) + sR'(s) - s^2R(s) = 0$ if $\eta > 0$,
3. $sR''(s) + R'(s) = 0$ if $\eta = 0$.

- **Case 1:** $\eta < 0$.

In this case the equation for $R(s)$ is known as the *Bessel equation of order zero*, with general solution

$$R(s) = C_1J_0(s) + C_2Y_0(s),$$

where C_1, $C_2 \in \mathbb{R}$ and J_n and Y_n are, respectively, the Bessel functions of first and second kind of order n. Since Y_0 has a singularity at $s = 0$, to ensure that function $R(s)$ is bounded, C_2 must be zero, and consequently, $R(s) = C_1J_0(s)$. It is well known that $J_0'(s) = -J_1(s)$ and $0 \in \{s \in [0,+\infty)\colon J_1(s) = 0\}$, which is a countable set $\{T_n\}_{n\in\mathbb{N}}$ with an infinite number of elements (see, e.g., [**?**]). Therefore, $R'(0) = 0$ is always satisfied and from the boundary condition at $s = a$ ($r = 1$), one has that the eigenvalues η are such that $J_0'(\sqrt{\frac{-\eta\text{Th}_\text{B}}{\sigma^2}}) = 0$. Consequently, $\eta \in \{\eta_n\}_{n\in\mathbb{N}}$, with

$$\eta_n = -\frac{(\sigma T_n)^2}{\text{Th}_\text{B}}, \tag{2.55}$$

and the solution $R(r)$ is given by

$$R(r) = \sum_{n\in\mathbb{N}} C_nJ_0(\frac{\sqrt{-\text{Th}_\text{B}\eta_n}}{\sigma}r).$$

- **Case 2:** $\eta > 0$.

In this case the equation for $R(s)$ is known as the *modified Bessel equation of order zero*, with general solution

$$R(r) = C_1I_0(s) + C_2K_0(s),$$

where C_1, $C_2 \in \mathbb{R}$ and I_n and K_n are, respectively, the modified Bessel functions of first and second kind of order n. Again, since K_n has a singularity at $s = 0$, we have that $R(s) = C_1I_0(s)$. It is well known that $I_0'(s) = I_1(s)$ and the boundary condition at $s = a$ implies that that the eigenvalues η satisfy that

$$C_1I_0'(\sqrt{\frac{\eta\text{Th}_\text{B}}{\sigma^2}}) = 0.$$

Nevertheless, $I_0'(s) = I_1(s) > 0$, so that C_1 must be zero and the corresponding solution $R(s)$ is the trivial one.

• **Case 3:** $\eta = 0$.

Denoting $Q(s) = R'(s)$, the second order differential equation in R can be rewritten as $sQ'(s) + Q(s) = 0$. Easy calculations lead to

$$R(s) = -C_1 \mathrm{e}^{-s} + C_2,$$

where C_1 and C_2 are constants to be determined with the boundary conditions. Thus, since $R'(0) = 0$, it follows that $C_1 = 0$ and one concludes that

$$R(s) = C_2.$$

Consequently, one has that the countable set of admissible eigenvalues η is

$$E = \{0\} \cup \{-\frac{(\sigma T_n)^2}{\mathrm{Th_B}}\}_{n\in\mathbb{N}}, \tag{2.56}$$

where T_n is such that $J_1(T_n) = 0$, J_1 being the Bessel function of first kind and order one. The general solution for the second order differential equation for R is

$$R(r) = C_0 + \sum_{n\in\mathbb{N}} C_n J_0(\frac{\sqrt{-\mathrm{Th_B}\eta_n}}{\sigma} r).$$

Step 1.3. Calculation of $Z(z)$.

Using the boundary conditions of system (2.53) on Γ_{in} and Γ_{out}, it is clear that function $Z(z)$ is solution of system

$$\begin{cases} (\mathrm{Th_B})^{-1} Z''(z) + (\mathrm{Da})^{-1} Z'(z) - (\lambda - \mu(1) - \eta) Z(z) = 0, \quad z \in (0,1), \\ (\mathrm{Th_B})^{-1} Z'(1) + (\mathrm{Da})^{-1} Z(1) = 0, \\ Z'(0) = 0, \end{cases} \tag{2.57}$$

which corresponds to a regular Sturm-Liouville eigenvalue problem (see Theorem A.2.6). The corresponding characteristic equation is

$$\frac{1}{\mathrm{Th_B}}\rho^2 + \frac{1}{\mathrm{Da}}\rho - (\lambda - \mu(1) - \eta) = 0,$$

with roots

$$\rho = \frac{-\mathrm{Th_B}}{2\mathrm{Da}} \pm \frac{\mathrm{Th_B}}{2}\sqrt{(\frac{1}{\mathrm{Da}})^2 + \frac{4(\lambda - \mu(1) - \eta)}{\mathrm{Th_B}}}.$$

Now, depending on the value of $\Delta = (\frac{1}{\mathrm{Da}})^2 + \frac{4(\lambda-\mu(1)-\eta)}{\mathrm{Th_B}}$, three possible solutions appear.

• **Case 1:** $\Delta = 0 \Leftrightarrow \lambda = \eta + \mu(1) - \mathrm{Th_B}(\frac{1}{2\mathrm{Da}})^2$**.**

In this case, the solution of system (2.57) is

$$Z(z) = D_1 \mathrm{e}^{\alpha z} + D_2 z \mathrm{e}^{\alpha z},$$

where $\alpha = \frac{-\mathrm{Th_B}}{2\mathrm{Da}}$ and D_1, D_2 are constants which are determined by the boundary conditions of the system. Since

$$Z'(z) = \alpha \mathrm{e}^{\alpha z}(D_1 + zD_2) + D_2 \mathrm{e}^{\alpha z},$$

then $Z'(0) = \alpha D_1 + D_2 = 0$ if and only if $D_2 = -\alpha D_1$. Thus, the solution and its derivative can be rewritten as

$$Z(z) = D_1 \mathrm{e}^{\alpha z}\big(1 - \alpha z\big) \qquad \text{and} \qquad Z'(z) = -D_1 \alpha^2 z \mathrm{e}^{\alpha z}.$$

From the boundary condition at $z = 1$ it follows that

$$D_1 \mathrm{e}^{\alpha}\big(\frac{1}{\mathrm{Da}}(1-\alpha) - \frac{\alpha^2}{\mathrm{Th_B}}\big) = 0. \tag{2.58}$$

By replacing α by its value into equation (2.58), we conclude that this equation is true either if $\frac{\mathrm{Th_B}}{\mathrm{Da}} = -4$ or if $D_1 = 0$. The first option is not possible since constants Da and $\mathrm{Th_B}$ are assumed strictly positive. Thus, the only solution in this case is $Z(z) = 0$.

- **Case 2:** $\Delta < 0 \Leftrightarrow \lambda < \eta + \mu(1) - \mathrm{Th_B}(\frac{1}{2\mathrm{Da}})^2$**.**

In this case, we have two complex conjugate roots $\rho = \alpha \pm i\beta$, where $\alpha \in (-\infty, 0)$ and $\beta \in (0, +\infty)$. Then, the solution of system (2.57) is of the form

$$Z(z) = \mathrm{e}^{\alpha z}\big(D_1 \cos(\beta z) + D_2 \sin(\beta z)\big),$$

where D_1 and D_2 are constants which will be determined by the boundary conditions.

Since

$$Z'(z) = \alpha Z(z) + \beta \mathrm{e}^{\alpha z}\big(-D_1 \sin(\beta z) + D_2 \cos(\beta z)\big),$$

then $Z'(0) = \alpha D_1 + \beta D_2 = 0$ if and only if $D_2 = -\frac{\alpha}{\beta} D_1$.

Thus, the solution and its derivative can be rewritten as

$$Z(z) = D_1 \mathrm{e}^{\alpha z}\big(\cos(\beta z) - \frac{\alpha}{\beta}\sin(\beta z)\big) \qquad \text{and} \qquad Z'(z) = -D_1 \mathrm{e}^{\alpha z}\sin(\beta z)(\frac{\alpha^2}{\beta} + \beta).$$

From the boundary condition at $z = 1$ it follows that:

$$D_1 \mathrm{e}^{\alpha}\Big(\frac{1}{\mathrm{Da}}\cos(\beta) - \sin(\beta)\big(\frac{1}{\mathrm{Da}}\frac{\alpha}{\beta} + \frac{1}{\mathrm{Th_B}}(\frac{\alpha^2}{\beta} + \beta)\big)\Big) = 0,$$

which solutions are $D_1 = 0$ or

$$\tan(\beta) = \frac{\frac{1}{\mathrm{Da}}}{\frac{\alpha}{\beta}\frac{1}{\mathrm{Da}} + (\frac{\alpha^2}{\beta} + \beta)\frac{1}{\mathrm{Th_B}}} = \frac{\beta}{\frac{\mathrm{Da}}{\mathrm{Th_B}}\beta^2 + \frac{\alpha}{2}} = \frac{\beta}{\frac{1}{2}(-\frac{\beta^2}{\alpha} + \alpha)} = \frac{2\alpha\beta}{-\beta^2 + \alpha^2}. \tag{2.59}$$

As $F(\beta) = \dfrac{2\alpha\beta}{\alpha^2 - \beta^2}$ is a decreasing function and has an asymptote at $\beta = -\alpha$, there exists a countable set $\{\beta_n\}_{n\in\mathbb{N}}$ with $\beta_n \in ((n-1)\pi, n\pi)$ satisfying $F(\beta_n) = \tan(\beta_n)$. Figure 2.6 shows some crossing points between functions $\tan(\beta)$ and $F(\beta)$ (i.e., some solutions of equation (2.59)) when $\alpha = -1$. Consequently,

$$Z(z) = \sum_{n\in\mathbb{N}} D_n \mathrm{e}^{-\frac{\mathrm{Th_B}}{2\mathrm{Da}}z}\big(\cos(\beta_n z) + \frac{\mathrm{Th_B}}{2\mathrm{Da}\beta_n}\sin(\beta_n z)\big),$$

where $\beta_n \in (0, +\infty)$ fulfills equation (2.59).

- **Case 3:** $\Delta > 0 \Leftrightarrow \lambda > \eta + \mu(1) - \mathrm{Th_B}(\frac{1}{2\mathrm{Da}})^2$**.**

In this case, we have two different real roots $\rho_{1,2} = \alpha \pm \beta$, with $\alpha = \frac{-\mathrm{Th_B}}{2\mathrm{Da}}$, $\beta = \frac{\mathrm{Th_B}}{2}\sqrt{(\frac{1}{\mathrm{Da}})^2 + \frac{4(\lambda-\mu(1)-\eta)}{\mathrm{Th_B}}}$, and the solution of equation (2.57) is of the form

$$Z(z) = D_1 \mathrm{e}^{(\alpha+\beta)z} + D_2 \mathrm{e}^{(\alpha-\beta)z},$$

where D_1 and D_2 are constants which will be determined by the boundary conditions.

Since $Z'(z) = (\alpha+\beta)D_1 \mathrm{e}^{(\alpha+\beta)z} + (\alpha-\beta)D_2 \mathrm{e}^{(\alpha-\beta)z}$, $\alpha < 0$ and $\beta > 0$, then $Z'(0) = (\alpha+\beta)D_1 + (\alpha-\beta)D_2 = 0$ if and only if $D_2 = -\frac{(\alpha+\beta)}{(\alpha-\beta)}D_1$.

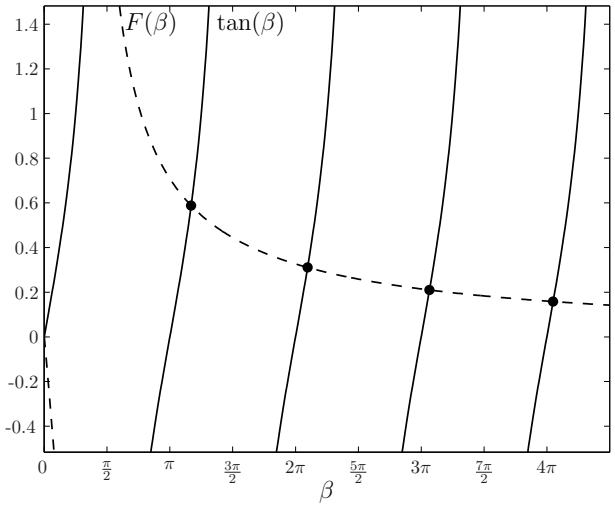

Figure 2.6: Solutions of equation (2.59) obtained when $\alpha = -1$.

Thus, the solution and its derivative can be rewritten as

$$Z(z) = D_1\big(\mathrm{e}^{(\alpha+\beta)z} - \frac{(\alpha+\beta)}{(\alpha-\beta)}\mathrm{e}^{(\alpha-\beta)z}\big) \qquad \text{and} \qquad Z'(z) = D_1(\alpha+\beta)\big(\mathrm{e}^{(\alpha+\beta)z} - \mathrm{e}^{(\alpha-\beta)z}\big).$$

From the boundary condition at $z = 1$, it follows that:

$$D_1\mathrm{e}^{\alpha}\frac{(\alpha+\beta)}{\mathrm{Th_B}}\big(\mathrm{e}^{\beta} - \mathrm{e}^{-\beta}\big) + D_1\mathrm{e}^{\alpha}\frac{1}{\mathrm{Da}}\big(\mathrm{e}^{\beta} - \frac{(\alpha+\beta)}{(\alpha-\beta)}\mathrm{e}^{-\beta}\big) = 0,$$

which implies $D_1 = 0$ or

$$\mathrm{e}^{\beta}\big(\frac{(\alpha+\beta)}{\mathrm{Th_B}} + \frac{1}{\mathrm{Da}}\big) = \mathrm{e}^{-\beta}\big(\frac{(\alpha+\beta)}{\mathrm{Th_B}} + \frac{(\alpha+\beta)}{(\alpha-\beta)}\frac{1}{\mathrm{Da}}\big) \Leftrightarrow$$

$$\mathrm{e}^{2\beta} = \frac{\frac{(\alpha+\beta)}{\mathrm{Th_B}} + \frac{1}{\mathrm{Da}}\frac{(\alpha+\beta)}{(\alpha-\beta)}}{\frac{(\alpha+\beta)}{\mathrm{Th_B}} + \frac{1}{\mathrm{Da}}} = \frac{(\alpha+\beta)}{(\alpha-\beta)}\big(\frac{(\alpha-\beta)\mathrm{Da} + \mathrm{Th_B}}{(\alpha+\beta)\mathrm{Da} + \mathrm{Th_B}}\big) = \frac{(\alpha+\beta)}{(\alpha-\beta)}\big(\frac{-(\beta+\alpha)\mathrm{Da}}{(\beta-\alpha)\mathrm{Da}}\big) \Leftrightarrow$$

$$\mathrm{e}^{2\beta} = \big(\frac{\alpha+\beta}{\alpha-\beta}\big)^2. \tag{2.60}$$

Again, as $\beta > 0$ and $\alpha < 0$, then $(\beta+\alpha)^2 < (\alpha-\beta)^2$ and thus $(\frac{\alpha+\beta}{\alpha-\beta})^2 < 1$. This implies that $D_1 = 0$ is the unique admissible solution and $Z(z) = 0$.

Step 1.4. General expression of $\bar{B}(r,z,t)$.
Given $\eta_n \in E$ (see equation (2.56)), there exists a countable set of admissible eigenvalues λ

$$\Lambda_n = \{\lambda_{nm}\}_{m\in\mathbb{N}} = \{\mu(1) + \eta_n - \frac{1}{(2\mathrm{Da})^2}\mathrm{Th_B} - \frac{\beta_m^2}{\mathrm{Th_B}}\}_{m\in\mathbb{N}}, \tag{2.61}$$

where β_m fulfills system (2.59).
Consequently,

$$\bar{B}(r,z,t) = \sum_{n\in\{0\}\cup\mathbb{N}}\sum_{m\in\mathbb{N}} A_{nm}\mathrm{e}^{\lambda_{nm}t}J_0(\frac{\sqrt{-\mathrm{Th_B}\eta_n}}{\sigma}r)\mathrm{e}^{-\frac{\mathrm{Th_B}}{2\mathrm{Da}}z}\big(\cos(\beta_m z) + \frac{\mathrm{Th_B}}{2\mathrm{Da}\beta_m}\sin(\beta_m z)\big),$$

where $\eta_n \in E$, β_m fulfills (2.59), $\lambda_{nm} \in \Lambda_n$ and the constants A_{nm} are chosen such that $\bar{B}(r,z,0) = \delta B_{\text{init}}(r,z)$. Notice that the constants A_{nm} are well defined since the two systems (2.54) and (2.57) are regular Sturm-Liouville eigenvalue problems (see Theorem A.2.6).

Using Parseval's equation (see (A.6)) one has that

$$\|\bar{B}(t)\|^2_{L^2(\Omega)} = \sum_{n\in\mathbb{N}\cup\{0\}} \sum_{m\in\mathbb{N}} A^2_{nm} \mathrm{e}^{2\lambda_{nm}t}.$$

Furthermore, it is straightforward to see that

$$\lambda_{nm} \leq \lambda_{01} = \mu(1) - \frac{1}{(2\mathrm{Da})^2}\mathrm{Th_B} - \frac{\beta_1^2}{\mathrm{Th_B}} \qquad \forall\ (n,m) \in (\{0\}\cup\mathbb{N})\times\mathbb{N}.$$

Therefore, if

$$\lambda_{01} = \mu(1) - (\frac{1}{2\mathrm{Da}})^2\mathrm{Th_B} - \frac{\beta_1^2}{\mathrm{Th_B}} < 0, \tag{2.62}$$

(which is the same condition as (2.51)) it follows that

$$\|\bar{B}(t)\|^2_{L^2(\Omega)} \leq \mathrm{e}^{2\lambda_{01}t} \sum_{n\in\mathbb{N}\cup\{0\}} \sum_{m\in\mathbb{N}} A^2_{nm} = \mathrm{e}^{2\lambda_{01}t}\|\bar{B}(0)\|^2_{L^2(\Omega)} \xrightarrow{t\to\infty} 0.$$

Notice that, if $\lambda_{01} < 0$, one can also deduce inequality (that will be used at the end of this proof)

$$\|\bar{B}(t)\|^2_{L^2(\Omega)} \leq \|\bar{B}(0)\|^2_{L^2(\Omega)} \leq K^2\|\delta B_{\text{init}}\|^2_{L^\infty(\Omega)}, \tag{2.63}$$

where K is a constant relating the norms $\|\cdot\|_{L^2(\Omega)}$ and $\|\cdot\|_{L^\infty(\Omega)}$.

Step 2. Let us prove that $\|\bar{S}(t)\|_{L^2(\Omega)} \longrightarrow 0$ as $t\to\infty$:
Regarding $\bar{S}$, the main equation involving the substrate in system (2.53) is a advection-diffusion equation with non-homogeneous term $-\mu(1)\bar{B}(r,z,t)$, which makes complex the use of separation of variables. Here, we prove that $\|\bar{S}(\cdot,\cdot,t)\|_{L^2(\Omega)} \xrightarrow{t\to\infty} 0$ by using variational techniques. To this aim, we multiply the first equation in system (2.53) by $r\bar{S}$ and integrate as follows

$$\begin{aligned}
\int_0^t\int_\Omega r\tfrac{\mathrm{d}\bar{S}}{\mathrm{d}\tau}\bar{S}\mathrm{d}r\mathrm{d}z\mathrm{d}\tau = \;& \tfrac{\sigma^2}{\mathrm{Th_S}}\int_0^t\int_\Omega \tfrac{\mathrm{d}}{\mathrm{d}r}(r\tfrac{\mathrm{d}\bar{S}}{\mathrm{d}r})\bar{S}\mathrm{d}r\mathrm{d}z\mathrm{d}\tau + \tfrac{1}{\mathrm{Th_S}}\int_0^t\int_\Omega r\tfrac{\mathrm{d}^2\bar{S}}{\mathrm{d}z^2}\bar{S}\mathrm{d}r\mathrm{d}z\mathrm{d}\tau \\
& + \tfrac{1}{\mathrm{Da}}\int_0^t\int_\Omega r\tfrac{\mathrm{d}\bar{S}}{\mathrm{d}z}\bar{S}\mathrm{d}r\mathrm{d}z\mathrm{d}\tau - \mu(1)\int_0^t\int_\Omega r\bar{B}\bar{S}\mathrm{d}r\mathrm{d}z\mathrm{d}\tau \\
= \;& \tfrac{\sigma^2}{\mathrm{Th_S}}\int_0^t\int_{\Gamma_{\text{sym}}\cup\Gamma_{\text{wall}}} r\tfrac{\mathrm{d}\bar{S}}{\mathrm{d}r}\bar{S}\mathrm{d}z\mathrm{d}\tau - \tfrac{\sigma^2}{\mathrm{Th_S}}\int_0^t\int_\Omega r(\tfrac{\mathrm{d}\bar{S}}{\mathrm{d}r})^2\mathrm{d}r\mathrm{d}z\mathrm{d}\tau \\
& + \int_0^t\int_{\Gamma_{\text{in}}} r\big(\tfrac{1}{\mathrm{Th_S}}\tfrac{\mathrm{d}\bar{S}}{\mathrm{d}z} + \tfrac{1}{\mathrm{Da}}\bar{S}\big)\bar{S}\mathrm{d}r\mathrm{d}\tau - \int_0^t\int_{\Gamma_{\text{out}}} r\big(\tfrac{1}{\mathrm{Th_S}}\tfrac{\mathrm{d}\bar{S}}{\mathrm{d}z} + \tfrac{1}{\mathrm{Da}}\bar{S}\big)\bar{S}\mathrm{d}r\mathrm{d}\tau \\
& - \tfrac{1}{\mathrm{Th_S}}\int_0^t\int_\Omega r\big(\tfrac{\mathrm{d}\bar{S}}{\mathrm{d}z}\big)^2\mathrm{d}r\mathrm{d}z\mathrm{d}\tau - \tfrac{1}{\mathrm{Da}}\int_0^t\int_\Omega r\tfrac{\mathrm{d}\bar{S}}{\mathrm{d}z}\bar{S}\mathrm{d}r\mathrm{d}z\mathrm{d}\tau \\
& - \mu(1)\int_0^t\int_\Omega r\bar{B}\bar{S}\mathrm{d}r\mathrm{d}z\mathrm{d}\tau \\
= \;& -\tfrac{\sigma^2}{\mathrm{Th_S}}\int_0^t\int_\Omega r(\tfrac{\mathrm{d}\bar{S}}{\mathrm{d}r})^2\mathrm{d}r\mathrm{d}z\mathrm{d}\tau - \tfrac{1}{\mathrm{Th_S}}\int_0^t\int_\Omega r(\tfrac{\mathrm{d}\bar{S}}{\mathrm{d}z})^2\mathrm{d}r\mathrm{d}z\mathrm{d}\tau \\
& - \tfrac{1}{\mathrm{Da}}\int_0^t\int_{\Gamma_{\text{out}}} r\bar{S}^2\mathrm{d}r\mathrm{d}z\mathrm{d}\tau \underbrace{- \frac{1}{\mathrm{Da}}\int_0^t\int_\Omega r\frac{\mathrm{d}\bar{S}}{\mathrm{d}z}\bar{S}\mathrm{d}r\mathrm{d}z\mathrm{d}\tau}_{(I)} \\
& - \mu(1)\int_0^t\int_\Omega r\bar{S}\bar{B}\mathrm{d}r\mathrm{d}z\mathrm{d}\tau.
\end{aligned} \tag{2.64}$$

The integral denoted by (I) in equation (2.64) can be rewritten as

$$(I) = -\frac{1}{2\mathrm{Da}}\int_0^t\int_\Omega r\frac{\mathrm{d}(\bar{S}^2)}{\mathrm{d}z}\mathrm{d}r\mathrm{d}z\mathrm{d}\tau = -\frac{1}{2\mathrm{Da}}\int_0^t\int_{\Gamma_{\mathrm{in}}} r\bar{S}^2\mathrm{d}r\mathrm{d}\tau + \frac{1}{2\mathrm{Da}}\int_0^t\int_{\Gamma_{\mathrm{out}}} r\bar{S}^2\mathrm{d}r\mathrm{d}\tau.$$

Thus, equation (2.64) leads to

$$\begin{aligned}&\tfrac{1}{2}\textstyle\int_0^t\int_\Omega r\frac{\mathrm{d}(\bar{S}^2)}{\mathrm{d}\tau}\mathrm{d}r\mathrm{d}z\mathrm{d}\tau + \frac{\sigma^2}{\mathrm{Th_S}}\int_0^t\int_\Omega r(\frac{\mathrm{d}\bar{S}}{\mathrm{d}r})^2\mathrm{d}r\mathrm{d}z\mathrm{d}\tau + \frac{1}{\mathrm{Th_S}}\int_0^t\int_\Omega r(\frac{\mathrm{d}\bar{S}}{\mathrm{d}z})^2\mathrm{d}r\mathrm{d}z\mathrm{d}\tau\\ &+\tfrac{1}{2\mathrm{Da}}\textstyle\int_0^t\int_{\Gamma_{\mathrm{in}}} r\bar{S}^2\mathrm{d}r\mathrm{d}\tau + \frac{1}{2\mathrm{Da}}\int_0^t\int_{\Gamma_{\mathrm{out}}} r\bar{S}^2\mathrm{d}r\mathrm{d}\tau = -\mu(1)\int_0^t\int_\Omega r\bar{S}\bar{B}\mathrm{d}r\mathrm{d}z\mathrm{d}\tau.\end{aligned} \tag{2.65}$$

By multiplying equation (2.65) by 2π and applying Young's inequality (see (A.1)) with $\epsilon > 0$ to be chosen afterward, we obtain

$$\begin{aligned}&\tfrac{1}{2}\textstyle\int_0^t \frac{\mathrm{d}}{\mathrm{d}\tau}\big(\|\bar{S}(\tau)\|^2_{L^2(\Omega^*)}\big)\mathrm{d}\tau + \frac{\min(1,\sigma^2)}{\mathrm{Th_S}}\int_0^t \|\nabla\bar{S}(\tau)\|^2_{L^2(\Omega^*)}\mathrm{d}\tau + \frac{1}{2\mathrm{Da}}\int_0^t \|\bar{S}(\tau)\|^2_{L^2(\Gamma^*_{\mathrm{out}})}\mathrm{d}\tau\\ &\le \epsilon\mu(1)\textstyle\int_0^t \|\bar{S}(\tau)\|^2_{L^2(\Omega^*)}\mathrm{d}\tau + \frac{\mu(1)}{4\epsilon}\int_0^t \|\bar{B}(\tau)\|^2_{L^2(\Omega^*)}\mathrm{d}\tau.\end{aligned} \tag{2.66}$$

Considering $A = \min\{\frac{1}{\mathrm{Th_S}}, \frac{\sigma^2}{\mathrm{Th_S}}, \frac{1}{2\mathrm{Da}}\}$, it follows that

$$\begin{aligned}&\tfrac{1}{2}\textstyle\int_0^t \frac{\mathrm{d}}{\mathrm{d}\tau}\big(\|\bar{S}(\tau)\|^2_{L^2(\Omega^*)}\big)\mathrm{d}\tau + A\int_0^t(\|\nabla\bar{S}(\tau)\|^2_{L^2(\Omega^*)} + \|\bar{S}(\tau)\|^2_{L^2(\Gamma^*_{\mathrm{out}})})\mathrm{d}\tau\\ &\le \epsilon\mu(1)\textstyle\int_0^t \|\bar{S}(\tau)\|^2_{L^2(\Omega^*)}\mathrm{d}\tau + \frac{\mu(1)}{4\epsilon}\|\bar{B}\|^2_{L^2((0,t)\times\Omega^*)}.\end{aligned} \tag{2.67}$$

Now, applying Friedrich's inequality (see (A.3)) to inequality (2.67) with $E = \Gamma^*_{\mathrm{out}}$, there exits a constant C depending on Ω^* and Γ^*_{out} such that

$$\tfrac{1}{2}\textstyle\int_0^t \frac{\mathrm{d}}{\mathrm{d}\tau}\big(\|\bar{S}(\tau)\|^2_{L^2(\Omega^*)}\big)\mathrm{d}\tau \le \big(\epsilon\mu(1) - \frac{A}{C}\big)\int_0^t \|\bar{S}(\tau)\|^2_{L^2(\Omega^*)}\mathrm{d}\tau + \frac{\mu(1)}{4\epsilon}\|\bar{B}\|^2_{L^2((0,t)\times\Omega^*)}. \tag{2.68}$$

Next, applying the Gronwall's inequality in its integral form (see (A.2)), it follows that

$$\|\bar{S}(t)\|^2_{L^2(\Omega^*)} \le \underbrace{\big(\|\delta S_{\mathrm{init}}\|^2_{L^2(\Omega^*)} + \frac{\mu(1)}{2\epsilon}\|\bar{B}\|^2_{L^2((0,t)\times\Omega^*)}\big)}_{(:=m(t))}\mathrm{e}^{\underbrace{2(\epsilon\mu(1) - \frac{A}{C})t}_{(:=\alpha)}}.$$

Since $\|\bar{B}(t)\|^2_{L^2(\Omega)} \le K^2\|\delta B_{\mathrm{init}}\|^2_{L^\infty(\Omega)}$ for all $t > 0$ (see equation (2.63)), taking $\epsilon < \frac{A}{\mu(1)C}$ it follows that $\alpha < 0$. Thus,

$$\|\bar{S}(t)\|^2_{L^2(\Omega^*)} \le \big(\|\delta S_{\mathrm{init}}\|^2_{L^2(\Omega^*)} + \frac{\mu(1)}{2\epsilon}tK^2\|\delta B_{\mathrm{init}}\|^2_{L^\infty(\Omega^*)}\big)\mathrm{e}^{\alpha t} \xrightarrow{t\to\infty} 0.$$

□

Taking into account Theorem 2.2.17, we conjecture (supported by the numerical experiments presented later on) that the following result holds:

Proposition 2.2.19. *If μ fulfills* (H1) *(or fulfills* (H2) *and $\mu(1) = \max_{S\in[0,1]}\mu(S)$), a sufficient condition for (S_2^*, B_2^*) to be an asymptotically stable steady state of system* (2.47) *is that*

$$\mu(1) > \frac{\mathrm{Th_B}}{(2\mathrm{Da})^2} + \frac{(\beta_1(\mathrm{Da},\mathrm{Th_B}))^2}{\mathrm{Th_B}}. \tag{2.69}$$

If μ fulfills (H2) *and $\mu(1) < \max_{S\in[0,1]}\mu(S) (= 1$ in this case), a sufficient condition for (S_2^*, B_2^*) to be an asymptotically stable steady state of system* (2.47) *is that*

$$1 > \frac{\mathrm{Th_B}}{(2\mathrm{Da})^2} + \frac{(\beta_1(\mathrm{Da},\mathrm{Th_B}))^2}{\mathrm{Th_B}}. \tag{2.70}$$

Remark 2.2.20. *In terms of the variables with dimensions appearing in system* (2.11)*, conditions* (2.69) *and* (2.70) *are reformulated, respectively, as*

$$\mu(S_{\mathrm{e}}) > \frac{u^2}{4D_{\mathrm{B}}} + \frac{D_{\mathrm{B}}}{H^2}(\tilde{\beta}_1(H,u,D_{\mathrm{B}}))^2,$$

and

$$\|\mu\|_{L^\infty(\mathbb{R})} > \frac{u^2}{4D_{\mathrm{B}}} + \frac{D_{\mathrm{B}}}{H^2}(\tilde{\beta}_1(H,u,D_{\mathrm{B}}))^2.$$

Remark 2.2.21. *From Theorem 2.2.17 and Proposition 2.2.19, it follows that if μ fulfills* (H2) *and $\mu(1) < \max_{S\in[0,1]} \mu(S)$ $(= 1$ in this case$)$, there is bistability in system* (2.47) *when*

$$\mu(1) < \frac{\mathrm{Th_B}}{(2\mathrm{Da})^2} + \frac{(\beta_1(\mathrm{Da},\mathrm{Th_B}))^2}{\mathrm{Th_B}} < 1.$$

Bounds for the flow rate assuring asymptotic stability of the steady states

Conditions (2.51) and (2.70) include in their analytical expression the model parameters Da, $\mathrm{Th_B}$ and $\mu(1)$, among which the flow rate Da can be seen as a bioreactor control parameter. Here, we present bounds for the parameter Da assuring the asymptotic stability of the steady states $(1,0)$ and (S_2^*, B_2^*). To do so, we first define the following function.

Definition 2.2.22. *For a fixed value* $\mathrm{Th_B}$*, one can define the function*

$$\begin{array}{rccc} f_{\mathrm{Th_B}}: & [0,+\infty) & \longrightarrow & [0,+\infty) \\ & \mathrm{Da} & \to & \dfrac{\mathrm{Th_B}}{(2\mathrm{Da})^2} + \dfrac{(\beta_1(\mathrm{Da},\mathrm{Th_B}))^2}{\mathrm{Th_B}}. \end{array}$$

In Figure 2.7 we plot the value of functions $\beta_1(\mathrm{Da},\mathrm{Th_B})$ and $f_{\mathrm{Th_B}}(\mathrm{Da})$ for $\mathrm{Th_B} \in \{\frac{1}{5}, 1, 5\}$ and $\mathrm{Da} \in [0,2]$. For a fixed value $\mathrm{Th_B}$, function $\beta_1(\cdot,\mathrm{Th_B})$ is decreasing, bounded by π (see the proof of Theorem 2.2.17 for a detailed explanation of this feature) and $\beta_1(\mathrm{Da},\mathrm{Th_B}) \xrightarrow{\mathrm{Da}\to+\infty} 0$. One can also conclude that, for a fixed value $\mathrm{Th_B}$, function $f_{\mathrm{Th_B}}$ is decreasing, $f_{\mathrm{Th_B}}(\mathrm{Da}) \xrightarrow{\mathrm{Da}\to 0} +\infty$ and $f_{\mathrm{Th_B}}(\mathrm{Da}) \xrightarrow{\mathrm{Da}\to+\infty} 0$. Taking into account these properties of $f_{\mathrm{Th_B}}$, we define the following variables.

Definition 2.2.23. *We define*

- $\mathrm{Da}^{\mathrm{W}}_{(2.47)}(\mathrm{Th_B},\mu(1)) := (f_{\mathrm{Th_B}})^{-1}(\mu(1))$.
- $\mathrm{Da}^{\mathrm{NW}}_{(\mathrm{H1}),(2.47)}(\mathrm{Th_B},\mu(1)) := \mathrm{Da}^{\mathrm{W}}_{(2.47)}(\mathrm{Th_B},\mu(1))$.
- $\mathrm{Da}^{\mathrm{NW}}_{(\mathrm{H2}),(2.47)}(\mathrm{Th_B}) := (f_{\mathrm{Th_B}})^{-1}(1)$.

Remark 2.2.24. *Following Theorem 2.2.17 and Proposition 2.2.19, it follows that:*

- *If* $\mathrm{Da} < \mathrm{Da}^{\mathrm{W}}_{(2.47)}(\mathrm{Th_B},\mu(1))$*, then the equilibrium state* $(1,0)$ *of system* (2.47) *is asymptotically stable.*
- *If μ fulfills* (H1) *(or fulfills* (H2) *and $\mu(1) = \max_{S\in[0,1]} \mu(S)$) and* $\mathrm{Da} > \mathrm{Da}^{\mathrm{NW}}_{(\mathrm{H1}),(2.47)}(\mathrm{Th_B},\mu(1))$*, then the equilibrium state (S_2^*, B_2^*) of system* (2.47) *is asymptotically stable.*
- *If μ fulfills* (H2)*, $\mu(1) < \max_{S\in[0,1]} \mu(S)$ $(= 1)$ and* $\mathrm{Da} > \mathrm{Da}^{\mathrm{NW}}_{(\mathrm{H2}),(2.47)}(\mathrm{Th_B})$*, then the equilibrium state (S_2^*, B_2^*) of system* (2.47) *is asymptotically stable.*

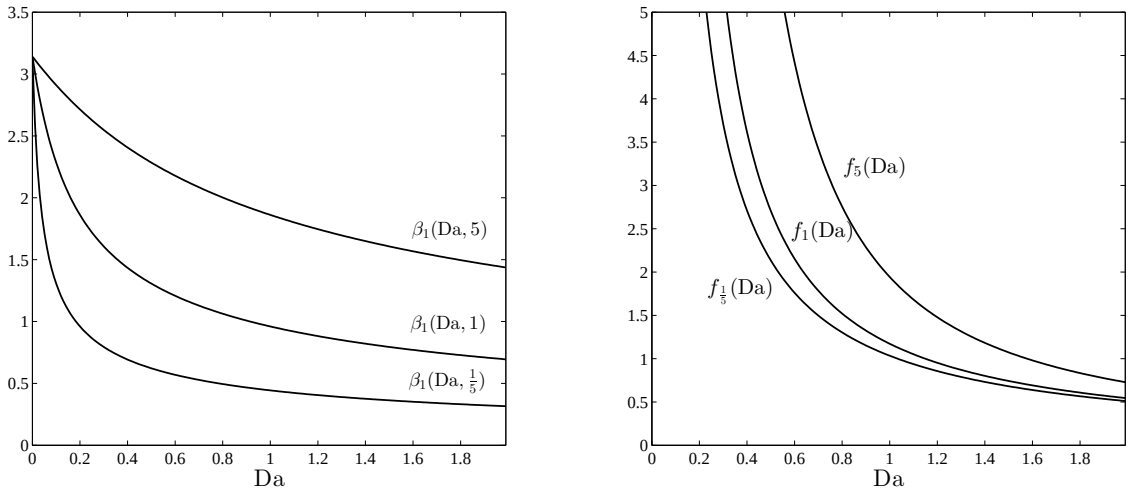

(a) $\beta_1(\mathrm{Da}, \mathrm{Th_B})$ (b) $f_{\mathrm{Th_B}}(\mathrm{Da})$

Figure 2.7: Graphical plots of functions $\beta_1(\mathrm{Da}, \mathrm{Th_B})$ and $f_{\mathrm{Th_B}}(\mathrm{Da})$ (described in Definitions 2.2.16 and 2.2.22, respectively) for $\mathrm{Th_B} \in \{\frac{1}{5}, 1, 5\}$ and $\mathrm{Da} \in [0, 2]$.

Definition 2.2.25. *In terms of the variables with dimensions appearing in system* (2.11)*, for fixed values* H *and* D_{B} *we define the function*

$$\begin{aligned} \tilde{f}_{H,D_{\mathrm{B}}}: \quad [0,+\infty) &\longrightarrow [0,+\infty) \\ u &\to \frac{u^2}{4D_{\mathrm{B}}} + \frac{D_{\mathrm{B}}}{H^2}(\tilde{\beta}_1(H,u,D_{\mathrm{B}}))^2. \end{aligned}$$

Similarly to Definition 2.2.23, we define:

- $u^{\mathrm{W}}_{(2.11)}(H, D_{\mathrm{B}}, \mu(S_{\mathrm{e}})) := (\tilde{f}_{H,D_{\mathrm{B}}})^{-1}(\mu(S_{\mathrm{e}}))$
- $u^{\mathrm{NW}}_{(\mathrm{H1}),(2.11)}(H, D_{\mathrm{B}}, \mu(S_{\mathrm{e}})) := u^{\mathrm{W}}_{(2.11)}(H, D_{\mathrm{B}}, \mu(S_{\mathrm{e}}))$.
- $u^{\mathrm{NW}}_{(\mathrm{H2}),(2.11)}(H, D_{\mathrm{B}}) := (\tilde{f}_{H,D_{\mathrm{B}}})^{-1}(\|\mu\|_{L^\infty(\mathbb{R})})$.

Remark 2.2.26. *Following Remarks 2.2.18 and 2.2.20, it follows that:*

- *If* $u > u^{\mathrm{W}}_{(2.11)}(H, D_{\mathrm{B}}, \mu(S_{\mathrm{e}}))$*, then the equilibrium state* $(S_{\mathrm{e}}, 0)$ *of system* (2.11) *is asymptotically stable.*
- *If* μ *fulfills* (H1) *(or fulfills* (H2) *and* $\mu(S_{\mathrm{e}}) = \max_{S\in[0,S_{\mathrm{e}}]} \mu(S)$*) and* $u < u^{\mathrm{NW}}_{(\mathrm{H1}),(2.11)}(H, D_{\mathrm{B}}, \mu(S_{\mathrm{e}}))$*, then the equilibrium state* (S_2^*, B_2^*) *of system* (2.11) *is asymptotically stable.*
- *If* μ *fulfills* (H2)*,* $\mu(S_{\mathrm{e}}) < \max_{S\in[0,S_{\mathrm{e}}]} \mu(S)$ $(= \|\mu\|_{L^\infty(\mathbb{R})})$ *and* $u < u^{\mathrm{NW}}_{(\mathrm{H2}),(2.11)}(H, D_{\mathrm{B}})$*, then the equilibrium state* (S_2^*, B_2^*) *of system* (2.47) *is asymptotically stable.*

Numerical Experiments

Here, we describe the results of the numerical experiments performed to analyze the validity and robustness of the stability analysis previously presented. First, we study the sensitivity of variables $\mathrm{Da}^{\mathrm{W}}_{(2.47)}(\mathrm{Th_B}, \mu(1))$ and $\mathrm{Da}^{\mathrm{NW}}_{(\mathrm{H2}),(2.47)}(\mathrm{Th_B})$ regarding the model parameters. Then, we carry out the numerical implementation

of system (2.47)-(2.48) in order to check the interest of these functions. Finally, we compare the results of the stability analysis of systems (2.6) and (2.47).

In what follows, the value of functions $\mathrm{Da}^{\mathrm{W}}_{(2.47)}(\mathrm{Th_B}, \mu(1))$ and $\mathrm{Da}^{\mathrm{NW}}_{(\mathrm{H2}),(2.47)}(\mathrm{Th_B})$ is approximated numerically using a self-implemented *Dichotomy method* (see Section 3.1.1 for a description of this method). Moreover, for each pair $(\mathrm{Th_B}, \mathrm{Da})$, the value of $\beta_1(\mathrm{Th_B}, \mathrm{Da})$ (see Definition 2.2.16) was computed by using the MATLAB function `vpasolve` (see `www.mathworks.com/help/symbolic/vpasolve.html`).

Sensitivity to model parameters

Here, we perform the sensitivity analysis of $\mathrm{Da}^{\mathrm{W}}_{(2.47)}(\mathrm{Th_B}, \mu(1))$ with respect to the nondimensional parameters $\mathrm{Th_B}$ and $\mu(1)$ (the sensitivity analysis of $\mathrm{Da}^{\mathrm{NW}}_{(\mathrm{H2}),(2.47)}(\mathrm{Th_B})$ can be obtained with a similar methodology).

• **Sensitivity with respect to** $\mu(1)$

Taking into account that $\mathrm{Da}^{\mathrm{W}}_{(2.47)}(\mathrm{Th_B}, \mu(1)) = (f_{\mathrm{Th_B}})^{-1}(\mu(1))$ and $f_{\mathrm{Th_B}}$ is decreasing, one concludes that, for any fixed value $\mathrm{Th_B}$, the function $\mathrm{Da}^{\mathrm{W}}_{(2.47)}(\mathrm{Th_B}, \mu(1))$ decreases as $\mu(1)$ increases. This is physically reasonable since, as parameter $\mu(1)$ increases, the range of flow rates $\frac{1}{\mathrm{Da}}$ suitable to avoid washout also increases (see, e.g., [**?**, **?**, **?**]).

• **Sensitivity with respect to** $\mathrm{Th_B}$

In order to easily analyze the sensitivity of $\mathrm{Da}^{\mathrm{W}}_{(2.47)}(\mathrm{Th_B}, \mu(1))$ with respect to $\mathrm{Th_B}$, we aim to approximate $\mathrm{Da}^{\mathrm{W}}_{(2.47)}(\mathrm{Th_B}, \mu(1))$ by using the following variables:

– $\overline{\mathrm{Da}}^{\mathrm{W}}_{(2.47)}(\mathrm{Th_B}, \mu(1)) := \frac{1}{2}\sqrt{\frac{\mathrm{Th_B}}{\mu(1)}}$. This should be a good approximation of $\mathrm{Da}^{\mathrm{W}}_{(2.47)}(\mathrm{Th_B}, \mu(1))$ assuming that the second term of the right hand side of condition (2.51) is negligible.

– $\widehat{\mathrm{Da}}^{\mathrm{W}}_{(2.47)}(\mathrm{Th_B}, \mu(1)) := (g_{\mathrm{Th_B}})^{-1}(\mu(1))$, where

$$g_{\mathrm{Th_B}} : [0, +\infty) \longrightarrow [0, +\infty)$$

$$\mathrm{Da} \rightarrow \frac{(\beta_1(\mathrm{Th_B}, \mathrm{Da}))^2}{\mathrm{Th_B}}.$$

This should be a good approximation of $\mathrm{Da}^{\mathrm{W}}_{(2.47)}(\mathrm{Th_B}, \mu(1))$ assuming that the first term of the right hand side of condition (2.51) is negligible. Since $\beta_1(\mathrm{Th_B}, \mathrm{Da}) < \pi$ (see the proof of Theorem 2.2.17 for a detailed explanation of this fact), if $\mathrm{Th_B}\mu(1) > \pi^2$, then the function $\widehat{\mathrm{Da}}^{\mathrm{W}}_{(2.47)}(\mathrm{Th_B}, \mu(1))$ is not defined. We approximate numerically $\widehat{\mathrm{Da}}^{\mathrm{W}}_{(2.47)}(\mathrm{Th_B}, \mu(1))$ applying the same methodology that the one used to approximate numerically $\mathrm{Da}^{\mathrm{W}}_{(2.47)}(\mathrm{Th_B}, \mu(1))$, described above.

Figure 2.8 illustrates the difference between the functions $\mathrm{Da}^{\mathrm{W}}_{(2.47)}(\mathrm{Th_B}, \mu(1))$, $\overline{\mathrm{Da}}^{\mathrm{W}}_{(2.47)}(\mathrm{Th_B}, \mu(1))$ and $\widehat{\mathrm{Da}}^{\mathrm{W}}_{(2.47)}(\mathrm{Th_B}, \mu(1))$ when $\mu(1) = 0.5$ and $\mathrm{Th_B} \in [5 \cdot 10^{-3}, 5 \cdot 10^{3}]$. We observe that $\widehat{\mathrm{Da}}^{\mathrm{W}}_{(2.47)}(\mathrm{Th_B}, 0.5)$ approximates $\mathrm{Da}^{\mathrm{W}}_{(2.47)}(\mathrm{Th_B}, 0.5)$ for values smaller than $\log(\mathrm{Th_B}) = -2$ ($\mathrm{Th_B} \approx 0.1$) while $\overline{\mathrm{Da}}^{\mathrm{W}}_{(2.47)}(\mathrm{Th_B}, 0.5)$ approximates $\mathrm{Da}^{\mathrm{W}}_{(2.47)}(\mathrm{Th_B}, 0.5)$ for values larger than $\log(\mathrm{Th_B}) = 6$ ($\mathrm{Th_B} \approx 400$). The comparison between the functions $\mathrm{Da}^{\mathrm{W}}_{(2.47)}(\mathrm{Th_B}, \mu(1))$, $\overline{\mathrm{Da}}^{\mathrm{W}}_{(2.47)}(\mathrm{Th_B}, \mu(1))$ and $\widehat{\mathrm{Da}}^{\mathrm{W}}_{(2.6)}(\mathrm{Th_B}, \mu(1))$, shown in Figure 2.8 for $\mu(1) = 0.5$, has been reproduced for reaction values $\mu(1) \in \{\frac{i}{20}\}_{i=1}^{20}$ and the results seems to indicate that in general: if $\mathrm{Th_B} \geq 10^4$, the function $\overline{\mathrm{Da}}^{\mathrm{W}}_{(2.47)}(\mathrm{Th_B}, \mu(1))$ can be used as an approximation of $\mathrm{Da}^{\mathrm{W}}_{(2.47)}(\mathrm{Th_B}, \mu(1))$; and if $\mathrm{Th_B} \leq 0.1$, the function $\widehat{\mathrm{Da}}^{\mathrm{W}}_{(2.47)}(\mu(1))$ can be used as an approximation of

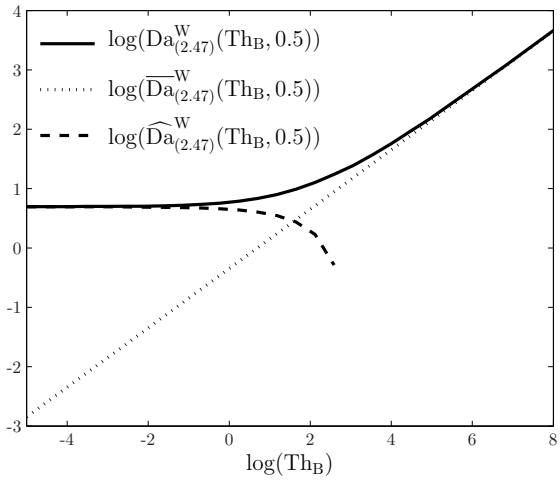

Figure 2.8: Comparison between the functions $\mathrm{Da}^{\mathrm{W}}_{(2.47)}(\mathrm{Th_B}, 0.5)$, $\overline{\mathrm{Da}}^{\mathrm{W}}_{(2.47)}(\mathrm{Th_B}, 0.5)$ and $\widehat{\mathrm{Da}}^{\mathrm{W}}_{(2.47)}(\mathrm{Th_B}, 0.5)$ (depicted with solid, dotted and dashed lines, respectively), when $\mathrm{Th_B} \in [5 \cdot 10^{-3}, 5 \cdot 10^{3}]$.

$\mathrm{Da}^{\mathrm{W}}_{(2.47)}(\mathrm{Th_B}, \mu(1))$.

Taking into account the approximations of $\mathrm{Da}^{\mathrm{W}}_{(2.47)}(\mathrm{Th_B}, \mu(1))$ presented above and Figure 2.8, the sensitivity of $\mathrm{Da}^{\mathrm{W}}_{(2.47)}(\mathrm{Th_B}, \mu(1))$ with respect to $\mathrm{Th_B}$ reads as follows:

- If $\mathrm{Th_B} \leq 0.1$, the variable $\mathrm{Da}^{\mathrm{W}}_{(2.47)}(\mathrm{Th_B}, \mu(1))$ is not sensible to parameter $\mathrm{Th_B}$. Indeed, small values of $\mathrm{Th_B}$ correspond, for instance, to high diffusion coefficients implying almost spatial homogeneous biomass concentration. In this case, there would be no differences when considering even higher diffusion coefficients. As we will see when comparing the stability analysis of systems (2.6) and (2.47), if $\mathrm{Th_B} \leq 0.1$, the dynamics of the bioreactor can be modeled with ordinary differential equations.

- If $\mathrm{Th_B} > 0.1$, the variable $\mathrm{Da}^{\mathrm{W}}_{(2.47)}(\mathrm{Th_B}, \mu(1))$ seems to increase with parameter $\mathrm{Th_B}$. This outcome is physically reasonable, since as parameter $\mathrm{Th_B}$ increases (equivalently, the diffusion coefficient decreases) the flow rate $\frac{1}{\mathrm{Da}}$ should be chosen smaller to favor the reaction between the substrate and the biomass (see Section 3.2).

- If $\mathrm{Th_B} \geq 10^4$, the variable $\mathrm{Da}^{\mathrm{W}}_{(2.47)}(\mathrm{Th_B}, \mu(1))$ is quadratically proportional to $\mathrm{Th_B}$.

Numerical validation of the results

Here, we check the properties given in Remark 2.2.24 for the threshold values $\mathrm{Da}^{\mathrm{W}}_{(2.47)}(\mathrm{Th_B}, \mu(1))$ and $\mathrm{Da}^{\mathrm{NW}}_{(\mathrm{H2}),(2.47)}(\mathrm{Th_B}, \mu(1))$ by using the numerical solution of system (2.47)-(2.48). To do that computation, we use the software COMSOL Multiphysics 5.0 (`www.comsol.com`), based on the Finite Element Method (see [**?**]). The numerical experiments were carried out in a 2.8Ghz Intel i7-930 64bits computer with 12Gb of RAM. We used a triangular mesh with around 1000 elements and final nondimensional time $T = 300$.

In order to validate the properties of the threshold values $\mathrm{Da}^{\mathrm{W}}_{(2.47)}(\mathrm{Th_B}, \mu(1))$ and $\mathrm{Da}^{\mathrm{NW}}_{(\mathrm{H2}),(2.47)}(\mathrm{Th_B}, \mu(1))$, we define the following variables:

- $\widetilde{\mathrm{Da}}^{\mathrm{W}}_{(2.47)}(\mathrm{Th_B}, \mu(1)) := \sup\{\mathrm{Da}$: the numerical solution of system (2.47)-(2.48) (with parameters $\mathrm{Th_B}$, Da, $\mathrm{Th_S} = \mathrm{Th_B}$, $\sigma = 1$, μ the nondimensional Monod function with $K_S = \frac{1-\mu(1)}{\mu(1)}$, $S_{\mathrm{init}} = 0.1$ and $B_{\mathrm{init}} = 0.9$) approaches asymptotically the steady state $(1, 0)\}$.

– $\widetilde{\mathrm{Da}}^{\mathrm{NW}}_{(\mathrm{H2}),(2.47)}(\mathrm{Th_B}) := \inf\{\mathrm{Da}$: the numerical solution of system (2.47)-(2.48) (with parameters $\mathrm{Th_B}$, Da, $\mathrm{Th_S} = \mathrm{Th_B}$, $\sigma = 1$, μ the nondimensional Haldane function with $\frac{\mu^*}{\|\mu\|_{L^\infty}} = 1.7071$, $K_\mathrm{S} = 0.3536$ and $K_\mathrm{I} = 2.8284$) approaches asymptotically a steady state different from $(1,0)\}$.

We approximate numerically the value of $\widetilde{\mathrm{Da}}^{\mathrm{W}}_{(2.47)}(\mathrm{Th_B}, \mu(1))$ and $\widetilde{\mathrm{Da}}^{\mathrm{NW}}_{(\mathrm{H2}),(2.47)}(\mathrm{Th_B})$ by using again a self-implemented *Dichotomy method*. Figure 2.9-(a) illustrates the difference between $\mathrm{Da}^{\mathrm{W}}_{(2.47)}(\mathrm{Th_B}, \mu(1))$ and $\widetilde{\mathrm{Da}}^{\mathrm{W}}_{(2.47)}(\mathrm{Th_B}, \mu(1))$ when $\mathrm{Th_B} \in [5 \cdot 10^{-3}, 1.5 \cdot 10^2]$ and $\mu(1) = 0.5$. Similarly, Figure 2.9-(b) shows the difference between $\mathrm{Da}^{\mathrm{NW}}_{(\mathrm{H2}),(2.47)}(\mathrm{Th_B})$ and $\widetilde{\mathrm{Da}}^{\mathrm{NW}}_{(\mathrm{H2}),(2.47)}(\mathrm{Th_B})$ when $\mathrm{Th_B} \in [5 \cdot 10^{-3}, 1.5 \cdot 10^2]$. We point out that these comparisons were also performed with $\widetilde{\mathrm{Da}}^{\mathrm{W}}_{(2.47)}(\mathrm{Th_B}, \mu(1))$ and $\widetilde{\mathrm{Da}}^{\mathrm{NW}}_{(\mathrm{H2}),(2.47)}(\mathrm{Th_B})$ defined using other model parameters σ, $\mathrm{Th_S}$ and μ and similar results were obtained. In Figure 2.10, we plot the

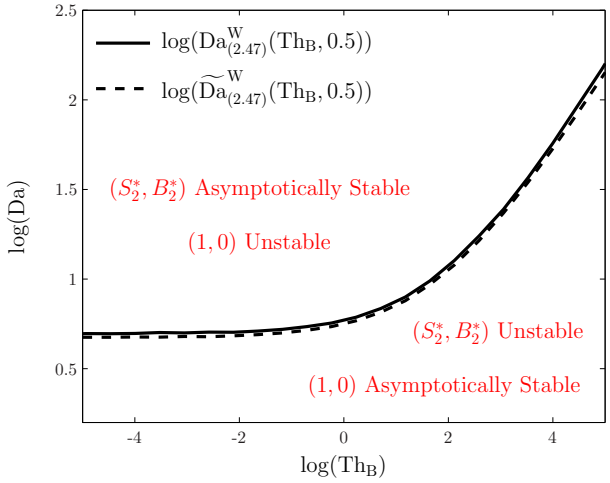

(a) Comparison between $\log(\mathrm{Da}^{\mathrm{W}}_{(2.47)}(\mathrm{Th_B}, 0.5))$ (depicted with solid line) and $\log(\widetilde{\mathrm{Da}}^{\mathrm{W}}_{(2.47)}(\mathrm{Th_B}, 0.5))$ (depicted with dashed lines).

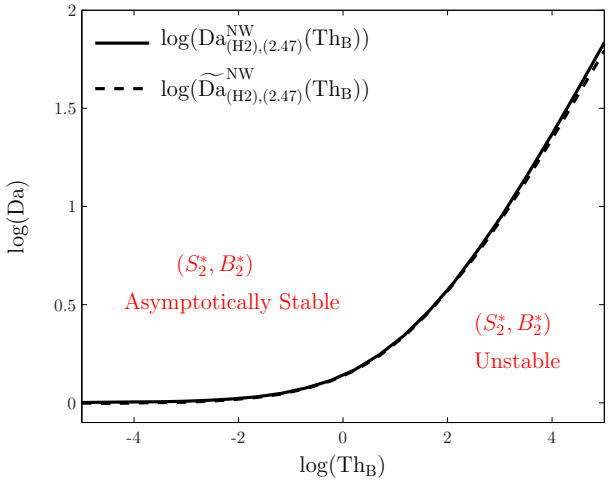

(b) Comparison between $\log(\mathrm{Da}^{\mathrm{NW}}_{(\mathrm{H2}),(2.47)}(\mathrm{Th_B})$ (depicted with solid line) and $\log(\widetilde{\mathrm{Da}}^{\mathrm{NW}}_{(\mathrm{H2}),(2.47)}(\mathrm{Th_B}))$ (depicted with dashed lines).

Figure 2.9: Numerical validation of the results.

steady-state solution (S_2^*, B_2^*) of system (2.47), computed numerically when $\mathrm{Th_B} = \mathrm{Th_S} = \mathrm{e}^4$, $\mathrm{Da} = \mathrm{e}^2$, $\sigma = 1$, $S_{\mathrm{init}} = 0.1$, $B_{\mathrm{init}} = 0.9$ and μ being the nondimensional Monod function with $K_\mathrm{S} = 1$ (so that $\mu(1) = 0.5$). With these parameters, i.e., when $\log(\mathrm{Th_B}) = 4$ and $\log(\mathrm{Da}) = 2$, the equilibrium solution (S_2^*, B_2^*) is asymptotically stable (see Figure 2.9-(a)). Notice that the same steady-state solution can be obtained with nonhomogeneous initial conditions (for instance, $S_{\mathrm{init}}(r,z) = rz$ and $B_{\mathrm{init}}(r,z) = r(1-z)$).
The bistability of system (2.47), stated in Remark 2.2.21, is perceivable when numerically solving system (2.47). For instance, if $\mathrm{Th_B} = 0.01$, $\mathrm{Da} = 1.5$ and $\mu(1) = 0.5$, we observe that the solution of system (2.47) (computed with parameters $\sigma = 1$, $\mathrm{Th_S} = 0.01$ and μ the nondimensional Haldane function with $\frac{\mu^*}{\|\mu\|_{L^\infty(\mathrm{R})}} = 1.7071$, $K_\mathrm{S} = 0.0529$ and $K_\mathrm{I} = 0.4235$) approaches $(1,0)$ if we choose $S_{\mathrm{init}} = 0.9$ and $B_{\mathrm{init}} = 0.1$, while it approaches a different equilibrium (similar to the one represented in Figure 2.10) solution if we set $S_{\mathrm{init}} = 0.1$ and $B_{\mathrm{init}} = 0.9$.

Comparison with the stability analysis of system (2.6)

In this section, we compare the stability analysis conditions associated to the ODE and PDE systems (2.6) and (2.47), respectively. As done previously for system (2.47), we define the following variables:

Definition 2.2.27.

- $\mathrm{Da}^{\mathrm{W}}_{(2.6)}(\mu(1)) := \frac{1}{\mu(1)}$.

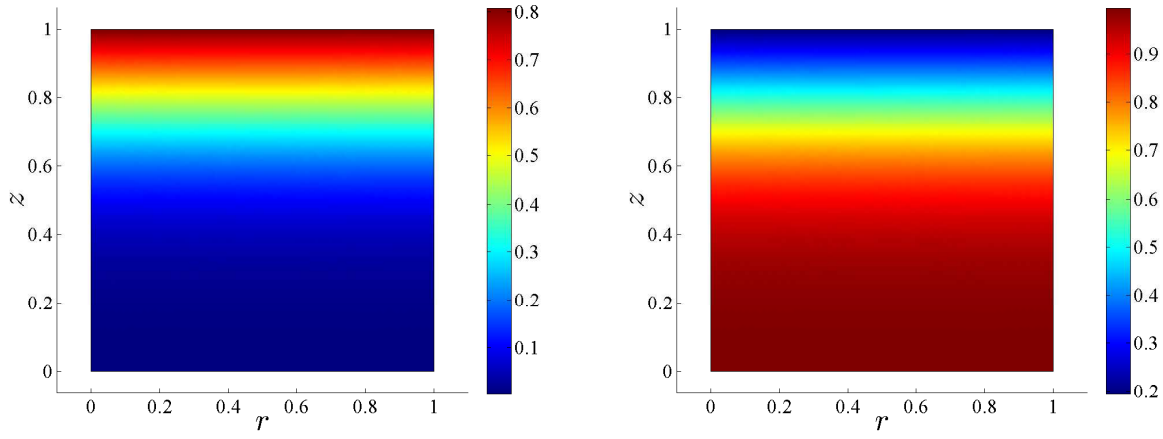

(a) $S_2^*(r,z)$ (b) $B_2^*(r,z)$

Figure 2.10: Representation of the steady-state solution (S_2^*, B_2^*) of system (2.47) computed numerically when $\mathrm{Th_B} = \mathrm{Th_S} = \mathrm{e}^4$, $\mathrm{Da} = \mathrm{e}^2$, $\sigma = 1$, $S_{\mathrm{init}} = 0.1$, $B_{\mathrm{init}} = 0.9$ and μ being the nondimensional Monod Function with $K_S = 1$ (so that $\mu(1) = 0.5$).

- $\mathrm{Da}^{\mathrm{NW}}_{(\mathrm{H1}),(2.6)}(\mu(1)) := \mathrm{Da}^{\mathrm{W}}_{(2.6)}(\mu(1))$.
- $\mathrm{Da}^{\mathrm{NW}}_{(\mathrm{H2}),(2.6)} := 1$.

Remark 2.2.28. *According to Remark 2.2.12 and Definition 2.2.27, the stability analysis of system* (2.6) *(shown in Section 2.1.4) can be rewritten as*

- *If* $\mathrm{Da} < \mathrm{Da}^{\mathrm{W}}_{(2.6)}(\mu(1))$*, then the equilibrium solution* $(1,0)$ *of system* (2.6) *is asymptotically stable.*
- *If* μ *fulfills* (H1) *(or fulfills* (H2) *and* $\mu(1) = \arg\max_{S\in[0,1]} \mu(S)$*) and* $\mathrm{Da} > \mathrm{Da}^{\mathrm{NW}}_{(\mathrm{H1}),(2.6)}(\mu(1))$*, then the equilibrium solution* (S_2^*, B_2^*) *of system* (2.6) *is asymptotically stable.*
- *If* μ *fulfills* (H2)*,* $\mu(1) < \max_{S\in[0,1]} \mu(S)$ *(*$= 1$*) and* $\mathrm{Da} > \mathrm{Da}^{\mathrm{NW}}_{(\mathrm{H2}),(2.6)}(\mu(1))$*, then the equilibrium solution* (S_2^*, B_2^*) *of system* (2.6) *is asymptotically stable.*

Figure 2.11 illustrates the difference between the variable $\mathrm{Da}^{\mathrm{NW}}_{(\mathrm{H2}),(2.47)}(\mathrm{Th_B})$ and the constant $\mathrm{Da}^{\mathrm{NW}}_{(\mathrm{H2}),(2.6)} = 1$ (and the difference, when $\mu(1) = 0.5$, between the variable $\mathrm{Da}^{\mathrm{W}}_{(2.47)}(\mathrm{Th_B}, \mu(1))$ and the constant $\mathrm{Da}^{\mathrm{W}}_{(2.6)}(\mu(1)) = 2$). In both cases $\mathrm{Th_B} \in [5\cdot 10^{-3}, 1.5\cdot 10^2]$. Notice that the area limited between the curves $\mathrm{Da}^{\mathrm{NW}}_{(\mathrm{H2}),(2.47)}(\mathrm{Th_B})$ and $\mathrm{Da}^{\mathrm{W}}_{(2.47)}(\mathrm{Th_B}, 0.5)$ is the region of bistability of system (2.47) (see Remark 2.2.21).

We observe that $\log(\mathrm{Da}^{\mathrm{NW}}_{(\mathrm{H2}),(2.47)}(\mathrm{Th_B})) \approx 0$ for values smaller than $\log(\mathrm{Th_B}) \approx -2$ ($\mathrm{Th_B} \approx 0.1$). Similarly, for the particular case when $\mu(1) = 0.5$, we observe that $\log(\mathrm{Da}^{\mathrm{W}}_{(2.47)}(\mathrm{Th_B}, 0.5)) \approx \log(2)$ also for values smaller than $\log(\mathrm{Th_B}) \approx -2$ ($\mathrm{Th_B} \approx 0.1$). This comparison, performed with other reaction values $\mu(1) \in \{\frac{i}{20}\}_{i=1}^{20}$, lead to the same conclusion, and consequently, we can deduce that, if $\mathrm{Th_B} < 0.1$, the stability results obtained for the ODE and PDE systems (2.6) and (2.47) are similar. This result is consistent with the physics of the problem. Indeed, small values of $\mathrm{Th_B}$ correspond, for instance, to high diffusion coefficients implying almost spatial homogeneous biomass concentration. In this case, the dynamics in the reactor can be modeled with an ordinary differential equation cheaper to implement numerically (see Section 3.2).

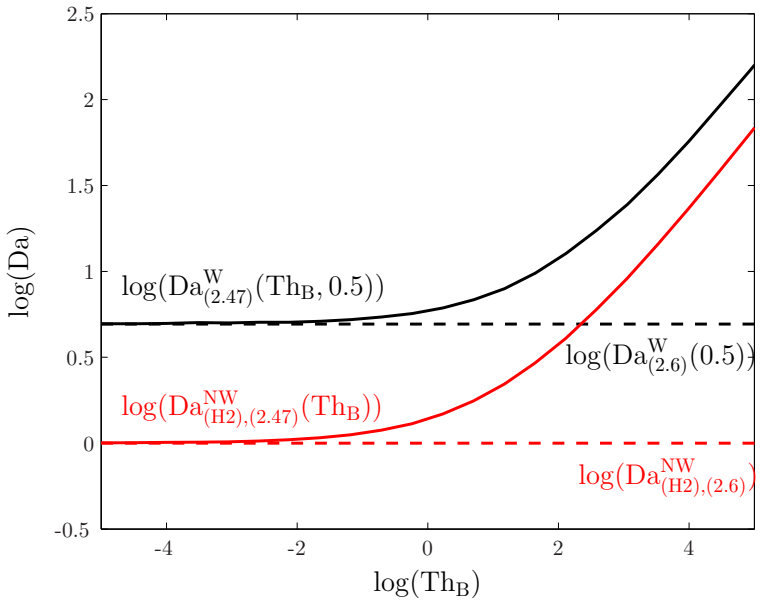

Figure 2.11: Comparison between $\log(\mathrm{Da}^{\mathrm{W}}_{(2.47)}(\mathrm{Th}_{\mathrm{B}}, 0.5))$, $\log(\mathrm{Da}^{\mathrm{NW}}_{(\mathrm{H2}),(2.47)}(\mathrm{Th}_{\mathrm{B}}))$ (depicted with solid lines) and constant values $\log(\mathrm{Da}^{\mathrm{W}}_{(2.6)}(0.5)) = \log(2)$, $\log(\mathrm{Da}^{\mathrm{NW}}_{(\mathrm{H2}),(2.6)}) = 0$ (depicted with dashed lines) when $\mathrm{Th}_{\mathrm{B}} \in [5 \cdot 10^{-3}, 1.5 \cdot 10^{2}]$.

Chapter 3

Optimization problems in Water Treatment

In this chapter, we tackle two optimization problems arising in bioreactor theory, whose objective is to decontaminate polluted water. In Section 3.1, we introduce a Hybrid Genetic Algorithm used in Sections 3.2 and 3.3 to solve two optimization problems. The problem presented in Section 3.2 aims to clean a natural water resource by using a continuous reactor, while the problem proposed in Section 3.3 aims to find an optimal shape of the bioreactor device.

3.1 Description and validation of the considered optimization method

We consider a general optimization problem of the form

$$\min_{x\in\Theta} f(x) \tag{3.1}$$

where $f : \Theta \to \mathbb{R}$ is the fitness function; x is the optimization parameter, $\Theta \subset \mathbb{R}^N$, $N \in \mathbb{N}$ is the search space. We propose to solve problem (3.1) by using a Hybrid Genetic Algorithm (HGA) based on a combination between a Genetic Algorithm (GA) (which performs a first coarse global search of the solution) and a Steepest Descent method (SD) (which performs a fine local search of the solution). Figure 3.1 illustrates the main steps followed by the considered HGA to approximate a solution of (3.1).

In Section 3.1.1, we give a detailed description of the HGA used in this work. Then, in Section 3.1.2,

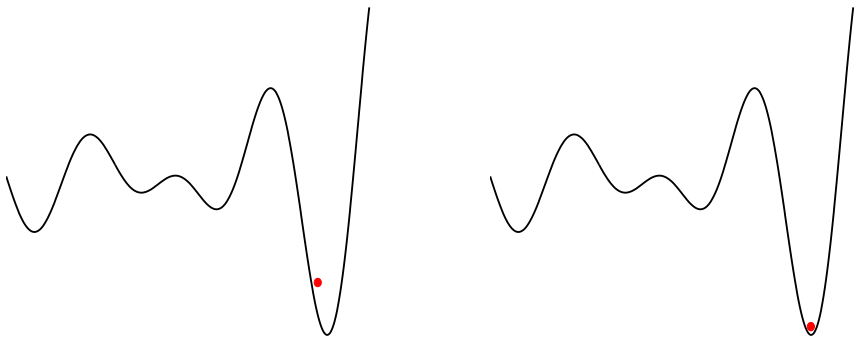

(a) Step 1: Global Search with GA (b) Step 2: Local Search with SD

Figure 3.1: Illustration of the main steps followed by the HGA when solving problem (3.1).

we present a general scheme for implementing the considered HGA. Finally, in Section 3.1.3, the HGA is validated by considering some classical benchmark problems.

3.1.1 Description of the algorithm

In this section, we detail the GA and the SD which, combined, conform the HGA used in this chapter.

Genetic Algorithm

A first family of possible solutions of the optimization problem (3.1) is randomly created in the search space Θ. We call it population and we denote it by $X^0 = \{x_j^0 = (x_{j,1}^0, \ldots, x_{j,N}^0) \in \Theta, j = 1, \ldots, N_{\mathrm{p}}\}$, where each x_j^0 is called *individual* and $N_{\mathrm{p}} \in \mathbb{N}$ is the size of the population. We call *gene* to each component $x_{j,k}^0$ of an individual, $k = 1, \ldots, N$. In our case $\Theta = \prod_{k=1}^{N}[l_k, u_k]$, where l_k and u_k are respectively the lower and upper bounds for the gene $x_{j,k}^i$.

Starting from the initial population X^0, we recursively create $N_{\mathrm{g}} \in \mathbb{N}$ new populations, which we call *generations*, by applying 4 stochastic steps, called *selection*, *crossover*, *mutation* and *elitism*, which are described below. More precisely, let $X^i = \{x_j^i \in \Theta,\ j = 1, ..., N_{\mathrm{p}}\}$ with $i = 1, ..., N_{\mathrm{g}} - 1$, denotes the population at iteration i. Thus, using the following (N_{p}, N)-real valued matrix notation

$$X^i = \begin{bmatrix} x_{1,1}^i & \cdots & x_{1,N}^i \\ \vdots & \vdots & \vdots \\ x_{N_p,1}^i & \cdots & x_{N_p,N}^i \end{bmatrix},$$

X^{i+1} is obtained by considering

$$X^{i+1} = (I_N - \mathcal{E}^i)(\mathcal{C}^i \mathcal{S}^i X^i + \mathcal{M}^i) + \mathcal{E}^i X^i \tag{3.2}$$

where matrices $\mathcal{S}^i$, $\mathcal{C}^i$, $\mathcal{M}^i$, $\mathcal{E}^i$ and I_N are described as follows.

Selection

This operator is used to select individuals according to their fitness value. There exists various selection techniques (see for instance [**?**, **?**, **?**]), among which we use the *Roulette Wheel Selection* method.

We randomly select N_{p} individuals from X^i with eventual repetitions. Each individual $x_j^i \in X^i$, with $j = 1, \ldots, N_{\mathrm{p}}$ has a probability to be selected during this process which is given by $\dfrac{f(x_j^i)^{-1}}{\sum_{j=1}^{N_{\mathrm{p}}} f(x_j^i)^{-1}}$. This step can be summarized as

$$X^{i+1,1} = \mathcal{S}^i X^i,$$

where $\mathcal{S}^i$ is a binary valued $(N_{\mathrm{p}}, N_{\mathrm{p}})$-matrix satisfying $S_{j,k}^i = 1$ if the k-th individual in X^i is the j-th selected individual, and $S_{j,k}^i = 0$ in other case.

Crossover

This operator is used to create a new individual by combining the genes of two existing individuals from the population X^i (chosen during the previous selection process). There are several methods for combining individuals (see for instance [**?**, **?**, **?**]), among which we use the *Arithmetic Crossover* method.

For each pair of consecutive individuals (rows) $2j-1$ and $2j$ in $X^{i+1,1}$, with $1 \leq j \leq \lfloor N_{\mathrm{p}}/2 \rfloor$ (where $\lfloor a \rfloor$ is the nearest integer lower than or equal to a), we determine, with a probability p_{c}, if those rows exchange data or if they are directly copied into an intermediate population denoted by $X^{i+1,2}$. Thus, matrix $\mathcal{C}^i$ is a real valued matrix of size $(N_{\mathrm{p}}, N_{\mathrm{p}})$, satisfying

$$\mathcal{C}_{2j-1,2j-1}^i = \lambda_1, \quad \mathcal{C}_{2j-1,2j}^i = 1 - \lambda_1, \quad \mathcal{C}_{2j,2j}^i = \lambda_2 \quad \text{and} \quad \mathcal{C}_{2j,2j-1}^i = 1 - \lambda_2,$$

where $\lambda_1 = \lambda_2 = 1$ with probability $1 - p_c$, or λ_1, λ_2 are randomly chosen in $(0, 1)$ considering a uniform distribution with probability p_c. Other coefficients of $\mathcal{C}^i$ are set to 0. If N_p is odd, then we also set $\mathcal{C}^i(N_p, N_p) = 1$, and then the N_p-th row of $X^{i+1,1}$ is directly copied into $X^{i+1,2}$.

Mutation

This operator randomly modifies the value of one or more genes of an individual from the population $X^{i+1,2}$ (obtained during the previous crossover process). It provides diversity in the population and intends to avoid the premature convergence phenomenon (i.e., population concentrated near a local minimum, see [**?**]). Each individual can be mutated with a probability p_m given by the user. There exists different techniques to randomly mutate individuals (see for instance [**?**, **?**]), among which we use the *Non-Uniform Mutation* method.

We decide, with a probability p_m, if each row of $X^{i+1,2}$ is randomly perturbed or not. This step is defined by

$$X^{i+1,3} = X^{i+1,2} + \mathcal{M}^i,$$

where $\mathcal{M}^i$ is a real valued matrix with size (N_p, N) and the j-th row satisfies

$$\mathcal{M}^i_j = \left\{ \begin{array}{ll} \vec{0} & \text{with probability } 1 - p_m \\ \Delta^i_j & \text{with probability } p_m \end{array} \right\}$$

and the k-th component of the vector Δ^i_j is defined as

$$\Delta^i_{j,k} = \left\{ \begin{array}{ll} (u_k - x^i_{j,k})(1 - r^{(1-\frac{i}{N_g})^\lambda}) & \text{if } \tau = 0 \\ (l_k - x^i_{j,k})(1 - r^{(1-\frac{i}{N_g})^\lambda}) & \text{if } \tau = 1 \end{array} \right.$$

where τ is a binary random number, r is a uniform random number in $[0, 1]$ and λ is a parameter given by the user, determining the degree of dependency on the iteration number. This mutation method decreases the mutation rate as the generation number increases.

Elitism

This operator ensures that at least one of the best individuals of the current generation is directly copied to the next generation. The main advantage of elitism is that a decreasing convergence is guaranteed. For more details about elitism methods see for instance [**?**, **?**].

Let x^i_b, where $b \in 1, ..., N_p$, be the individual in X^i with the lowest value of the fitness function (or, if there exists various, one of those individuals selected randomly with a uniform distribution). If x^i_b has a lower fitness value than all the individuals in $X^{i+1,3}$, it is directly copied at the b-th row of X^{i+1}. This step can be formalized as

$$X^{i+1} = (I_N - \mathcal{E}^i)(X^{i+1,3}) + \mathcal{E}^i X^i,$$

where I_N is the identity matrix of size N and $\mathcal{E}^i$ is a real-valued (N_p, N_p)-matrix such that $\mathcal{E}^i(b, b) = 1$ if x^i_b has a lower fitness value than all the individuals in $X^{i+1,3}$ and 0 otherwise, $\mathcal{E}^i = 0$ elsewhere.

Stopping Criteria for GA

At the end of each generation step, a stopping criterion is applied to determine if the GA continues to its next iteration or it is stopped. Indeed, the genetic search is terminated when N_g generations have been computed or when a user-specified criteria is satisfied. There are many types of conditions that can be used to stop the search (see for instance [**?**, **?**, **?**]), among which we use the subsequent criteria:

– *No improvement through generations*: The genetic search is terminated after a user-specified number of generations, $\hat{g}$, without improvement of the fitness value (i.e., the fitness value of the best element has not decreased).

– *Fitness threshold*: This criterion is well-suited for minimization problems for which the solution is known. The genetic search is stopped when the best fitness value of the current population is close enough to the fitness of a global minimum. If x^* is a global minimum, we consider that x is significantly close to x^* if

$$|f(x^*) - f(x)| \leq \epsilon_1 |f(x^*)| + \epsilon_2,$$

where ϵ_1 and ϵ_2 are real numbers (close to zero) chosen by the user.

When GA stops, the best individual, denoted by $x_{\text{GA,sol}}$, is returned as an output. Then, $x_{\text{GA,sol}}$ is used by the considered SD as its starting point.

Steepest Descent Method

Descent methods are used in optimization theory in order to obtain a local minimum value of functions $f \in C^1(\mathbb{R}^N, \mathbb{R})$, by choosing an appropriate descent direction ρ_k. Starting from a given $x_0 \in \mathbb{R}^N$ (in our case $x_0 = x_{\text{GA,sol}}$), the SD iteration is given by

$$x_{k+1} = x_k + \alpha_k \rho_k,$$

where the positive scalar α_k is called the step length.

The success of a descent method depends on the suitable choices of both direction ρ_k and step length α_k. Particularly, Steepest Descent method uses the descent direction $\rho_k = -\nabla f(x_{\text{k}})$. Moreover, α_k must fulfill the equation

$$f(x_k + \alpha_k \rho_k) \leq f(x_k + \alpha \rho_k), \qquad \text{for all } \alpha \geq 0.$$

This is equivalent to solve another optimization problem, given by

$$\min_{\alpha} f(x_k - \alpha \nabla f(x_k)). \tag{3.3}$$

Solving the optimization problem (3.3) could be computationally expensive. Therefore, in practice, we use a Dichotomy method in order to approximate the step length α_k (for more detailes see [**?**]).

Dichotomy method

We calculate α_k as follows:

1. We first compute $f(x_k - \alpha \nabla f(x_k))$ for $\alpha = 10^{-6}, 10^{-5}, \ldots, 10^5, 10^6$, and we choose $\bar{\alpha}$, the value of α for which the lowest fitness value is attained.

2. We compute $f(x_k - w\bar{\alpha} \nabla f(x_k))$ for $w = \frac{1}{2}, 1, 2$. Then, we choose $\bar{w}$, the value of w for which the lowest fitness value is reached.

3. If $\bar{w} = 1$, then go to Step 4, else repeat Step 2 with $\bar{\alpha} = \bar{w}\bar{\alpha}$.

4. Return $\alpha_k = \bar{w}\bar{\alpha}$ as the output.

Stopping Criteria for SD

At the end of each SD step, we apply a stopping condition to determine if we continue or stop the algorithm. There exists different methods to stop the search (see for instance [**?**, **?**, **?**]), among which we use the following two criteria:

– *Maximum number of iterations*: The descent method is terminated when a maximum number of iterations, N_{it}, is reached.

– *Fitness convergence*: The descent method is terminated when the fitness value does not decrease significantly over two successive iterations. More precisely, the SD stops if

$$|f(x^{i+1,*})| \geq \tau |f(x^{i,*})|,$$

where τ is a user-specified real number between 0 and 1.

– *Fitness threshold*: defined as in the GA description.

When SD stops, the individual of the last iteration, denoted by x_{sol}, is returned as the output and is considered as an approximated solution of problem (3.1).

3.1.2 Implementation of HGA

We have implemented the Hybrid Genetic Algorithm in MATLAB script language, following the pseudo-code presented below:

Inputs
- N_{g} (*natural*): Number of generations.
- N_{p} (*natural*): Size of the population for each generation.
- p_{c} (*float*): Crossover probability.
- p_{m} (*float*): Mutation probability.
- l (*float*): Vector of length N corresponding to the lower bounds of our variable.
- u (*float*): Vector of length N corresponding to the upper bounds of our variable.
- $f_{\min}$ (*float*): Fitness of the global minimum (in the case it is known beforehand).

Outputs
- x_{sol} (*float*): Vector of length N, approximated solution of the minimization problem (3.1).
- $f(x_{\text{sol}})$ (*float*): Fitness value of x_{sol}.

Pseudo-Code

```
% We perform a global search with GA
 call INITIAL_SOLUTIONS          % We randomly create an initial population X = X^0 ∈ Θ.
 call FITNESS_EVALUATION         % We calculate f(X)

 Repeat (Loop 1)
       call THREE_STEPS_GENETIC  % Starting from X, we obtain X' following the
                                   three stochastic processes below
            call SELECTION
            call CROSSOVER
            call MUTATION

       call FITNESS_EVALUATION   % We calculate f(X')
       call ELITISM              % We calculate X'' by applying the elitism process
                                   to X'
       X = X''                   % We update the population
until GA stopping criteria (end Loop1)
x_GA,sol                         % Output of the global search with GA

% We perform a local refinement with SD
x = x_GA,sol                     % We start SD with the solution returned by GA
```

```
Repeat (Loop 2)
       call GRADIENT            % We calculate the value of ∇f(x)
       call DICHOTOMY           % We calculate α
       x = x − α∇f(x)           % We update the solution
until SD stopping criteria (end Loop2)
x_sol , f(x_sol)                % Output of the local refinement with SD
```

3.1.3 Validation

In order to validate the efficiency of the considered HGA we study its behavior with some benchmark functions, available in literature (see, for instance, [**?**]). The global minima of these functions is known and they present some difficulties found in many optimization problems, such as: the existence of various local minima, flat fitness function, high oscillations, etc. Among the multiple classes of test functions found in literature (one dimensional / multidimensional, convex / nonconvex, etc.) we choose 8 representative benchmark functions, detailed below. Note that some of the proposed functions (except the *Branin* and the *Zakharov* functions) exhibit several local minima.

- **Branin function**

$$f(x) = (x_2 - \frac{5}{4\pi^2}x_1^2 + \frac{1}{\pi}5x_1 - 6)^2 + 10(1 - \frac{1}{8\pi})\cos(x_1) + 10, \qquad x \in [-5, 15]^2.$$

  Its minimum $f_{\min} = 0.397887$ is reached at points $(-\pi, 12.275)$, $(\pi, 2.275)$ and $(9.42478, 2.475)$. A two-dimensional representation of this function depicted in Figure 3.2-(a).

- **Easom function**

$$f(x) = -\cos(x_1)\cos(x_2) = e^{-(x_1-\pi)^2-(x_2-\pi)^2}, \qquad x \in [-100, 100]^2.$$

  Its minimum $f_{\min} = -1$ is reached at $(-\pi, \pi)$. A two-dimensional representation of this function is depicted in Figure 3.2-(b).

- **Goldstein and Price function**

$$f(x) = \begin{array}{l}\big(1 + (x_1 + x_2 + 1)^2(19 - 14x_1 + 3x_1^2 - 14x_2 + 6x_1x_2 + 3x_2^2)\big) \\ \cdot\big(30 + (2x_1 - 3x_2)^2(18 - 32x_1 + 12x_1^2 + 48x_2 - 36x_1x_2 + 27x_2^2)\big),\end{array} \qquad x \in [-2, 2]^2.$$

  Its minimum $f_{\min} = 3$ is reached at $(0, -1)$. A two-dimensional representation of this function is depicted in Figure 3.2-(c).

- **Shubert function**

$$f(x) = \big(\sum_{i=1}^{5} i\cos((i+1)x_1 + i)\big)\big(\sum_{i=1}^{5} i\cos((i+1)x_2 + i)\big), \qquad x \in [-10, 10]^2.$$

  Its minimum $f_{\min} = -186.7309$ is reached at 18 global minima points. A two-dimensional representation of this function is depicted in Figure 3.2-(d).

- **Hartmann-3 function**

$$f(x) = -\sum_{i=1}^{4} \alpha_i \mathrm{e}^{-\sum_{j=1}^{3} A_{ij}^{(3)}(x_j - P_{ij}^{(3)})^2}, \qquad x \in [0, 1]^3,$$

where

$$\alpha = [1, 1.2, 3, 3.2]^T, \quad A^{(3)} = \begin{bmatrix} 3.0 & 10 & 30 \\ 0.1 & 10 & 35 \\ 3.0 & 10 & 30 \\ 0.1 & 10 & 35 \end{bmatrix} \text{ and } P^{(3)} = 10^{-4} \begin{bmatrix} 6890 & 1170 & 2673 \\ 4699 & 4387 & 7470 \\ 1091 & 8732 & 5547 \\ 381 & 5743 & 8838 \end{bmatrix}.$$

Its minimum $f_{\min} = -3.8627$ is reached at $(0.114614, 0.555649, 0.852547)$.

- **Rosenbrock function**

$$f(x) = (\sum_{j=1}^{n-1} \big(100(x_j^2 - x_{j+1})^2 + (x_j - 1)^2\big), \quad , x \in [-10, 10]^n.$$

Its minimum $f_{\min} = 0$ is reached at $(1, \ldots, 1)$. A two-dimensional representation of this function is depicted in Figure 3.2-(e).

- **Shekel function**

$$f(x) = -\sum_{j=1}^{m} \big(\sum_{i=1}^{4} (x_i - a_{ij})^2 + c_i\big)^{-1}, \quad x \in [0, 10]^4,$$

where $c = [0.1, 0.2, 0.2, 0.4, 0.4, 0.6, 0.3, 0.7, 0.5, 0.5]$ and

$$a = \begin{bmatrix} 4.0 & 1.0 & 8.0 & 6.0 & 3.0 & 2.0 & 5.0 & 8.0 & 6.0 & 7.0 \\ 4.0 & 1.0 & 8.0 & 6.0 & 7.0 & 9.0 & 5.0 & 1.0 & 2.0 & 3.6 \\ 4.0 & 1.0 & 8.0 & 6.0 & 3.0 & 2.0 & 5.0 & 8.0 & 6.0 & 7.0 \\ 4.0 & 1.0 & 8.0 & 6.0 & 7.0 & 9.0 & 5.0 & 1.0 & 2.0 & 3.6 \end{bmatrix}.$$

Its minimum $f_{\min}$ depends on the value of $m \in \mathbb{N}$ (for instance $f_{\min} = -10.153195380$ if $m = 5$ and $f_{\min} = -10.40281868$ if $m = 7$) and is reached at $(4, 4, 4, 4)$.

- **Zakharov function**

$$f(x) = \sum_{i=1}^{n} x_i^2 + (\sum_{i=1}^{n} 0.5 i x_i)^2 + (\sum_{i=1}^{n} 0.5 i x_i)^4, \quad x \in [-5, 10]^n.$$

Its minimum $f_{\min} = 0$ is reached at $(0, \ldots, 0)$. A two-dimensional representation of this function is depicted in Figure 3.2-(f).

For numerical experiments, we have chosen the GA and SD parameters following [**?**]. More precisely, we use $N_g = N_p = 100$, $p_c = 0.4$, $\lambda = 1$ and $p_m = 0.2$. When validating the HGA, since for the considered benchmark functions the global minimum is known, we use the *Fitness threshold* stopping criterion with $\epsilon_1 = 10^{-2}$ and $\epsilon_2 = 10^{-3}$ for GA and a combination of the *Maximum number of iterations* and *Fitness convergence* criteria (with $N_{it} = 100$ and $\tau = 0.99$, respectively) for SD.

In order to validate our results, we compare the convergence success with the MATLAB genetic algorithm function *ga*, denoted by MGA. For *ga* documentation see
`http://www.mathworks.com/discovery/geneticalgorithm.html`. We consider the same processes and parameters values than for our HGA .
The comparison can be seen in Table 3.1, where the number of function evaluations is also compared.
In the case of the benchmarks *Branin*, *Easom*, *Goldstein Price*, *Schubert*, *Hartmann -3*, *Rosenbrock-2* and *Zakharov-5* both algorithms converge, and the number of function evaluations is comparable. Benchmark *Shekel-5* does not converge with MGA, but converge with HGA. Regarding those results, we conclude that the presented Hybrid Genetic Algorithm (HGA) works as least as well than the MGA, improving it in some cases. This algorithm will be used in next sections to solve some particular optimization problems.

Function	Convergence HGA	Convergence MGA	Evaluations HGA	Evaluations MGA
Branin	Yes	Yes	1926	2056
Easom	Yes	Yes	5237	2133
Goldstein Price	Yes	Yes	4433	4293
Shubert	Yes	Yes	8167	7393
Hartmann 3	Yes	Yes	3863	6073
Rosenbrock 2	Yes	Yes	33760	2783
Shekel 5	Yes	No	260257	-
Zakharov 5	Yes	Yes	5002	3766

Table 3.1: Comparison between HGA and MGA using some benchmarks.

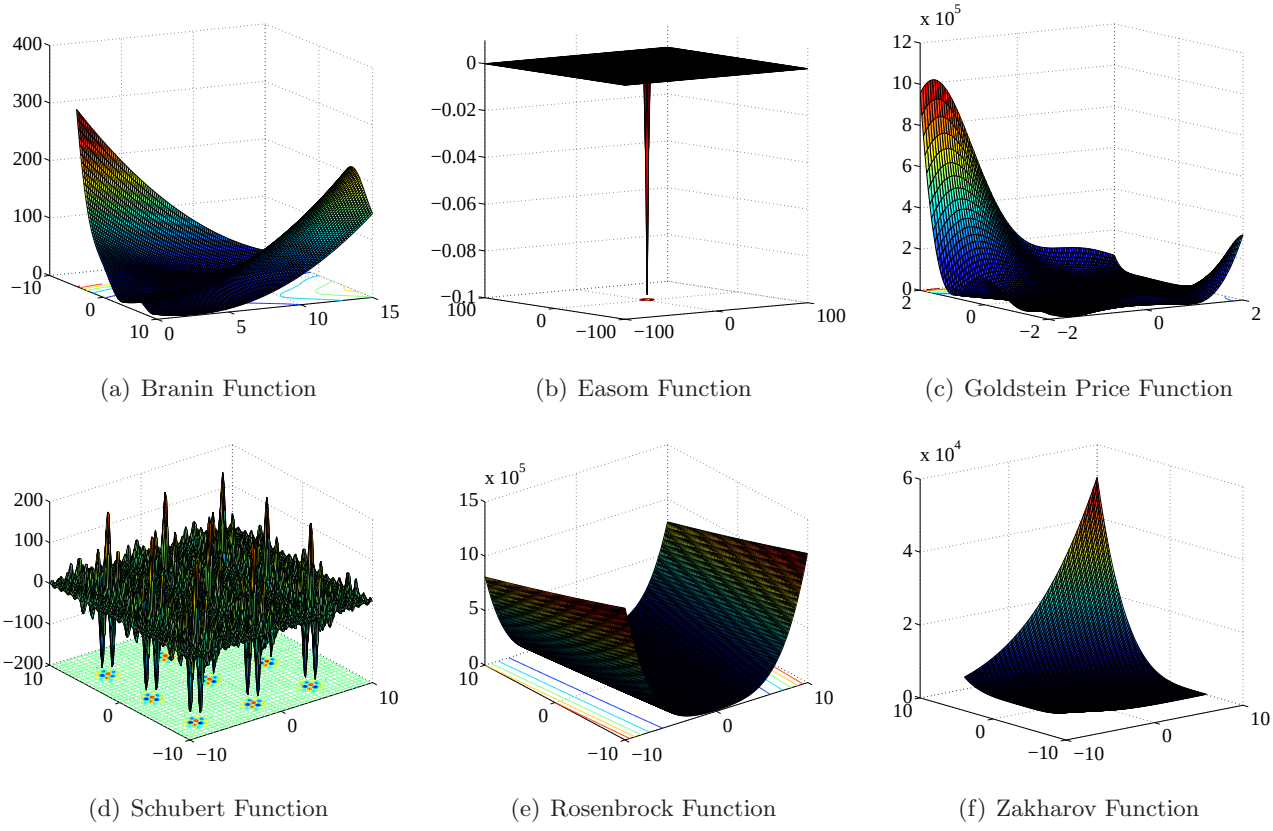

(a) Branin Function (b) Easom Function (c) Goldstein Price Function

(d) Schubert Function (e) Rosenbrock Function (f) Zakharov Function

Figure 3.2: Benchmarck Functions

3.2 Bioremediation of natural water resources

Following [**?**], we consider a natural resource polluted with a substrate concentration S_r. The objective of the treatment is to decrease S_r, as fast as possible, to a target value S_{lim}, with the help of a bioreactor. The bioreactor is fed from the resource with a volumetric flow rate Q, and its output returns to the resource with the same flow rate Q (we implicitly assume that the impact of the volume of the collected biomass on the flow rate is negligible), after separation of biomass in a settler (see Figure 3.3). We study optimal and suboptimal control strategies for the treatment of the polluted water resource by choosing the inlet volumetric flow rate Q. We analyze the influence of inhomogeneities of concentrations in the bioreactor (due for instance to diffusion and flow motions) on the optimization results.

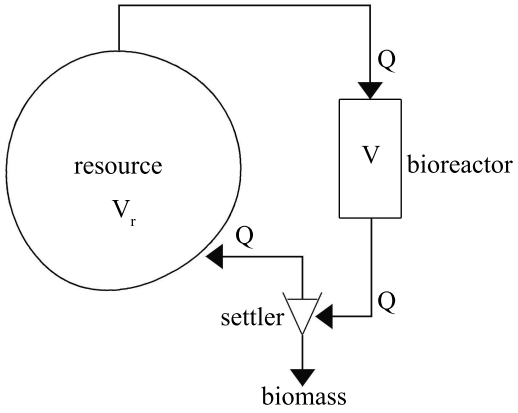

Figure 3.3: Connection of the bioreactor with the resource

3.2.1 Mathematical modeling

In this section, we detail the mathematical models used to describe the dynamics of the bioreactor and the water resource. More precisely, we present an ODE system under the assumption of uniform concentration of contaminant in the resource. We justify such an assumption for very large resource volumes for which the treatment takes long time. The output flow Q induces then a very small dilution rate of the contaminant in the resource compared to the diffusion of the contaminant, that maintains an (almost) homogeneous distribution in the resource. As the bioreactor volume is much smaller, the induced advection could make the assumption of homogeneous concentrations inside the bioreactor, questionable depending on the process characteristics (reactor shape, agitation, diffusivity...). When describing the dynamics of the bioreactor we use models (2.1) and (2.11), presented respectively in Sections 2.1.1 and 2.2.1.

Water resource model

Since we assume homogeneous distribution of substrate in the water resource, its dynamics can be described as follows [**?**]:

$$\begin{cases} \dfrac{\mathrm{d}S_{\mathrm{r}}}{\mathrm{d}t}(t) = \dfrac{Q(t)}{V_{\mathrm{r}}}(S_{\mathrm{out}}(t) - S_{\mathrm{r}}(t)) \qquad t > 0, \\ \\ S_{\mathrm{r}}(0) = S_{\mathrm{r},0}, \end{cases} \tag{3.4}$$

where S_{r} (kg/m^3) is the concentration of substrate in the water resource; V_{r} (m^3) is the water resource volume; Q (m^3/s) is the volumetric flow rate and S_{out} (kg/m^3) denotes the concentration of substrate at the outlet of the bioreactor, which is calculated differently depending on the mathematical modeling considered for the bioreactor (see more details below).
The explicit solution of (3.4) is

$$S_{\mathrm{r}}(t) = \mathrm{e}^{-\int_0^t \frac{Q(s)}{V_{\mathrm{r}}}\mathrm{d}s}\left(\int_0^t \frac{Q(s)}{V_{\mathrm{r}}} S_{\mathrm{out}}(s)\mathrm{e}^{\int_0^s \frac{Q(\tau)}{V_{\mathrm{r}}}\mathrm{d}\tau}\mathrm{d}s + S_{\mathrm{r},0}\right). \tag{3.5}$$

In order to obtain a characteristic time scale for system (3.4), we non-dimensionalize it by setting

$$\hat{S}_{\mathrm{r}} = \frac{S_{\mathrm{r}}}{s}, \qquad \hat{S}_{\mathrm{out}} = \frac{S_{\mathrm{out}}}{o}, \qquad \hat{t} = \frac{t}{\tau_{\mathrm{r}}}, \qquad \hat{Q} = \frac{Q}{\gamma},$$

where s, o, τ and γ are suitable scales. Proceeding as in Section 2.1.3, we set $s = o = S_{\mathrm{r},0}$ and $\gamma = \frac{Q}{V\|\mu\|_{L^\infty(\mathbb{R})}}$ is chosen, so that $\tau_{\mathrm{r}} = \frac{V_{\mathrm{r}}}{V\|\mu\|_{L^\infty(\mathbb{R})}}$. This time scale will be used below in order to compare it with the

obtained characteristic time scales for the bioreactor. System (3.4) in non-dimensional form is therefore given by

$$\begin{cases} \dfrac{\mathrm{d}\hat{S}_\mathrm{r}}{\mathrm{d}\hat{t}} = \hat{Q}(\hat{t})(\hat{S}_\mathrm{out}(\hat{t}) - \hat{S}_\mathrm{r}(\hat{t})) \qquad \hat{t} > 0, \\ \\ \hat{S}_\mathrm{r}(0) = 1. \end{cases} \tag{3.6}$$

Notice that the numerical experiments performed in Section 3.2.3 consider the model with dimensions (i.e., model (3.4)) since it provides a more intuitive description of the processes occurring in the water resource.

Bioreactor Models

Following Chapter 2, we assume that the behaviour of the substrate and biomass concentrations in the considered reactor is described either with system (2.1) or with system (2.11). In both systems, we assume that the growth rate function μ fulfills assumption (H1).

Well-mixed bioreactor

In order to couple systems (2.1) and (3.4), we proceed as follows

- We set $S_\mathrm{e}(t) = S_\mathrm{r}(t)$ in system (2.1) (i.e., the substrate concentration in the reactor inlet at time t corresponds to the water resource concentration at time t).
- We set $S_\mathrm{out}(t)$ in system (3.4) following the reasoning below:
  The nondimensional analysis of systems (2.1) (see Section 2.1.3) and (3.4) provides us with a time scale for the bioreactor, $\tau = \frac{1}{\|\mu\|_{L^\infty(\mathbb{R})}}$ and for the water resource, $\tau_\mathrm{r} = \frac{V_r}{V}\tau$. Since a reasonable hypothesis is to assume that the volume of the resource is much larger than that of the bioreactor, i.e., $V_\mathrm{r} \gg V$, one has that $\tau_\mathrm{r} \gg \tau$. This implies that the dynamics of (2.1) is faster than that of (3.4), i.e., for a reasonable process time for the bioreactor, the changes in the entering substrate and the fluid flow velocity are negligible (therefore, they can be treated as constants) and one can make the quasi-steady state approximation, setting

  $$S_\mathrm{out}(t) = S^\mathrm{qs}(Q(t)) \tag{3.7}$$

  in system (3.4), where $S^\mathrm{qs}(Q(t))$ denotes the steady state of system (2.1) fulfilling

  $$Q(t) = V\mu(S^\mathrm{qs}(Q(t))),$$

  which is asymptotically stable if $Q(t) < V\mu(S_\mathrm{r}(t))$ (see Section 2.1.4 for more details on the stability analysis of system (2.1)).

We point out that the hypothesis $Q(t) < V\mu(S_\mathrm{r}(t))$ can be rewritten as $S^\mathrm{qs}(Q(t)) \in [0, S_\mathrm{r}(t))$. We observe that, when $\tau_\mathrm{r} \gg \tau$, the model given by (2.1),(3.4) is not needed and we can use (3.4),(3.7) instead. Furthermore, according to (3.5), when Q is constant the explicit solution of system (3.4),(3.7) is given by

$$S_\mathrm{r}(t) = S^\mathrm{qs}(Q) + (S_{\mathrm{r},0} - S^\mathrm{qs}(Q))\mathrm{e}^{-\frac{V}{V_\mathrm{r}}\mu(S^\mathrm{qs}(Q))t}. \tag{3.8}$$

Remark 3.2.1. *Since the mapping $Q \to S^\mathrm{qs}(Q)$ given by $Q = V\mu(S^\mathrm{qs}(Q))$ is a bijection from $[0, +\infty)$ to $[0, V\|\mu\|_{L^\infty(\mathbb{R})})$ we can use as the ODE model for the water resource*

$$\begin{cases} \frac{\mathrm{d}S_\mathrm{r}}{\mathrm{d}t}(t) = \frac{Q}{V_\mathrm{r}}(\mu^{-1}(\frac{Q}{V}) - S_\mathrm{r}(t)) \qquad t > 0, \\ \\ S_\mathrm{r}(0) = S_{\mathrm{r},0}, \end{cases} \tag{3.9}$$

or, equivalently

$$\begin{cases} \frac{\mathrm{d}S_\mathrm{r}}{\mathrm{d}t}(t) = \frac{V}{V_\mathrm{r}}\mu(S^\mathrm{qs})(S^\mathrm{qs} - S_\mathrm{r}(t)) \qquad t > 0, \\ \\ S_\mathrm{r}(0) = S_{\mathrm{r},0}. \end{cases} \tag{3.10}$$

Due to the bijection mentioned above we will use the notation $Q = Q(S^\mathrm{qs})$ and $S^\mathrm{qs} = S^\mathrm{qs}(Q)$. Giving a function S^qs is equivalent to give a function Q, and viceversa.

Unmixed bioreactor

In order to couple systems (2.11) and (3.4) we proceed as follows:

- We set $S_\mathrm{e}(t) = S_\mathrm{r}(t)$ at the boundary condition Γ_in, for S, in system (2.11) (i.e., the substrate concentration in the reactor inlet at time t corresponds to the water resource concentration at time t).
- We set $S_\mathrm{out}(t)$ in system (3.4) following the reasoning below:
  Taking into account that both substrate concentration and outlet flow velocity at the reactor may depend on the position of the exiting particle, we consider an average value of the exiting substrate concentration weighted by the flow velocity, computed as

$$S_\mathrm{out}(t) = \frac{\int_0^{2\pi}\int_0^L ru(r,0,t)S(r,0,t)\,\mathrm{d}r\mathrm{d}\theta}{\int_0^{2\pi}\int_0^L ru(r,0,t)\,\mathrm{d}r\mathrm{d}\theta} = \frac{\int_0^L ru(r,0,t)S(r,0,t)\,\mathrm{d}r}{\int_0^L ru(r,0,t)\,\mathrm{d}r}. \tag{3.11}$$

  We consider two types of flow velocity fields, which do not change along the z-axis

  - Homogeneous flow velocity field: As a first approach, we consider that the flow velocity field is as in (2.9), where

$$u(r,z,t) = u(t) = Q(t)/A, \tag{3.12}$$

    Q (m^3/s) being the volumetric flow rate in model (3.4) and A (m^2) is the area of the basis of the cylinder, i.e., $A = \pi L^2$. In this case, $S_\mathrm{out}(t) = \frac{2}{L^2}\int_0^L rS(r,0,t)\mathrm{d}r$.
  - Ellipsoidal flow velocity field: As a second approach, we consider that the flow velocity field has the shape of an ellipsoid of revolution, which is classical in Fluid Dynamics (see, for instance [**?**]) and more realistic than the previous homogeneous flow velocity profile. More precisely, the flow velocity field is as in (2.9), where $u(r,z,t) = u(r,t) = -C(t)\sqrt{L^2 - r^2}$, and $C(t)$ chosen so that the volume covered by half of the ellipsoid of revolution is equal to $Q(t)$ (m^3/s). Since the volume generated is $v = C(t)\frac{2}{3}\pi L^3$, we conclude that $C(t) = \frac{3Q(t)}{2\pi L^3}$ and thus

$$u(r,z,t) = u(r,t) = \frac{3Q(t)}{2\pi L^3}\sqrt{L^2 - r^2}. \tag{3.13}$$

    In this case, $S_\mathrm{out}(t) = \frac{3}{L^3}\int_0^L r\sqrt{L^2 - r^2}S(r,0,t)\mathrm{d}r$.

The nondimensional analysis of systems (2.11) (see Section 2.2.3) and (3.4) provides us with a time scale for the bioreactor,

$$\tau = \max\Big(\frac{H^2}{D_\mathrm{S}}, \frac{H^2}{D_\mathrm{B}}, \frac{H}{\|u\|_{L^\infty(\bar\Omega\times(0,T))}}, \frac{1}{\|\mu\|_{L^\infty(\mathbb{R})}}\Big) \tag{3.14}$$

and for the water resource, $\tau_\mathrm{r} = \frac{V_\mathrm{r}}{V\|\mu\|_{L^\infty(\mathbb{R})}}$. For the cases where $\tau_\mathrm{r} \gg \tau$, one can consider that the dynamics of (2.11) is faster than that of (3.4). Consequently, when dealing with time intervals of the order of τ_r, we

consider that the bioreactor is in quasi-steady state. Under this hypothesis, the solution of system (2.11) can be changed, at each time $t \in (0, +\infty)$, by its limit when $t \to \infty$, which is a solution of

$$\begin{cases} \frac{1}{r}\frac{\partial}{\partial r}(rD_{\mathrm{S}}\frac{\partial S^{\mathrm{qs}}}{\partial r}) + \frac{\partial}{\partial z}(D_{\mathrm{S}}\frac{\partial S^{\mathrm{qs}}}{\partial z}) - u\frac{\partial S^{\mathrm{qs}}}{\partial z} = \mu(S^{\mathrm{qs}})B^{\mathrm{qs}} & \text{in } \Omega, \\ \frac{1}{r}\frac{\partial}{\partial r}(rD_{\mathrm{B}}\frac{\partial B^{\mathrm{qs}}}{\partial r}) + \frac{\partial}{\partial z}(D_{\mathrm{B}}\frac{\partial B^{\mathrm{qs}}}{\partial z}) - u\frac{\partial B^{\mathrm{qs}}}{\partial z} = -\mu(S^{\mathrm{qs}})B^{\mathrm{qs}} & \text{in } \Omega, \\ D_{\mathrm{S}}\frac{\partial S^{\mathrm{qs}}}{\partial z} - uS^{\mathrm{qs}} = -uS_{\mathrm{r}} & \text{in } \Gamma_{\mathrm{in}}, \\ D_{\mathrm{B}}\frac{\partial B^{\mathrm{qs}}}{\partial z} - uB^{\mathrm{qs}} = 0 & \text{in } \Gamma_{\mathrm{in}}, \\ \frac{\partial S^{\mathrm{qs}}}{\partial r} = \frac{\partial B^{\mathrm{qs}}}{\partial r} = 0 & \text{in } \Gamma_{\mathrm{wall}} \cup \Gamma_{\mathrm{sym}}, \\ \frac{\partial S^{\mathrm{qs}}}{\partial z} = \frac{\partial B^{\mathrm{qs}}}{\partial z} = 0 & \text{in } \Gamma_{\mathrm{out}}, \end{cases} \tag{3.15}$$

where $u(\cdot, t)$ and $S_{\mathrm{r}}(t)$ are time dependent and $(S^{\mathrm{qs}}(r, z, t), B^{\mathrm{qs}}(r, z, t))$ (kg/m^3) are the substrate and biomass concentrations of the bioreactor in quasi-steady state, respectively.

Remark 3.2.2. *A usual way to find numerically stable stationary solutions of* (2.11) *satisfying the nonlinear system* (3.15) *is to solve numerically* (2.11) *and then take the solution corresponding to large values of* t *as solution of* (3.15) *(see [**?**]). Therefore, in the following, we consider and solve system* (2.11),(3.4),(3.11)*, also for the cases where* $\tau \ll \tau_{\mathrm{r}}$*. As a representative example, we have computed numerically the solution of systems* (2.11) *and* (3.15) *by using the solver COMSOL Multyphisics 5.0 (*`www.comsol.com`*) (using, respectively, the Time Dependent and Stationary Studies options for that software) and the model parameters* $D_{\mathrm{S}}, D_{\mathrm{B}}, H, L, \mu_{\max}, K_{\mathrm{S}}$ *proposed in Section 3.2.3. Moreover,* u *(m/s) has been taken of the form* (3.13) *(with* $Q = 0.25$*) and the values* S_{e} *in* (2.11) *and* S_{r} *in* (3.15) *have been set to* 10 *(kg/m*^{3}*). Finally, when solving system* (2.11)*, we have used the initial conditions* $S_{\mathrm{init}} = 10$ *(kg/m*^{3}*),* $B_{\mathrm{init}} = 0.5$ *(kg/m*^{3}*) and final time* $T = 100$ *(s). Notice that, with those model parameters,* $\tau \approx 46$ *(see* (3.14)*), and so, at final time* $T = 100$*, the solution of system* (2.11) *should be numerically close enough to a stable solution of system* (3.15)*. Figures 3.4 and 3.5 plot the final substrate and biomass concentrations obtained with this procedure. Furthermore, in order to quantify the difference between both solutions we have chosen a set of points* $\{(r_i, z_j)\}_{i,j=1}^{70}$*, with* $r_i = \frac{(i-1)}{69}L$ *and* $z_j = \frac{(j-1)}{69}H$*, and computed the value of the substrate and the biomass concentrations at these points. Thus, denoting* $(S_{i,j}^{\mathrm{TDEP}}, B_{i,j}^{\mathrm{TDEP}})$ *(respectively,* $(S_{i,j}^{\mathrm{STAT}}, B_{i,j}^{\mathrm{STAT}})$*), the solution of system* (2.11) *at final time* $T = 100$ *(s) (respectively, system* (3.15)*) evaluated at point* (r_i, z_j)*, we quantify the relative error between both solutions as*

$$\mathrm{E_S} = 100\frac{\left(\sum_{i,j=1}^{70}(S_{i,j}^{\mathrm{TDEP}} - S_{i,j}^{\mathrm{STAT}})^2\right)^{\frac{1}{2}}}{\left(\sum_{i,j=1}^{70}(S_{i,j}^{\mathrm{STAT}})^2\right)^{\frac{1}{2}}} = 5.12 \cdot 10^{-4},$$

$$\mathrm{E_B} = 100\frac{\left(\sum_{i,j=1}^{70}(B_{i,j}^{\mathrm{TDEP}} - B_{i,j}^{\mathrm{STAT}})^2\right)^{\frac{1}{2}}}{\left(\sum_{i,j=1}^{70}(B_{i,j}^{\mathrm{STAT}})^2\right)^{\frac{1}{2}}} = 5.92 \cdot 10^{-4}.$$

From Figures 3.4 and 3.5 and the values of $\mathrm{E_S}$ *and* $\mathrm{E_B}$*, we conclude that, for this particular case, the solution of system* (2.11) *seems to be an accurate approximation of the solution of system* (3.15)*.*

If the flow velocity field is taken as in (3.12) (i.e., $u(t) = \frac{Q(t)}{\pi L^2}$), we can apply the stability results obtained in Section 2.2.4. In this case, a sufficient condition assuring that the *washout* (see Definition 3.2.3) is an unstable equilibrium of system (2.11) is that

$$Q(t) < Q^{\mathrm{NW}}(L, H, D_{\mathrm{B}}, \mu(S_{\mathrm{r}}(t))) := \frac{u^{\mathrm{NW}}_{(\mathrm{H1}),(2.11)}(H, D_{\mathrm{B}}, \mu(S_{\mathrm{r}}(t)))}{\pi L^2}. \tag{3.16}$$

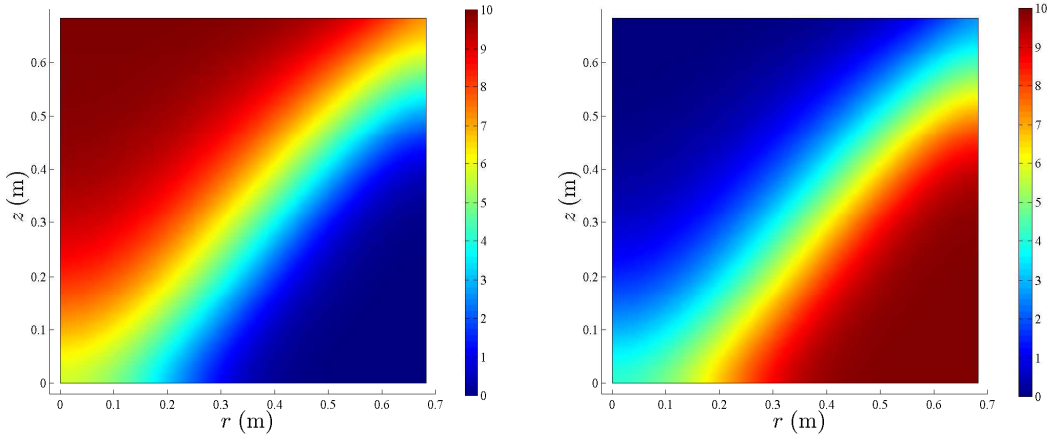

(a) Substrate concentration (kg/m^3) (b) Biomass concentration (kg/m^3)

Figure 3.4: Solution of system (2.11) obtained by considering: $H = L = 0.68$ (m), $D_{\mathrm{B}} = D_{\mathrm{S}} = 0.01$ (m^2/s), $S_{\mathrm{e}} = 10$ (kg/m^3), u (m/s) has been taken as in (3.13) (with $Q = 0.25$), μ is the Monod function (see (2.2)) with $\mu_{\max} = 1$ (1/s) and $K_{\mathrm{S}} = 1$ (kg/m^3), $S_{\mathrm{init}} = 10$ (kg/m^3), $B_{\mathrm{init}} = 0.5$ (kg/m^3) and $T = 100$ (s).

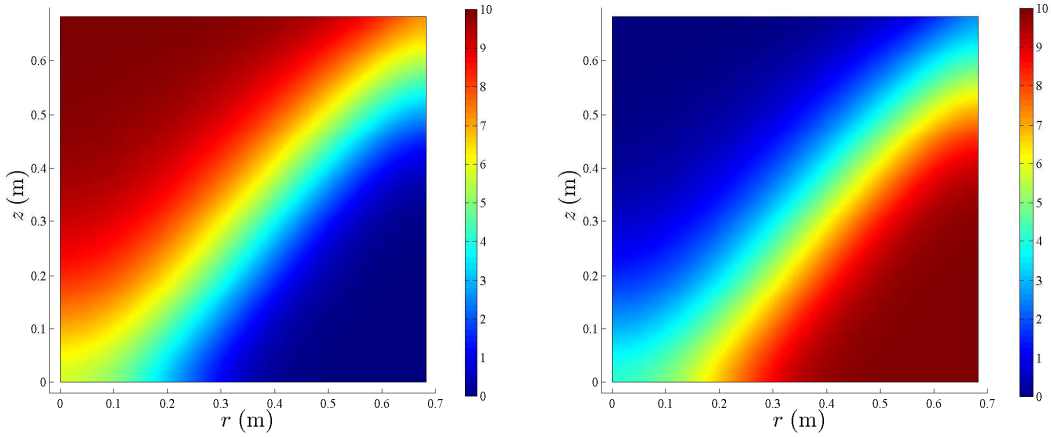

(a) Substrate concentration (kg/m^3) (b) Biomass concentration (kg/m^3)

Figure 3.5: Solution of system (3.15) obtained by considering: $H = L = 0.68$ (m), $D_{\mathrm{B}} = D_{\mathrm{S}} = 0.01$ (m^2/s), $S_{\mathrm{r}} = 10$ (kg/m^3), u (m/s) has been taken as in (3.13) (with $Q = 0.25$), and μ is the Monod function (see (2.2)) with $\mu_{\max} = 1$ (1/s) and $K_{\mathrm{S}} = 1$ (kg/m^3).

Furthermore, if the flow profile is nonhomogeneous, the liquid located at the reactor center could be ejected faster than if we use the homogeneous profile. In this context, flow rates smaller than those that are suitable for the homogeneous case, are required to ensure that the substrate and biomass react in the whole tank (see Remark 3.2.17). Thus, one can conclude that, if u is taken as in (3.13) and $Q(t) > Q^{\mathrm{NW}}(L, H, D_{\mathrm{B}}, \mu(S_{\mathrm{r}}(t)))$, then the washout phenomena (see Definition (3.2.3)) is produced in system (2.11).

Definition 3.2.3. *We recall that the washout is the bioreactor equilibrium with no biomass (see Sections 2.1.4 and 2.2.4 for more details of the stability analysis of systems* (2.1) *and* (2.11)*, respectively).*

3.2.2 Optimization problem

We consider the optimization problem consisting in making decrease the substrate concentration of the water resource, to a prescribed value $S_{\lim} > 0$ (kg/m^3), in a minimal amount of time by choosing a suitable control strategy for the input variable Q.

Definition 3.2.4. *We denote by Σ_0 and Σ the initial state and the state at an arbitrary time, respectively. Therefore, when considering system (3.9) $\Sigma_0 = S_{\mathrm{r},0}$ and $\Sigma = S_{\mathrm{r}} \in [0, +\infty)$; and when considering system (2.11),(3.4),(3.11) we have $\Sigma_0 = (S_{\mathrm{r},0}, S_0, B_0)$ and $\Sigma = (S_{\mathrm{r}}, S, B) \in [0, +\infty) \times (L^\infty(\Omega))^2$.*

Definition 3.2.5.

1. *For each initial state Σ_0 we consider the set of admissible time-dependent control functions given by $\mathcal{Q}^{\mathrm{OL}} = \{Q : [0, +\infty) \to [0, +\infty)$ Lebesgue measurable such that $Q(0) < V\mu(S_{\mathrm{r},0})$ (resp. $Q(0) < Q^{\mathrm{NW}}(L, H, D_{\mathrm{B}}, \mu(S_{\mathrm{r},0}))$), where $S_{\mathrm{r},0}$ is initial state of system (3.9) (resp. of system (3.4) coupled with (2.11),(3.11))$\}$. A function $Q(\cdot) \in \mathcal{Q}^{OL}$ is called an open loop-control and in the following is denoted by Q^{OL}.*

2. *We consider the set of admissible state-dependent control functions given by $\mathcal{Q}^{\mathrm{FB}} = \{Q : [0, +\infty) \to [0, +\infty)$ (resp. $Q : [0, +\infty) \times (L^\infty(\Omega))^2 \to [0, +\infty)$) such that system (3.9) (resp. (2.11),(3.4),(3.11)) admits a unique absolutely continuous solution for any initial condition Σ_0 and $Q(\Sigma) < V\mu(S_{\mathrm{r}})$ (resp. $Q(\Sigma) < Q^{\mathrm{NW}}(L, H, D_{\mathrm{B}}, \mu(S_{\mathrm{r}}))$) $\}$. A functional $Q \in \mathcal{Q}^{FB}$ is called a feedback control and in the following is denoted by Q^{FB}. †*

Remark 3.2.6. *A particular case of open-loop is when Q is constant, which in the following will be denoted by Q^{C}. For each initial state Σ_0 we consider the set of admissible constant control functions given by $\mathcal{Q}^C = \{Q : [0, +\infty) \to [0, +\infty) : Q(t) \equiv c$ with $c \in [0, V\mu(S_{\mathrm{r},0}))$ in system (3.9) (resp. $c \in [0, Q^{\mathrm{NW}}(L, H, D_{\mathrm{B}}, \mu(S_{\mathrm{r},0})))$ in system (2.11),(3.4),(3.11)) $\}$. Furthermore, since the objective is to decrease the substrate concentration of the water resource to a prescribed value $S_{\lim}$ in minimal time, the set of admissible constant control functions is reduced to $\mathcal{Q}^C = \{Q : [0, +\infty) \to [0, +\infty) : Q(t) = c$ for all $t \geq 0$, with $c \in [0, V\mu(S_{\lim}))$ in system (3.9) (resp. $c \in [0, Q^{\mathrm{NW}}(L, H, D_{\mathrm{B}}, \mu(S_{\lim})))$ in system (2.11),(3.4),(3.11)) $\}$.*

Remark 3.2.7. *For an initial state Σ_0, we call open-loop representation of the feedback Q^{FB} to the time function $Q^{\mathrm{FB}}(\cdot) = Q^{\mathrm{FB}}(\Sigma(\cdot))$ where $\Sigma(\cdot)$, is the solution of system (either (3.9) or (2.11),(3.4),(3.11)) with initial state Σ_0.*

Remark 3.2.8. *For cases where $\tau \ll \tau_{\mathrm{r}}$, we can assume that system (2.11),(3.4),(3.11) is in quasi-steady state (see Section 3.2.1). In this situation, we can approximate the state of system by $\Sigma = S_{\mathrm{r}}$ and open-loops and feedbacks can be assumed, respectively, functionals of the form $Q^{OL}(\cdot) = Q^{OL}(S_{\mathrm{r},0}; \cdot)$ and $S_{\mathrm{r}} \mapsto Q^{\mathrm{FB}}(S_{\mathrm{r}})$, where $Q^{\mathrm{FB}} \in \mathcal{Q}^{\mathrm{FB}} = \{Q : [0, +\infty) \to (0, +\infty)$ such that system (2.11),(3.4),(3.11) admits a unique absolutely continuous solution for any initial condition Σ_0 and $Q(S_{\mathrm{r}}) < Q^{\mathrm{NW}}(L, H, D_{\mathrm{B}}, \mu(S_{\mathrm{r}}))\}$.*

Given an initial state Σ_0, the optimization problem when using open-loops can be formulated as follows:

$$\begin{cases} \text{Find } Q^{\mathrm{OL,opt}}(\cdot) \in \mathcal{Q}^{\mathrm{OL}}, \text{ such that} \\ T(\Sigma_0, Q^{\mathrm{OL,opt}}(\cdot)) = \min\limits_{Q^{\mathrm{OL}}(\cdot) \in \mathcal{Q}^{\mathrm{OL}}} T(\Sigma_0, Q^{\mathrm{OL}}(\cdot)), \end{cases} \tag{3.17}$$

where $T(\Sigma_0, Q^{\mathrm{OL}}(\cdot))$ denotes the time required to achieve $S_{\mathrm{r}}(T(\Sigma_0, Q^{\mathrm{OL}}(\cdot))) = S_{\lim}$ when solving system (3.9) (or system (2.11),(3.4),(3.11)) with the flow rate $Q = Q^{\mathrm{OL}}(\cdot)$. If the target is not achieved we set $T(\Sigma_0, Q^{\mathrm{OL}}(\cdot)) = +\infty$.

†The definition of $\mathcal{Q}^{FB}$ will be modified in Remark 3.2.8 for a special case that we will studied in this section

The optimization problem when using feedback controls can be formulated as follows:

$$\begin{cases} \text{Find } Q^{\mathrm{FB,opt}} \in \mathcal{Q}^{\mathrm{FB}}, \text{ such that for every initial state } \Sigma_0 \\ T(\Sigma_0, Q^{\mathrm{FB,opt}}(\cdot)) = \min\limits_{Q^{\mathrm{FB}} \in \mathcal{Q}^{\mathrm{FB}}} T(\Sigma_0, Q^{\mathrm{FB}}(\cdot)), \end{cases} \tag{3.18}$$

where $T(\Sigma_0, Q^{\mathrm{FB}}(\cdot))$ denotes the time required to achieve $S_{\mathrm{r}}(T(\Sigma_0, Q^{\mathrm{FB}}(\cdot))) = S_{\mathrm{lim}}$ when solving system (3.9) (or system (2.11),(3.4),(3.11)) with the flow rate $Q = Q^{\mathrm{FB}}$. If the target is not achieved we set $T(\Sigma_0, Q^{\mathrm{FB}}(\cdot)) = +\infty$.

Now, we solve these problems considering first the ODE model (3.9) and then the PDE-ODE system (2.11),(3.4),(3.11).

Optimization problem with the ODE model (3.9)

When using the ODE model (3.9), we assume $\tau_{\mathrm{r}} \gg \tau$. We distinguish between the cases in which Q is a constant open-loop control or a feedback control. The case where Q is a time-varying open loop is derived from the case in which Q is a feedback control (as explained in Remark 3.2.13). Notice that the results about problems (3.17) and (3.18), presented in this section, are proved in [**?**].

Constant open-loop control

Given an initial state $\Sigma_0 = S_{\mathrm{r},0} \in [0, +\infty)$ we look for an optimal constant $Q^{\mathrm{C,opt}} \in \mathcal{Q}^{\mathrm{C}}$ solution of (3.17). Under assumption (H1), if control variable Q is equivalently replaced by control variable S^{qs} (see Remark 3.2.1) and if we denote $\mathcal{S}^{\mathrm{qs,C}} = \{S^{\mathrm{qs}} = S^{\mathrm{qs}}(Q) \text{ such that } Q \in \mathcal{Q}^{\mathrm{C}}\}$, then problem (3.17) becomes

$$\begin{cases} \text{Find } S^{\mathrm{qs,C,opt}} \in \mathcal{S}^{\mathrm{qs,C}} \text{ such that} \\ T(S_{\mathrm{r},0}, S^{\mathrm{qs,C,opt}}) = \min\limits_{S^{\mathrm{qs,C}} \in \mathcal{S}^{\mathrm{qs,C}}} T(S_{\mathrm{r},0}, S^{\mathrm{qs,C}}), \end{cases} \tag{3.19}$$

where $T(S_{\mathrm{r},0}, S^{\mathrm{qs,C}})$ denotes the time required to achieve $S_{\mathrm{r}}(T(S_{\mathrm{r},0}, S^{\mathrm{qs,C}})) = S_{\mathrm{lim}}$ when solving system (3.10) with the control variable $S^{\mathrm{qs}} = S^{\mathrm{qs,C}}$. We now present some theoretical results about problem (3.19).

Lemma 3.2.9. *If Q is constant (i.e., S^{qs} is constant),*

$$T(S_{\mathrm{r},0}, S^{\mathrm{qs,C}}) = \frac{1}{\frac{V}{V_{\mathrm{r}}}\mu(S^{\mathrm{qs,C}})} \ln\left(\frac{S_{\mathrm{r},0} - S^{\mathrm{qs,C}}}{S_{\mathrm{lim}} - S^{\mathrm{qs,C}}}\right). \tag{3.20}$$

Proof. From (3.8), given an initial condition $S_{\mathrm{r},0}$ it may be calculated the time T for which variable S_{r} achieves the prescribed value S_{lim}.

$$S_{\mathrm{lim}} = (S_{\mathrm{r},0} - S^{\mathrm{qs,C}})\mathrm{e}^{-\frac{V}{V_{\mathrm{r}}}\mu(S^{\mathrm{qs,C}})T} + S^{\mathrm{qs,C}},$$

and so

$$\frac{S_{\mathrm{r},0} - S^{\mathrm{qs,C}}}{S_{\mathrm{lim}} - S^{\mathrm{qs,C}}} = \mathrm{e}^{\frac{V}{V_{\mathrm{r}}}\mu(S^{\mathrm{qs,C}})T}.$$

Taking logarithms we obtain

$$\ln\left(\frac{S_{\mathrm{r},0} - S^{\mathrm{qs,C}}}{S_{\mathrm{lim}} - S^{\mathrm{qs,C}}}\right) = \frac{V}{V_{\mathrm{r}}}\mu(S^{\mathrm{qs,C}})T,$$

and therefore

$$T(S_{\mathrm{r},0}, S^{\mathrm{qs,C}}) = \frac{1}{\frac{V}{V_{\mathrm{r}}}\mu(S^{\mathrm{qs,C}})} \ln\left(\frac{S_{\mathrm{r},0} - S^{\mathrm{qs,C}}}{S_{\mathrm{lim}} - S^{\mathrm{qs,C}}}\right).$$

□

Lemma 3.2.10. *Assuming $S_{\mathrm{r},0} > S_{\mathrm{lim}}$, the optimization problem (3.19) has a unique solution.*

Proof. Lemma 3.2.9 implies that $T(S_{\mathrm{r},0}, S^{\mathrm{qs,C}}) \to +\infty$ as $S^{\mathrm{qs,C}} \to S_{\mathrm{lim}}$ or $S^{\mathrm{qs,C}} \to 0$, and consequently its minimum is reached on the interval $(0, S_{\mathrm{lim}})$. In terms of Q, the minimum time is attained with $Q \in (0, V\mu(S_{\mathrm{lim}}))$. Even though it cannot be concluded that the function (3.20) is convex, it has a minimum that we denote as T^* and there is an associated constant control $S^{\mathrm{qs,C}}$ which realizes the minimum T^* in (3.20). Considering $S^{\mathrm{qs,C}}$ as a variable parameter, let us reformulate equation (3.8) as:

$$S_{\mathrm{r}}(t, S^{\mathrm{qs,C}}) = (S_{\mathrm{r},0} - S^{\mathrm{qs,C}})\mathrm{e}^{-\frac{V}{V_{\mathrm{r}}}\mu(S^{\mathrm{qs,C}})t} + S^{\mathrm{qs,C}}.$$

For a fix $t > 0$, the map

$$\begin{aligned} F_t : (0, S_{\mathrm{lim}}) &\longrightarrow (0, S_{\mathrm{r},0}) \\ S^{\mathrm{qs,C}} &\longrightarrow F_t(S^{\mathrm{qs,C}}) = S_{\mathrm{r}}(t, S^{\mathrm{qs,C}}) \end{aligned}$$

is strictly convex. Indeed,

$$\begin{aligned} \frac{\mathrm{dF}_t}{\mathrm{dS}^{\mathrm{qs,C}}} &= 1 + (-1)\mathrm{e}^{-\frac{V}{V_{\mathrm{r}}}\mu(S^{\mathrm{qs,C}}(Q))t} + (S_{\mathrm{r},0} - S^{\mathrm{qs,C}})\big(-\tfrac{V}{V_{\mathrm{r}}}\mu'(S^{\mathrm{qs,C}})t\mathrm{e}^{-\frac{V}{V_{\mathrm{r}}}\mu(S^{\mathrm{qs}})t}\big) \\ &= 1 - (\mathrm{e}^{-\frac{V}{V_{\mathrm{r}}}\mu(S^{\mathrm{qs,C}})t})\big(1 + \tfrac{V}{V_{\mathrm{r}}}\mu'(S^{\mathrm{qs,C}})t(S_{\mathrm{r},0} - S^{\mathrm{qs,C}})\big), \end{aligned}$$

and so

$$\begin{aligned} \frac{\mathrm{d}}{\mathrm{dS}^{\mathrm{qs,C}}}\Big(\frac{\mathrm{dF}_t}{\mathrm{dS}^{\mathrm{qs,C}}}\Big) = {} & \tfrac{V}{V_{\mathrm{r}}}\mu'(S^{\mathrm{qs,C}})t\mathrm{e}^{-\frac{V}{V_{\mathrm{r}}}\mu(S^{\mathrm{qs,C}})t}\big(1 + \tfrac{V}{V_{\mathrm{r}}}\mu'(S^{\mathrm{qs,C}})t(S_{\mathrm{r},0} - S^{\mathrm{qs,C}})\big) \\ & -\tfrac{V}{V_{\mathrm{r}}}t\mathrm{e}^{-\frac{V}{V_{\mathrm{r}}}\mu(S^{\mathrm{qs,C}})t}\big(\mu''(S^{\mathrm{qs,C}})(S_{\mathrm{r},0} - S^{\mathrm{qs,C}}) - \mu'(S^{\mathrm{qs,C}})\big) \\ = {} & \underbrace{\frac{V}{V_{\mathrm{r}}}t\mathrm{e}^{-\frac{V}{V_{\mathrm{r}}}\mu(S^{\mathrm{qs,C}})t}}_{>0}\Big(\underbrace{2\mu'(S^{\mathrm{qs,C}}) + \frac{V}{V_{\mathrm{r}}}t(\mu'(S^{\mathrm{qs,C}}))^2(S_{\mathrm{r},0} - S^{\mathrm{qs,C}})}_{>0\,(\mathrm{H1})} \\ & -\underbrace{\mu''(S^{\mathrm{qs,C}})}_{<0\,(\mathrm{H1})}\underbrace{(S_{\mathrm{r},0} - S^{\mathrm{qs,C}})}_{>0}\Big) > 0. \end{aligned}$$

Particularly, if we consider $t = T^*$, the map $F_{T^*}(\cdot) := S_{\mathrm{r}}(T^*, \cdot)$ is strictly convex. Moreover, $F_{T^*}(S^{\mathrm{qs,C}}) \geq S_{\mathrm{lim}}$ for all $S^{\mathrm{qs,C}} \in (0, S_{\mathrm{lim}})$, and $F_{T^*}(S^{\mathrm{qs,C,opt}}) = S_{\mathrm{lim}}$. Consequently the constant control $S^{\mathrm{qs,C,opt}}$ is unique. □

We approximate the solution of problem (3.19) by computing

$$S^{\mathrm{qs,C,opt}} = \arg \min_{S^{\mathrm{qs,C}} \in \mathcal{S}^{\mathrm{qs,C,N}}} T(S_{\mathrm{r},0}, S^{\mathrm{qs,C}}), \tag{3.21}$$

where $\mathcal{S}^{\mathrm{qs,C,N}} = \{S_i^{\mathrm{qs,C}}\}_{i=1}^N$, with $N \in \mathbb{N}$ large enough and $S_i^{\mathrm{qs,C}} = \frac{i}{N+1}S_{\mathrm{lim}}$.

Feedback control

In this case, we look for an optimal feedback $Q^{\mathrm{FB,opt}} \in \mathcal{Q}^{\mathrm{FB}}$ solution of (3.18). Under assumption (H1), if control variable Q is equivalently replaced by control variable S^{qs} and if we denote $\mathcal{S}^{\mathrm{qs,FB}} = \{S^{\mathrm{qs}} = S^{\mathrm{qs}}(Q)$ where $Q \in \mathcal{Q}^{\mathrm{FB}}\}$, then $S^{\mathrm{qs,FB,opt}} = S^{\mathrm{qs}}(Q^{\mathrm{FB,opt}})$ is called an optimal feedback. We have the following result.

Lemma 3.2.11. *An optimal feedback $S^{\mathrm{qs,FB,opt}} : [0, +\infty) \to \mathbb{R}$ must fulfill*

$$S^{\mathrm{qs,FB,opt}} = \arg \min_{S^{\mathrm{qs,FB}} \in \mathcal{S}^{\mathrm{qs,FB}}} \frac{V}{V_{\mathrm{r}}}\mu(S^{\mathrm{qs,FB}})(S^{\mathrm{qs,FB}} - S_{\mathrm{r}}) \tag{3.22}$$

or, equivalently,

$$\mu'(S^{\mathrm{qs,FB,opt}})(S_{\mathrm{r}} - S^{\mathrm{qs,FB,opt}}) = \mu(S^{\mathrm{qs,FB,opt}}). \tag{3.23}$$

Moreover, $Q^{\mathrm{FB,opt}}(\cdot)$ (see Remark 3.2.7) is decreasing along any optimal trajectory.

Proof. It is clear that any optimal feedback $S^{\mathrm{qs,FB,opt}}$ must make the time derivative of $S_{\mathrm{r}}(t)$ in equation (3.9) the most negative at any given time, i.e., it must fulfill

$$S^{\mathrm{qs,FB,opt}}(t) \in \arg \min_{S^{\mathrm{qs,FB}}(t)\in(0,S_{\mathrm{r}}(t))} \frac{V}{V_{\mathrm{r}}}\mu(S^{\mathrm{qs,FB}}(t))(S^{\mathrm{qs,FB}}(t) - S_{\mathrm{r}}(t)).$$

Considering $S^{\mathrm{qs,FB}}$ as a time variable and for a fix $t > 0$, we define the map:

$$\begin{aligned} G_t : (0, S_{\mathrm{r}}(t)) &\longrightarrow \mathbb{R} \\ s &\longrightarrow G_t(s) = \tfrac{V}{V_{\mathrm{r}}}\mu(s)(s - S_{\mathrm{r}}(t)). \end{aligned}$$

One can see that function G_t is convex, i.e., $\frac{\mathrm{d}^2 G_t}{\mathrm{d}s^2} > 0$. Thus,

$$\frac{\mathrm{d}G_t}{\mathrm{d}s} = \frac{V}{V_{\mathrm{r}}}\big(\mu'(s)(s - S_{\mathrm{r}}(t)) + \mu(s)\big),$$

$$\frac{\mathrm{d}^2 G_t}{\mathrm{d}s^2} = \frac{V}{V_{\mathrm{r}}}\big(\underbrace{\mu''(s)}_{<0(\mathrm{H1})} \underbrace{(s - S_{\mathrm{r}}(t))}_{<0} + 2 \underbrace{\mu'(s)}_{>0(\mathrm{H1})} \big) > 0.$$

Consequently, for any $t \geq 0$ we have that $S^{\mathrm{qs,FB,opt}}(t)$ is unique. Thus, the control variable $S^{\mathrm{qs,FB,opt}}$ is unique, and the equality in (3.22) holds.

In order to look for a explicit expression for $S^{\mathrm{qs,FB,opt}}$, we recall that a necessary condition for optimality in (3.22) is that $\frac{\mathrm{d}G_t}{\mathrm{d}s}(S^{\mathrm{qs,FB,opt}}(t)) = 0$. Therefore,

$$\frac{\mathrm{d}G_t}{\mathrm{d}s}(S^{\mathrm{qs,FB,opt}}(t)) = \frac{V}{V_{\mathrm{r}}}\big(\mu'(S^{\mathrm{qs,FB,opt}}(t))(S^{\mathrm{qs,FB,opt}}(t) - S_{\mathrm{r}}(t)) + \mu(S^{\mathrm{qs,FB,opt}}(t))\big) = 0$$

$$\Leftrightarrow \mu'(S^{\mathrm{qs,FB,opt}}(t))(S_{\mathrm{r}}(t) - S^{\mathrm{qs,FB,opt}}(t)) = \mu(S^{\mathrm{qs,FB,opt}}(t)).$$

It remains to prove that the map $t \to Q^{\mathrm{FB,opt}}(t)$ is decreasing along any optimal trajectory, i.e., $\frac{\mathrm{d}Q^{\mathrm{FB,opt}}}{\mathrm{d}t} < 0$. Since $Q^{\mathrm{FB,opt}}(t) = V\mu(S^{\mathrm{qs,FB,opt}}(t))$, one has $\frac{\mathrm{d}Q^{\mathrm{FB,opt}}}{\mathrm{d}t} = V \underbrace{\mu'(S^{\mathrm{qs,FB,opt}})}_{>0(\mathrm{H1})} \frac{\mathrm{d}S^{\mathrm{qs,FB,opt}}}{\mathrm{d}t}$. Thus, we only need to prove that $\frac{\mathrm{d}S^{\mathrm{qs,FB,opt}}}{\mathrm{d}t} < 0$, to show that $Q^{\mathrm{FB,opt}}(\cdot)$ is decreasing.

Taking the time derivative of expression (3.23), one obtains

$$\frac{\mathrm{d}S^{\mathrm{qs,FB,opt}}}{\mathrm{d}t}\mu''(S^{\mathrm{qs,FB,opt}})(S_{\mathrm{r}} - S^{\mathrm{qs,FB,opt}}) + \mu'(S^{\mathrm{qs,FB,opt}})\big(\frac{\mathrm{d}S_{\mathrm{r}}}{\mathrm{d}t} - \frac{\mathrm{d}S^{\mathrm{qs,FB,opt}}}{\mathrm{d}t}\big) = \frac{\mathrm{d}S^{\mathrm{qs,FB,opt}}}{\mathrm{d}t}\mu'(S^{\mathrm{qs,FB,opt}}),$$

$$\frac{\mathrm{d}S^{\mathrm{qs,FB,opt}}}{\mathrm{d}t}\big(2\mu'(S^{\mathrm{qs,FB,opt}}) + \mu''(S^{\mathrm{qs,FB,opt}})(S^{\mathrm{qs,FB,opt}} - S_{\mathrm{r}})\big) = \mu'(S^{\mathrm{qs,FB,opt}})\frac{\mathrm{d}S_{\mathrm{r}}}{\mathrm{d}t},$$

and therefore

$$\frac{\mathrm{d}S^{\mathrm{qs,FB,opt}}}{\mathrm{d}t} = \frac{\overbrace{\mu'(S^{\mathrm{qs,FB,opt}})}^{>0(\mathrm{H1})}\overbrace{\frac{\mathrm{d}S_{\mathrm{r}}}{\mathrm{d}t}}^{<0}}{2\underbrace{\mu'(S^{\mathrm{qs,FB,opt}})}_{>0(\mathrm{H1})} - \underbrace{\mu''(S^{\mathrm{qs,FB,opt}})}_{<0(\mathrm{H1})}\underbrace{(S_{\mathrm{r}} - S^{\mathrm{qs,FB,opt}})}_{>0}} < 0,$$

which completes the proof. □

If the Monod function (see (2.2)) is used, we can solve explicitly equation (3.23) with $S^{\mathrm{qs,FB,opt}}(S_{\mathrm{r}}) = \sqrt{K_{\mathrm{S}}^2 + K_{\mathrm{S}} S_{\mathrm{r}}} - K_{\mathrm{S}}$.

Remark 3.2.12. *The fact that the open loop realization of the feedback $Q^{\mathrm{FB,opt}}$ is decreasing along time can be interpreted physically as follows: as time goes on, the substrate in the water resource is decreasing and the water that enters the bioreactor is less polluted. Therefore, if $Q(\cdot)$ does not decrease, the biomass has not enough time to be in contact with the substrate in order to grow, and eventually becomes extinct.*

Remark 3.2.13. *If $Q^{\mathrm{FB,opt}}$ is solution of problem (3.18) when using the model (3.9), given an initial state $\Sigma_0 = S_{\mathrm{r},0} \in [0, +\infty)$, the open-loop representation of $Q^{\mathrm{FB,opt}}$ (see Remark 3.2.7) is solution of problem (3.17).*

Optimization problem with the PDE-ODE model (2.11),(3.4),(3.11)

As done previously for system (3.9), we consider the cases in which Q is chosen as an open-loop control or as a feedback control.

Constant open-loop control

Given an initial state $\Sigma_0 \in [0, +\infty) \times (L^\infty(\Omega))^2$ (or $\Sigma_0 \in [0, +\infty)$ for the cases where $\tau \ll \tau_{\mathrm{r}}$, see Remark 3.2.8), we look for an optimal constant $Q^{\mathrm{C,opt}} \in \mathcal{Q}^{\mathrm{C}}$ solution of problem (3.17), that we approximate by taking N equidistant points in the interval $(0, Q^{\mathrm{NW}}(L, H, D_{\mathrm{B}}, \mu(S_{\mathrm{lim}})))$ proceeding as in problem (3.21).

Time varying open-loop control

Given an initial state $\Sigma_0 \in [0, +\infty) \times (L^\infty(\Omega))^2$ (or $\Sigma_0 \in [0, +\infty)$ for the cases where $\tau \ll \tau_{\mathrm{r}}$, see Remark 3.2.8), we look for a time variable function $Q^{\mathrm{OL,opt}} \in \mathcal{Q}^{\mathrm{OL}}$ close to a solution of (3.17). With that aim, we consider a family of time varying functions with 5 optimization parameters, denoted by Q_0, Q_1, Q_2, Q_3 and Q_4. Those optimization parameters correspond to the value of the flow rate $Q^{\mathrm{OL}}(\cdot)$ at five different given fixed times t_0, t_1, t_2, t_3 and t_4, starting from time $t_0 = 0$, so that function Q^{OL} is given by:

$$Q^{\mathrm{OL}}(t) = \begin{cases} Q_0 & \text{if} \quad t = 0, \\ Q_1 & \text{if} \quad t = t_1, \\ Q_2 & \text{if} \quad t = t_2, \\ Q_3 & \text{if} \quad t = t_3, \\ Q_4 & \text{if} \quad t > t_4 \end{cases}$$

and $Q^{\mathrm{OL}}(t)$ is calculated with the *monotone piecewise cubic hermite interpolation*, with null derivatives at t_0 and t_4 (see for instance [**?**]), for $t \in (t_i, t_{i+1})$ $(i = 0, \ldots, 3)$.
Following Remark 3.2.12, we only consider decreasing time functions $Q(\cdot)$. Thus, we compute the optimization parameters Q_0, Q_1, Q_2, Q_3 and Q_4 with the following constraints

$$Q_0 > Q_1 > Q_2 > Q_3 > Q_4.$$

To that end, we consider the optimization parameter $Q_0 \in [0, Q^{\mathrm{NW}}(L, H, D_{\mathrm{B}}, \mu(S_{\mathrm{r},0})))$ and we define new optimization parameters α_1, α_2, α_3 and α_4 in $[0, 1]$ such that the interpolation data are given by

$$Q_1 = \alpha_1 Q_0, \qquad Q_2 = \alpha_2 Q_1, \qquad Q_3 = \alpha_3 Q_2, \qquad Q_4 = \alpha_4 Q_3.$$

Therefore, we approximate $Q^{\mathrm{OL,opt}}(\cdot)$ by a function defined by interpolation, as explained above, and where the corresponding vector $\gamma^{\mathrm{opt}} = (Q_0^{\mathrm{opt}}, \alpha_1^{\mathrm{opt}}, \alpha_2^{\mathrm{opt}}, \alpha_3^{\mathrm{opt}}, \alpha_4^{\mathrm{opt}})$ is solution of

$$\begin{cases} \text{Find } \gamma^{\mathrm{opt}} \in (0, Q^{\mathrm{NW}}(L, H, D_{\mathrm{B}}, \mu(S_{\mathrm{r},0}))) \times (0, 1)^4 \text{ such that} \\ T(\Sigma_0, Q^{\mathrm{OL,opt}}(\cdot)) = \min\limits_{\gamma \in (0, Q^{\mathrm{NW}}(L, H, D_{\mathrm{B}}, \mu(S_{\mathrm{r},0}))) \times (0,1)^4} T(\Sigma_0, Q^{\mathrm{OL}}(\cdot)), \end{cases} \tag{3.24}$$

where $T(\Sigma_0, Q^{\mathrm{OL}}(\cdot))$ denotes the time required to achieve $S_{\mathrm{r}}(T(\Sigma_0, Q^{\mathrm{OL}}(\cdot))) = S_{\mathrm{lim}}$ when solving (with any suitable solver; see Section 3.2.3) system (3.4) coupled with (2.11),(3.11) with the flow rate $Q = Q^{\mathrm{OL}}(\cdot)$. We solve problem (3.24) with the Hybrid Genetic Algorithm presented in Section 3.1, applying the stopping criterion *No improvement through generations* (with $\hat{g} = 25$) for GA and the stopping criterion *Maximum number of iterations* (with $N_{\mathrm{it}} = 25$) for SD.

Feedback Approximation

In this case, we look for an optimal feedback $Q^{\mathrm{FB,opt}} \in \mathcal{Q}^{\mathrm{FB}}$ solution of problem (3.18). To this end, proceeding similarly as done in Lemma 3.2.11 for perfectly mixed bioreactors, we perform a suboptimal strategy as a greedy policy that consists in choosing a control maximizing the instantaneous decrease of the contaminant concentration in the resource.
For cases where $\tau \ll \tau_{\mathrm{r}}$, we assume that the feedback only depends on S_{r}, i.e., $\Sigma = S_{\mathrm{r}}$ (see Remark 3.2.8) and we approximate the feedback function that we are looking for by solving the following optimization problem: Given an arbitrary resource substrate concentration $s_{\mathrm{r}} \in [0, +\infty)$ and a small time interval $\Delta t > 0$ (chosen of the order of the water resource time scale τ_{r} in order to assure that the bioreactor is in quasi-steady state during the time interval Δt)

$$\begin{cases} \text{Find } Q^{\mathrm{FB,opt}}(s_{\mathrm{r}}) \in [0, Q^{\mathrm{NW}}(L, H, D_{\mathrm{B}}, \mu(s_{\mathrm{r}}))) \text{ such that} \\ \\ S_{\mathrm{r}}(s_{\mathrm{r}}, Q^{\mathrm{FB,opt}}; \Delta t) = \min_{Q^{\mathrm{FB}} \in [0, Q^{\mathrm{NW}}(L,H,D_{\mathrm{B}},\mu(s_{\mathrm{r}})))} S_{\mathrm{r}}(s_{\mathrm{r}}, Q^{\mathrm{FB}}; \Delta t), \end{cases} \tag{3.25}$$

where $S_{\mathrm{r}}(s_{\mathrm{r}}, Q^{\mathrm{FB}}; \Delta t)$ is the solution (computed with any suitable solver; see Section 3.2.3) of system (3.4) coupled with (2.11),(3.11) at time Δt, with $S_{\mathrm{r},0} = s_{\mathrm{r}}$ and $Q = Q^{\mathrm{FB}}(s_{\mathrm{r}})$. Since $\tau \ll \tau_{\mathrm{r}}$ the bioreactor is in quasi-steady state and the choice of the concentration values S_0 and B_0 does not have influence on the solution of problem (3.25). Particularly, we take $S_0 = B_0 = s_{\mathrm{r}}$. We estimate the solution of problem (3.25) by taking N equidistant points in the interval $(0, Q^{\mathrm{NW}}(L, H, D_{\mathrm{B}}, \mu(s_{\mathrm{r}})))$ and proceeding as in problem (3.21). Then, in order to obtain a function of the form

$$\begin{array}{rccc} Q^{\mathrm{FB,opt}}: & [S_{\mathrm{lim}}, S_{\mathrm{r},0}] & \longrightarrow & [0, Q^{\mathrm{NW}}(L, H, D_{\mathrm{B}}, \mu(S_{\mathrm{r},0}))) \\ & s_{\mathrm{r}} & \to & Q^{\mathrm{FB,opt}}(s_{\mathrm{r}}), \end{array} \tag{3.26}$$

we solve problem (3.25) for a range of concentration values $s_{\mathrm{r}} \in \mathcal{S}_{\mathrm{r}} = \{s_{\mathrm{r},i}\}_{i=1}^{I+1}$, where $I \in \mathbb{N}$ is large enough and $s_{\mathrm{r},i} = S_{\mathrm{r},0} - \frac{i-1}{I}(S_{\mathrm{r},0} - S_{\mathrm{lim}})$. Finally, $Q^{\mathrm{FB,opt}}(s_{\mathrm{r}})$ is calculated with the *monotone piecewise cubic hermite interpolation* with null derivatives at S_{lim} and $S_{\mathrm{r},0}$ (see [**?**]) for $s_{\mathrm{r}} \notin \mathcal{S}_{\mathrm{r}}$.

For cases where $\tau \ll \tau_{\mathrm{r}}$ is not satisfied, we approximate the feedback function that we are looking for by solving the following optimization problem: Given arbitrary concentration values $(s_{\mathrm{r}}, s, b) \in [0, +\infty) \times (L^{\infty}(\Omega))^2$ and a small time interval $\Delta t > 0$

$$\begin{cases} \text{Find } Q^{\mathrm{FB,opt}}(s_{\mathrm{r}}, s, b) \in [0, Q^{\mathrm{NW}}(L, H, D_{\mathrm{B}}, \mu(s_{\mathrm{r}}))) \text{ such that} \\ \\ S_{\mathrm{r}}(\Sigma_0, Q^{\mathrm{FB,opt}}; \Delta t) = \min_{Q^{\mathrm{FB}} \in [0, Q^{\mathrm{NW}}(L,H,D_{\mathrm{B}},\mu(s_{\mathrm{r}})))} S_{\mathrm{r}}(\Sigma_0, Q^{\mathrm{FB}}; \Delta t), \end{cases} \tag{3.27}$$

where $S_{\mathrm{r}}(\Sigma_0, Q^{\mathrm{FB}}; \Delta t)$ is the solution (obtained with a suitable numerical solver; see Section 3.2.3) of system (3.4) coupled with (2.11),(3.11) at time Δt, with $\Sigma_0 = (s_{\mathrm{r}}, s, b)$ and $Q = Q^{\mathrm{FB}}(s_{\mathrm{r}}, s, b)$. We estimate the solution of problem (3.27) by taking N equidistant points in the interval $(0, Q^{\mathrm{NW}}(L, H, D_{\mathrm{B}}, \mu(s_{\mathrm{r}})))$ and proceeding as in problem (3.21).
Then, in order to obtain a function of the form

$$\begin{array}{rccc} Q^{\mathrm{FB,opt}}: & [S_{\mathrm{lim}}, S_{\mathrm{r},0}] \times (L^{\infty}(\Omega))^2 & \longrightarrow & [0, Q^{\mathrm{NW}}(L, H, D_{\mathrm{B}}, \mu(S_{\mathrm{r},0}))) \\ & (s_{\mathrm{r}}, s, b) & \to & Q^{\mathrm{FB,opt}}(s_{\mathrm{r}}, s, b), \end{array} \tag{3.28}$$

we solve problem (3.27) for a range of concentration values $(s_{\rm r}, s, b)$ in the set $\mathcal{M} = \{(s_{\rm r}, s, b) : \exists i \in \{1, \ldots, I+1\}$ such that $s_{\rm r} = s_{{\rm r},i} \in \mathcal{S}_{\rm r}$, $s \in \mathcal{S}_i$ and $b \in \mathcal{B}_i\}$ where $s_{{\rm r},i} = S_{{\rm r},0} - \frac{i-1}{I}(S_{{\rm r},0} - S_{\rm lim})$, $\mathcal{S}_i = \mathcal{B}_i = \{s_{i,j}\}_{j\in J}$ with $J \subset \mathbb{N}$ and $s_{i,j} = \frac{s_{{\rm r},i}}{j}$. If $(s_{\rm r}, s, b) \notin \mathcal{M}$, we compute the mean value of the concentrations s and b in the bioreactor (which we denote by $\overline{s}$ and $\overline{b}$) by

$$\overline{s} = \frac{2\displaystyle\int_0^L \int_0^H rS(r,z)\,{\rm d}z{\rm d}r}{L^2 H}, \quad \overline{b} = \frac{2\displaystyle\int_0^L \int_0^H rB(r,z)\,{\rm d}z{\rm d}r}{L^2 H},$$

and $Q^{\rm FB,opt}(s_{\rm r}, s, b)$ is approximated by $Q^{\rm FB,opt}(s_{\rm r}, \overline{s}, \overline{b})$, which is given by *spatial interpolation*. More specifically, $Q^{\rm FB,opt}(s_{\rm r}, \overline{s}_{\rm b}, \overline{b}_{\rm b})$ is calculated with a suitable *trilinear* or *neighbour interpolation* method depending if $(s_{\rm r}, s, b)$ is or not inside the convex hull of $\mathcal{M}$.

Remark 3.2.14. *Set $\mathcal{M}$ has been chosen following the stability analysis of the ODE system* (2.1)*, presented in Section 2.1.4, which shows that the value of concentration of both substrate and biomass at their equilibria state is below the substrate concentration in the resource. Nevertheless, in order to obtain a function of the form (3.28), the same methodology can be applied with more general sets $\mathcal{M}$.*

Remark 3.2.15. *Solution of problems (3.25) and (3.27) are approximations of the solution of problem (3.18) which, as shown in Section 3.2.3, provide satisfactory results.*

3.2.3 Numerical experiments

In this section, we first introduce the numerical solvers used for computing the solutions of systems (3.10) and (2.11),(3.4),(3.11). Then, we present the numerical results obtained when looking for constant and feedback controls, respectively. Notice that, in order to shorten the presentation of this work, the results obtained when looking for time varying open-loop controls has been included in the section devoted to Feedback.

Numerical solvers used for systems (3.10) and (2.11),(3.4),(3.11)

The solution of system (3.10) was computed numerically by using a fourth-order Runge-Kutta method and the solution of system (2.11),(3.4),(3.11) was computed numerically by coupling a fourth-order Runge-Kutta method with a Finite Element Method (see [**?**]). The computational experiments were carried out with a 2.8Ghz Intel i7-930 64bits computer with 12Gb of RAM. We used a triangular mesh with around 600 elements. A numerical simulation of system (2.11),(3.4),(3.11) with time step $\Delta t = 100$s and final time 10^5s, computed using MATLAB (`mathworks.com`) and COMSOL Multyphisics 5.0 (`www.comsol.com`), takes approximately 12 seconds.

The model parameters were taken following [**?**, **?**]: μ was the Monod function (see (2.2)) with $\mu_{\max} = 1$ (1/s) and $K_{\rm S} = 1$ (kg/m^3). For the bioreactor and water resource volumes we took $V = 1$ (m^3) and $V_{\rm r} = 1000$ (m^3), respectively. In order to obtain a cylinder of volume $V = 1$ (m^3), we used a 2D bioreactor domain with $H = L = 0.68$ (m). We considered a case for which the time scale of the bioreactor was comparable to the time scale of the water resource by using diffusion coefficients $D_{\rm S} = D_{\rm B} = 0.01$ (m^2/s). We also consider a case where the time scale for the bioreactor was much smaller than the time scale of the water resource by using diffusion coefficients $D_{\rm S} = D_{\rm B} = 100$ (m^2/s). When computing a constant open loop control, $N = 100$ was chosen to solve problem (3.21). When computing a time-varying open loop, the interpolation times were $t_0 = 0$ (s), $t_1 = 20000$(s), $t_2 = 40000$(s), $t_3 = 60000$(s) and $t_4 = 80000$(s). Those values where taken equidistant and having estimated experimentally that the time needed to achieve the prescribed value in the resource is around 10^5s. Finally, when computing a feedback, problems (3.25) and (3.27) were solved by using the MATLAB functions `interp1` and `interp3` (see `https://www.mathworks.com/moler/interp.pdf`), respectively, with $\Delta t = 100$ s.

Remark 3.2.16. *The model parameters considered here were chosen as in [?, ?] in order to obtain a straightforward comparison between the methodologies proposed in this article and the ones introduced here. Of course, they could be replaced by other values found in the literature.*

Constant Open-Loop Control

Here, we solve numerically the optimization problem (3.17) when the volumetric flow rate Q is considered a constant. Firstly, we show the numerical results for the ODE model (3.10), and secondly, we show the numerical results obtained for the PDE-ODE system (2.11),(3.4),(3.11). Then, we make a comparison of the results, obtained for the two systems, in terms of the optimal constant open-loop controls and the time needed to achieve the prescribed value of substrate concentration in the water resource, $S_{\lim}$. We also compare the models (3.10) and (2.11),(3.4),(3.11) in terms of the minimum substrate concentration achieved in the water resource if the constant flow rate obtained for system (3.10) is used in system (2.11),(3.4),(3.11). Simulations were done with initial substrate concentration in the resource $S_{\mathrm{r},0} = 5$ and 10 (kg/m^3) and with $S_{\lim} = 0.1$ (kg/m^3).

ODE model (3.10)

We solve the optimization problem (3.21), using system (3.10), with $N = 200$, the corresponding optimal constant flow rate being $Q^{\mathrm{C,opt}} = V\mu(S^{\mathrm{qs,C,opt}})$. Following Remark 3.2.6, the interval of admissible constant controls for model (3.9) is $\mathcal{Q}^{\mathrm{C}} = [0, V\mu(S_{\lim}))$, here $\mathcal{Q}^{\mathrm{C}} \approx [0, 0.0909)$. Table 3.2 shows the results.

$S_{\mathrm{r},0}$ (kg/m^3)	$Q^{\mathrm{C,opt}}_{\mathrm{ODE}}$ (m^3/s)	$T(S_{\mathrm{r},0}, Q^{\mathrm{C,opt}}_{\mathrm{ODE}})(s)$
5	0.0776	74090
10	0.0790	81830

Table 3.2: ODE model: Value of the optimal constant open-loop $Q^{\mathrm{C,opt}}_{\mathrm{ODE}}$ and the corresponding decontamination time for two different initial values $S_{\mathrm{r},0}$.

PDE-ODE model (2.11),(3.4),(3.11)

Here, we solve the optimization problem (3.17) using the model given by system (2.11),(3.4),(3.11). We denote $Q^{\mathrm{C,opt}}_{\mathrm{HOM}}$ and $Q^{\mathrm{C,opt}}_{\mathrm{ELL}}$ the optimal constant flow rates when considering the homogeneous and the ellipsoidal flow velocity fields, respectively. Equivalently, we denote $S^{\mathrm{HOM}}_{\mathrm{r,ach}}$ and $S^{\mathrm{ELL}}_{\mathrm{r,ach}}$ the minimum substrates concentrations achieved in the water resource if $Q^{\mathrm{C,opt}}_{\mathrm{ODE}}$ is used in system (2.11),(3.4),(3.11). For these concentration values, the flow rate $Q^{\mathrm{C,opt}}_{\mathrm{ODE}}$ is high enough to drive system (2.11),(3.4),(3.11) to washout.

We distinguish between the cases where the time scale of the bioreactor is much smaller than the time scale of the water resource (i.e., $\tau \ll \tau_{\mathrm{r}}$) and the case where that condition is not satisfied.

- **Case $\tau \ll \tau_{\mathrm{r}}$:**

Following Remark 3.2.6, the interval of admissible constant controls for model (2.11),(3.4),(3.11) is $\mathcal{Q}^{\mathrm{C}} = [0, Q^{\mathrm{NW}}(L, H, D_{\mathrm{B}}, \mu(S_{\lim})))$, here, for the case $\tau \ll \tau_{\mathrm{r}}$, $\mathcal{Q}^{\mathrm{C}} \approx [0, 0.0898)$. Table 3.3 shows optimal constant open loops and the corresponding decontamination times and Table 3.4 shows the substrate concentrations achieved in the resource.

$S_{r,0}$ (kg/m^3)	$Q_{HOM}^{C,opt}$ (m^3/s)	$T(S_{r,0}, Q_{HOM}^{C,opt})$ (s)	$Q_{ELL}^{C,opt}$ (m^3/s)	$T(S_{r,0}, Q_{ELL}^{C,opt})$ (s)
5	0.0758	72750	0.0658	87040
10	0.0778	81840	0.0666	97770

Table 3.3: PDE-ODE model: case $\tau \ll \tau_r$. Values of the optimal constant open-loops $Q_{HOM}^{C,opt}$ and $Q_{ELL}^{C,opt}$ and the corresponding decontamination times for two initial values $S_{r,0}$.

$S_{r,0}$ (kg/m^3)	$S_{r,ach}^{HOM}$ (kg/m^3)	$S_{r,ach}^{ELL}$ (kg/m^3)
5	0.08404	0.1006
10	0.08569	0.1026

Table 3.4: PDE-ODE model: case $\tau \ll \tau_r$. Substrate concentrations achieved if the constant flow rate $Q_{ODE}^{C,opt}$ is used in system (2.11),(3.4),(3.11) for two initial values $S_{r,0}$.

- **Case $\tau \approx \tau_r$:**

In this case, the optimal constant open loop also depends on the initial state at the bioreactor. Since we aim to compare the optimal constant open-loop controls obtained for the ODE model (3.10) and the PDE-ODE model (2.11),(3.4),(3.11), we estimate a function of the form $S_{r,0} \to Q_{HOM}^{C,opt}(S_{r,0})$ by solving problem (3.17) for a range of initial states in the set $\mathcal{M}$ defined to solve problem (3.27) with $I = 1$ and $J = \{1, 2, 4, 10\}$. Then, $Q_{HOM}^{C,opt}$ is approximated by computing the mean value of the set of optimal constant open-loop controls obtained for the different initial states. This procedure is also used to obtain the optimal constant $Q_{ELL}^{C,opt}$ and the substrate concentrations $S_{r,ach}^{HOM}$ and $S_{r,ach}^{ELL}$.
Following Remark 3.2.6, we recall that the interval of admissible constant controls when using the model (2.11),(3.4),(3.11) is $\mathcal{Q}^C = [0, Q^{NW}(L, H, D_B, \mu(S_{lim})))$ and so, in the case $\tau \ll \tau_r$, $\mathcal{Q}^C \approx [0, 0.0596)$. Table 3.5 shows the optimal constant flow rates and the corresponding decontamination times, and Table 3.6 shows the substrate concentrations achieved in the resource.

$S_{r,0}$ (kg/m^3)	$Q_{HOM}^{C,opt}$ (m^3/s)	$T(S_{r,0}, Q_{HOM}^{C,opt})$ (s)	$Q_{ELL}^{C,opt}$ (m^3/s)	$T(S_{r,0}, Q_{ELL}^{C,opt})$ (s)
5	0.0540	89260	0.0467	103160
10	0.0547	102190	0.0470	118790

Table 3.5: PDE-ODE model: case $\tau \approx \tau_r$. Values of the optimal constant open-loops $Q_{HOM}^{C,opt}$ and $Q_{ELL}^{C,opt}$ and the corresponding decontamination times for two different initial values $S_{r,0}$.

$S_{r,0}$ (kg/m^3)	$S_{r,ach}^{HOM}$ (kg/m^3)	$S_{r,ach}^{ELL}$ (kg/m^3)
5	0.14811	0.1754
10	0.1524	0.1802

Table 3.6: PDE-ODE model: case $\tau \approx \tau_r$. Substrate concentration achieved if the constant $Q_{ODE}^{C,opt}$ is used in system (2.11),(3.4),(3.11) for two different initial values $S_{r,0}$.

Discussion

An interesting study is to check if the optimization results obtained for the ODE system (3.10) and the PDE-ODE system (2.11),(3.4),(3.11) are similar. We make the comparison for both flow velocity fields, described in Section 3.2.1.

– Homogenous flow velocity field:
We can observe from Tables 3.2 and 3.3 that the volumetric flow rates $Q^{\mathrm{C,opt}}_{\mathrm{ODE}}$ and $Q^{\mathrm{C,opt}}_{\mathrm{HOM}}$ (obtained with the PDE-ODE system (2.11),(3.4),(3.11) when $\tau \ll \tau_{\mathrm{r}}$) are significantly close and the decontamination times are comparable (the difference is below 1% for both values of $S_{\mathrm{r},0}$). Nevertheless, from Tables 3.2 and 3.5 one notice that the flow rate $Q^{\mathrm{C,opt}}_{\mathrm{HOM}}$ (obtained with the PDE-ODE system (2.11),(3.4),(3.11) when $\tau \approx \tau_{\mathrm{r}}$) is around 70% of the value of $Q^{\mathrm{C,opt}}_{\mathrm{ODE}}$. Furthermore, from Table 3.6 we conclude that if the constant $Q^{\mathrm{C,opt}}_{\mathrm{ODE}}$ is applied in system (2.11),(3.4),(3.11) in the case where $\tau \approx \tau_{\mathrm{r}}$, the bioreactor is driven to washout before the decontamination target is achieved. This is due to the fact that $Q^{\mathrm{C,opt}}_{\mathrm{ODE}}$ (> 0.07) is not in the admissible space $\mathcal{Q}^{\mathrm{C}}$ obtained when $\tau \approx \tau_{\mathrm{r}}$. Generally, these results seem to indicate that, when high diffusions are considered, the optimal constant controls obtained with the ODE model are similar to those obtained with the PDE-ODE model, whereas for low diffusion coefficients, the PDE-ODE model exhibits better results, in the sense that it provides smaller volumetric flow rates which favor that the biomass does not become extinct in the bioreactor before the target is achieved.

– Ellipsoidal flow velocity field:
We can observe from Tables 3.2, 3.3 and 3.5 than the volumetric flow rates $Q^{\mathrm{C,opt}}_{\mathrm{ELL}}$, obtained with the PDE-ODE system (2.11),(3.4),(3.11) in the cases where $\tau \ll \tau_{\mathrm{r}}$ and $\tau \approx \tau_{\mathrm{r}}$, are around 84% and 60% of the value of the flow rate $Q^{\mathrm{C,opt}}_{\mathrm{ODE}}$, respectively. Furthermore, from Tables 3.4 and 3.6 we conclude that if the constant $Q^{\mathrm{C,opt}}_{\mathrm{ODE}}$ is used in the PDE-ODE system (2.11),(3.4),(3.11), the bioreactor is driven to washout before the decontamination target is achieved. These results seem to indicate that when the ellipsoidal flow velocity field is considered, the model (2.11),(3.4),(3.11) exhibits better results, in the sense that it provides smaller volumetric flow rates which favor that the biomass does not become extinct in the bioreactor before the target is achieved. The influence of the ellipsoidal flow velocity field in the *washout* phenomena is explained in Remark 3.2.17.

Remark 3.2.17. *We recall from Section 3.2.1 that the washout phenomena is produced when* $Q(t) \geq V\mu(S_{\mathrm{r}}(t))$ *in system* (2.1) *(resp., when* $Q(t) > Q^{\mathrm{NW}}(L, H, D_{\mathrm{B}}, \mu(S_{\mathrm{r}}(t)))$ *in system* (2.11),(3.4),(3.11)*). Moreover, in Section 2.2.4 we concluded that for high values of* D_{S} *and* D_{B}*, the substrate and biomass concentrations become homogeneous in the bioreactor and* $Q^{\mathrm{NW}}(L, H, D_{\mathrm{B}}, \mu(S_{\mathrm{r}}(t))) \approx V\mu(S_{\mathrm{r}}(t))$*. Nevertheless, this analogy only takes place when using the homogeneous flow velocity field in system (2.11),(3.4), (3.11). As detailed in Section 3.2.1, the ellipsoidal flow velocity field is taken as* $u(r,t) = \frac{3Q(t)\sqrt{L^2-r^2}}{2\pi L^3}$*, so it attains its maximum depth at* $r = 0$*. This maximum depth is* $\frac{3}{2}$ *the maximum depth if the homogeneous profile is taken, so we can conclude that when using the ellipsoidal flow velocity field, washout occurs for* $Q(t) \geq Q_{\max}(t)$*, where* $Q_{\max}(t)$ *is some value in the interval* $[\frac{2}{3}V\mu(S_{\mathrm{r}}(t)), V\mu(S_{\mathrm{r}}(t))]$*. In order to find a physical explanation, we observe Figure 3.6-(a), pointing out that if the ellipsoidal flow velocity field is used, the liquid located in region* 1 *is ejected from the bioreactor faster than if we use the homogeneous flow velocity field. Thus, the substrate is in contact with the biomass less time and, consequently, the water remains polluted in this region when going out from the reactor. Furthermore, due to diffusion, the particles situated in the regions 1 and 2 are mixed and the resulting contamination value is higher than the required threshold. Figure 3.6-(b) shows the difference, in terms of decontamination time, between using the homogeneous and the ellipsoidal flow velocity fields when* Q *(*m^3/s*) is considered constant (*$Q \in \mathcal{Q}^{\mathrm{C}}$*). Particularly, taking* $S_{\mathrm{r},0} = 5$ *(*kg/m^3*) and the objective value* $S_{\lim} = 0.5$ *(*kg/m^3*), one obtains that, in order to avoid washout,* Q *should be in the interval* $[0, 0.33)$*. We observe that the washout phenomena starts at the value* $Q \approx 0.33$ *in the case of considering the homogeneous flow velocity field, but starts earlier if we use the ellipsoidal flow velocity field.*

Feedback

Here, we look for an optimal feedback, denoted by $Q^{\mathrm{FB,opt}}$ solution of problem (3.18). Firstly, we show the results for the ODE model (3.10), obtained using Lemma 3.2.11, and secondly, we show the feedback ap-

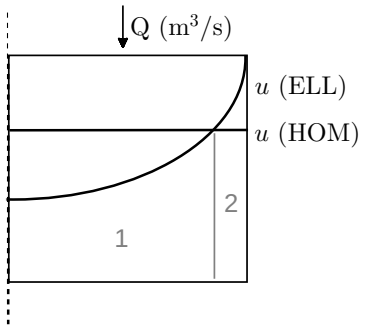

(a) Typical homogeneous and ellipsoidal flow velocity fields

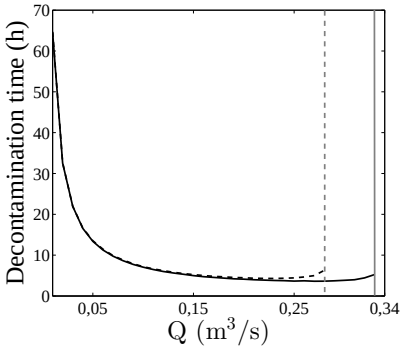

(b) Decontamination times obtained by using the homogeneous flow velocity field (depicted by a solid line) or the ellipsoid flow velocity field (depicted by a dashed line). Notice that the vertical lines are allocated at the value of Q for which washout starts.

Figure 3.6: Scheme of the washout phenomena when using the homogeneous and the ellipsoidal flow velocity fields.

proximations for the PDE-ODE system (2.11),(3.4),(3.11), obtained when solving the suboptimal problems (3.25) and (3.27). We also shows the feedback synthesis (see definition below) of the optimal time varying open-loops, obtained when solving (3.24). Then, we make a comparison of the results, obtained for the two systems, in terms of the feedback controls. We also compare the models (3.10) and (2.11),(3.4),(3.11) in terms of the minimum substrate concentration achieved in the water resource if the optimal feedback obtained for system (3.10) is used in system (2.11),(3.4),(3.11).

ODE model (3.10)

As detailed in Section 3.2.2 if the Monod function (2.2) is taken, the optimal feedback, denoted by $Q_{\mathrm{ODE}}^{\mathrm{FB,opt}}$, fulfills

$$Q_{\mathrm{ODE}}^{\mathrm{FB,opt}} = V\mu(S^{\mathrm{qs,FB,opt}}) = V\mu(\sqrt{K_{\mathrm{S}}^2 + K_{\mathrm{S}} \cdot S_{\mathrm{r}}} - K_{\mathrm{S}}).$$

PDE-ODE model (2.11),(3.4),(3.11)

As a first approach, we solve problem (3.18) by solving the optimization problems (3.25) and (3.27) (considering a feedback approximation, as described in Section 3.2.2), for both homogeneous and ellipsoidal flow velocity fields, denoting the solution by $Q_{\mathrm{HOM}}^{\mathrm{FB,opt}}$ and $Q_{\mathrm{ELL}}^{\mathrm{FB,opt}}$, respectively.
In order to compare with time varying open-loop controls (see Section 3.2.2), as a second approach we solve problem (3.18) by solving the optimization problem (3.24) and then taking the feedback synthesis of the time varying open-loop, i.e., for any time t with corresponding values $Q(t)$ and $\Sigma(t)$, we can reconstruct the map $\Sigma(t) \to Q(t)$, that can be seen as a state-dependent control function, which in the following we denote by $Q_{\mathrm{HOM}}^{\mathrm{OL,opt}}(\Sigma)$ and $Q_{\mathrm{ELL}}^{\mathrm{OL,opt}}(\Sigma)$, for the homogeneous and the ellipsoidal flow velocity fields, respectively. Equivalently, we denote $S_{\mathrm{r,ach}}^{\mathrm{HOM}}$ and $S_{\mathrm{r,ach}}^{\mathrm{ELL}}$ the minimum substrate concentrations achieved in the water resource if $Q_{\mathrm{ODE}}^{\mathrm{FB,opt}}$ is used in system (2.11),(3.4),(3.11). For these concentration value, the flow rate $Q_{\mathrm{FB,opt}}^{\mathrm{ODE}}$ is high enough to drive system (2.11),(3.4),(3.11) to washout.

Simulations have been conducted for substrate concentration $S_{\mathrm{r},0} = 10$ (kg/m^3) $S_{\mathrm{lim}} = 0.1$ (kg/m^3).

- **Case** $\tau \ll \tau_{\mathrm{r}}$

Figure 3.7 shows the similarities between the feedbacks obtained with the two approaches described above. More precisely, Figure 3.7-(a) shows the feedbacks $Q^{\mathrm{FB,opt}}_{\mathrm{HOM}}$ and $Q^{\mathrm{OL,opt}}_{\mathrm{HOM}}(\Sigma)$ and Figure 3.7-(b) shows the feedbacks $Q^{\mathrm{FB,opt}}_{\mathrm{ELL}}$ and $Q^{\mathrm{OL,opt}}_{\mathrm{ELL}}(\Sigma)$.

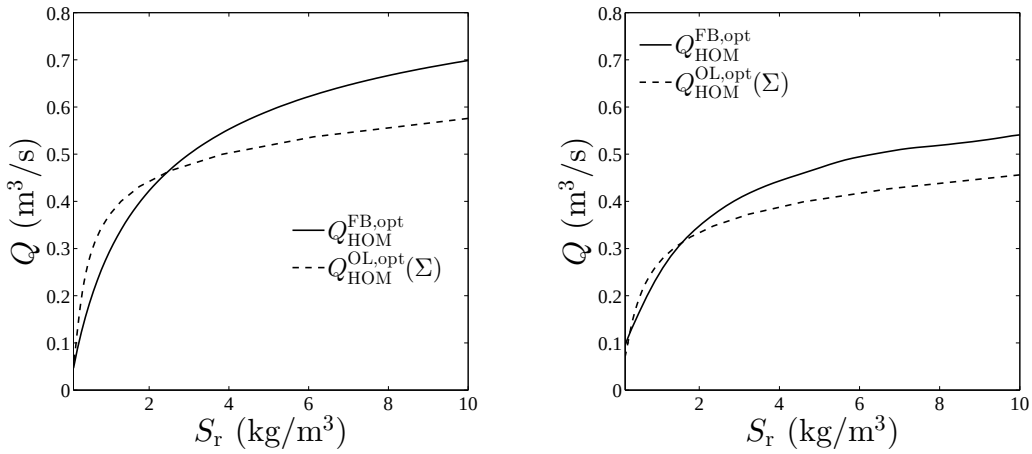

(a) Homogeneous flow velocity field

(b) Ellipsoidal flow velocity field

Figure 3.7: PDE-ODE model: case $\tau \ll \tau_{\mathrm{r}}$. Comparison between the feedback approximations $Q^{\mathrm{FB,opt}}$ (depicted with solid lines) and $Q^{\mathrm{OL,opt}}$ (depicted with dashed lines).

- **Case** $\tau \approx \tau_{\mathrm{r}}$

In this case, time varying open loops and feedbacks depend on the bioreactor state. Since we aim to compare the optimal feedback obtained for the ODE model (3.10) with the two feedback schemes obtained for the PDE-ODE model (2.11),(3.4),(3.11), we approximate functions of the form $S_{\mathrm{r}} \to Q^{\mathrm{FB,opt}}_{\mathrm{HOM}}(S_{\mathrm{r}})$ and $S_{\mathrm{r},0} \to Q^{\mathrm{OL,opt}}_{\mathrm{HOM}}(S_{\mathrm{r},0};\cdot)$. In order to compute $Q^{\mathrm{FB,opt}}_{\mathrm{HOM}}(S_{\mathrm{r}})$ (or $Q^{\mathrm{FB,opt}}_{\mathrm{ELL}}(S_{\mathrm{r}})$) we solve problem (3.27) for (s_{r}, s, b) in the set $\mathcal{M}$, defined to solve problem (3.25), with $I = 20$ and $J = \{1, 2, 4, 10\}$. Thus, for each $S \in \mathcal{S}$, $Q^{\mathrm{FB,opt}}(S)$ is approximated by computing the mean value of the set of optimal feedbacks $Q^{\mathrm{FB,opt}}(S, S, B)$ with $(S, S, B) \in \mathcal{M}$. Similarly, in order to compute $Q^{\mathrm{OL,opt}}_{\mathrm{HOM}}(S_{\mathrm{r},0};\cdot)$ we solve problem (3.24), taking $\Sigma_0 \in \mathcal{M}$ with $I = 1$ and $J = \{1, 2, 4, 10\}$. Then, each component of vector γ^{opt} is approximated by computing the mean value of the set of its optimal values obtained for the different initial states. This procedure is also used to obtain the average optimal time varying open loop $Q^{\mathrm{C,opt}}_{\mathrm{ELL}}(S_{\mathrm{r},0};\cdot)$ and substrate concentrations $S^{\mathrm{HOM}}_{\mathrm{r,ach}}$ and $S^{\mathrm{ELL}}_{\mathrm{r,ach}}$.

Figure 3.8 shows the similarities between the feedbacks obtained with the two approaches described above. More precisely, Figure 3.8-(a) shows the feedbacks $Q^{\mathrm{FB,opt}}_{\mathrm{HOM}}$ and $Q^{\mathrm{OL,opt}}_{\mathrm{HOM}}(\Sigma)$, obtained when considering the homogeneous flow velocity field. Figure 3.8-(b) shows the feedbacks $Q^{\mathrm{FB,opt}}_{\mathrm{ELL}}$ and $Q^{\mathrm{OL,opt}}_{\mathrm{ELL}}(\Sigma)$, obtained when considering the ellipsoidal flow velocity field. Table 3.7 shows the substrate concentrations achieved in the resource.

$S_{\mathrm{r},0}$ (kg/m^3)	$S^{\mathrm{HOM}}_{\mathrm{r,ach}}$ (kg/m^3)	$S^{\mathrm{ELL}}_{\mathrm{r,ach}}$ (kg/m^3)
10	9.9888	10.1841

Table 3.7: PDE-ODE model: Case $\tau \approx \tau_{\mathrm{r}}$. Substrate concentration achieved if the feedback $Q^{\mathrm{FB,opt}}_{\mathrm{ODE}}$ is used in system (2.11),(3.4),(3.11).

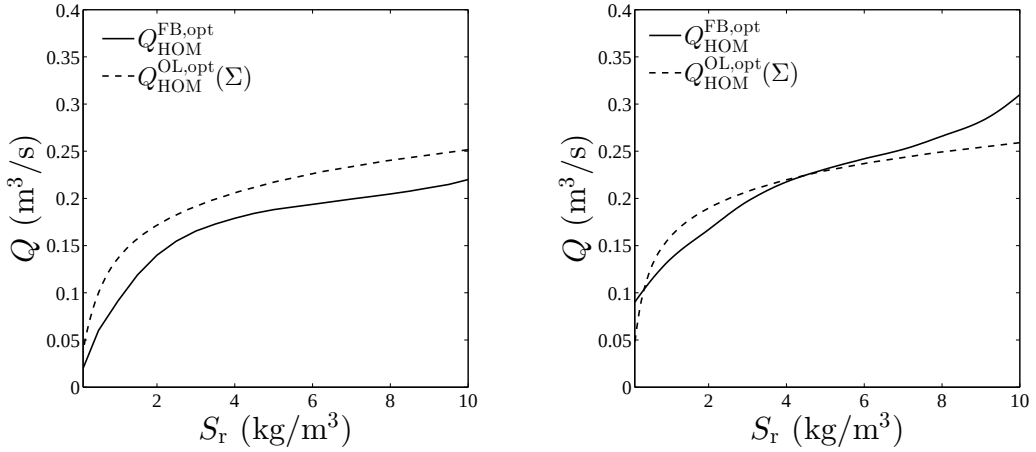

(a) Homogeneous flow velocity field (b) Ellipsoidal flow velocity field

Figure 3.8: PDE-ODE model: Case $\tau \approx \tau_{\mathrm{r}}$. Comparison between the feedback approximations $Q^{\mathrm{FB,opt}}$ (depicted with solid lines) and $Q^{\mathrm{OL,opt}}(\Sigma)$ (depicted with dashed lines).

Discussion

An interesting study is to check if both approaches, open-loop controls and feedbacks, present similar numerical results. From Figure 3.7 and Figure 3.8 one can observe significant similarities between the two volumetric flow rates $Q^{\mathrm{FB,opt}}$ and $Q^{\mathrm{OL,opt}}(\Sigma)$, being the first one a bit faster than the second one in most of the cases. This result is not surprising, since the open-loop approach takes into account the concentrations only at initial time, while the feedback strategy is intrinsically more robust.

Another interesting study is to check if the optimization results obtained for the model (3.10) and the model (2.11),(3.4),(3.11) are similar. We make the comparison for both flow velocity profiles, described in Section 3.2.1.

– Homogenous flow velocity field:
In order to analyze the similarities between the obtained optimal controls $Q^{\mathrm{FB,opt}}_{\mathrm{ODE}}$, $Q^{\mathrm{FB,opt}}_{\mathrm{HOM}}$ and $Q^{\mathrm{OL,opt}}_{\mathrm{HOM}}(\Sigma)$, we plot them in Figure 3.9. It is easy to observe that the volumetric flow rates $Q^{\mathrm{FB,opt}}_{\mathrm{HOM}}$ and $Q^{\mathrm{OL,opt}}_{\mathrm{HOM}}(\Sigma)$ (obtained with the PDE-ODE system (2.11),(3.4),(3.11) in the case where $\tau \ll \tau_{\mathrm{r}}$) are significantly close to the flow rate $Q^{\mathrm{FB,opt}}_{\mathrm{ODE}}$. Nevertheless, the flow rates $Q^{\mathrm{FB,opt}}_{\mathrm{HOM}}$ and $Q^{\mathrm{OL,opt}}_{\mathrm{HOM}}(\Sigma)$ (obtained with the PDE-ODE system (2.11),(3.4),(3.11) when $\tau \approx \tau_{\mathrm{r}}$) are much slower than $Q^{\mathrm{FB,opt}}_{\mathrm{ODE}}$. For instance, for $S_{\mathrm{r}} = 10$ (kg/m^3) the values of $Q^{\mathrm{FB,opt}}_{\mathrm{HOM}}$ and $Q^{\mathrm{OL,opt}}_{\mathrm{HOM}}(\Sigma)$ are around 35% the value of $Q^{\mathrm{FB,opt}}_{\mathrm{ODE}}$. Furthermore, from Table 3.7, we conclude that if the feedback $Q^{\mathrm{FB,opt}}_{\mathrm{ODE}}$ is used in system (2.11),(3.4),(3.11) the bioreactor is driven to washout before the decontamination target is achieved. These results seem to show that when high diffusions are considered, the optimal controls obtained with the ODE and PDE-ODE models are similar, whereas for low diffusion coefficients the PDE-ODE model exhibits better results, in the sense that it provides smaller volumetric flow rates that favor that the biomass does not become extinct before the target is achieved.

– Ellipsoidal flow velocity field:
In order to analyze the similarities between the obtained optimal controls $Q^{\mathrm{FB,opt}}_{\mathrm{ODE}}$, $Q^{\mathrm{FB,opt}}_{\mathrm{ELL}}$ and $Q^{\mathrm{OL,opt}}_{\mathrm{ELL}}(\Sigma)$, we plot them in Figure 3.10. It is easy to observe that the volumetric flow rates $Q^{\mathrm{FB,opt}}_{\mathrm{ELL}}$ and $Q^{\mathrm{OL,opt}}_{\mathrm{ELL}}(\Sigma)$, obtained with the PDE-ODE system (2.11),(3.4),(3.11) when $\tau \ll \tau_{\mathrm{r}}$ and $\tau \approx \tau_{\mathrm{r}}$,

are respectively around 75% and 35% the value of the flux $Q_{\mathrm{ODE}}^{\mathrm{FB,opt}}$. As a result we can conclude that the PDE-ODE systems exhibits better results when computing the optimal feedback, in the sense that it provides smaller volumetric flow rates that favor that the biomass does not become extinct before the target is achieved.

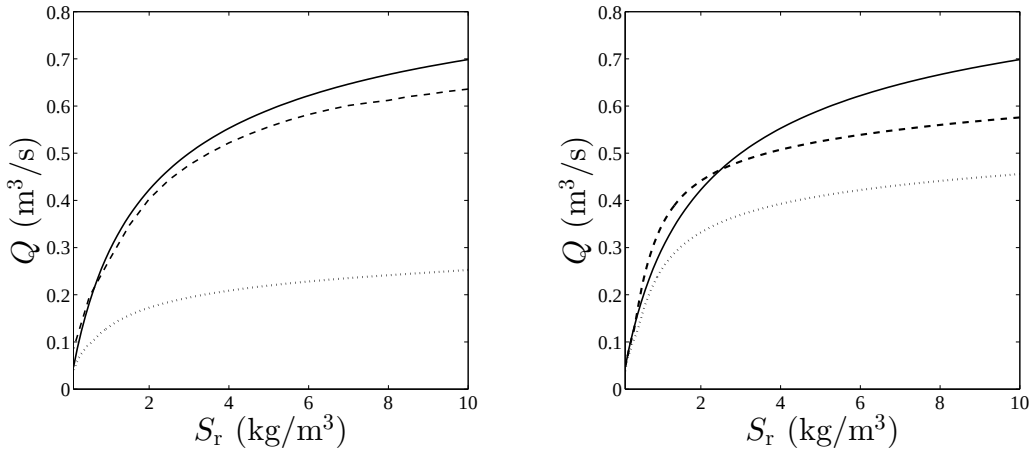

(a) $Q_{\mathrm{ODE}}^{\mathrm{FB,opt}}$ vs $Q_{\mathrm{HOM}}^{\mathrm{FB,opt}}$ (b) $Q_{\mathrm{ODE}}^{\mathrm{FB,opt}}$ vs $Q_{\mathrm{HOM}}^{\mathrm{OL,opt}}(\Sigma)$

Figure 3.9: Homogeneous flow velocity field: Comparison between the feedback obtained for the ODE model (depicted with solid line), the feedback obtained for the PDE-ODE model when $\tau \ll \tau_{\mathrm{r}}$ (depicted with dashed lines) and the feedback obtained for the PDE-ODE model when $\tau \approx \tau_{\mathrm{r}}$ (depicted with dotted lines).

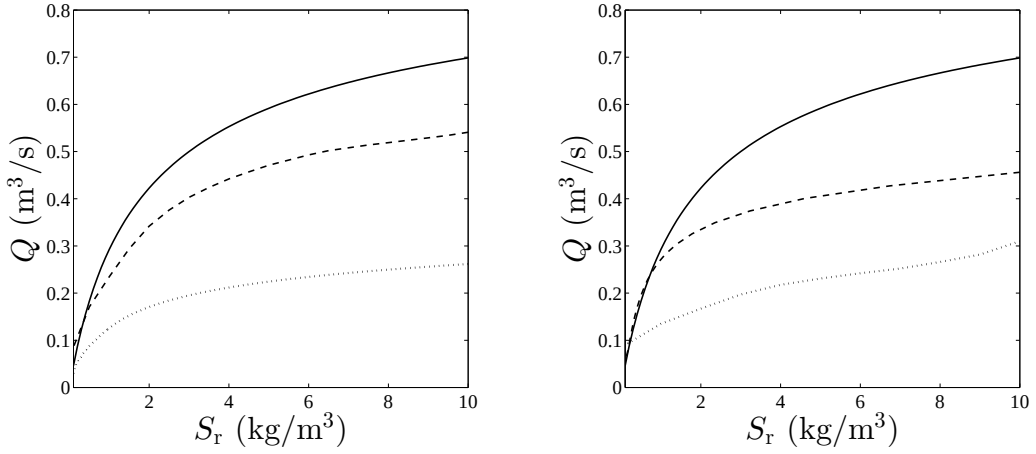

(a) $Q_{\mathrm{ODE}}^{\mathrm{FB,opt}}$ vs $Q_{\mathrm{ELL}}^{\mathrm{FB,opt}}$ (b) $Q_{\mathrm{ODE}}^{\mathrm{FB,opt}}$ vs $Q_{\mathrm{ELL}}^{\mathrm{OL,opt}}(\Sigma)$

Figure 3.10: Ellipsoidal flow velocity field: Comparison between the feedback obtained for the ODE model (depicted with solid line), the feedback obtained for the PDE-ODE model when $\tau \ll \tau_{\mathrm{r}}$ (depicted with dashed lines) and the feedback obtained for the PDE-ODE model when $\tau \approx \tau_{\mathrm{r}}$ (depicted with dotted lines).

3.2.4 Conclusions

In this section, we have focused on the modeling of the problem of water treatment by using continuous bioreactors. We have presented two mathematical models, assuming homogeneity or inhomogeneity of

substrate and biomass concentrations in the bioreactor. We have also made a difference between considering that the fluid flow velocity in the bioreactor is homogeneous through the inlet, or follows an ellipsoidal profile.

We have tackled an optimization problem which aims to minimize the time needed to clean the polluted resource, by choosing an optimal bioreactor volumetric inflow rate. In the case of considering homogeneity of the contaminant in the bioreactor, it is possible to obtain an optimal flow rate from previous theoretical results. In the case of considering inhomogeneity of the contaminant in the bioreactor, we show here how to obtain an optimal flow rate using an hybrid genetic algorithm. The results show that in the cases where the time scale in the bioreactor is comparable with the time scale of the resource (for instance, by using $D_S = D_B = 0.01$ (m^2/s)), the optimal flow rates are smaller than the optimal flow rates obtained for the mathematical model which considers homogeneity in the bioreactor.

Our goal was to compare the numerical optimization results obtained for the ODE and PDE-ODE models presented for coupled system between the bioreactor and the water resource. The results show that when the time scale of the bioreactor is much smaller than the one of the water resource, (for instance, by using $D_S = D_B = 100$ (m^2/s)), the PDE-ODE system with homogeneous flow velocity field approaches the ODE system. Contrarily, the PDE-ODE system with ellipsoidal flow velocity field does not approach the ODE system in the sense that, when using the control strategy that is optimal under the homogeneous assumption in the bioreactor, the biomass becomes extinct and it is not able to make the substrate in the water resource decrease to the objective value. Let us notice that the ellipsoidal flow velocity field has been presented in order to approach a more realistically behavior of the reactor (see [**?**]). An important conclusion is that an optimal feedback derived for perfectly mixed bioreactor can lead a bioreactor with non negligible diffusion terms to washout, preventing the desired decontamination objective, while a simple open loop control, obtained with the method presented in this section, can solve the problem.

3.3 Optimal shape of the continuous bioreactor

We consider the same continuous bioreactor as the one introduced previously in Section 2.2. In this section, we focus on an optimization problem which aims to minimize the considered reactor volume, with an outflow substrate concentration maintained to a desired threshold, by choosing a suitable bioreactor shape.

Here, the processes taking place in the bioreactor are described by using the coupled system (2.8),(2.10). More precisely, the fluid dynamics is modeled with the Navier–Stokes equations while the behavior of the reactants is described through an Advection-Diffusion-Reaction system coupled with Danckwerts boundary conditions. The growth rate function μ is considered either monotonic (see the Monod function (2.2)) or non-monotonic (see the Haldane function (2.3)). As explained in Remark 3.2.2, we assume that, after finite time $\hat{T}$ large enough (which is determined by numerical experiments), system (2.8) is numerically close enough to an equilibrium state, denoted by (S^*, B^*).

This section is organized as follows: in Section 3.3.1, we present a general shape optimization problem and two particular numerical implementations of this problem. In Section 3.3.2, we describe the numerical experiments used to validate our approach and exhibit the obtained results. Finally, in Section 3.3.3 we discuss and compare the obtained numerical solutions.

3.3.1 Optimization Problem

In this section, we first introduce the general formulation of the considered continuous optimization problem. Then, we propose two particular discrete implementations of this problem to be solved numerically in Section 3.3.2.

General Problem

Let us consider cylindrical bioreactors $\Omega^* \subset \mathbb{R}^3$ whose corresponding (r, z)-domain, $\Omega \subset \mathbb{R}^2$, is similar to the one depicted in Figure 3.11, where H (m) is the bioreactor height; r (m) is the radius of the inlet

Γ_{in} and the outlet Γ_{out}; h (m) is the height of the inlet and outlet pipes; R_1 (m) and R_2 (m) are the radius of the bioreactor wall perpendicular to the inlet and outlet pipes, respectively; the curve of the exterior wall corresponds to the graph of the function $\psi : [h, H-h] \to [r, +\infty)$, which satisfies $\psi(h) = r + R_2$ and $\psi(H-h) = r + R_1$. Since, in practice, the inlet and outlet pipes have standard dimensions (depending on the desired industrial application), we assume that r and h have fixed values. Similarly, we take into account that the height and width of the reactor can not exceed certain values (for example, due to a limitation of the physical space in an industrial factory).

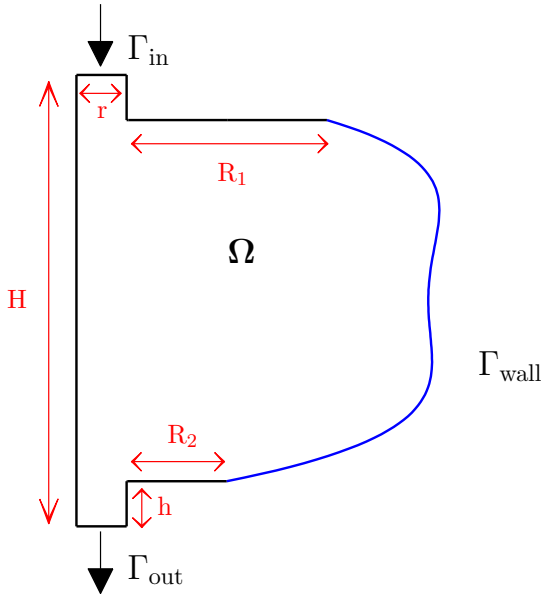

Figure 3.11: Schematic representation of the bioreactor geometries used to solve problem (3.29). The exterior curve (depicted in blue), which corresponds to the bioreactor exterior wall, is defined as $(z, \psi(z))$, where $z \in [h, H-h]$.

Given a prescribed output substrate concentration S_{lim} (kg/m^3), we state the following optimization problem

$$\begin{cases} \text{Find } \phi^{\text{opt}} \in \Phi, \text{ such that} \\ \text{Vol}(\phi^{\text{opt}}) = \min_{\phi \in \Phi} \text{Vol}(\phi), \\ S^*_{\text{out}}(\phi^{\text{opt}}) < S_{\text{lim}}, \end{cases} \tag{3.29}$$

where $\phi = (H, R_1, R_2, \psi) \in \Phi$ defines a particular bioreactor shape and $\Phi = \{[H_{\min}, H_{\max}] \times [R_{1,\min}, R_{1,\max}] \times [R_{2,\min}, R_{2,\max}] \times \mathcal{C}([h, H-h], [R_{\min}, R_{\max}])\}$ is the admissible space; $\text{Vol}(\phi)$ (m^3) is the volume of the reactor, computed as

$$\text{Vol}(\phi) = \int_{\Omega^*(\phi)} 1 \mathrm{d}x, \tag{3.30}$$

with $\Omega(\phi) \subset \mathbb{R}^2$ is the (r, z)-domain obtained with the set ϕ and $\Omega^*(\phi) \subset \mathbb{R}^3$ is the corresponding 3D domain; and $S^*_{\text{out}}(\phi)$ (kg/m^3) denotes the concentration of substrate that leaves the bioreactor (at steady state), computed as

$$S^*_{\text{out}}(\phi) = \frac{\int_{\Omega^*(\phi)} S(x, y, 0, \hat{T}) |u_3(x, y, 0)| \mathrm{d}x\mathrm{d}y}{\int_{\Omega^*(\phi)} |u_3(x, y, 0)| \mathrm{d}x\mathrm{d}y}, \tag{3.31}$$

with $S(\cdot, \cdot, \cdot, \hat{T})$ the solution of system (2.8) at time $\hat{T}$ and u_3 the third component of the velocity vector in (2.10).

Numerical Problem

Here, we present two discrete versions of the optimization problem (3.29), related to two different discrete parametrizations of the bioreactor geometry. For the sake of simplicity, the objective function and the restriction in problem (3.29) are combined into a new objective function $J(\phi)$ (m^3) as

$$J(\phi) = \mathrm{Vol}(\phi)\left(1 + \beta\frac{\max(S^*_{\mathrm{out}}(\phi) - S_{\mathrm{lim}}, 0)}{S_{\mathrm{lim}}}\right), \tag{3.32}$$

β is a huge real number (here, $\beta = 10^9$) and the term multiplied by the coefficient β is a barrier function used to penalize solutions with S_{lim} smaller than an average of the substrate concentration exiting the bioreactor.

We state a methodology to create different bioreactor geometries using either 2 or 5 parameters. The first parametrization allow us to better understand the influence of the parameter S_{lim} on the optimization results. The second parametrization offers the possibility to obtain a wider range of reactor geometries.

Domains built with 2 parameters

As a first approach, we consider bioreactor geometries as depicted in Figure 3.12-(a). The exterior wall corresponds to a semi-ellipse with center $(\frac{H}{2}, r)$ and with lengths of the semi-axis given by the pair $(\frac{H}{2} - h, R - r)$, where $R \in [R_{\min}, R_{\max}]$ (m). The set ϕ in problem (3.29) is taken as $\phi = (H, 0, 0, \psi)$, where

$$\begin{array}{rccl} \psi: & [h, H-h] & \longrightarrow & [R_{\min}, R_{\max}] \\ & z & \longmapsto & \psi(z) = r + (R-r)\sqrt{1 - \left(\frac{z - H/2}{h - H/2}\right)^2}. \end{array}$$

It is straightforward to see that, if $R \in [R_{\min}, R_{\max}]$, then $\psi \in \mathcal{C}([h, H-h], [R_{\min}, R_{\max}])$.

In this case, the bioreactor geometry only depends on parameters H and R and the optimization problem (3.29) can be reformulated as

$$\begin{cases} \text{Find } \tilde{\phi}^{2,\mathrm{opt}} \in \tilde{\Phi}^2, \text{ such that} \\ J(\tilde{\phi}^{2,\mathrm{opt}}) = \min_{\tilde{\phi}^2 \in \tilde{\Phi}^2} J(\tilde{\phi}^2), \end{cases} \tag{3.33}$$

where $\tilde{\phi}^{2,\mathrm{opt}} = (H^{\mathrm{opt}}, R^{\mathrm{opt}})$ and $\tilde{\Phi}^2 := \{(H, R) \in [H_{\min}, H_{\max}] \times [R_{\min}, R_{\max}]\} \subset \mathbb{R}^2$ is the admissible space.

We approximate the solution of problem (3.33) by computing the value of

$$\tilde{\phi}^{2,\mathrm{opt}} = \arg \min_{\tilde{\phi} \in \tilde{\Phi}^{2,N_{\mathrm{H}},N_{\mathrm{R}}}} J(\tilde{\phi}), \tag{3.34}$$

where $\tilde{\Phi}^{2,N_{\mathrm{H}},N_{\mathrm{R}}} = \big\{(H_i, R_j)\colon i \in \{1, \ldots, N_{\mathrm{H}}\},\ j \in \{1, \ldots, N_{\mathrm{R}}\}\big\}$, with N_{H}, $N_{\mathrm{R}} \in \mathbb{N}$ large enough, $H_i = H_{\min} + \frac{i-1}{N_{\mathrm{H}}-1}(H_{\max} - H_{\min})$ and $R_j = R_{\min} + \frac{j-1}{N_{\mathrm{R}}-1}(R_{\max} - R_{\min})$.

Domains built with 5 parameters

As a second approach, we parametrize the bioreactor shapes as shown in Figure 3.12-(b). The shape of the exterior wall is a quadratic *Bézier curve* (see, for example, [**?**]), associated to the control points $\mathbf{P} = (r + R_1, H - h)$, $\mathbf{Q} = (r + R_2, h)$ and $\mathbf{E} = (E_1, E_2)$, where $(E_1, E_2) \in [E_{1,\min}, E_{1,\max}] \times [E_{2,\min}, E_{2,\max}]$, by the formula

$$\mathbf{B}(\sigma) = (B_1(\sigma), B_2(\sigma)) = (1-\sigma)^2\mathbf{P} + 2(1-\sigma)\sigma\mathbf{E} + \sigma^2\mathbf{Q}, \qquad \sigma \in [0, 1]. \tag{3.35}$$

The set ϕ appearing in problem (3.29) is taken as $\phi = (H, R_1, R_2, \psi)$, where

$$\begin{array}{rccc} \psi: & [h, H-h] & \longrightarrow & [R_{\min}, R_{\max}] \\ & z & \longmapsto & \psi(z) = B_1(B_2^{-1}(z)). \end{array}$$

Following Lemma 3.3.1, one has that $B_1 \circ B_2^{-1} \in \mathcal{C}([h, H-h], [R_{\min}, R_{\max}])$.

Now, we define two new optimization parameters $\alpha_1, \alpha_2 \in [0,1]$ such that

$$E_1 = E_{1,\min} + \alpha_1 \cdot (E_{1,\max} - E_{1,\min}) \qquad \text{and} \qquad E_2 = h + \alpha_2 \cdot (H - 2h). \tag{3.36}$$

In that case, the bioreactor geometry only depends on parameters H, R_1, R_2, α_1 and α_2. The solution of the optimization problem (3.29) is approximated by computing

$$\left\{ \begin{array}{l} \text{Find } \tilde{\phi}^{5,\text{opt}} \in \tilde{\Phi}^5, \text{ such that} \\ J(\tilde{\phi}^{5,\text{opt}}) = \min_{\tilde{\phi}^5 \in \tilde{\Phi}^5} J(\tilde{\phi}^5), \end{array} \right. \tag{3.37}$$

where $\tilde{\phi}^{5,\text{opt}} = (H^{\text{opt}}, R_1^{\text{opt}}, R_2^{\text{opt}}, \alpha_1^{\text{opt}}, \alpha_2^{\text{opt}})$ and

$$\tilde{\Phi}^5 := \{(H, R_1, R_2, \alpha_1, \alpha_2) \in [H_{\min}, H_{\max}] \times [R_{1,\min}, R_{1,\max}] \times [R_{2,\min}, R_{2,\max}] \times [0,1]^2\} \subset \mathbb{R}^5$$

is the admissible space. We solve problem (3.37) by using the Hybrid Genetic Algorithm, presented in Section 3.1, applying the stopping criterion *No improvement through generations* (with $\hat{g} = 25$) for GA and the stopping criterion *Maximum number of iterations* (with $N_{\text{it}} = 25$) for SD.

Lemma 3.3.1. *Let us denote* $E_{1,\min} = R_{\min} - \sqrt{(R_1 + r - R_{\min})(R_2 + r - R_{\min})}$ *and* $E_{1,\max} = R_{\max} + \sqrt{(R_1 + r - R_{\max})(R_2 + r - R_{\max})}$. *If* $(E_1, E_2) \in [E_{1,\min}, E_{1,\max}] \times [h, H-h]$, *then* $B_1 \circ B_2^{-1} \in \mathcal{C}([h, H-h], [R_{\min}, R_{\max}])$.

Proof. We divide the proof in four steps:

Step 1. Let us prove that, if $E_2 \in [h, H-h]$, then $B_2([0,1]) = [h, H-h]$.
In order to obtain the minimum and maximum values of $B_2(\sigma)$, $\sigma \in [0,1]$, we compute the critical points σ_2^* satisfying the equation $\dfrac{\mathrm{d}B_2}{\mathrm{d}\sigma}(\sigma_2^*) = 0$. When considering E_2 as a variable, one can see that σ_2^* depends on E_2 through the expression $\sigma_2^*(E_2) = \dfrac{E_2 - H + h}{2E_2 - H}$, with corresponding value $B_2(\sigma_2^*(E_2)) = \dfrac{E_2^2 + h^2 - Hh}{2E_2 - h}$.
Now, in order to find the lower and upper bounds for variable E_2 (assuring that $B_2(\sigma) \in [h, H-h]$ $\forall \sigma \in [0,1]$), we respectively solve equations $B_2(\sigma_2^*(E_{2,\text{m}})) = h$ and $B_2(\sigma_2^*(E_{2,\text{M}})) = H - h$. It is easy to prove that the unique solutions of these equations are $E_{2,\text{m}} = h$ and $E_{2,\text{M}} = H - h$. Finally, taking into account that $\dfrac{\mathrm{d}B_2^2}{\mathrm{d}\sigma^2} = 2H - 4E_2$, it follows that $\dfrac{\mathrm{d}^2 B_2}{\mathrm{d}\sigma^2}\Big|_{E_2 = h} = 2(H - 2h) > 0$ and $\dfrac{\mathrm{d}^2 B_2}{\mathrm{d}\sigma^2}\Big|_{E_2 = H-h} = 2(2h - H) < 0$, and so, one can conclude that $E_{2,\min} = h$ and $E_{2,\max} = H - h$.

Step 2. Let us prove that the function $B_2 : [0,1] \to [h, H-h]$ is injective.
Let $\sigma, \bar{\sigma} \in [0,1]$ satisfying $B_2(\sigma) = B_2(\bar{\sigma})$. By definition, this implies that

$$(1-\sigma)^2(H-h) + 2(1-\sigma)\sigma E_2 + \sigma^2 h = (1-\bar{\sigma})^2(H-h) + 2(1-\bar{\sigma})\bar{\sigma} E_2 + \bar{\sigma}^2 h.$$

Easy calculations lead to

$$(H-h)\big(\sigma^2 - \bar{\sigma}^2 - 2\sigma + 2\bar{\sigma}\big) + 2E_2\big(\sigma - \bar{\sigma} - \sigma^2 + \bar{\sigma}^2\big) + h\big(\sigma^2 - \bar{\sigma}^2\big) = 0.$$

Denoting $x = \bar{\sigma} - \sigma$ and $y = \bar{\sigma} + \sigma$, the previous equation can be rewritten as

$$x(2-y)(H-h) + 2x(y-1)E_2 - xyh = 0 \Leftrightarrow x\left(2(H-h) - 2E_2 + y(2E_2 - H)\right) = 0.$$

This implies that either $x = 0$ or $y = \dfrac{2(H-h-E_2)}{H-2E_2}$. In the second case, it is easy to see that $y = 1 + \dfrac{H-2h}{H-2E_2}$ and, since we assume that $E_2 > h$, it follows that $y > 2$, but this enters in a contradiction with the definition of y. Thus, we can conclude that $x = 0$, so $\sigma = \bar{\sigma}$ and the injectivity is proved.

Step 3. Let us prove that, if $E_1 \in [E_{1,\min}, E_{1,\max}]$, then $B_1([0,1]) = [R_{\min}, R_{\max}]$.
Similarly to step 1, in order to obtain the minimum and maximum values of $B_1(\sigma)$, $\sigma \in [0,1]$, we compute the critical points σ_1^* satisfying the equation $\dfrac{\mathrm{d}B_1}{\mathrm{d}\sigma}(\sigma_1^*) = 0$. When considering E_1 as a variable, one can see that σ_1^* depends on E_1 through the expression $\sigma_1^*(E_1) = \dfrac{r + R_1 - E_1}{2r + R_1 + R_2 - 2E_1}$, with corresponding value $B_1(\sigma_1^*(E_1)) = \dfrac{(r+R_1)(r+R_2) - E_1^2}{2r + R_1 + R_2 - 2E_1}$. Now, in order to obtain lower and upper bounds for the variable E_1 (assuring that $B_1(\sigma) \in [R_{\min}, R_{\max}]\ \forall \sigma \in [0,1]$), we respectively solve equations $B_1(\sigma_1^*(E_{1,\mathrm{m}})) = R_{\min}$ and $B_1(\sigma_1^*(E_{1,\mathrm{M}})) = R_{\max}$. Each of these equations has two solutions, given by $E_{1,\mathrm{m}}^{\pm} = R_{\min} \pm \sqrt{(r + R_1 - R_{\min})(r + R_2 - R_{\min})}$ and $E_{1,\mathrm{M}}^{\pm} = R_{\max} \pm \sqrt{(r + R_1 - R_{\max})(r + R_2 - R_{\max})}$. Taking into account that $\dfrac{\mathrm{d}^2 B_1}{\mathrm{d}\sigma^2} = 2(2r + R_1 + R_2 - 2E_1)$, it follows that

$$\frac{\mathrm{d}^2 B_1}{\mathrm{d}\sigma^2}\Big|_{E_1 = E_{1,\mathrm{m}}^{\pm}} = 2(2r + R_1 + R_2 - 2R_{\min}) \mp 4\sqrt{(r + R_1 - R_{\min})(r + R_2 - R_{\min})}$$

and

$$\frac{\mathrm{d}^2 B_1}{\mathrm{d}\sigma^2}\Big|_{E_1 = E_{1,\mathrm{M}}^{\pm}} = 2(2r + R_1 + R_2 - 2R_{\max}) \mp 4\sqrt{(r + R_1 - R_{\max})(r + R_2 - R_{\max})},$$

and so, one can conclude that $E_{1,\min} = E_{1,\mathrm{m}}^{-}$ and $E_{1,\max} = E_{1,\mathrm{M}}^{+}$.

Step 4. Let us prove that $B_1 \circ B_2^{-1} \in \mathcal{C}([h, H-h], [R_{\min}, R_{\max}])$.
Since $B_1 : [0,1] \to [R_{\min}, R_{\max}]$ and $B_2 : [0,1] \to [h, H-h]$ are continuous functions and B_2 is injective, we conclude that $B_1 \circ B_2^{-1}$ is continuous because it is the composition of continuous functions. □

3.3.2 Numerical Experiments

In this section, we first describe the considered numerical experiments based on the optimization problems (3.34) and (3.37). Then, we analyze and compare the obtained results.

Numerical implementation of the model

The solution of system (2.8),(2.10) was computed using the software COMSOL Multyphisics 5.0 (`www.comsol.com`), based on the Finite Element method (see [**?**]). The numerical experiments were carried out in a 2.8Ghz Intel i7-930 64bits computer with 12Gb of RAM. We used a triangular mesh with around 3000 elements. We assumed that the solution of system (2.8) at finite time $\hat{T} = 10^7$ (s) could be considered as a reasonable approximation the steady state (S^*, B^*) of system (2.8). Model variables (3.30) and (3.31) were computed using the functions *Domain Integration* and *Boundary Integration* of COMSOL, respectively. Thus, the value of the cost function (3.32) was an output of the COMSOL model. Depending on the considered case (detailed below), each function evaluation in problems (3.34) and (3.37) may take from 15 up to 60 minutes.

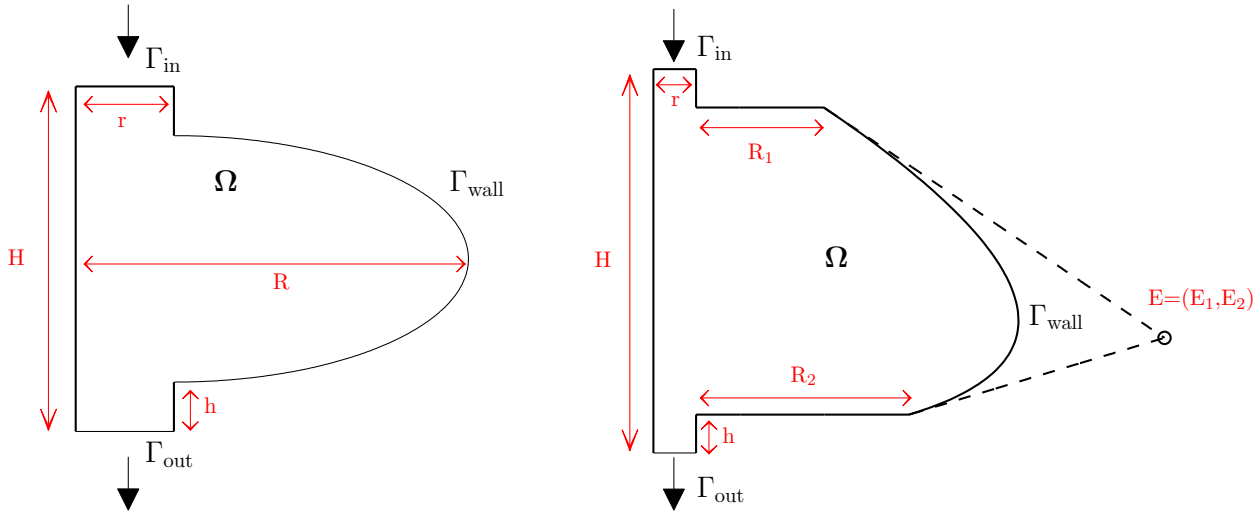

(a) Domain in problem (3.34) (b) Domain in problem (3.37)

Figure 3.12: Schematic representation of the bioreactor geometries used to solve the discrete problems (3.34) and (3.37).

Considered cases

Model parameters were set as follows [**?**, **?**]: $D_S = 4.3 \cdot 10^{-12}$(m^2/s), $D_B = 5 \cdot 10^{-10}$ (m^2/s), $S_e = 15$ (kg/m^3), $B_0 = 1$ (kg/m^3), $S_0 = 15$ (kg/m^3), $p_{atm} = 10^5$ (Pa), $\rho = 10^3$ (kg/m^3), $\eta = 10^{-3}$ (kg/m s) and $u_{in} = 0.8$ (m/h). We consider four different reaction functions μ_1, μ_2, μ_3 and μ_4, which are described in Table 3.8 (see pages 132, 182 and 187 in [**?**]). In Figure 3.13, we plot those four growth rate functions. We can observe that they have the same order of magnitude but with different slopes.

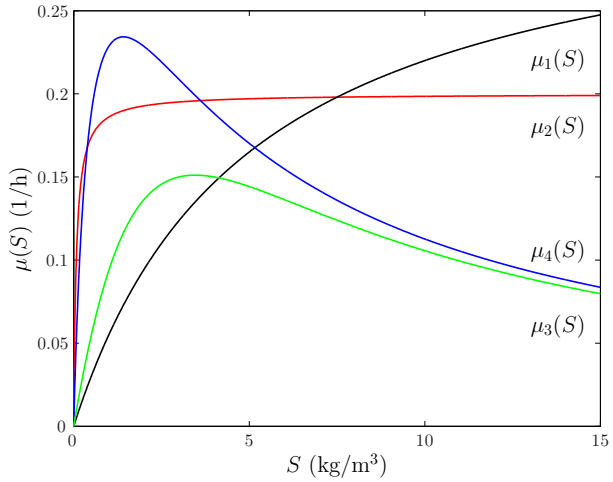

Figure 3.13: Functions $\mu_1(S)$, $\mu_2(S)$, $\mu_3(S)$ and $\mu_4(S)$ (1/h), detailed in Table 3.8, with $S \in [0, 15]$ (kg/m^3).

When solving problem (3.34), design parameters $H_{min} = 2$ (m), $H_{max} = 10$ (m), $R_{min} = 0.55$ (m) and $R_{max} = 5$ (m), $N_H = 30$ and $N_R = 50$ were taken to generate the admissible space $\tilde{\Phi}^{2,N_H,N_R}$. On the other hand, when solving problem (3.37), the admissible space $\tilde{\Phi}^5$ was generated with design parameters $H_{min} = 2$ (m) $H_{max} = 10$ (m), $R_{1,min} = R_{2,min} = 0$ and $R_{1,max} = R_{2,max} = 3.5$ (m). In order to compute the values $E_{1,min}$ and $E_{1,max}$, we chose $R_{min} = 0.5$ (m) and $R_{max} = 10$ (m). In all cases we set $r = h = 0.5$ (m).

$\mu_1(\cdot)$	$\mu_2(\cdot)$	$\mu_3(\cdot)$	$\mu_4(\cdot)$
Monod function (2.2)	Monod function (2.2)	Haldane function (2.3)	Haldane function (2.3)
$\mu_{\max} = 0.33$ 1/h	$\mu_{\max} = 0.2$ 1/h	$\mu_{\max} = 0.5$ 1/h	$\mu_{\max} = 0.4$ 1/h
$K_{\mathrm{S}} = 5$ kg/m^3	$K_{\mathrm{S}} = 0.075$ kg/m^3	$K_{\mathrm{S}} = 4$ kg/m^3,	$K_{\mathrm{S}} = 0.5$ kg/m^3,
		$K_{\mathrm{I}} = 3$ kg/m^3	$K_{\mathrm{I}} = 4$ kg/m^3

Table 3.8: Considered growth rate functions

Remark 3.3.2. *It would be interesting to run the numerical simulations with higher values of parameters N_{H} and N_{R} when considering bioreactor geometries created with 2 parameters. However, when considering the current parameters $N_{\mathrm{H}} = 30$ and $N_{\mathrm{R}} = 50$, the total computational time for solving the optimization problem (3.34) for each considered case is around 40 days. Thus, higher values of N_{H} and N_{R} could increase drastically the computational time and will be tackled as a future work.*

Optimal domains with 2 parameters

Here, we solve numerically the optimization problem (3.34) for prescribed output concentrations $S_{\mathrm{lim}} \in \{10^{-4}\} \cup \{\frac{i}{2}\}_{i=1}^{20}$ (kg/m^3). Figure 3.14 shows the optimization results obtained with μ_i, $i = 1, \ldots, 4$ in function of S_{lim}. More precisely, in Figures 3.14-(a), 3.14-(b) and 3.14-(c), we plot the values of the objective function $J(\tilde{\phi}^{2,\mathrm{opt}})$, the optimal height H^{opt} and the optimal radius R^{opt} according to S_{lim}, respectively. We point out that, in all the considered cases, the optimal solution $\tilde{\phi}^{2,\mathrm{opt}}$ is such that the second term in (3.32) is zero, and therefore, the value $J(\tilde{\phi}^{2,\mathrm{opt}})$ corresponds to the reactor volume $\mathrm{Vol}(\tilde{\phi}^{2,\mathrm{opt}})$.

As it can be observed in Figure 3.14-(a), the value of $J(\tilde{\phi}^{2,\mathrm{opt}})$ increases as the value of S_{lim} decreases. This behavior is physically reasonable, since one may need to increase the reactor volume in order to increase the region of interaction between the biomass and the substrate, and thus obtain a lower outflow substrate concentration.

Figures 3.14-(b) and 3.14-(c) seem to show that, in general, the height of the optimal reactor is greater than its width. This outcome is in line with the results found in [**?**, **?**], where the authors performed experimental studies to conclude that the most efficient reactor was a tubular reactor with its height much greater than its radius. Nevertheless, this strategy is not always applicable due to the restriction on the reactor height. When the maximum height is reached, the reactor radius may be increased to reduce the output substrate concentration.

When comparing the results obtained with the reaction functions, we observe that, for instance, the values of $J(\tilde{\phi}^{2,\mathrm{opt}})$ are higher with μ_3 than with μ_1. This difference seems to be due to the fact that function μ_3 is qualitative smaller than function μ_1 (see Figure 3.13) and thus, the optimal volume must be bigger to ensure that the prescribed value S_{lim} is reached.

As a representative case, the optimal shapes obtained when solving problem (3.34) with $S_{\mathrm{lim}} = 1$ (kg/m^3) are depicted in Figure 3.15. One can observe that the optimized reactors exhibit similar heights and the main difference lies in the reactor radius. The influence of the reactor width on the bioreactor dynamics is explained in Remarks 3.3.4 and 3.3.5 below.

Optimal domains with 5 parameters

Here, as the computational time to obtain one numerical solution of system (2.8),(2.10) is long (around 40 minutes), we solve numerically the optimization problem (3.37) considering only the case $S_{\mathrm{lim}} = 1$ (kg/m^3). Table 3.9 shows the optimal results, while the optimized shapes are depicted in Figure 3.16.

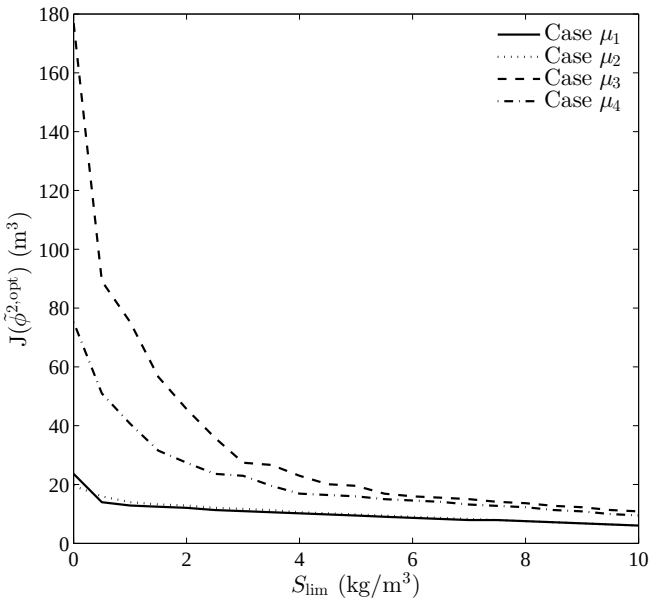

(a) $J(\tilde{\phi}^{2,\mathrm{opt}})$ vs S_{lim}

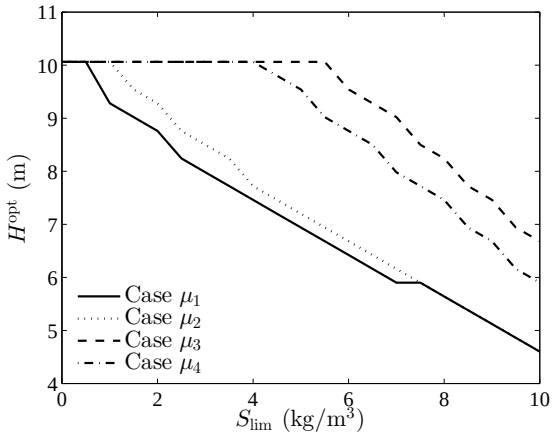

(b) H^{opt} vs S_{lim}

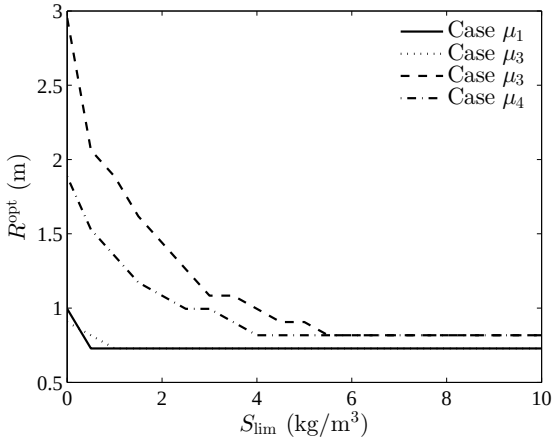

(c) R^{opt} vs S_{lim}

Figure 3.14: Domains built with 2 parameters: Comparison of the results of problem (3.34) obtained for growth rate functions μ_i, $i = 1, \ldots, 4$ (depicted with solid, dotted, dashed and dashed-dotted lines, respectively) when $S_{\mathrm{lim}} \in (0, 10]$ (kg/m^3).

Remark 3.3.3. *We observe from Table 3.9 that the value $S^*_{\mathrm{out}}(\tilde{\phi}^{5,\mathrm{opt}})$ is clearly smaller than the prescribed value S_{lim} in all the considered cases, which seems to indicate that smaller (and therefore better) domains could be obtained with this value closer to S_{lim}. This inaccuracy may be due to the lack of numerical precision of the COMSOL model, which in turn is caused by the restriction on the computational time. This fact highlights the difficulties tackled during the numerical resolution of our optimization problem.*

From Figure 3.16 we observe that, as stated when considering domains created with 2 parameters, the optimal reactors have height larger than width. Moreover, the exterior wall of the optimized reactors is concave (as said previously, the influence of the reactor radius in the bioreactor dynamics will be explained in Remarks 3.3.4 and 3.3.5 below).

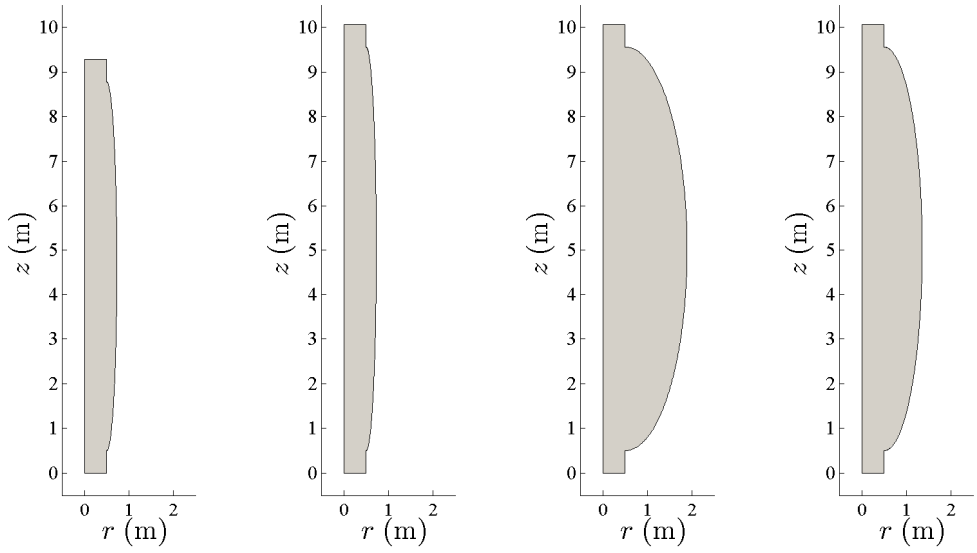

(a) μ_1 (b) μ_2 (c) μ_3 (d) μ_4

Figure 3.15: Domains built with 2 parameters: Shape of the optimized reactors, $\Omega(\tilde{\phi}^{2,\text{opt}})$, where $\tilde{\phi}^{2,\text{opt}}$ is the solution of problem (3.34) with $S_{\text{lim}} = 1$ (kg/m^3).

μ	H^{opt}	R_1^{opt}	R_2^{opt}	α_1^{opt}	α_2^{opt}	E_1	E_2	$\text{S}_{\text{out}}^*(\tilde{\phi}^{5,\text{opt}})$	$\text{Vol}(\tilde{\phi}^{5,\text{opt}})$
μ_1	9.6359	0.0931	0.4214	$1.6358 \cdot 10^{-5}$	0.0059	0.3022	0.5480	0.9540	10.0790
μ_2	9.0814	0.0730	0.6024	0.0064	0.0922	0.4111	1.1990	0.8923	12.0855
μ_3	9.8879	1.5432	0.7402	0.0093	0.9940	−0.3928	8.8376	0.9545	27.1679
μ_4	9.6401	0.5210	1.5805	$1.9301 \cdot 10^{-4}$	0.0273	−0.4038	0.7222	0.6083	22.0094

Table 3.9: Domains built with 5 parameters: Value of the optimal parameters (H^{opt}(m), R_1^{opt}(m), R_2^{opt}(m), α_1^{opt} and α_2^{opt}) in $\tilde{\phi}^{5,\text{opt}}$, solution of problem (3.37) with functions $\mu_i, i = 1, \ldots, 4$; and exterior control point coordinates (E_1 (m) and E_2 (m)), associated to $\tilde{\phi}^{5,\text{opt}}$ and computed using equation (3.36) and Lemma 3.3.1; outflow substrate concentrations ($\text{S}_{\text{out}}^*(\tilde{\phi}^{5,\text{opt}}$(kg/m^3)); and reactor volumes ($\text{Vol}(\tilde{\phi}^{5,\text{opt}})$(m^3)).

When comparing reaction functions, Figures 3.16-(a) and 3.16-(c) seem to show that, for instance, the radius expansion of the domain $\Omega(\tilde{\phi}^{5,\text{opt}})$ is wider for growth rate function μ_3 than for μ_1, as observed with 2 parameters. On the other hand, the main difference between considering Monod (μ_1 and μ_2) or Haldane (μ_3 and μ_4) reaction functions is observed in the concavity at the upper part of the exterior wall (see Remark 3.3.4 for a physical interpretation).

Comparison between the optimized reactors

Here, we compare the solutions obtained when solving the optimization problems (3.34) and (3.37). For example, Figures 3.15 and 3.16 seem to show that the optimized reactors have height larger than width (indeed, $H_{\max}$ set to 10 (m) limits the optimal shape height and the optimal heights in all the considered cases approach this limit) and generally, the width approach its lower bound (the minimum reactor radius

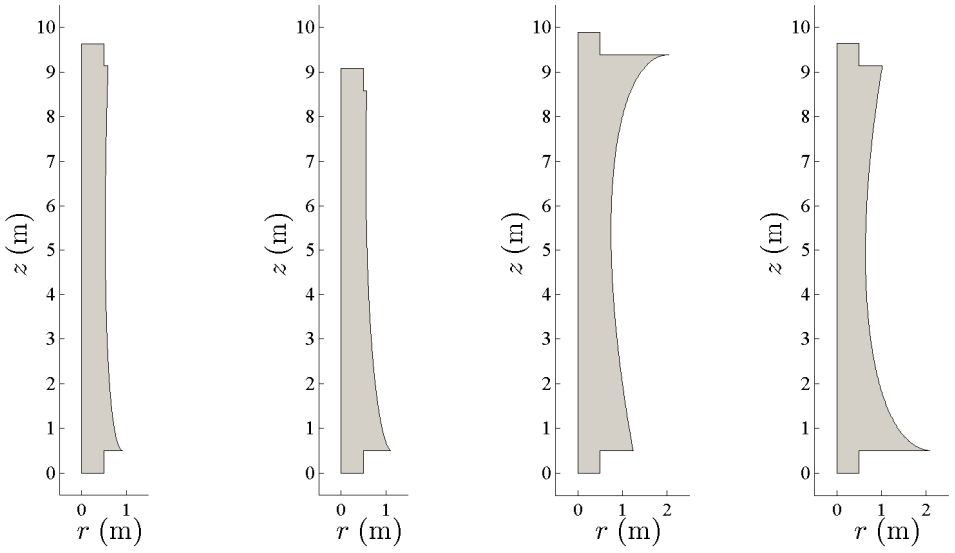

(a) μ_1 (b) μ_2 (c) μ_3 (d) μ_4

Figure 3.16: Optimal domains with 5 parameters: Shape of the optimized reactors, $\Omega(\tilde{\phi}^{5,\text{opt}})$, where $\tilde{\phi}^{5,\text{opt}}$ is the solution of problem (3.37).

allowed was $r = 0.5$ (m)). However, in some of the considered cases (see Figures 3.15-(c), 3.15-(d) and 3.16), a radius expansion (at least in some limited part of the reactor) is observed. We think that, increasing the reactor width, favors the reaction due to two main reasons:

- It helps that the vertical flow velocity decreases (in absolute value), and so the time that the biomass and the substrate remain in contact for reacting increases (see Remark 3.3.4 for a more detailed analysis of the relation between the reactor width and the vertical flow).
- It originates an area of biomass storage. For example, due to the apparition of Dean vortices in this area (see, e.g., [**?**]) the biomass located near the device exterior wall remains more time inside the bioreactor (compared to the biomass located at the reactor center), and so the amount of reaction between biomass and substrate increases (see Remark 3.3.5 for an specific explanation about the distribution of substances in the reactor).

Remark 3.3.4. *In order to understand the influence of the bioreactor width on the vertical flow velocity, we used four different domains, denoted by Ω_i, $i = 1, \ldots, 4$. The first reactor is cylindrical (depicted in Figure 3.17-(a)) and the other three present a radius extension on the top, center and bottom parts of the domain, (depicted in Figures 3.17-(b) to 3.17-(d), respectively). We solved system (2.10) with domains Ω_i, $i = 1, \ldots, 4$ and denoted u_{3,Ω_i} (m/s) the vertical flow velocity obtained when solving system (2.10) in the domain Ω_i, evaluated at $r = 0$ (i.e., symmetry streamline). Figure 3.17-(e) represents $|u_{3,\Omega_i}|$, $i \in \{1, \ldots, 4\}$, which can be seen as functions of z. We observe that, in regions where the reactor radius increases, the absolute value of the vertical velocity decreases. This physical interpretation may explain the optimal domains $\Omega(\tilde{\phi}^{5,\text{opt}})$ obtained with reactions μ_3 and μ_4 (see Figures 3.16-(c) and 3.16-(d)), since the Haldane function shows inhibition for large values of substrate (see Figure 3.13) and the maximum value of substrate appears at the reactor inlet.*

Remark 3.3.5. *Figures 3.18-(a) and 3.18-(b) represent the distributions of substrate and biomass at steady state, respectively, computed with the optimal reactor $\Omega(\tilde{\phi}^{2,\text{opt}})$, obtained for the growth rate function μ_3. One observes that the substrate concentration is mainly agglomerated in the area originated by the inlet streamlines (see Figure 3.18-(d)). On the other hand, the biomass becomes ejected from this central area*

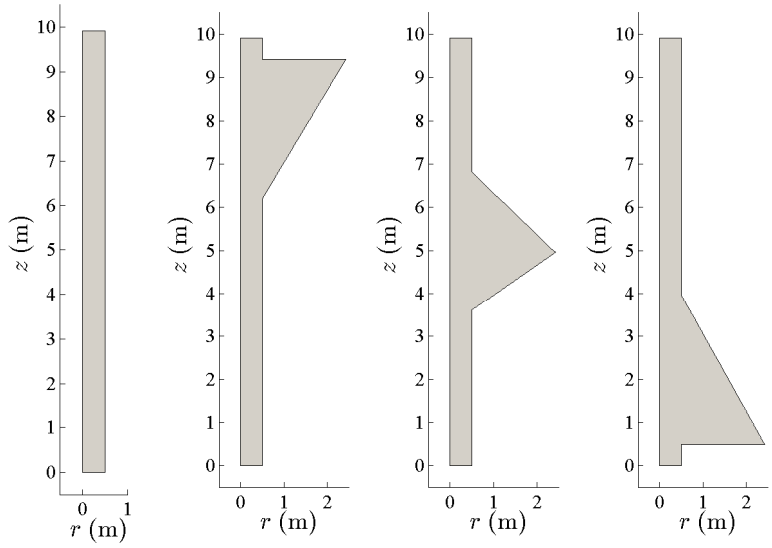

(a) Ω_1 (b) Ω_2 (c) Ω_3 (d) Ω_4

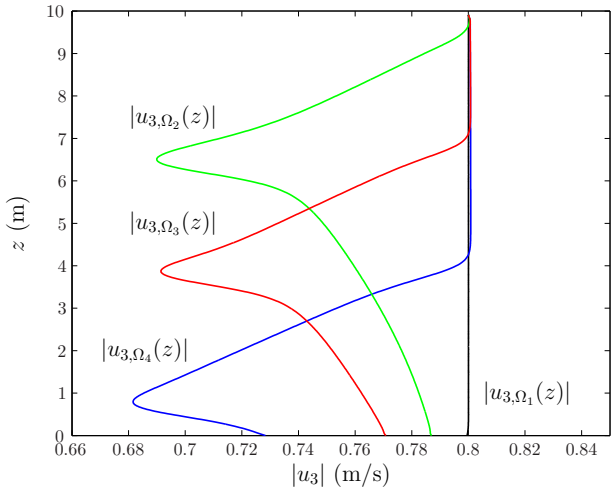

(e) Vertical velocity profile along the symmetry streamline obtained for reactor domains Ω_i, $i = 1, \ldots, 4$.

Figure 3.17: Influence of the reactor width into the vertical flow velocity.

and is mainly concentrated around the reactor wall (where Dean vortices appear [?], see Figure 3.18-(d)). Thus, a reaction front is created between the central area and the outer part of the reactor (as shown in Figure 3.18-(c)) favoring the reaction between the two species. Similar analysis can be performed by observing Figures 3.19, 3.20, 3.21, 3.22, 3.23, 3.24 and 3.25, related to the rest of optimized reactors shown in Figures 3.15 and 3.16. Although the optimization problems (3.34) *and* (3.37) *have been solved for a singular pair of diffusion coefficients* (D_S, D_B)*, numerical experiments seem to show that the analysis of the distribution of substances in the reactor, performed above, is suitable in the range of typical diffusion coefficients* D_S *(from* 10^{-10} *to* 10^{-7} *(*m^2/s*) [?, ?, ?]) and* D_B *(from* 10^{-13} *to* 10^{-7} *(*m^2/s*) [?, ?, ?]).*

Now, it is of interest to compare the optimized reactors obtained when solving the optimization problems (3.34) and (3.37). Table 3.10 shows the comparison, in terms of reactor volume, between the optimized reactors obtained when creating the domain with 2 and 5 parameters. One observes that the range of value of $\text{Vol}(\tilde{\phi}^{5,\text{opt}})$ is between 35% and 85% of $\text{Vol}(\tilde{\phi}^{2,\text{opt}})$.

μ	Vol($\tilde{\phi}^{2,\text{opt}}$) (m^3)	Vol($\tilde{\phi}^{5,\text{opt}}$) (m^3)
μ_1	12.8479	10.0790
μ_2	13.9843	12.0855
μ_3	75.2551	27.1679
μ_4	40.6650	22.0094

Table 3.10: Comparison, in terms of reactor volume (m^3), between optimized reactors obtained when solving problems (3.34) (Vol($\tilde{\phi}^{2,\text{opt}}$)) and (3.37) (Vol($\tilde{\phi}^{5,\text{opt}}$)) with $S_{\text{lim}} = 1$ (kg/m^3).

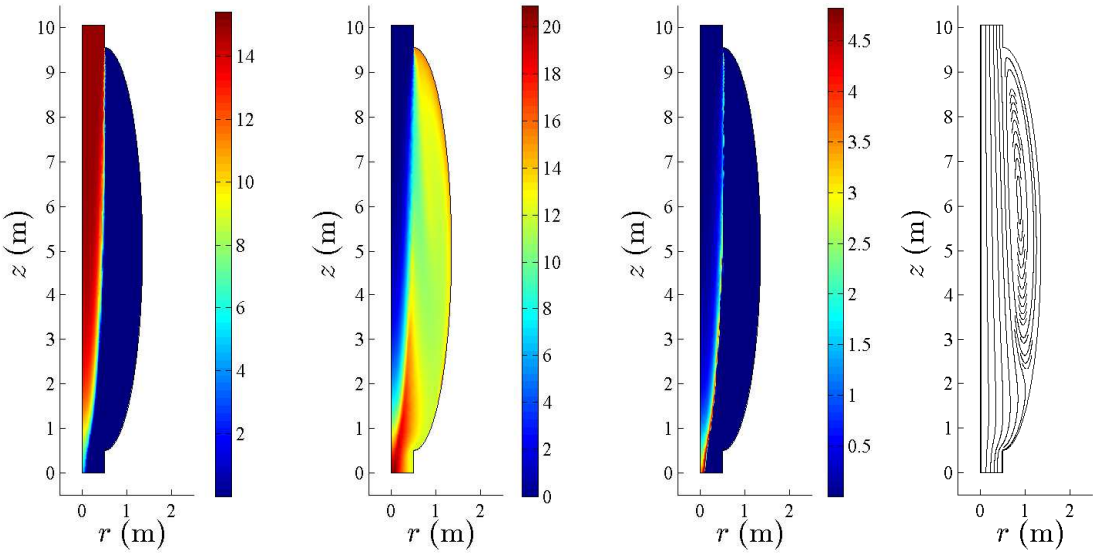

(a) $S^*(r,z)$ (kg/m^3) (b) $B^*(r,z)$ (kg/m^3) (c) $\mu(S^*)B^*$ (kg/m^3 h) (d) Streamlines

Figure 3.18: Case μ_3: (a) substrate concentration (at steady state). (b) biomass concentration (at steady state). (c) reaction (at steady state) (d) streamlines. (a)-(d) associated to the optimal reactor $\Omega(\phi^{2,\text{opt}})$.

3.3.3 Conclusions

We have explored the shape design of a particular biological reactor. The main objective was to reduce the reactor volume, ensuring that a prescribed output concentration value was reached. We have used a mathematical model that couples hydrodynamics (described with the incompressible Navier–Stokes equations) with biological phenomena (described with an Advection-Diffusion-Reaction system). Using the Finite Element Method, we have numerically computed the output substrate concentration and the volume of a reactor associated to a particular set of design parameters. Then, we have defined two discrete optimization problems related to the design of our device and solved them by using different optimization techniques. We have taken into account that the reaction between species may be modeled by either monotonic or non-monotonic functions, and we have analyzed the influence of this factor on the optimization results.

From a general point of view, the optimized reactors exhibit height much larger than width and their exterior wall is concavely curved. The magnitude of the radius extension is related to the reaction function. The slower is the reaction the wider should be the device. The advantage of the radius extensions in the reactor performance could be attributed to two main factors:

1. The width of the reactor helps to decrease the absolute value of the vertical flow velocity, and

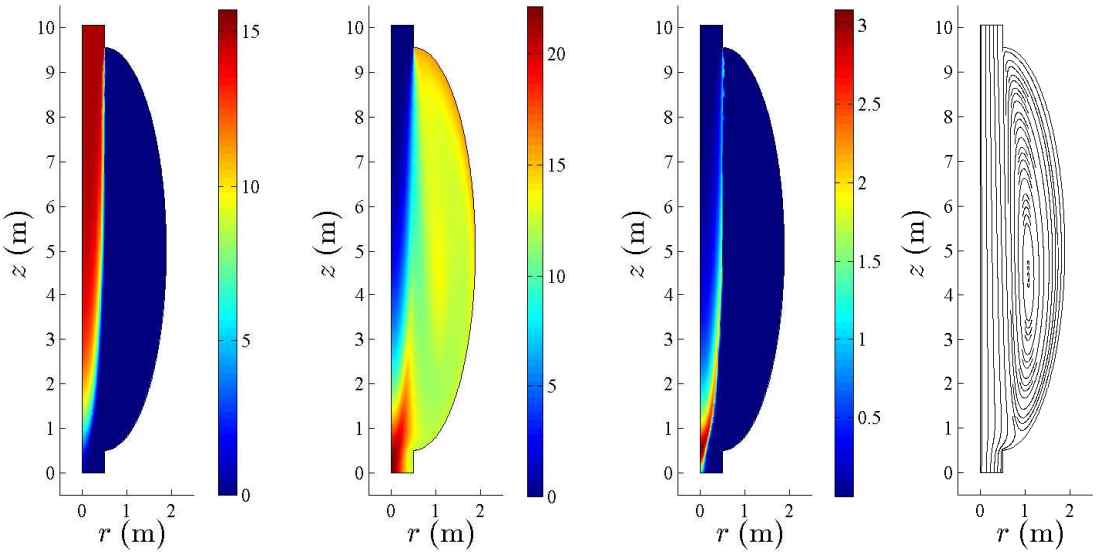

(a) $S^*(r,z)$ (kg/m^3) (b) $B^*(r,z)$ (kg/m^3) (c) $\mu(S^*)B^*$ (kg/m^3 h) (d) Streamlines

Figure 3.19: Case μ_4: (a) substrate concentration (at steady state). (b) biomass concentration (at steady state). (c) reaction (at steady state) (d) streamlines. (a)-(d) associated to the optimal reactor $\Omega(\phi^{2,\text{opt}})$.

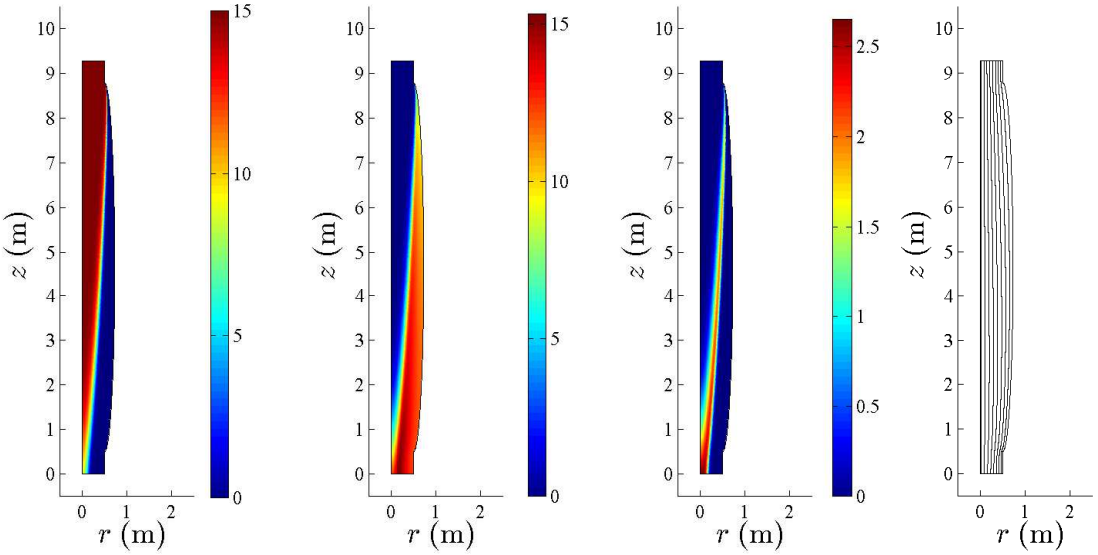

(a) $S^*(r,z)$ (kg/m^3) (b) $B^*(r,z)$ (kg/m^3) (c) $\mu(S^*)B^*$ (kg/m^3 h) (d) Streamlines

Figure 3.20: Case μ_1: (a) substrate concentration (at steady state). (b) biomass concentration (at steady state). (c) reaction (at steady state) (d) streamlines. (a)-(d) associated to the optimal reactor $\Omega(\phi^{2,\text{opt}})$.

consequently, increases the time of potential reaction between substances.

2. The reactor corners may act as a biomass storage. The biomass located near the reactor exterior wall is ejected slower from the device than the biomass located near the device center, favoring the reaction between species.

When comparing the optimized reactors obtained for both monotonic and non-monotonic growth rate

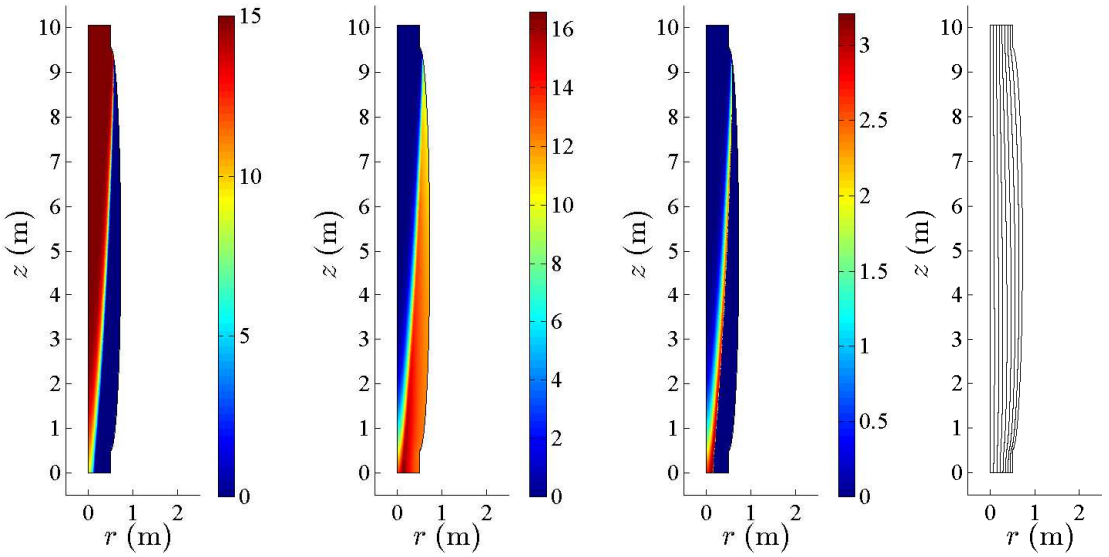

(a) $S^*(r,z)$ (kg/m^3) (b) $B^*(r,z)$ (kg/m^3) (c) $\mu(S^*)B^*$ (kg/m^3 h) (d) Streamlines

Figure 3.21: Case μ_2: (a) substrate concentration (at steady state). (b) biomass concentration (at steady state). (c) reaction (at steady state) (d) streamlines. (a)-(d) associated to the optimal reactor $\Omega(\phi^{2,\text{opt}})$.

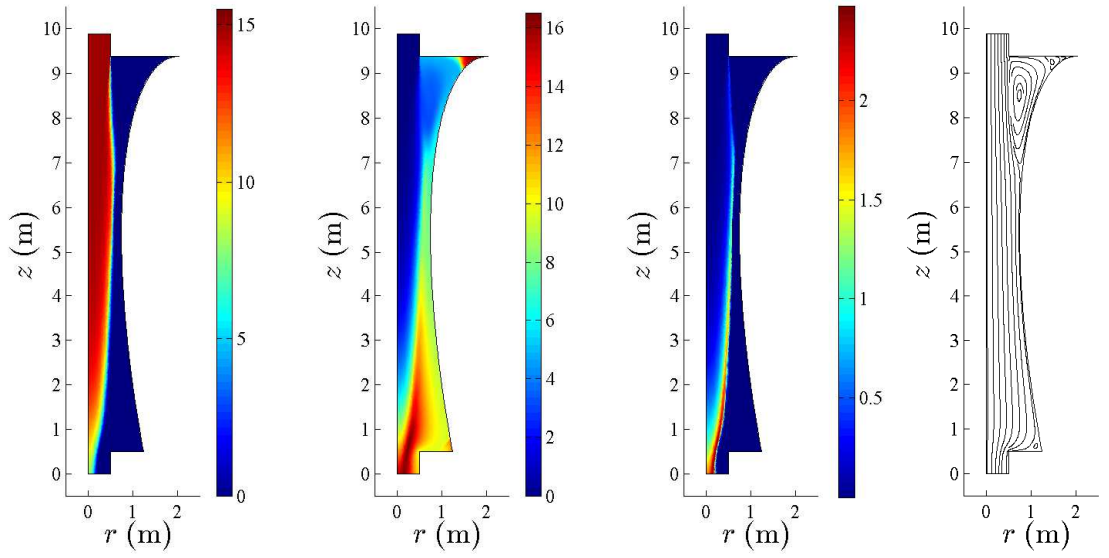

(a) $S^*(r,z)$ (kg/m^3) (b) $B^*(r,z)$ (kg/m^3) (c) $\mu(S^*)B^*$ (kg/m^3 h) (d) Streamlines

Figure 3.22: Case μ_3: (a) substrate concentration (at steady state). (b) biomass concentration (at steady state). (c) reaction (at steady state) (d) streamlines. (a)-(d) associated to the optimal reactor $\Omega(\phi^{5,\text{opt}})$.

functions, one observes that, if the reactor is modeled with non-monotonic kinetics (e.g., Haldane function), the radius expansion located at the top of the reactor is more pronounced. We believe that this difference relays on the fact that for large values of substrate (i.e., at the inlet of the device) the Haldane reaction shows inhibition, and so the radius expansion should be bigger to make decrease the absolute value of the vertical flow near the reactor inlet.

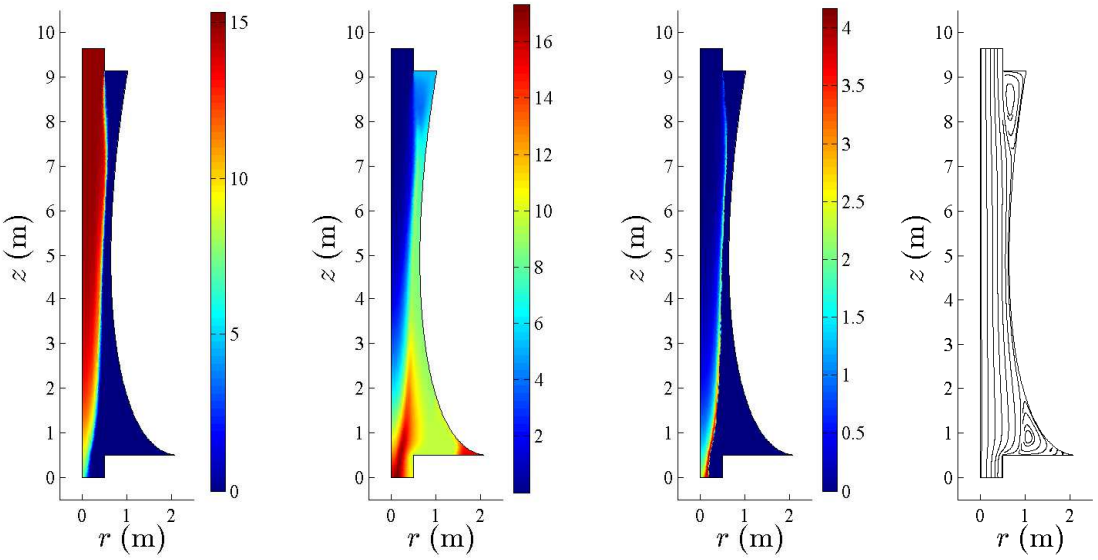

(a) $S^*(r,z)$ (kg/m^3) (b) $B^*(r,z)$ (kg/m^3) (c) $\mu(S^*)B^*$ (kg/m^3 h) (d) Streamlines

Figure 3.23: Case μ_4: (a) substrate concentration (at steady state). (b) biomass concentration (at steady state). (c) reaction (at steady state) (d) streamlines. (a)-(d) associated to the optimal reactor $\Omega(\phi^{5,\text{opt}})$.

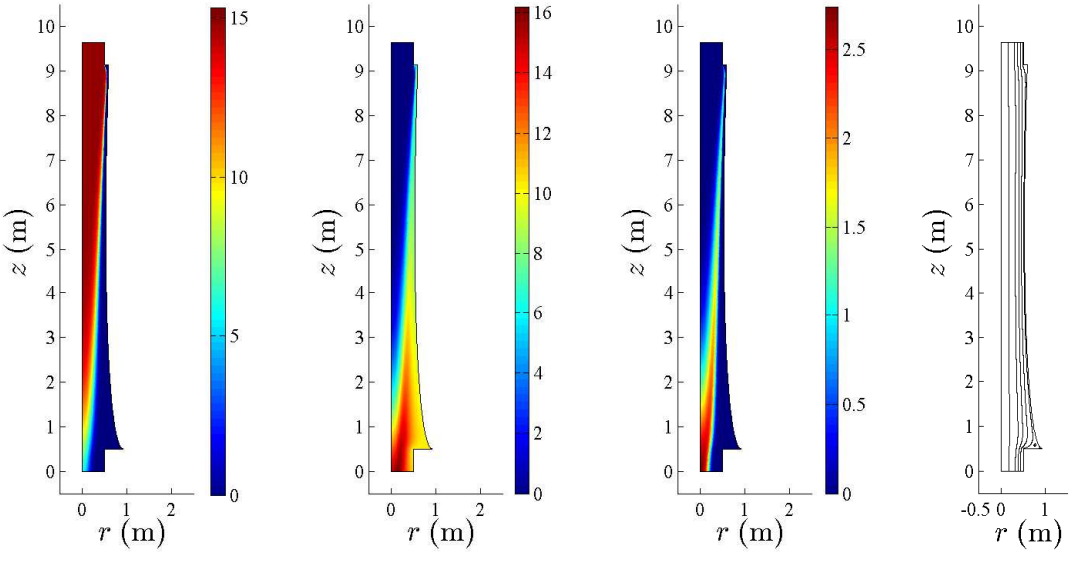

(a) $S^*(r,z)$ (kg/m^3) (b) $B^*(r,z)$ (kg/m^3) (c) $\mu(S^*)B^*$ (kg/m^3 h) (d) Streamlines

Figure 3.24: Case μ_1: (a) substrate concentration (at steady state). (b) biomass concentration (at steady state). (c) reaction (at steady state) (d) streamlines. (a)-(d) associated to the optimal reactor $\Omega(\phi^{5,\text{opt}})$.

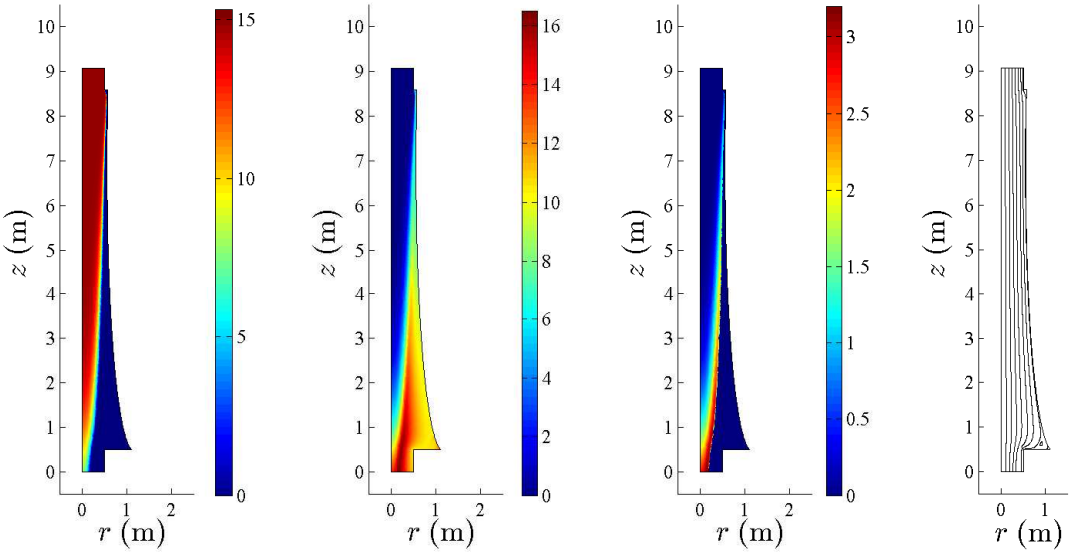

(a) $S^*(r,z)$ (kg/m^3) (b) $B^*(r,z)$ (kg/m^3) (c) $\mu(S^*)B^*$ (kg/m^3 h) (d) Streamlines

Figure 3.25: Case μ_2: (a) substrate concentration (at steady state). (b) biomass concentration (at steady state). (c) reaction (at steady state) (d) streamlines. (a)-(d) associated to the optimal reactor $\Omega(\phi^{5,\mathrm{opt}})$.

Chapter 4

Conclusions and future work

In this part of the thesis, we have described, modeled and analyzed the dynamics in a continuous bioreactor, our main goal being to study the influence of spatial inhomogeneities in the bioreactor dynamics. Then, we have tackled two optimization problems in which continuous bioreactors are used for water treatment.

Chapter 2 is devoted to the mathematical modeling of the bioreactor. Particularly, in Section 2.1 we presented the renowned *chemostat* model, based on ordinary differential equations, which describes the dynamics in a well-mixed reactor. We have reviewed previous results on the existence, uniqueness, nonnegativity and boundedness of the solution, as well as the usual stability analysis of the chemostat model. The system exhibits two stable equilibrium states: the *washout* state (in which the biomass becomes extinct and no reaction is produced) and another steady state, which corresponds to the partial elimination of substrate. Then, in Section 2.2, we proposed to describe the behavior of an unmixed reactor with a coupled system of Advection-Diffusion-Reaction equations. In contrast with previous works [**?**, **?**, **?**], we have considered cylindrical reactors and allowed the diffusion rates of the substrate and the biomass to be distinct. The existence, uniqueness, nonnegativity and boundedness of the solution have been proved using a combination of the Schauder Fixed Point Theorem and variational techniques. When performing the stability analysis of the Advection-Diffusion-Reaction system, we have applied linearization techniques to obtain sufficient conditions for the asymptotic stability of the different equilibria. Results seem to indicate that, as the diffusion coefficients decrease, the fluid flow velocity must be smaller (favoring the reaction between the substrate and the biomass) to avoid the washout state. Moreover, when high diffusion coefficients are considered (so that the concentration of substances becomes nearly spatially homogeneous in the reactor) the stability analysis results obtained for the chemostat model are similar to those obtained for the Advection-Diffusion-Reaction system.

In Chapter 3, we firstly introduced a global optimization algorithm, called Hybrid Genetic Algorithm (HGA), used to solve the two optimization problems appearing in that chapter. The first problem, presented in Section 3.2, aims to minimize the time needed to clean a polluted water resource, by choosing an optimal bioreactor volumetric inflow rate (which is taken either time or state dependent). This problem was tackled in [**?**] by applying well-mixed reactors and our goal was to study the influence of spatial inhomogeneities into the optimization results obtained in [**?**]. We showed that, when considering small diffusion parameters or non-uniform flow velocity profiles in the bioreactor, the optimal state-dependent control obtained in [**?**] can lead the bioreactor to washout (preventing the desired decontamination objective), while a simple constant control, obtained with the methodology proposed in this work, can solve the problem. Notice that, when modeling the coupled system between the water resource and the bioreactor, we assumed that the substances were homogeneously distributed throughout the resource. More accurate optimization results might be obtained if one studies the influence of spatial inhomogeneities in the full system.

The second problem, presented in Section 3.3, aims to reduce the reactor volume, assuring that a prescribed output concentration is attained, by optimizing its shape. Results seem to indicate that, generally, the optimized reactor shows height much bigger than width and its outer wall is concavely curved, with the radius extensions acting as a biomass storage and helping to decrease the vertical inflow (so that the time of potential reaction between substances increase). Moreover, when considering non-monotonic growth rate functions (i.e., when assuming that the growth rate of the biomass do not always increase with the substrate concentration), the radius expansion located at the top is more pronounced. The optimization results obtained in this section may guide companies in the industry sector to build on smaller reactors, reducing not only the production cost of the tank, but also the physical space set aside for the water treatment.

Part II

Liquid Crystals

Chapter 5

Introduction

Liquid crystals are states of matter which are sometimes observed to occur between the solid crystal state and the conventional liquid state. They may flow like fluids and also possess features that are characteristic of solid crystals, such as certain optical properties: they therefore display both liquid and crystal properties, hence the name *liquid crystals*. Liquid crystals are also known to be *anisotropic* because they exhibit different physical properties in different directions.

History

The discovery of liquid crystals is generally attributed to the austrian botanical physiologist Reinitzer, who reported his observations in 1888 [**?**, **?**]. He observed that the *cholesteryl benzoate*, which is solid at room temperature, exhibits two melting points. At 145.5°C it melts into a cloudy liquid and at 178.5°C it melts again and the cloudy liquid becomes clear. Seeking help from a physicist, he wrote to Otto Lehman, who started a systematic research by observing *cholesteryl benzoate* and related compounds with a polarized light. Lehman [**?**] found that the intermediate cloudy phase sustained flow but exhibited several compound features that convinced him that he was dealing with a solid.

Liquid crystals revolutionized the industry of electronic visual displays (see [**?**, **?**]), a market valued at 75 millions of dollars in 2008. A typical Liquid Crystal Device (LCD), composed of millions of liquid crystal layers, exploits the birefringence property of liquid crystals to obtain distinct optical configurations (for instance, the amount of light passing through the layers) [**?**]. Figure 5.1 shows a liquid crystal observed with polarized light.

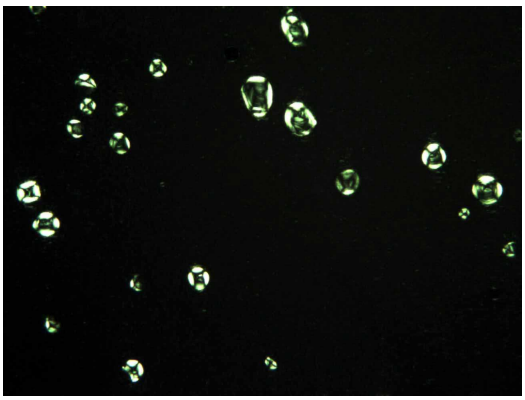

Figure 5.1: Liquid crystal viewed under a polarized light microscope. This picture is courtesy of Nuria Crespo Moya.

Basic descriptions

Most liquid crystals are organic substances which can be induced to exhibit liquid crystals phases by either two ways: changing the temperature or changing the concentration in a solvent. Those obtained by a change of concentration are called *lyoptropic* liquid crystals and those obtained by changing the temperature are called *thermotropic* liquid crystals, the latter being extensively studied in the literature. In the simplest description, liquid crystals can be thought as elongated rod-like molecules which have a preferred local average direction. Figure 5.2 is a schematic illustration of the solid crystal, liquid crystal and isotropic liquid phases of a possible material as the temperature T increases.

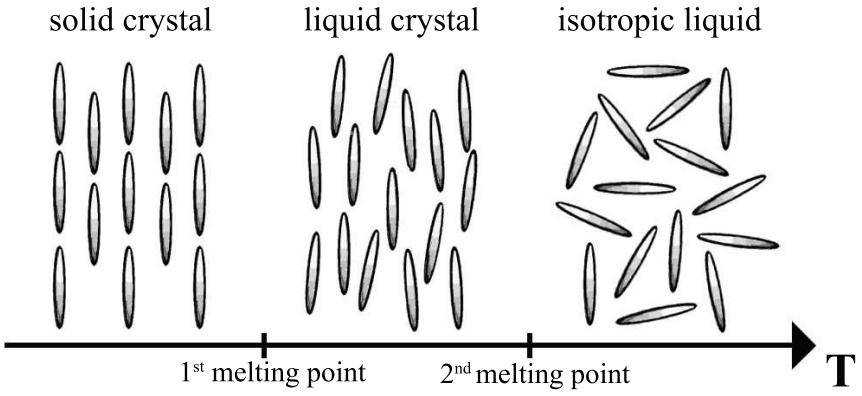

Figure 5.2: Schematic representation of the possible solid crystal, liquid crystal and isotropic liquid phases of a substance as the temperature T increases.

The liquid crystal phase can be, at the same time, subdivided in several phases, characterized by the type of ordering of the molecules. One can distinguish positional order (whether molecules are arranged in any sort of ordered lattice) and directional order (whether molecules are mostly pointing in the same direction). Following this characterization, we distinguish three main phases of thermotropic liquid crystals: nematic, smectic and chiral (a schematic representation of these phases is depicted in Figure 5.3).

- Nematic phase: molecules possess directional order but no positional order (they are randomly distributed as in a liquid).
- Smectic phase: molecules show directional order and positional order (they are arranged in some ordered pattern).
- Chiral phase (also called cholesteric phase): molecules exhibit a directional order that is helical (in the sense depicted in Figure 5.3) but no positional order.

In this part of the thesis, we focus on *thermotropic* liquid crystals in its nematic phase, where the long axes of the constitutive molecules tend to align parallel to each other along a single preferred direction (sometimes refereed as the *anisotropic axis*). A unit vector $\boldsymbol{n}$, called the director, describes the local direction of the average molecular alignment in liquid crystals, as shown in Figure 5.4. Here, $\boldsymbol{n}$ and -$\boldsymbol{n}$ are physically indistinguishable (in the absence of polarity the sign of $\boldsymbol{n}$ has no physical meaning).

When the nematic phase is limited by a surface, created by contact with another phase (solid, liquid, gas), its orientation may change in a drastic manner. This phenomena of orientation of a liquid crystal by a surface is called *anchoring*. Two typical types of anchoring are *strong* and *weak* anchoring, described as follows.

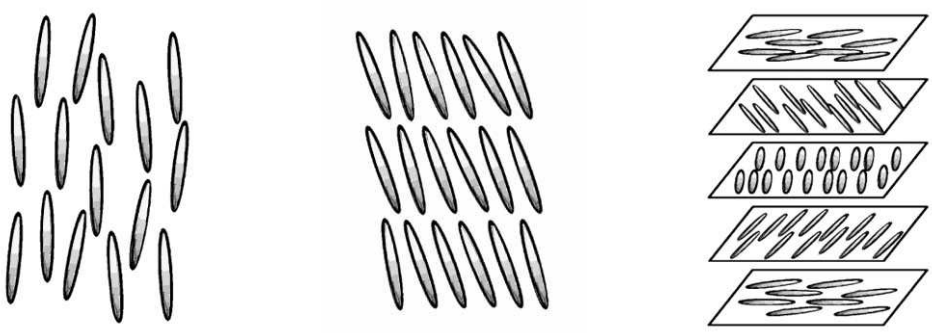

(a) Nematic Phase (b) Smectic Phase (c) Chiral Phase

Figure 5.3: Schematic representation of the possible nematic, smectic phases observed in thermotropic liquid crystals.

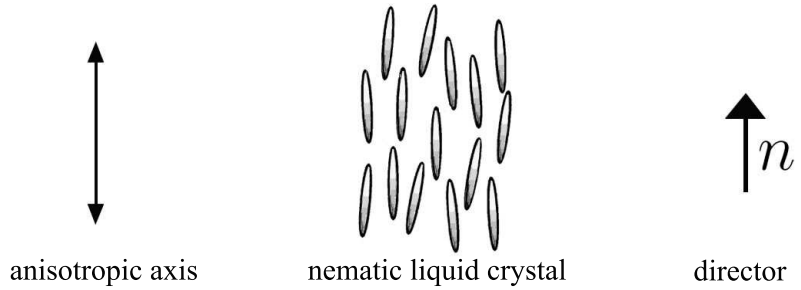

Figure 5.4: Schematic representation of a nematic liquid crystal. A unit vector $\boldsymbol{n}$, called the director, describes the average direction of the molecular alignment along the anisotropic axis.

- Strong Anchoring: the director $\boldsymbol{n}$ is defined on the physical surface of the boundary. Two examples of strong anchoring between parallel plates are *homeotropic* anchoring (the director is forced to be perpendicular to the boundary plates) and *homogeneous* anchoring (the director is forced to be parallel to the boundary plates).
- Weak Anchoring: the angle between the director $\boldsymbol{n}$ and the boundary or interface may vary under the influence of applied fields.

In Section 5.1 we give a brief review the state of art of the mathematical modeling of nematic liquid crystals. Then, in Section 5.2, we report some of the works studying the effect of flow fields on pattern formation in confined nematic systems.

5.1 Mathematical Modeling

The first accepted mathematical model describing the behavior of liquid crystals was developed by Oseen and Frank [**?**], who derived a static theory in which the configuration of nematic liquid crystals is described with a vector director $\boldsymbol{n}$. In 1961, Leslie [**?**] proceeded to generalize the static theory developed by Oseen and Frank and completed a model which describes the evolution of the director $\boldsymbol{n}$ under the application of external fields (for instance, electric, magnetic or flow fields), giving birth to the celebrated Leslie–Ericksen dynamic theory for nematic liquid crystals. In 1993, de Gennes and Prost [**?**] proposed to replace the director $\boldsymbol{n}$ by a $\boldsymbol{Q}$-tensor field, that accounts for biaxial systems (with a primary and a secondary director of molecular alignment) and variations in the degree of orientational order. The introduction of the $\boldsymbol{Q}$-tensor led to the development of the Beris–Edwards dynamic theory for nematic liquid crystals [**?**]. Since we want to model nematic liquid crystals with uniaxial directional order and build on the work

performed in Anderson et al. [**?**], we focus on the the Leslie–Ericksen model. A general description of the Leslie–Ericksen governing equations is introduced in Chapter 6.

5.2 Flow induced behavior of nematic liquid crystals

Microfluidics is a thriving area of research; scientists typically manipulate fluid flow (say conventional isotropic fluids) in narrow channels complemented by different boundary treatments, leading to novel transport and mixing phenomena for fluids and potentially new health and pharmaceutical applications (see, e.g., [**?**, **?**, **?**]). A natural question to ask (see [**?**]) is: what happens when we replace a conventional isotropic liquid with an anisotropic liquid, such as a nematic liquid crystal? Nematic microfluidics have recently generated substantial interest by virtue of their optical, rheological and backflow properties along with their defect profiles (see for instance [**?**]).

In Sengupta et al. [**?**], the authors investigated, both experimentally and numerically (using the equations in the Beris–Edwards theory), microfluidic channels filled with nematic solvents. The authors worked with homeotropic boundary conditions on the top and bottom channel surfaces and imposed a flow field transverse to the anchoring conditions so that there were at least two competing effects in the experiment: anchoring normal to the boundaries and flow along the length of the microfluidic channel. They worked with weak, medium, and strong flow speeds in qualitative terms and observed complex flow transitions. In the weak-flow regime, the molecules were only weakly affected by the flow and the molecular orientations were largely determined by the anchoring conditions. As the flow strength increased, a complex coupling between the molecular alignments and the flow field emerged and the nematic molecules reoriented to align somewhat with the flow field. The medium-flow director field exhibited boundary layers near the centre and the boundaries where the director field was strongly influenced by either the flow field or the boundary conditions. In the strong-flow regime, the molecules were almost entirely oriented with the flow field, with the exception of thin boundary layers near the channel surfaces to match the boundary conditions. The authors studied these transitions experimentally and their experimental results suggested a largely *uniaxial* profile wherein the molecules exhibited a single distinguished direction of molecular alignment and this direction was referred to as being the *director* in the literature.

In Anderson et al. [**?**], the authors modeled this experimental set-up within the Leslie–Ericksen model for nematodynamics. They presented governing equations for the flow field and the nematic director field (along with the constitutive relations that described the coupling between both fields) and assumed that all dependent variables only varied along the channel depth, with a unidirectional flow along the channel length, consistent with the experiments. These assumptions greatly simplified the mathematical model, yielding a decoupled system of partial differential equations for the director field, which captured the flow dynamics through a single variable: the pressure gradient, $\mathcal{G}$, along the channel length. The authors defined two separate boundary-value problems: one for weak-flow solutions and one for strong-flow solutions, described by two different sets of boundary conditions for the director field. They found weak- and strong-flow solutions for all values of the pressure gradient and they related the resulting flow profile to the mean flow speed by a standard Poiseuille-flow-type relation. The energy of the weak-flow solution was lower than the strong-flow solution for small $\mathcal{G}$ and there was an energy cross-over at some critical value, $\mathcal{G}^*$, that depended on the anchoring strength, at the channel surfaces.

In Chapter 7, we build on the work in Anderson et al. [**?**] by performing an extensive study of the static solution landscape, complemented by some numerical investigations of the dynamical behavior, as the system evolves to these equilibrium configurations. We adopt the same model with the same underpinning assumptions as in Anderson et al. [**?**], but we do not define two separate boundary-value problems. We impose weak anchoring conditions for the director field on the top and the bottom surfaces since it includes both the weak and strong anchoring configurations and allow us to capture the competition between the

flow field and the anchoring strength.

Notation and conventions

The following notation and summation convention is used through Chapter 6.
Given a set of basis vectors $\{e_1, e_2, e_3\} \in \mathbb{R}^3$, a vector $\mathbf{a} = (a_1, a_2, a_3)$ can be written as

$$\mathbf{a} = \sum_{i=1}^{3} a_i e_i := a_i e_i.$$

The summation convention can be applied to vectors, matrices and tensors. For instance, if $A = (a_{ij})$, $B = (b_{ij})$ are $n \times n$ matrices, the product $AB \equiv C = (c_{ij})$ is the matrix with components

$$c_{ij} = a_{ik} b_{kj},$$

with a summation over the index k from 1 to n being implied. It is also a common convention to denote by $p_{,i}$ the partial derivate of quantity p with respect to its i-th variable.

Chapter 6

Mathematical Modeling

This chapter is devoted to the mathematical modeling of nematic liquid crystals. In Section 6.1 we present the governing equations of a general Leslie–Ericksen model. Then, in Section 6.2 we simplify the general Leslie–Ericksen model to describe the dynamics of a unidirectional nematic flow. Finally, in Section 6.2.1 we propose a dimensional analysis of the simplified system.

6.1 General Leslie–Ericksen model

The Leslie–Ericksen dynamic theory is widely accepted to model dynamic phenomena in nematic liquid crystals. A unit vector $\boldsymbol{n} = (n_1, n_2, n_3)$, called the *director*, is defined to describe the local direction of the average molecular alignment in liquid crystals, while the instantaneous motion of the fluid is described by its velocity vector $\boldsymbol{v} = (v_1, v_2, v_3)$. The full equations for the dynamics of nematic liquid crystals describe the evolution of $\boldsymbol{n}$ and $\boldsymbol{v}$. When electromagnetic and gravitational forces are disregarded, the Leslie–Ericksen model for incompressible fluids is (see, e.g., [**?**, **?**, **?**]):

$$v_{i,i} = 0 \qquad \text{in } \Omega \times (0, +\infty), \tag{6.1a}$$

$$\rho \frac{\mathrm{d}v_i}{\mathrm{d}t} = \sigma_{ji,j} \qquad \text{in } \Omega \times (0, +\infty), \tag{6.1b}$$

$$\rho_1 \frac{\mathrm{d}}{\mathrm{d}t}\Big(\frac{\mathrm{d}n_i}{\mathrm{d}t} + \boldsymbol{v} \cdot \nabla n_i\Big) = g_i + \pi_{ji,j} \qquad \text{in } \Omega \times (0, +\infty), \tag{6.1c}$$

where t represents the time. Equations (6.1a)-(6.1c) represent mass, linear and angular momentum conservation, respectively, with Ω being the domain occupied by the liquid crystal, ρ is the mass density (assumed constant) and ρ_1 is a constant, measured in terms of weight divided by distance, that arises from the consideration of a rotational kinetic energy of the material element. Here, σ, π and g represent, respectively, the stress tensor, the director stress tensor and the intrinsic director body force. They are defined as

$$\begin{aligned} \sigma_{ji} &= -P\delta_{ij} - \frac{\mathrm{d}F}{\mathrm{d}n_{k,j}} n_{k,i} + \bar{\sigma}_{ji}, \\ \pi_{ji} &= \beta_j n_i + \frac{\mathrm{d}F}{\mathrm{d}n_{i,j}}, \\ g_i &= \gamma n_i - \beta_j n_{i,j} - \frac{\mathrm{d}F}{\mathrm{d}n_i} + \bar{g}_i, \end{aligned} \tag{6.2}$$

where P is the pressure of the fluid flow and δ_{ij} is the Kronecker delta. The vector $(\beta_1, \beta_2, \beta_3)$ and the scalar function γ (sometimes called direction tension) are Lagrange multipliers ensuring $\|\boldsymbol{n}\| = 1$ (see [**?**] for more details). F represents the Frank–Oseen free elastic energy, which is associated to distortions of the anisotropic axis. In the case of nematic liquid crystals, F depends on four elastic constants K_i $(i = 1, 2, 3, 4)$, corresponding to the curvature components describing splay, twist, bend and saddle-splay

effects (see for instance equation (4.130) in Stewart [**?**]). Here, we exploit the one-constant approximation of the Frank–Oseen elastic free energy density given by (see [**?**])

$$F = \frac{K}{2} n_{i,j} n_{i,j}, \tag{6.3}$$

where K is the only elastic constant considered. Note that in this framework, F does not depend on n_i, so that the term $\frac{\mathrm{d}F}{\mathrm{d}n_i}$ appearing in the definition of g_i can be disregarded. Furthermore,

$$\bar{\sigma}_{ji} = \alpha_1 n_k n_p A_{kp} n_i n_j + \alpha_2 N_i n_j + \alpha_3 N_j n_i + \alpha_4 A_{ij} + \alpha_5 A_{ik} n_k n_j + \alpha_6 A_{jk} n_k n_i, \tag{6.4}$$

$$N_i = \frac{\mathrm{d}n_i}{\mathrm{d}t} + \boldsymbol{v} \cdot \nabla n_i - \omega_{ij} n_j,\ \omega_{ij} = \frac{v_{i,j} - v_{j,i}}{2},\ A_{ij} = \frac{v_{i,j} + v_{j,i}}{2},$$

$$\text{and } \bar{g}_i = -\gamma_1 N_i - \gamma_2 n_j A_{ji},$$

where α_i are constant viscosities satisfying the Parodi relation (see [**?**]) $\alpha_2 + \alpha_3 = \alpha_6 - \alpha_5$, and $\gamma_1 = \alpha_3 - \alpha_2$, $\gamma_2 = \alpha_6 - \alpha_5$. More details about these parameters can be found in Section 6.2.2.

Remark 6.1.1. *Liu et al. [**?**] proved that, if* $\boldsymbol{v}(x,0) \in (L^2(\Omega))^3$ *and* $\boldsymbol{n}(x,0) \in (H^1(\Omega))^3$ *with* $\boldsymbol{n}(x,0) \in (H^{\frac{3}{2}}(\delta\Omega))^3$ *and under suitable boundary conditions, system* (6.1) *has a unique global weak solution* $(\boldsymbol{v}, \boldsymbol{n})$ *such that*

$$\boldsymbol{v} \in \left(L^2(0,T,H^1(\Omega)) \cap L^\infty(0,T,L^2(\Omega))\right)^3,$$
$$\boldsymbol{n} \in \left(L^2(0,T,H^1(\Omega)) \cap L^\infty(0,T,L^2(\Omega))\right)^3,$$

for all $T \in (0,\infty)$.

Boundary conditions

System (6.1) must be supplemented by a relevant description of the alignment of the director $\boldsymbol{n}$ on the boundary surfaces of the channel, these descriptions entering the mathematics via appropriate boundary conditions. In their simplest description, the boundary conditions are obtained by computing the Euler–Lagrange equations associated to the total energy of the nematic liquid crystal (see [**?**] for more details), i.e.,

$$J(\boldsymbol{n}) = \int_\Omega F(x, \boldsymbol{n}, \nabla \boldsymbol{n})\ \mathrm{d}x + \int_{\delta\Omega} S(\boldsymbol{n})\ \mathrm{d}s,$$

where F is the free energy (in our case, given by equation (6.3)) and S is the surface energy. Following the work developed by Anderson et al. [**?**], we exploit the well-known Rapini–Papoular surface energy, which describes the energy forcing the director $\boldsymbol{n}$ to orient parallel to an easy direction $\boldsymbol{n}_0$ and it can be written as

$$S = \frac{W}{2}(n_i n_{0_i})^2, \tag{6.5}$$

where W is the surface anchoring strength.

Remarks on Coefficients

The coefficients α_i and γ_i are usually called *Leslie Coefficients* (see for instance Lee [**?**] or Wang et al. [**?**] for further information about their physical meaning and how to approximate them experimentally). They depend only on the temperature and have dimension of viscosity. Some constraints on the *Leslie Coefficients* come from the nonnegativity of the *Dissipative function* (see for instance [**?**, **?**]). When the Parodi relation (see [**?**]) is used, the dissipative function is defined as (see, e.g., [**?**]):

$$\mathcal{D} = \alpha_1 (n_i A_{ij} n_j)^2 + 2\gamma_2 N_i A_{ij} n_j + \alpha_4 A_{ij} A_{ij} + (\alpha_5 + \alpha_6) A_{ij} A_{jk} n_i n_k + \gamma_1 N_i N_i. \tag{6.6}$$

6.2 Simplified model

As in Anderson et al. [?], we model the nematic liquid crystals within the microfluidic channel in the Leslie–Ericksen framework. Here, the domain is $\Omega = (0, l) \times (0, w) \times (-h, h)$, where we assume that the length l is much greater than width w and the width is much greater than height $2h$, so that the director and the flow fields may be assumed to depend only on the z-coordinate (consistent with the experimental set-up in Anderson et al. [?] and Sengupta et al. [?]). Here, $\boldsymbol{n}$ and $-\boldsymbol{n}$ are physically indistinguishable (in the absence of polarity the sign of $\boldsymbol{n}$ has no physical meaning). We additionally assume that all dependent variables only depend on the z-coordinate, along the channel depth, as depicted in Figure 6.1. Then the

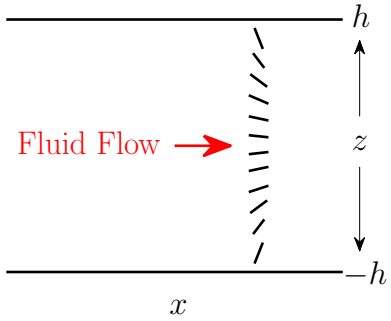

Figure 6.1: Schematic of the microfluidic channel set-up. The nematic molecules are anchored at the top and bottom surfaces and are deformed by the fluid flow from the left.

director field is of the form $\boldsymbol{n} = (\sin(\theta(z,t)), 0, \cos(\theta(z,t)))$ and the velocity field is unidirectional, of the form $\boldsymbol{v} = (u(z,t), 0, 0)$, with $-h \leq z \leq h$. Since $\boldsymbol{n}$ and $-\boldsymbol{n}$ are indistinguishable, θ and $\theta + k\pi$, $k \in \mathbb{Z}$, describe the same director profile. We assume that $u(z,t)$ is symmetric around the center-line (i.e., around $z = 0$) and no-slip conditions are imposed on the channel walls (i.e., $u(\pm h, t) = 0$).

Using this information in the constitutive formulae (6.1), one has that

- $A_{ij} = 0$ except for $A_{13} = A_{31} = \dfrac{u_z}{2}$.
- $\omega_{ij} = 0$ except for $\omega_{13} = \dfrac{u_z}{2}$ and $\omega_{31} = \dfrac{-u_z}{2}$.
- $N_1 = n_{1,t} - w_{13} n_3 = \cos(\theta)\theta_t - \dfrac{u_z}{2}\cos(\theta) = \cos(\theta)(\theta_t - \dfrac{u_z}{2})$.
- $N_2 = 0$.
- $N_3 = n_{3,t} - w_{31} n_1 = -\sin(\theta)\theta_t + \dfrac{u_z}{2}\sin(\theta) = \sin(\theta)(\dfrac{u_z}{2} - \theta_t)$.
- $\bar{g}_1 = -\gamma_1 N_1 - \gamma_2 A_{31} n_3 = \dfrac{\cos(\theta) u_z}{2}(\gamma_1 - \gamma_2) - \gamma_1 \cos(\theta)\theta_t$.
- $\bar{g}_2 = 0$.
- $\bar{g}_3 = -\gamma_1 N_3 - \gamma_2 A_{13} n_1 = -\dfrac{\sin(\theta) u_z}{2}(\gamma_1 + \gamma_2) + \gamma_1 \sin(\theta)\theta_t$.

Now, taking into account that F only depends on the variables $n_{1,3}$ and $n_{3,3}$ one has that $\pi_{ij,i} = 0$ except for $\pi_{31,3}$ and $\pi_{33,3}$. Thus,

- $\pi_{31,3} = \left(\dfrac{\mathrm{d}F}{\mathrm{d}n_{1,3}}\right)_{,3} = K n_{1,33}$.

- $\pi_{33,3} = \left(\dfrac{\mathrm{d}F}{\mathrm{d}n_{3,3}}\right)_{,3} = Kn_{3,33}$.
- $g_1 = \gamma n_1 + \bar{g}_1 = \gamma n_1 + \dfrac{\cos(\theta)u_z}{2}(\gamma_1 - \gamma_2) - \gamma_1 \cos(\theta)\theta_t$.
- $g_2 = 0$.
- $g_3 = \gamma n_3 + \bar{g}_3 = \gamma n_3 - \dfrac{\sin(\theta)u_z}{2}(\gamma_1 + \gamma_2) + \gamma_1 \sin(\theta)\theta_t$.
- $\bar{\sigma}_{ij} = 0$ except for $\bar{\sigma}_{11}, \bar{\sigma}_{13}, \bar{\sigma}_{31}$ and $\bar{\sigma}_{33}$.

In our case, it follows from the linear momentum equation (6.1b) that

$$\begin{aligned} \rho\tfrac{\mathrm{d}u}{\mathrm{d}t} &= \sigma_{11,1} + \sigma_{31,3} = -P_{,1} + \bar{\sigma}_{31,3}, \\ 0 &= \sigma_{22,2} = -P_{,2}, \\ 0 &= \sigma_{33,3} = -(P + 2F)_{,3} + \bar{\sigma}_{33,3}. \end{aligned}$$

Note that we will use the notation $f_{,1}$, $f_{,2}$, $f_{,3}$; $f_{,x}$, $f_{,y}$, $f_{,z}$ and f_x, f_y, f_z interchangeably. Therefore, it follows from (6.1b) that

$$-(P + 2F)_x + \bar{\sigma}_{31,z} = \rho\frac{\mathrm{d}u}{\mathrm{d}t} \text{ in } (0,l)\times(0,w)\times(-h,h)\times(0,+\infty), \tag{6.7a}$$

$$(P + 2F)_y = 0 \quad \text{in } (0,l)\times(0,w)\times(-h,h)\times(0,+\infty), \tag{6.7b}$$

$$-(P + 2F)_z + \bar{\sigma}_{33,z} = 0 \quad \text{in } (0,l)\times(0,w)\times(-h,h)\times(0,+\infty). \tag{6.7c}$$

We suppose that the inertia of the liquid crystal molecules can be ignored in typical cells having small depths (see, e.g., [**?**]), so that $\rho\dfrac{\mathrm{d}u}{\mathrm{d}t} = 0$ in equation (6.7a). From (6.7b), one has that $P + 2F = q(x,z,t)$. Now, if we integrate with respect to x in equation (6.7a) and take into account that F only depends on z and t,

$$P + 2F = x\bar{\sigma}_{31,z} + r(z,t). \tag{6.8}$$

If the relation (6.8) is introduced in equation (6.7c), one has that $(x\bar{\sigma}_{31,z} + r(z,t))_{,z} = \bar{\sigma}_{33,z}$. Consequently, $\bar{\sigma}_{31,zz} = 0$, and so

$$\bar{\sigma}_{31} = C(t)z + D(t), \tag{6.9}$$

where $C(t)$ and $D(t)$ are functions to be determined. Then, from the relation (6.8), one has that

$$P + 2F = C(t)x + r(z,t). \tag{6.10}$$

From equations (6.7c) and (6.10) it follows that $(C(t)x + r(z,t))_{,z} = (r(z,t))_{,z} = \bar{\sigma}_{33,z}$, where integrating with respect to z one has that $r(z,t) = \bar{\sigma}_{33} + s(t)$, s being a time-dependent function to be determined. Returning to equation (6.10), it follows that

$$P = -2F + C(t)x + s(t) + \bar{\sigma}_{33}. \tag{6.11}$$

Replacing the value of $\bar{\sigma}_{31}$ (obtained following (6.4)) in equation (6.9) one has that

$$u_z g(\theta) + \theta_t m(\theta) = C(t)z + D(t),$$

where

$$g(\theta) = \alpha_1 \cos^2(\theta)\sin^2(\theta) + \frac{\alpha_5 - \alpha_2}{2}\cos^2(\theta) + \frac{\alpha_3 + \alpha_6}{2}\sin^2(\theta) + \frac{\alpha_4}{2}, \tag{6.12a}$$

$$m(\theta) = \alpha_2 \cos^2(\theta) - \alpha_3 \sin^2(\theta). \tag{6.12b}$$

A consequence of the symmetry of u enforces $\frac{\partial\theta}{\partial t} = 0$ at $z = 0$. Any scenario for which $\frac{\partial\theta}{\partial t} \neq 0$ would induce a velocity profile that is non-symmetric and thus violate our original assumption. As a result, this implies that $D(t) = 0$ for our system and hence

$$u_z g(\theta) + \theta_t m(\theta) = C(t)z. \tag{6.13}$$

Note that we have reduced equations (6.7a)–(6.7c) to equation (6.13), the pressure being available via equation (6.11). Now, the angular momentum balance equation (6.1c) for $i = 1$ and $i = 3$ reduces, respectively, to

$$\begin{aligned}\rho_1 n_{1,tt} &= g_1 + \pi_{31,3} = \gamma n_1 + \bar{g}_1 + \pi_{31,3} = \gamma n_1 + \bar{g}_1 + K n_{1,33},\\ \rho_1 n_{3,tt} &= g_3 + \pi_{33,3} = \gamma n_3 + \bar{g}_3 + \pi_{33,3} = \gamma n_3 + \bar{g}_3 + K n_{3,33}.\end{aligned}$$

It remains to compute $n_{1,33}$, $n_{3,33}$, $n_{1,tt}$ and $n_{2,tt}$:

- $n_1 = \sin(\theta) \Rightarrow n_{1,3} = \cos(\theta)\theta_z \Rightarrow n_{1,33} = -\sin(\theta)(\theta_z)^2 + \cos(\theta)\theta_{zz}$,
- $n_{1,t} = \cos(\theta)\theta_t \Rightarrow n_{1,tt} = -\sin(\theta)(\theta_t)^2 + \cos(\theta)\theta_{tt}$,
- $n_3 = \cos(\theta) \Rightarrow n_{3,3} = -\sin(\theta)\theta_z \Rightarrow n_{3,33} = -\cos(\theta)(\theta_z)^2 - \sin(\theta)\theta_{zz}$,
- $n_{3,t} = -\sin(\theta)\theta_t \Rightarrow n_{3,tt} = -\cos(\theta)(\theta_t)^2 - \sin(\theta)\theta_{tt}$.

Thus, equation (6.1c) when $i = 1$ and $i = 3$ becomes

$$\begin{aligned}\rho_1(-\sin(\theta)(\theta_t)^2 + \cos(\theta)\theta_{tt}) = \;& \gamma\sin(\theta) - \gamma_1\cos(\theta)\theta_t + \cos(\theta)\frac{u_z}{2}(\gamma_1 - \gamma_2)\\ & + K(-\sin(\theta)\theta_z^2 + \cos(\theta)\theta_{zz}),\\ \rho_1(-\cos(\theta)(\theta_t)^2 - \sin(\theta)\theta_{tt}) = \;& \gamma\cos(\theta) + \gamma_1\sin(\theta)\theta_t - \sin(\theta)\frac{u_z}{2}(\gamma_1 + \gamma_2)\\ & + K(-\cos(\theta)\theta_z^2 - \sin(\theta)\theta_{zz}).\end{aligned}$$

We neglect the term $\rho_1\theta_{tt}$ (it is accepted as being negligible in physical situations, see [**?**]). Then, multiplying the first equation by $\cos(\theta)$, the second one by $\sin(\theta)$ and subtracting them, one obtains:

$$\gamma_1\theta_t = K\theta_{zz} + \frac{u_z}{2}\big(\gamma_1 - \gamma_2\cos(2\theta)\big). \tag{6.14}$$

Thus, the evolution of θ and u are described by the following system

$$\begin{aligned}\gamma_1\theta_t &= K\theta_{zz} - u_z m(\theta) && z \in (-h,h), t > 0, && (6.15a)\\ C(t)z &= u_z g(\theta) + \theta_t m(\theta) && z \in (-h,h), t > 0, && (6.15b)\\ \theta(z,0) &= \Theta(z) && z \in (-h,h), && (6.15c)\\ u(\pm h,t) &= 0 && t > 0, && (6.15d)\end{aligned}$$

where Θ is the initial condition for θ and $C(t) = P_x$, i.e., the channel direction component of the pressure gradient.

The boundary conditions for the variable θ are obtained as explained in Section 6.1, i.e., taking into account that the total energy of the nematic liquid crystals in this simplified model is given by

$$J(\theta) = \int_0^l\int_0^w\int_{-h}^h \frac{K}{2}\theta_z^2 \, dz \, dy \, dx + \int_0^l\int_0^w\int_{z=\pm h} \frac{W}{2}\sin^2\theta \, dy \, dx. \tag{6.16}$$

The Euler–Lagrange equations associated to (6.16) lead to (see [**?**] for more details)

$$-K\theta_z(-h) + \frac{W}{2}\sin(2\theta(-h)) = 0 \quad \text{and} \quad K\theta_z(h) + \frac{W}{2}\sin(2\theta(h)) = 0. \tag{6.17}$$

We refer to (6.17) as *weak anchoring* boundary conditions, since $\theta(-h)$ and $\theta(h)$ may vary depending on model parameters (see Chapter 5 for a general review of the different types of *anchoring*). Notice that the Rapini–Papoular surface energy enforces $\theta(-h) = k_1\pi$ and $\theta(h) = k_2\pi$ ($k_1, k_2 \in \mathbb{Z}$) for large anchoring coefficients $W > 0$. In other words, the surface energy enforces homeotropic anchoring (along the normal to the surface) described by, $\boldsymbol{n} = \pm\,(0,0,1)$ on $z = \pm h$.

Using (6.15*a,b*), we obtain the following decoupled initial-boundary-value problem for θ:

$$\begin{cases} \big(\gamma_1 g(\theta) - m(\theta)^2\big)\dfrac{\partial\theta}{\partial t} = Kg(\theta)\dfrac{\partial^2\theta}{\partial z^2} + Gzm(\theta) & z \in (-h,h),\ t>0, \\ K\dfrac{\partial\theta}{\partial z}(h,t) = -\dfrac{W}{2}\sin(2\theta(h,t)) & t>0, \\ K\dfrac{\partial\theta}{\partial z}(-h,t) = \dfrac{W}{2}\sin(2\theta(-h,t)) & t>0, \\ \theta(z,0) = \Theta(z) & z \in (-h,h), \end{cases} \tag{6.18}$$

where K (N) is the elastic constant of the nematic liquid crystal, Θ is the initial condition, $-G = \frac{\partial P}{\partial x}$ is the component of the pressure gradient in the channel direction and W (Nm^{-1}) is the surface anchoring strength. Note that for a physically realistic solution, we expect that as $W \to \infty$, 2θ tends to an integer multiple of π on $z = \pm h$. The functions

$$m(\theta) = \alpha_2\cos^2(\theta) - \alpha_3\sin^2(\theta) \text{ and}$$

$$g(\theta) = \alpha_1\cos^2(\theta)\sin^2(\theta) + \frac{\alpha_5-\alpha_2}{2}\cos^2(\theta) + \frac{\alpha_3+\alpha_6}{2}\sin^2(\theta) + \frac{\alpha_4}{2},$$

the α_i (N m^{-2}s), $i \in \{1,\dots,6\}$, are constant viscosities related to each other by the Parodi relation (see [**?**]) $\alpha_2 + \alpha_3 = \alpha_6 - \alpha_5$.

Remark 6.2.1. *Taking into account the regularity of the vectors $\boldsymbol{n}$ and $\boldsymbol{v}$ (see Remark 6.1.1), we assume that there exists a unique solution $\theta \in L^2((-h,h)\times(0,T))$ of system* (6.18)

Remark 6.2.2 (Remarks on coefficients)**.** *As explained in Section 6.1, there exist some constraints on the coefficients α_i and γ_i coming from the nonnegativity of the Dissipative function* (6.6)*, which in our particular case can be rewritten as*

$$\mathcal{D} = \alpha_1 u_z^2\sin^2(\theta)\cos^2(\theta) + 2\gamma_2\frac{u_z}{2}(\theta_t - \frac{u_z}{2})(\cos^2(\theta) - \sin^2(\theta)) + \alpha_4\frac{u_z^2}{2}$$

$$+(\alpha_5+\alpha_6)\frac{u_z^2}{4} + \gamma_1(\theta_t - \frac{u_z}{2})^2 = 2\theta_t u_z m(\theta) + \gamma_1\theta_t^2 + g(\theta)u_z^2.$$

This expression is a quadratic form and can be rewritten as:

$$\mathcal{D} = \begin{bmatrix} X & Y \end{bmatrix}\begin{bmatrix} g(\theta) & m(\theta) \\ m(\theta) & \gamma_1 \end{bmatrix}\begin{bmatrix} X \\ Y \end{bmatrix},\ \textit{with } X = u_z,\ Y = \theta_t.$$

*A reasonable assumption is that the dissipation function is positive (see for instance [**?**]) which is fulfilled if and only if the determinant of every principal submatrix is positive (see, e.g., [**?**]), i.e.,*

$$g(\theta) > 0 \qquad \textit{and} \qquad \gamma_1 g(\theta) - m^2(\theta) > 0. \tag{6.19}$$

When $\theta = 0$, this implies that

$$\gamma_1 > 0, \quad \alpha_5 - \alpha_2 + \alpha_4 > 0 \quad \textit{and} \quad \gamma_1(\alpha_5 - \alpha_2 + \alpha_4) > 2\alpha_2^2.$$

6.2.1 Non-dimensional analysis

We non-dimensionalize system (6.18) using the scalings

$$\hat{z} = \frac{z}{h}, \qquad \hat{\alpha}_i = \frac{\alpha_i}{\alpha_4}, \qquad \hat{\gamma}_1 = \frac{\gamma_1}{\alpha_4}, \qquad \hat{t} = \frac{Kt}{\alpha_4 h^2}.$$

For ease of notation we drop the $\hat{}$ notation. The dimensionless version of (6.18) is then

$$\big(\gamma_1 g(\theta) - m(\theta)^2\big)\frac{\partial \theta}{\partial t} = g(\theta)\frac{\partial^2 \theta}{\partial z^2} + \mathcal{G} z m(\theta) \qquad z \in (-1,1),\ t > 0, \tag{6.20a}$$

$$\mathcal{B}\frac{\partial \theta}{\partial z}(1,t) = -\sin(2\theta(1,t)) \qquad t > 0, \tag{6.20b}$$

$$\mathcal{B}\frac{\partial \theta}{\partial z}(-1,t) = \sin(2\theta(-1,t)) \qquad t > 0, \tag{6.20c}$$

$$\theta(z,0) = \Theta(z) \qquad z \in (-1,1), \tag{6.20d}$$

where $\mathcal{G} = h^3 G/K$ and $\mathcal{B} = 2K/Wh$ are the dimensionless pressure gradient and the dimensionless inverse anchoring strength respectively,

$$m(\theta) = \alpha_2 \cos^2(\theta) - \alpha_3 \sin^2(\theta) \text{ and}$$

$$g(\theta) = \alpha_1 \cos^2(\theta)\sin^2(\theta) + \frac{1}{2}\big((\alpha_5 - \alpha_2)\cos^2(\theta) + (\alpha_3 + \alpha_6)\sin^2(\theta) + 1\big).$$

Characteristic values for the dimensionless nematic viscosities (see [**?**]) are $\alpha_1 = -0.1549$, $\alpha_2 = -0.9859$, $\alpha_3 = -0.0535$, $\alpha_5 = 0.7324$ and $\alpha_6 = -0.39$.

Chapter 7

Asymptotic Behavior

In this chapter we study the asymptotic behavior of the nematic liquid crystals described by system (6.20). Particularly, in Section 7.1 we compute the static equilibrium solutions of the system as a function of the pressure gradient and the anchoring strength. Then, in Section 7.2 we study the dynamic model, with focus on the effects of initial conditions and the time-dependent forms of the pressure grandient and anchoring strength.

7.1 Equilibrium Solutions

The static equilibria of system (6.20), $\theta^*(z)$, satisfy

$$\begin{cases} g(\theta^*(z))\dfrac{\mathrm{d}^2\theta^*}{\mathrm{d}z^2}(z) = -\mathcal{G}zm(\theta^*(z)) \quad z \in (-1,1), \\ \mathcal{B}\dfrac{\mathrm{d}\theta^*}{\mathrm{d}z}(1) = -\sin(2\theta^*(1)), \\ \mathcal{B}\dfrac{\mathrm{d}\theta^*}{\mathrm{d}z}(-1) = \sin(2\theta^*(-1)). \end{cases} \tag{7.1}$$

We characterize the equilibrium solutions in terms of their winding number, defined to be

$$\omega(\theta^*) = \frac{\theta^*(1) - \theta^*(-1)}{2\pi}. \tag{7.2}$$

The winding number (see [**?**]) is a measure of the rotation of the director field between the top and bottom surfaces. The limit $\mathcal{B} \to 0$ is the strong anchoring limit, when the boundary conditions on $z = \pm 1$ are strongly enforced and both $\theta^*(1)$ and $\theta^*(-1)$ are integer multiples of $\frac{\pi}{2}$ at this limit. Particularly, as we will see in Section 7.1.1, as $\mathcal{B} \to 0$, the stable equilibria at $z = \pm 1$ tend to $\theta^*(\pm 1) = n\pi, n \in \mathbb{Z}$ (homeotropic anchoring at the boundaries); the unstable equilibria to $\theta^*(1)$ (and/or $\theta^*(-1)$) $= (n + \frac{1}{2})\pi$, $n \in \mathbb{Z}$ (planar anchoring at at least one of the boundaries). This is simply because $\theta^*(\pm 1) = n\pi$ is a minimum of the surface energy used to derive the anchoring conditions at $z = \pm 1$ (see the expression for the surface energy (6.16)). In what follows, we track some stable and unstable solutions of (7.1) as the model parameters are varied.

7.1.1 No fluid flow ($\mathcal{G} = 0$)

In this section, under the assumption of $\mathcal{G} = 0$, we analytically compute the solutions of system (6.20) as a function of the inverse anchoring strength $\mathcal{B}$. Then, we perform an stability analysis of the equilibria based on linearization techniques and demonstrate that, depending on the value of $\mathcal{B}$, system (6.20) may exhibit multistability. Finally, we build on a solution landscape by characterizing the equilibria in terms of their winding number and parameter $\mathcal{B}$.

Computation of the equilibrium solutions

When $\mathcal{G} = 0$, we can explicitly solve the first equation of system (7.1) to obtain

$$\theta^*(z) = az + b,$$

where a and b are constants to be determined by the boundary conditions, i.e., a and b must fulfill

$$\mathcal{B}a = -\sin(2(a+b)) = -\sin(2a)\cos(2b) - \sin(2b)\cos(2a),$$

$$\mathcal{B}a = \sin(2(-a+b)) = -\sin(a)\cos(2b) + \sin(2b)\cos(2a).$$

Substracting them, one obtains that

$$0 = 2\sin(2b)\cos(2a),$$

and then two cases appear:

- $\sin(2b) = 0$.
  In this case $b = \frac{k\pi}{2}$ for some $k \in \mathbb{Z}$ and from the boundary condition at $z = 1$, it follows that

  $$\mathcal{B}a = -\sin(2a + k\pi) = -\sin(2a)(-1)^k = (-1)^{k+1}\sin(2a). \tag{7.3}$$

  Thus, for any $k \in \mathbb{Z}$, there exists a collection $a_n = a_n(\mathcal{B})$ $n = 0, \pm 1, \pm 2$ fulfilling the transcendental equation (7.3). One observes that this collection depends on the parity of the integer k.

- $\cos(2a) = 0$.
  In this case $a = \frac{(2k+1)\pi}{4}$ for some $k \in \mathbb{Z}$ and from the boundary condition at $z = 1$, it follows that

  $$\mathcal{B}\frac{(2k+1)\pi}{4}(-1)^{k+1} = \cos(2b). \tag{7.4}$$

  Thus, for any $k \in \mathbb{Z}$, there exists a collection $b_m = b_m(\mathcal{B})$ $m = 0, \pm 1, \pm 2$ fulfilling the transcendental equation (7.4). One observes that this collection depend on the value of the integer k.

Taking this computations into account, we categorize the solutions of (7.1) as

$$\text{Type I } \theta^*_{a_n}(z) = a_n z + m\pi, \qquad \text{where } m \in \mathbb{Z} \text{ and } \mathcal{B}a_n = -\sin(2a_n), \tag{7.5}$$

$$\text{Type II } \theta^*_{\tilde{a}_n}(z) = \tilde{a}_n z + (m + \frac{1}{2})\pi, \qquad \text{where } m \in \mathbb{Z} \text{ and } \mathcal{B}\tilde{a}_n = \sin(2\tilde{a}_n), \tag{7.6}$$

$$\text{Type III } \theta^*_{(n+\frac{1}{4})\pi}(z) = (n + \frac{1}{4})\pi z + b_m, \qquad \text{where } n \in \mathbb{Z} \text{ and}$$

$$\cos(2b_m) = -\mathcal{B}(n + \frac{1}{4})\pi, \tag{7.7}$$

$$\text{Type IV } \theta^*_{(n+\frac{3}{4})\pi}(z) = (n + \frac{3}{4})\pi z + \tilde{b}_m, \qquad \text{where } n \in \mathbb{Z} \text{ and}$$

$$\cos(2\tilde{b}_m) = \mathcal{B}(n + \frac{3}{4})\pi. \tag{7.8}$$

For every value of $\mathcal{B}$, we obtain an ordered set of solutions for (7.5), with $0 = a_0 < a_1 < \ldots < a_n$ ($n \in \mathbb{N} \cup \{0\}$ depending on $\mathcal{B}$). Furthermore, if a_n provides a solution, so does $-a_n$, which we denote by a_{-n}. Equivalent statement can be made for $\tilde{a}_n$, b_m and $\tilde{b}_m$, solutions of equations (7.6), (7.7) and (7.8), respectively.
We observe that constant solutions of Type I and II, $\theta^* \equiv k\frac{\pi}{2}$ ($k \in \mathbb{Z}$) exist for all values of $\mathcal{B}$, while solutions of Types III and IV exist only if $\mathcal{B} \leq \frac{4}{\pi}$. The associated director fields are

$$\begin{aligned}
\text{Type I} \quad & \boldsymbol{n}(z) = (-1)^m(\sin(a_n z), 0, \cos(a_n z)),\\
\text{Type II} \quad & \boldsymbol{n}(z) = (-1)^m(\cos(\tilde{a}_n z), 0, -\sin(\tilde{a}_n z)),\\
\text{Type III} \quad & \boldsymbol{n}(z) = (-1)^m(\sin((n+\tfrac{1}{4})\pi z + b_0), 0, \cos((n+\tfrac{1}{4})\pi z + b_0))\\
\text{Type IV} \quad & \boldsymbol{n}(z) = (-1)^m(\sin((n+\tfrac{3}{4})\pi z + \tilde{b}_0), 0, \cos((n+\tfrac{3}{4})\pi z + \tilde{b}_0))
\end{aligned}$$

and thus, since director fields with $m \in \mathbb{Z}$ are the same but with opposite direction, all possible director profiles in (7.5)–(7.8) are covered by $m = 0$. Figure 7.1 shows the solution landscape in terms of a, b and $\mathcal{B}$, restricted to $a \in [2\pi, 2\pi]$ and $b \in [0, \frac{\pi}{2}]$. Figures 7.2 and 7.3 show the director profiles associated,

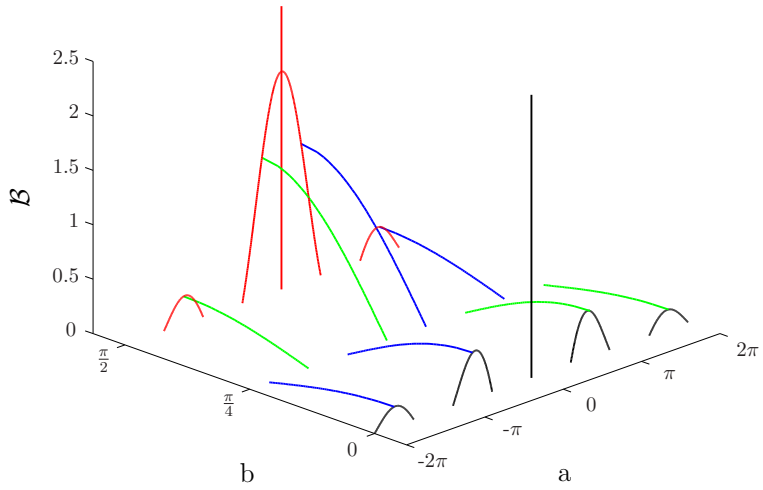

Figure 7.1: Solution landscape with $a \in [-2\pi, 2\pi]$ and $b \in [0, \frac{\pi}{2}]$. Solutions of Type I (Type II) correspond to $b = 0$ ($b = \frac{\pi}{2}$) and are plotted in black (red). Solutions of Types III and IV correspond to $b \in [0, \frac{\pi}{2}]$ and are plotted in blue and green, respectively.

respectively, to solutions $\theta^*_{a_n}$ and $\theta^*_{\tilde{a}_n}$, $n = 0, \pm 1, \pm 2 \pm 3, \pm 4$. Similarly, Figure 7.4 show the director profiles associated to solutions $\theta^*_{(n+\frac{1}{4})\pi}$ ($n \in \{-1, 0, 1, 2\}$) and $\theta^*_{(n+\frac{3}{4})\pi}$ ($n \in \{-2, -1, 0, 1\}$).

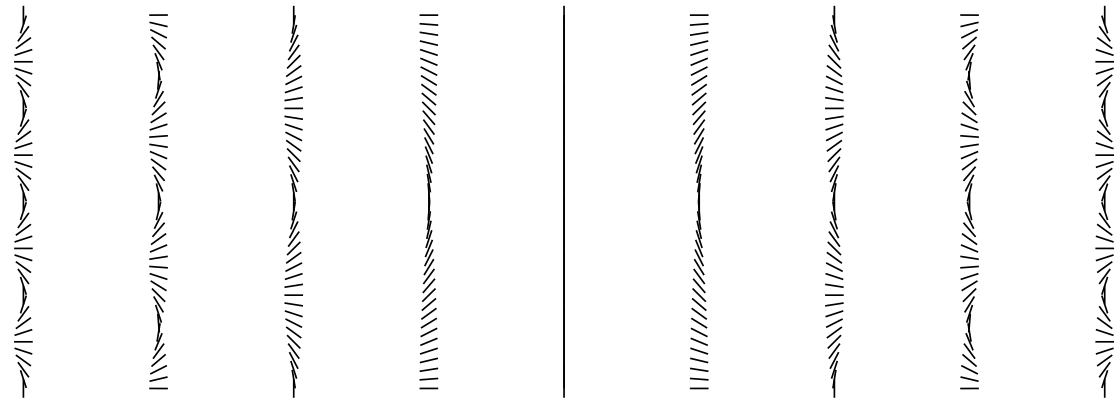

(a) $\theta^*_{a_{-4}}$ (b) $\theta^*_{a_{-3}}$ (c) $\theta^*_{a_{-2}}$ (d) $\theta^*_{a_{-1}}$ (e) $\theta^*_{a_0}$ (f) $\theta^*_{a_1}$ (g) $\theta^*_{a_2}$ (h) $\theta^*_{a_3}$ (i) $\theta^*_{a_4}$

Figure 7.2: $\boldsymbol{n}$ associated with steady states $\theta^*_{a_n}$ (Type I), obtained with $\mathcal{B} = 0.001$ and $\mathcal{G} = 0$. These states are stable if n is even and unstable if n is odd.

Stability analysis

The asymptotic stability of an equilibrium solution of system (6.20) is defined as follows (see Definition A.3.10).

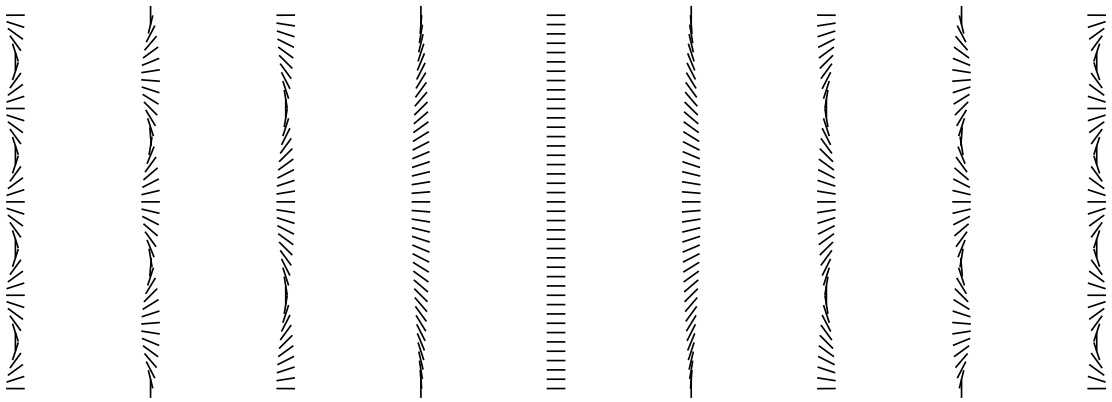

(a) $\theta^*_{\tilde{a}_{-4}}$ (b) $\theta^*_{\tilde{a}_{-3}}$ (c) $\theta^*_{\tilde{a}_{-2}}$ (d) $\theta^*_{\tilde{a}_{-1}}$ (e) $\theta^*_{\tilde{a}_0}$ (f) $\theta^*_{\tilde{a}_1}$ (g) $\theta^*_{\tilde{a}_2}$ (h) $\theta^*_{\tilde{a}_{3,0}}$ (i) $\theta^*_{\tilde{a}_{4,0}}$

Figure 7.3: $\boldsymbol{n}$ associated with steady states $\theta^*_{\tilde{a}_n}$ (Type II), obtained with $\mathcal{B} = 0.001$ and $\mathcal{G} = 0$. These states are stable if n is odd and unstable if n is even.

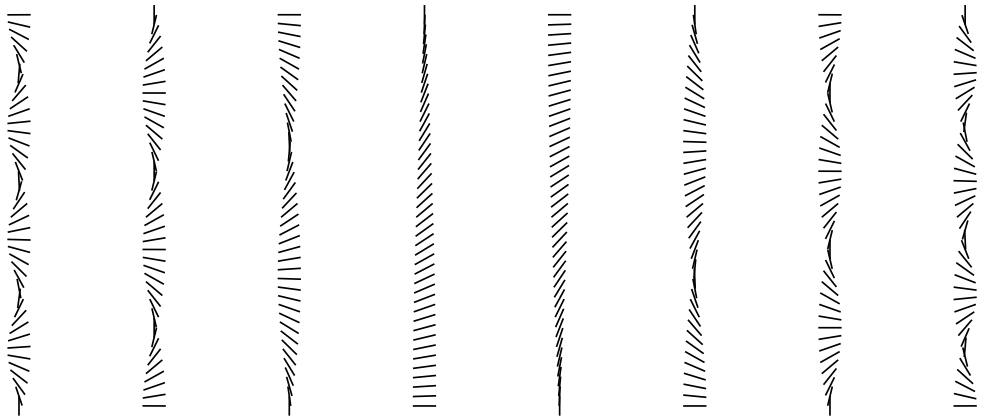

(a) $\theta^*_{\frac{-7\pi}{4}}$ (b) $\theta^*_{\frac{-5\pi}{4}}$ (c) $\theta^*_{\frac{-3\pi}{4}}$ (d) $\theta^*_{\frac{-\pi}{4}}$ (e) $\theta^*_{\frac{\pi}{4}}$ (f) $\theta^*_{\frac{3\pi}{4}}$ (g) $\theta^*_{\frac{5\pi}{4}}$ (h) $\theta^*_{\frac{7\pi}{4}}$

Figure 7.4: $\boldsymbol{n}$ associated with steady states $\theta^*_{(n+\frac{1}{4})\pi}$ (Type III) and $\theta^*_{(n+\frac{3}{4})\pi}$ (Type IV), obtained with $\mathcal{B} = 0.001$ and $\mathcal{G} = 0$. These states are unstable.

Definition 7.1.1 (Asymptotically Stable Equilibrium)**.** *An equilibrium solution θ^* of system (6.20.a-c) is said to be asymptotically stable if there exists $\delta > 0$ such that*

$$\text{if } \|\Theta - \theta^*\|_{L^2(\Omega)} < \delta, \text{ then } \lim_{t\to\infty} \|\theta(t) - \theta^*\|_{L^2(\Omega)} = 0, \tag{7.9}$$

where θ is the solution of system (6.20)*.*

In order to analyze the stability of the equilibria (7.5)–(7.8) we choose initial conditions close to $\theta^*(z)$ and of the form $\Theta(z,0) = \theta^* + \delta\Theta$, with $\|\delta\Theta\|_{L^2(\Omega)} \ll 1$.

Linearizing around θ^*, we obtain

$$\theta(z,t) \approx \theta^*(z) + \bar{\theta}(z,t),$$

with $\bar{\theta}(z,t)$ satisfying

$$\begin{cases} \bar{\theta}_t = F(\theta^*(z))\bar{\theta}_{zz}, \\ \bar{\theta}(z,0) = \delta\Theta(z), \\ \mathcal{B}\bar{\theta}_z(1,t) = -2\cos(2\theta^*(1))\bar{\theta}(1,t), \\ \mathcal{B}\bar{\theta}_z(-1,t) = 2\cos(2\theta^*(-1))\bar{\theta}(-1,t), \end{cases} \tag{7.10}$$

where $F(\theta^*) = \dfrac{g(\theta^*)}{\gamma_1 g(\theta^*) + m(\theta^*)h(\theta^*)}$. We prove that the steady state, θ^*, is asymptotically stable by showing that (see Definition 7.1.1)

$$\|\bar{\theta}(t)\|_{L^2(\Omega)} \longrightarrow 0 \text{ as } t \to \infty.$$

It is straightforward to show that (7.10) admits a separable solution of the form

$$\bar{\theta}(z,t) = \sum_{k=0}^{\infty} C_k e^{-\lambda_k t} Z_k(z),$$

for suitable eigenvalues $\{\lambda_k\}_{k\in\mathbb{N}} \subset \mathbb{R}$ and $\{C_k\}_{k\in\mathbb{N}} \subset \mathbb{R}$ such that $\delta\Theta(z) = \sum_{k=0}^{\infty} C_k Z_k(z)$, $\{Z_k\}_{k\in\mathbb{N}}$ solving the following second-order ordinary differential equation

$$\begin{array}{l} F(\theta^*(z))Z_k''(z) + \lambda_k Z_k(z) = 0 \\ \mathcal{B}Z_k'(1) = -2\cos(2\theta^*(1))Z_k(1) \\ \mathcal{B}Z_k'(-1) = 2\cos(2\theta^*(-1))Z_k(-1). \end{array} \tag{7.11}$$

Notice that (7.11) is a regular Sturm-Liouville eigenvalue problem (see Theorem A.2.6), so that the family $\{Z_k\}_{k\in\mathbb{N}}$ form an orthogonal basis on $L^2([-1,1])$ and the constants C_k are well defined. Using Parseval's equality (see (A.6)) one has that

$$\|\bar{\theta}(t)\|^2_{L^2(\Omega)} = \sum_{k\in\mathbb{N}} e^{-2\lambda_k t} C_k^2.$$

Therefore, if $0 < \lambda_1 < \lambda_2 < \cdots < \lambda_k$ it follows that

$$\|\bar{\theta}(t)\|^2_{L^2(\Omega)} \leq e^{-2\lambda_1 t}\|\delta\Theta\|^2_{L^2(\Omega)} \xrightarrow{t\to\infty} 0.$$

Proposition 7.1.2. *When $\theta^*(z) = 0$, the collection of eigenvalues $\{\lambda_k\}_{k\in\mathbb{N}}$ are positive. Consequently, the equilibrium solution $\theta^*(z) = 0$ is asymptotically stable.*

Proof. Making the change of variables $\varsigma = \frac{z+1}{2}$, system (7.11) with θ^* can be rewritten as

$$\begin{array}{l} \rho Z_k''(\varsigma) + \lambda_k Z_k(\varsigma) = 0 \\ \mathcal{B}Z_k'(1) = -2Z_k(1) \\ \mathcal{B}Z_k'(0) = 2Z_k(0), \end{array} \tag{7.12}$$

where $\rho = F(0)$. Depending on the value of λ_k, three possible solutions appear:

- **Case 1:** $\lambda_k = 0$.

In this case, the solution of system (7.12) is

$$Z_k(\varsigma) = C_1\varsigma + C_2,$$

where C_1 and C_2 are constants determined by the boundary conditions, which imply respectively $\mathcal{B}C_1 = -2(C_1 + C_2)$ and $\mathcal{B}C_1 = 2C_2$. Substracting them one obtains that $C_1 = -2C_2$. Replacing this equality in the second boundary condition one has that $(\mathcal{B}+1)C_2 = 0$, which implies that $C_2 = 0$, since $\mathcal{B}$ is assumed positive. Consequently the only solution in this case is $Z_k(\varsigma) = 0$.

• **Case 2:** $\lambda_k < 0$.
In this case, the solution of system (7.12) is

$$Z_k(\varsigma) = C_1 e^{\alpha\varsigma} + C_2 e^{-\alpha\varsigma},$$

where $\alpha = \sqrt{-\frac{\lambda_k}{\rho}}$ and C_1,C_2 are constants which are determined by the boundary conditions. Since

$$Z_k'(\varsigma) = \alpha\Big(C_1 e^{\alpha\varsigma} - C_2 e^{-\alpha\varsigma}\Big),$$

then the second boundary condition (evaluated at $\varsigma = 0$) implies that $\mathcal{B}\alpha(C_1 - C_2) = 2(C_1 + C_2)$, so that $C_1 = \big(\frac{\mathcal{B}\alpha+2}{\mathcal{B}\alpha-2}\big)C_2$. Thus, the solution and its derivative can be rewritten as

$$Z_k(\varsigma) = C_2\big(\big(\frac{\mathcal{B}\alpha+2}{\mathcal{B}\alpha-2}\big)e^{\alpha\varsigma} + e^{-\alpha\varsigma}\big) \text{ and } Z_k'(\varsigma) = C_2\alpha\big(\big(\frac{\mathcal{B}\alpha+2}{\mathcal{B}\alpha-2}\big)e^{\alpha\varsigma} - e^{-\alpha\varsigma}\big).$$

From the first boundary condition (evaluated at $\varsigma = 1$) we have that

$$-2\big(\big(\frac{\mathcal{B}\alpha+2}{\mathcal{B}\alpha-2}\big)e^{\alpha} + e^{-\alpha}\big) = \mathcal{B}\alpha\big(\big(\frac{\mathcal{B}\alpha+2}{\mathcal{B}\alpha-2}\big)e^{\alpha} - e^{-\alpha}\big) \Leftrightarrow$$

$$-(2+\mathcal{B}\alpha)\big(\frac{\mathcal{B}\alpha+2}{\mathcal{B}\alpha-2}\big)e^{\alpha} = (2-\mathcal{B}\alpha)e^{-\alpha} \Leftrightarrow e^{2\alpha} = \big(\frac{\mathcal{B}\alpha-2}{\mathcal{B}+2}\big)^2 \Leftrightarrow$$

$$e^{\alpha} = \big|1 - \frac{4}{\mathcal{B}\alpha+2}\big|.$$

Since $e^{\alpha} > 1$, then $\big|1 - \frac{4}{\mathcal{B}\alpha+2}\big| > 1$ and thus $\frac{4}{\mathcal{B}\alpha+2} > 2$. This contradicts the assumption that $\mathcal{B} > 0$ and consequently, the unique admissible solution is $Z_k(\varsigma) = 0$.

• Case 3: $\lambda_k > 0$.
In this case, the solution of system (7.12) is

$$Z_k(\varsigma) = C_1\cos(\alpha\varsigma) + C_2\sin(\alpha\varsigma),$$

where $\alpha = \sqrt{\frac{\lambda_k}{\rho}}$ and C_1, C_2 are constants which are determined by the boundary conditions. Since

$$Z_k'(\varsigma) = \alpha\big(-C_1\sin(\alpha\varsigma) + C_2\cos(\alpha\varsigma)\big),$$

then the second boundary condition (evaluated at $\varsigma = 0$) implies that $\mathcal{B}\alpha C_2 = 2C_1$, so that $C_1 = C_2\frac{\mathcal{B}}{2\alpha}$. Thus, the solution and its derivative can be rewritten as

$$Z_k(\varsigma) = C_2\big(\frac{\mathcal{B}\alpha}{2}\cos(\alpha\varsigma) + \sin(\alpha\varsigma)\big) \text{ and } Z_k'(\varsigma) = C_2\alpha\big(-\frac{\mathcal{B}\alpha}{2}\sin(\alpha\varsigma) + \cos(\alpha\varsigma)\big).$$

From the first boundary condition (evaluated at $\varsigma = 1$) we have that

$$-2\big(\frac{\mathcal{B}\alpha}{2}\cos(\alpha) + \sin(\alpha)\big) = \mathcal{B}\alpha\big(-\frac{\mathcal{B}\alpha}{2}\sin(\alpha) + \cos(\alpha)\big) \Leftrightarrow \big(-2 + \frac{(\mathcal{B}\alpha)^2}{2}\big)\sin(\alpha) = 2\alpha\mathcal{B}\cos(\alpha) \Leftrightarrow$$

$$\tan(\alpha) = \frac{4\mathcal{B}\alpha}{(\mathcal{B}\alpha)^2 - 4}.$$

In terms of λ_k, this transcendental equation can be rewritten as:

$$\tan\left(\sqrt{\frac{\lambda_k}{\rho}}\right) = -\frac{4\mathcal{B}\sqrt{\frac{\lambda_k}{\rho}}}{4 - \mathcal{B}^2\frac{\lambda_k}{\rho}}. \tag{7.13}$$

Thus, one can conclude that, when $\theta^*(z) = 0$, any solution λ_k of problem (7.11) is positive. □

For the other steady states in (7.5)-(7.8), we follow the same paradigm as above and numerically compute the eigenvalues λ_k using the function *eigs*, in the MATLAB package *Chebfun* (`http://www.chebfun.org`). We find that, in terms of the type of solution θ^*, the stability can be classified as:

Type I	is stable if n is even and unstable if n is odd
Type II	is stable if n is odd and unstable if n is even
Type III - IV	is unstable.

Solution Landscape

We have categorized the solutions of system (7.1) as in (7.5)–(7.8) (the integer m has been set to 0 since we assume that the director fields $\boldsymbol{n}$ and $-\boldsymbol{n}$ are physically indistinguishable). For simplicity, in what follows we only track the equilibria of Types I - II (since the equilibrium solutions of Types III - IV are unstable):

$$\text{Type I } \theta^*_{a_n}(z) = a_n z, \qquad \text{where } \mathcal{B}a_n = -\sin(2a_n), \tag{7.14}$$

$$\text{Type II } \theta^*_{\tilde{a}_n}(z) = \tilde{a}_n z + \frac{\pi}{2}, \qquad \text{where } \mathcal{B}\tilde{a}_n = \sin(2\tilde{a}_n). \tag{7.15}$$

It follows that $\theta^*_{a_n} = -\theta^*_{a_{-n}}$ and $\omega(\theta^*_{a_n}) = -\omega(\theta^*_{a_{-n}}) = \frac{a_n}{\pi}$, where $\omega(\theta^*_{a_n})$ satisfies the transcendental equation

$$\mathcal{B} = -\frac{\sin(2\pi\omega(\theta^*_{a_n}))}{\pi\omega(\theta^*_{a_n})}. \tag{7.16}$$

Analogous statements apply to solutions $\theta^*_{\tilde{a}_n}$ with $\tilde{a}_n$ a solution of equation (7.15), where $\omega(\theta^*_{\tilde{a}_n})$ satisfies the transcendental equation

$$\mathcal{B} = \frac{\sin(2\pi\omega(\theta^*_{\tilde{a}_n}))}{\pi\omega(\theta^*_{\tilde{a}_n})}. \tag{7.17}$$

Thus, there is a symmetric (with respect to $\omega(\theta^*) = 0$) arrangement of solutions, which is physically reasonable since we do not expect to have a preferred twist direction when $\mathcal{G} = 0$. It is clear that the

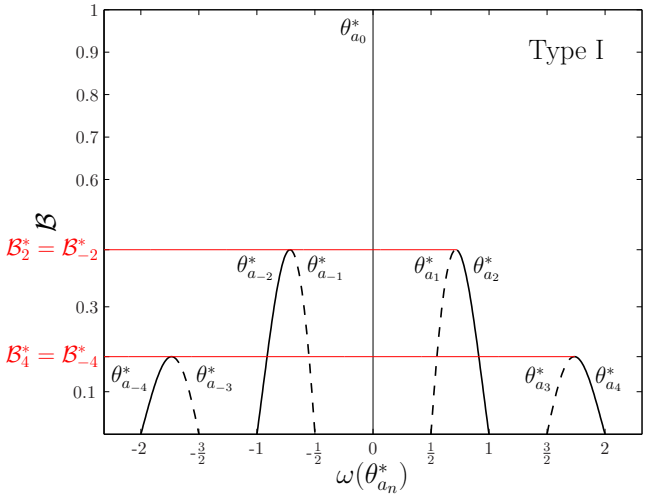

Figure 7.5: Case $\mathcal{G} = 0$: Solutions of (7.16) indicating the emergence of non-constant steady-state solutions $\theta^*_{a_n}$, $n = 0, \pm 1, \ldots$ at critical values $\mathcal{B}^*_{2n}$ for $n = \pm 1, \pm 2, \ldots$. The solid and dashed lines represent, respectively, the values of $\omega(\theta^*_{a_n})$ for which the steady state $\theta^*_{a_n}$ is stable or unstable.

director profiles for $\theta^*_{a_n}$ and $\theta^*_{a_{-n}}$ are reflections of each other about the angle $\theta = 0$. The constant solutions $\theta^*_{a_0} \equiv 0$ and $\theta^*_{\tilde{a}_0} \equiv \frac{\pi}{2}$ exist for all values of $\mathcal{B}$. These are the only solutions for large values of $\mathcal{B}$. Non-constant solutions subject to (7.14) and (7.15) emerge as $\mathcal{B}$ decreases.

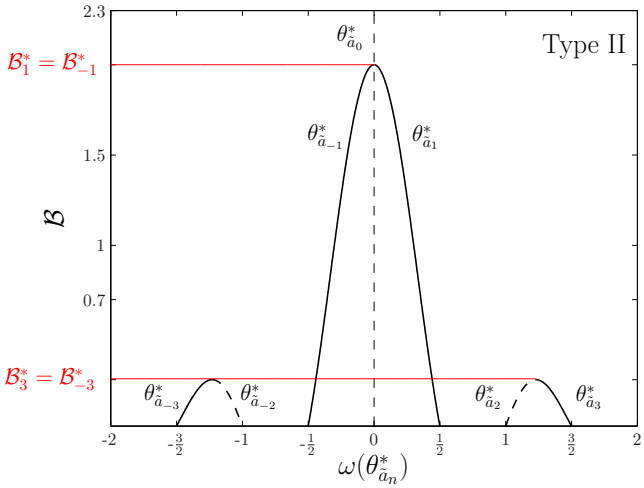

Figure 7.6: Case $\mathcal{G} = 0$: Solutions of (7.17) indicating the emergence of non-constant steady-state solutions $\theta^*_{\tilde{a}_n}$, $n = 0, \pm 1, \ldots$ at critical values $\mathcal{B}^*_{2n+1}$ for $n = 0, \pm 1, \ldots$. The solid and dashed lines represent, respectively, the values of $\omega(\theta^*_{\tilde{a}_n})$ for which the steady state $\theta^*_{\tilde{a}_n}$ is stable or unstable.

We define critical values $\mathcal{B}^*_{2n}$ with $n = \pm 1, \pm 2, \ldots$ such that, for $n > 0$, the solution branches, $\big(\omega(\theta^*_{a_{2n}}), \mathcal{B}\big)$ and $\big(\omega(\theta^*_{a_{2n-1}}), \mathcal{B}\big)$ (and $\big(\omega(\theta^*_{a_{2n+1}}), \mathcal{B}\big)$ if $n < 0$) coalesce at the critical value $\mathcal{B} = \mathcal{B}^*_{2n}$ and cease to exist for $\mathcal{B} > \mathcal{B}^*_{2n}$ (see Figure 7.5). Similarly, we define the critical values $\mathcal{B}^*_{2n+1}$ with $n = 0, \pm 1, \ldots$ as the coalescence points for solutions of Type II (see Figure 7.6 for a complete description). For $\mathcal{G} = 0$, $\mathcal{B}^*_i = \mathcal{B}^*_{-i}$ $(i \in \mathbb{N})$. For $\mathcal{B} > \mathcal{B}^*_1$, $\theta^*_{a_0}$ and $\theta^*_{\tilde{a}_0}$ are the only constant steady states of system (7.1). Solutions with large winding numbers are only observable in the strong-anchoring limit. Notice that for $\mathcal{B} \to 0$ the stable equilibria are either $\theta^*_{a_n}$ with $\omega(\theta^*_{a_n}) = k\pi$ or $\theta^*_{\tilde{a}_n}$ with $\omega(\theta^*_{\tilde{a}_n}) = (k + \frac{1}{2})\pi$, $k \in \mathbb{Z}$, and in both cases $\theta^*(\pm 1)$ tends to a multiple of π. We can apply the same reasoning to deduce that for $\mathcal{B} \to 0$, the unstable equilibria are such that $\theta^*(\pm 1) \to (k + \frac{1}{2})\pi$, as previously claimed before Section 7.1.1. For weaker anchoring, the director profile has greater freedom to reorient at the boundaries and escape from the energetically expensive fixed rotation imposed by large winding numbers. For simplicity, in what follows we denote the equilibrium solutions as θ^*_a, where $\theta^*_a = \theta^*_{a_n}$ if it is of Type I and $\theta^*_a = \theta^*_{\tilde{a}_n}$ if it is of Type II.

7.1.2 Fluid flow ($\mathcal{G} > 0$)

In this section, under the assumption that $\mathcal{G} > 0$, we numerically compute the steady-state solutions of system (6.20) as a function of $\mathcal{G}$ and the inverse anchoring strength $\mathcal{B}$. Then, we perform an asymptotic analysis of the equilibria in the limits $\mathcal{G} \to 0$ and $\mathcal{G} \to \infty$, with the latter regime yielding useful information about the boundary layers near channel surfaces (see [**?**]). Finally, we study how the static solution landscape (presented in Section 7.1.1 when $\mathcal{G} = 0$) for system (6.20) evolves as the pressure gradient $\mathcal{G}$ increases.

Computation of the equilibrium solutions

We study the static equilibria of system (7.1) when we apply a pressure difference $\mathcal{G} > 0$ across the microfluidic channel, inducing a fluid flow. The solutions are computed numerically for all values of $\mathcal{G}$ using *Chebfun* via the method of continuation (see, i.e., [**?**]) When the $\mathcal{G} = 0$ solution θ^*_a is taken as the initial condition (see Section 7.1.1), the corresponding solution with $\mathcal{G} > 0$ is denoted by $\theta^*_{a,\mathcal{G}}$.

Asymptotics when $\mathcal{G} \ll 1$

When $\mathcal{G} \ll 1$, we can approximate $\theta^*_{a,\mathcal{G}}$ by the expansion $\theta^*_{a,\mathcal{G}}(z) = \theta^*_a(z) + \mathcal{G}\theta^{(1)}_{\mathcal{G}}(z) + \cdots$, where θ^*_a is the corresponding solution for $\mathcal{G} = 0$. It is straightforward to

verify that $\theta_{\mathcal{G}}^{(1)}$ satisfies

$$\begin{cases} \dfrac{\mathrm{d}^2\theta_{\mathcal{G}}^{(1)}}{\mathrm{d}z^2}(z) = zQ(\theta_a^*(z)) \quad z \in (-1,1) \\ \mathcal{B}\dfrac{\mathrm{d}\theta_{\mathcal{G}}^{(1)}}{\mathrm{d}z}(1) = -2\theta_{\mathcal{G}}^{(1)}(1)\cos(2\theta_a^*(1)), \\ \mathcal{B}\dfrac{\mathrm{d}\theta_{\mathcal{G}}^{(1)}}{\mathrm{d}z}(-1) = 2\theta_{\mathcal{G}}^{(1)}(-1)\cos(2\theta_a^*(-1)), \end{cases} \tag{7.18}$$

where $Q(s) = -m(s)/g(s)$. The solution to (7.18) is given by

$$\theta_{\mathcal{G}}^{(1)}(z) = J(z) + Cz + D, \tag{7.19}$$

where

$$I(r) = \int_0^r sQ(as+b)\mathrm{d}s, \qquad J(z) = \int_0^z I(r)\mathrm{d}r, \tag{7.20}$$

$$C = \frac{2(-1)^k\cos(2a)\big(J(-1) - J(1)\big) - \mathcal{B}\big(I(1) + I(-1)\big)}{2\mathcal{B} + 4(-1)^k\cos(2a)}, \tag{7.21}$$

$$D = -\frac{1}{2}\big(J(1) + J(-1)\big) + \frac{\mathcal{B}(-1)^k\big(I(-1) - I(1)\big)}{4\cos(2a)}, \tag{7.22}$$

with $b = k = 0$ for Type I solutions where a satisfies (7.14) and $b = \frac{\pi}{2}$ and $k = 1$ for Type II solutions, where a satisfies (7.15). We validate the asymptotic analysis performed above by numerically computing

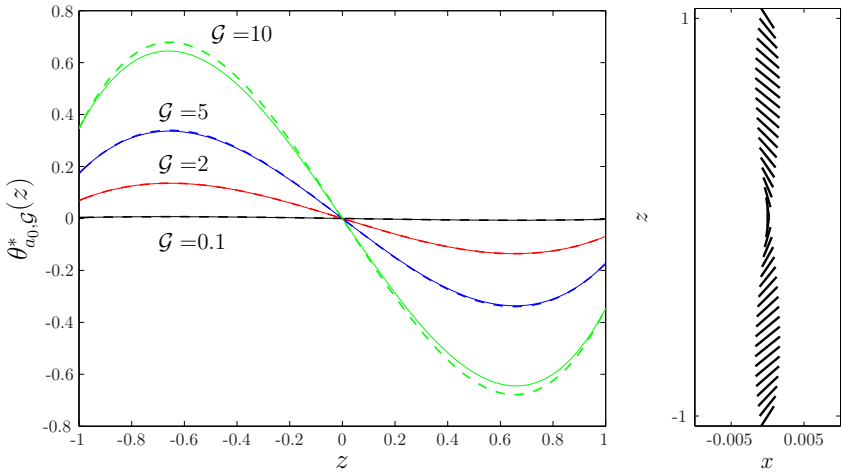

(a) Comparison of asymptotic solution given by (7.19) (dashed) with the full numerical solution to (7.1) (solid)

(b) $\boldsymbol{n}$ with $\theta^*_{a_0,0.5}$

Figure 7.7: Static equilibra $\theta^*_{a_0,\mathcal{G}}$ when $\mathcal{B} = \frac{1}{3}$. (b) We note that $\boldsymbol{n} \approx (0,0,1)$ but different scales have been used in the x and z axis to allow the reader to appreciate the change between $\theta^*_{a_0,0.5}$ and $\theta^*_{a_0,0}$ (corresponding to $\boldsymbol{n} = (0,0,1)$).

the equilibria $\theta^*_{a,\mathcal{G}}$ of (6.20) for small values of $\mathcal{G}$ by solving (7.1) with *Chebfun* and comparing this with the asymptotic result (7.19). When $\theta_a^* = \theta^*_{a_0} \equiv 0$ and $\theta_a^* = \theta^*_{\tilde{a}_1}$ the asymptotic solution approximates the actual solution for values of $\mathcal{G}$ significantly beyond the expected regime (see respectively Figures 7.7(a) and 7.8(a), where we find that the asymptotic solution approximates the full numerical solution well for values of $\mathcal{G}$ as large as 7). Figures 7.7(b) and 7.8(b) show the director field $\boldsymbol{n}$ associated with the equilibria $\theta^*_{a_0,\mathcal{G}}$ and $\theta^*_{\tilde{a}_1,\mathcal{G}}$, computed when $\mathcal{G} = 0.5$ and $\mathcal{B} = \frac{1}{3}$. We chose a moderate anchoring strength to illustrate the differences between the numerics and asymptotics clearly. The asymptotic approximations rapidly improve as $\mathcal{B} \to 0$.

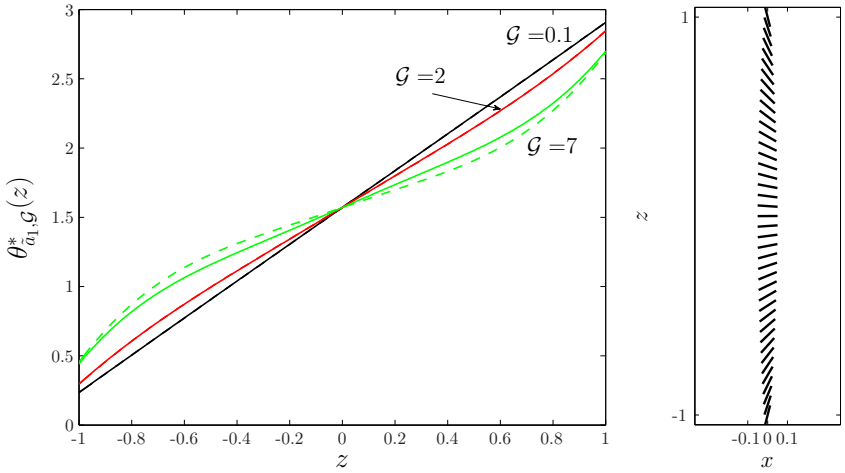

(a) Comparison of asymptotic solution given by (7.19) (dashed) with the full numerical solution to (7.1) (solid)

(b) $\boldsymbol{n}$ with $\theta^*_{\tilde{a}_1,0.5}$

Figure 7.8: Static equilibria $\theta^*_{\tilde{a}_1,\mathcal{G}}$ when $\mathcal{B} = \frac{1}{3}$. (b) In contrast with Figure 7.7(b), here x and z axis have the same scale, which corresponds to the real configuration of the molecules.

Asymptotics when $\mathcal{G} \to \infty$

For $\mathcal{G} \gg 1$, we can perform a similar asymptotic expansion of the form $\theta^*_{\mathcal{G}}(z) = \theta^{(0)}_{\mathcal{G}}(z) + (1/\mathcal{G})\theta^{(1)}_{\mathcal{G}}(z) + \cdots$. Substituting this expansion into (7.1) and equating terms at leading order gives

$$zQ(\theta^{(0)}_{\mathcal{G}}(z)) = 0, \qquad z \in (-1,1) \tag{7.23a}$$

$$\mathcal{B}\frac{\mathrm{d}\theta^{(0)}_{\mathcal{G}}}{\mathrm{d}z}(1) = -\sin(2\theta^{(0)}_{\mathcal{G}}(1)), \tag{7.23b}$$

$$\mathcal{B}\frac{\mathrm{d}\theta^{(0)}_{\mathcal{G}}}{\mathrm{d}z}(-1) = \sin(2\theta^{(0)}_{\mathcal{G}}(-1)). \tag{7.23c}$$

Equation (7.23a) implies that $\theta^{(0)}_{\mathcal{G}}(0)$ can take arbitrary values in $\mathbb{R}$ and

$$\theta^{(0)}_{\mathcal{G}}(z) \equiv \pm\arctan\left(\sqrt{\frac{\alpha_2}{\alpha_3}}\right) + k\pi \equiv \sigma^{\pm}_k \qquad \forall z \neq 0, \tag{7.24}$$

with $k \in \mathbb{Z}$ arbitrary. However, the boundary conditions (7.23$b.c$) are not satisfied by (7.24) and hence we expect to find boundary layers near $z = -1$, 0 and 1, in order to match the boundary conditions. The solution in the two outer regions $-1 < z < 0$ and $0 < z < 1$ are given by (7.24) for any two particular integer values of k, say k_1 and k_2.

Near $z = -1$, we rescale in (7.1) by introducing the variable $\eta = \sqrt{\mathcal{G}}(z+1)$ and perform an asymptotic expansion in powers of $1/\sqrt{\mathcal{G}}$. The corresponding leading-order term in $\mathcal{G}$, $\theta^{(0)}_{\mathrm{L},\mathcal{G}}(\eta)$, is a solution of

$$\frac{\mathrm{d}^2\theta^{(0)}_{\mathrm{L},\mathcal{G}}}{\mathrm{d}\eta^2}(\eta) = -Q(\theta^{(0)}_{\mathrm{L},\mathcal{G}}(\eta)), \eta > 0 \tag{7.25a}$$

$$\bar{\mathcal{B}}\frac{\mathrm{d}\theta^{(0)}_{\mathrm{L},\mathcal{G}}}{\mathrm{d}\eta}(0) = \sin(2\theta^{(0)}_{\mathrm{L},\mathcal{G}}(0)), \tag{7.25b}$$

$$\lim_{\eta\to\infty} \theta^{(0)}_{\mathrm{L},\mathcal{G}}(\eta) = \sigma^{\pm}_{k_1}, \tag{7.25c}$$

where we have rescaled $\bar{\mathcal{B}} = \sqrt{\mathcal{G}}\mathcal{B}$ assuming that $\bar{\mathcal{B}} = O(1)$ to obtain the richest asymptotic limit. We point out that the asymptotic analysis could be done without this assumption. Then (7.25b) would be

$\mathcal{B}\frac{\mathrm{d}\theta^{(0)}_{\mathrm{L},\mathcal{G}}}{\mathrm{d}\eta} = 0$ and $\theta^{(0)}_{\mathrm{L},\mathcal{G}}(\eta) = \sigma^{\pm}_{k_1}$. We would need to use the second term, $\theta^{(1)}_{\mathrm{L},\mathcal{G}}$, of the asymptotic expansion (at least) and the results with these two terms would be worse than those obtained here. Equation (7.25c) is the matching condition between $\theta^{(0)}_{\mathrm{L},\mathcal{G}}$ and $\theta^{(0)}_{\mathcal{G}}$.

Near $z = 0$, we set $\xi = \mathcal{G}^{1/3}z$ and the corresponding leading-order term, $\theta^{(0)}_{\mathrm{C},\mathcal{G}}(\xi)$, satisfies

$$\frac{\mathrm{d}^2\theta^{(0)}_{\mathrm{C},\mathcal{G}}}{\mathrm{d}\xi^2} = \xi Q(\theta^{(0)}_{\mathrm{C},\mathcal{G}}(\xi)),\ \xi \in (-\infty, \infty), \tag{7.26a}$$

$$\lim_{\xi\to-\infty} \theta^{(0)}_{\mathrm{C},\mathcal{G}}(\xi) = \sigma^{\pm}_{k_1}, \tag{7.26b}$$

$$\lim_{\xi\to\infty} \theta^{(0)}_{\mathrm{C},\mathcal{G}}(\xi) = \sigma^{\pm}_{k_2}, \tag{7.26c}$$

where (7.26b,c) describe the matching conditions.

Finally, we introduce the variable $\zeta = \sqrt{\mathcal{G}}(1 - z)$ near $z = 1$ and $\theta^{(0)}_{\mathrm{R},\mathcal{G}}(\zeta)$, the leading–order solution in $\mathcal{G}$, satisfies

$$\frac{\mathrm{d}^2\theta^{(0)}_{\mathrm{R},\mathcal{G}}}{\mathrm{d}\zeta^2} = Q(\theta^{(0)}_{\mathrm{R},\mathcal{G}}(\zeta)),\ \zeta > 0, \tag{7.27a}$$

$$\bar{\mathcal{B}}\frac{\mathrm{d}\theta^{(0)}_{\mathrm{R},\mathcal{G}}}{\mathrm{d}\zeta}(0) = \sin(2\theta^{(0)}_{\mathrm{R},\mathcal{G}}(0)), \tag{7.27b}$$

$$\lim_{\zeta\to\infty} \theta^{(0)}_{\mathrm{R},\mathcal{G}}(\zeta) = \sigma^{\pm}_{k_2}, \tag{7.27c}$$

where (7.27c) is the matching condition.

We numerically solve the three boundary layer problems (7.25), (7.26) and (7.27), using *Chebfun*, matching to the constant values in (7.24). For our particular choice of dimensionless nematic viscosities α_2 and α_3, all values of $\sigma^{\pm}_k$ (defined in (7.24)) are close to some odd multiple of $\frac{\pi}{2}$, and thus the inner director field is largely flow-aligned and is rotated $k\pi$ times with respect to the flow direction. There are multiple choices for the outer solutions, $\sigma^{\pm}_{k_1}$ and $\sigma^{\pm}_{k_2}$, for $-1 < z < 0$ and $0 < z < 1$ respectively, yielding different asymptotic approximations. In Figures 7.9(a) and 7.10(a) we compare the asymptotic approximations (7.24), (7.25), (7.26) and (7.27) with numerical solutions of the full system (7.1) for large values of $\mathcal{G}$. The two cases are labeled as $\theta^*_{a_0,\mathcal{G}}$ and $\theta^*_{\tilde{a}_1,\mathcal{G}}$ respectively, depending on the initial condition used to generate them. The values of $\sigma^{\pm}_{k_1}$ and $\sigma^{\pm}_{k_2}$ are extracted from the numerical solution and used in the asymptotic approximation (7.24)-(7.27) (these values are different for solutions $\theta^*_{a_0,\mathcal{G}}$ and $\theta^*_{\tilde{a}_1,\mathcal{G}}$). Once the outer values are determined, we can compute the asymptotic approximation using the methodology outlined above. The asymptotic solution approximates the full numerical solution well. The asymptotic solutions also show that the boundary layers near the walls have width proportional to $\mathcal{G}^{-1/2}$, consistent with the experimental findings in Sengupta et al. [**?**] In Figures 7.9(b) and 7.10(b), we plot the director field $\boldsymbol{n}$ associated with the equilibria $\theta^*_{a_0,\mathcal{G}}$ and $\theta^*_{\tilde{a}_1,\mathcal{G}}$, computed for $\mathcal{G} = 100$ and $\mathcal{B} = \frac{1}{3}$. The director field is largely flow-aligned and the director field associated with $\theta^*_{a_0,\mathcal{G}}$ exhibits a third transition layer near the centre as predicted by the asymptotic analysis.

Equilibrium solution landscape in $\mathcal{G}$

In this section, we study how the static solution landscape for system (6.20) evolves as the pressure gradient $\mathcal{G}$ increases. In Section 7.1.1, we compute the static equilibria, θ^*_a for $\mathcal{G} = 0$. In what follows, we let $\theta^*_{a,\mathcal{G}}$ denote the numerically computed equilibrium, via continuation methods with θ^*_a as initial condition. We numerically compute the stability of the equilibria with $\mathcal{G} > 0$ (using the function *eigs* of the MATLAB package *Chebfun*) and find that the stability properties of the $\mathcal{G} = 0$ equilibria propagate to the $\mathcal{G} > 0$ cases. Figures 7.11 and 7.12 show the evolution of the steady state solutions, $\theta^*_{a_n}$ and $\theta^*_{\tilde{a}_n}$, as $\mathcal{G}$ increases.

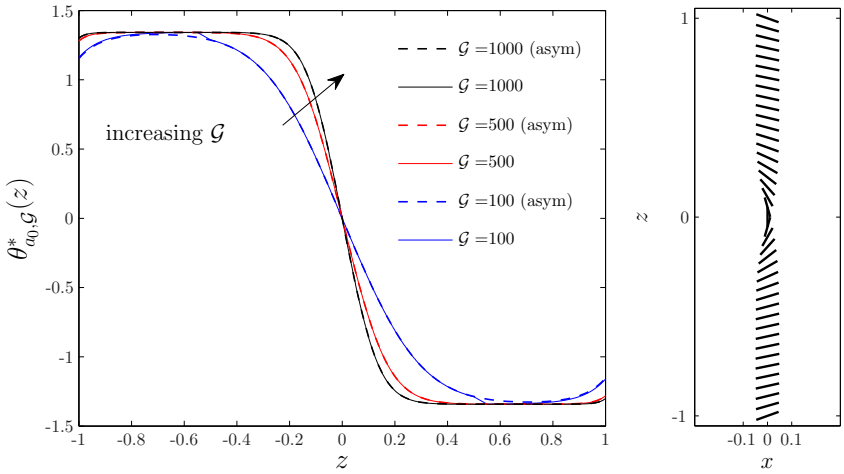

(a) Comparison of asymptotic solution given by (7.19) (dashed) with the full numerical solution to (7.1) (solid) (b) $\boldsymbol{n}$ with $\theta^*_{a_0,100}$

Figure 7.9: Static equilibria $\theta^*_{a_0,\mathcal{G}}$ with $\mathcal{G} \to \infty$ and $\mathcal{B} = \frac{1}{3}$.

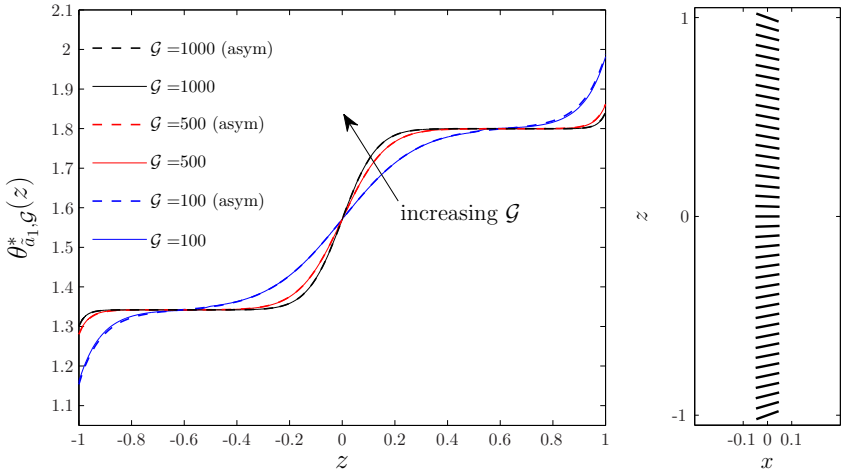

(a) Comparison of asymptotic solution given by (7.19) (dashed) with the full numerical solution to (7.1) (solid) (b) $\boldsymbol{n}$ with $\theta^*_{\tilde{a}_1,100}$

Figure 7.10: Static equilibria $\theta^*_{\tilde{a}_1,\mathcal{G}}$ when $\mathcal{G} \to \infty$ and $\mathcal{B} = \frac{1}{3}$.

For $\mathcal{G} = 0$ and $\mathcal{B} > \mathcal{B}_1^*$, the trivial solution $\theta^*_{a_0} \equiv 0$ is the unique stable equilibrium. For $\mathcal{G} > 0$ the trivial solution is not an equilibrium and for $\mathcal{B} > \mathcal{B}_1^*$, $\theta^*_{a_0,\mathcal{G}}$ is not the unique stable equilibrium. As the pressure gradient $\mathcal{G}$ increases, new equilibria appear for $\mathcal{B} > \mathcal{B}_1^*$. Additionally, some equilibria, e.g. those with a large positive winding number, become suppressed or have a smaller window of existence in $\mathcal{B}$, as $\mathcal{G}$ increases.

We believe that the asymmetry in the solution branches with positive and negative winding numbers for $\mathcal{G} > 0$ is a consequence of the fact that we work with unit-vector fields, and not director fields without a direction. We speculate that a more sophisticated model, such as the Beris–Edwards model for nematodynamics which accounts for the head–tail symmetry of nematic molecules, may resolve this asymmetry between positive and negative winding numbers for large $\mathcal{G}$.

Let $\mathcal{B}^*_{i,\mathcal{G}}$ denote a critical value of $\mathcal{B}$ for a fixed $\mathcal{G} > 0$; this definition is analogous to the definition of $\mathcal{B}_i^*$ for $\mathcal{G} = 0$. We conjecture that there is a saddle-node bifurcation at each critical value such that if $n > 0$, the stable branch, $\theta^*_{a_{2n},\mathcal{G}}$, and the unstable branch, $\theta^*_{a_{2n-1},\mathcal{G}}$ ($\theta^*_{a_{2n+1},\mathcal{G}}$ for $n < 0$), collide at $\mathcal{B} = \mathcal{B}^*_{2n,\mathcal{G}}$ and

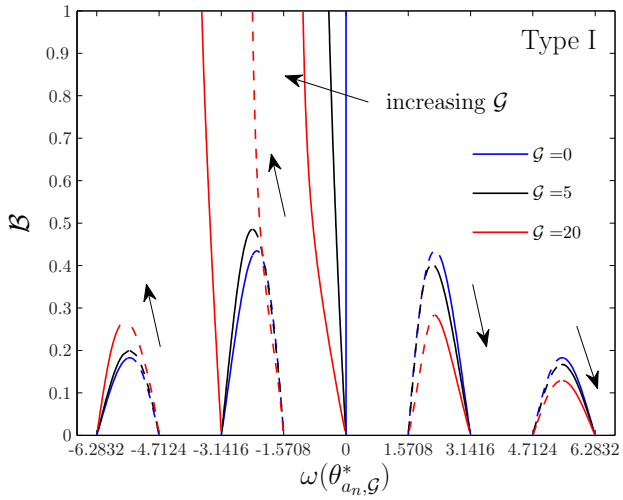

Figure 7.11: Evolution of the steady-state solutions of Type I as $\mathcal{G}$ increases. The solid and dashed lines represent, respectively, the values of $\omega(\theta^*_{a_n,\mathcal{G}})$ for which the steady states, $\theta^*_{a_n,\mathcal{G}}$, are stable or unstable.

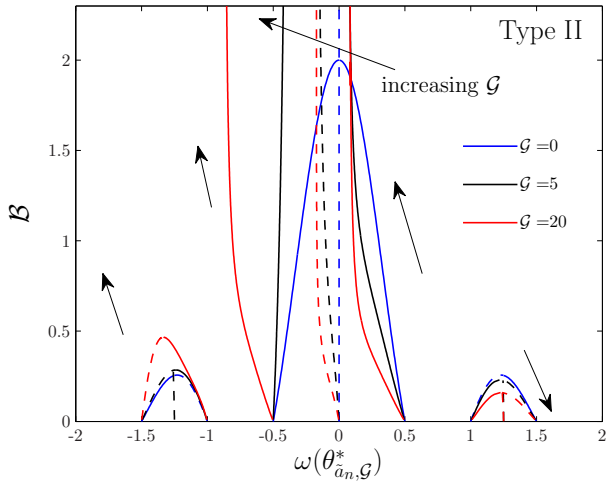

Figure 7.12: Evolution of the steady-state solutions of Type II as $\mathcal{G}$ increases. The solid and dashed lines represent, respectively, the values of $\omega(\theta^*_{\tilde{a}_n,\mathcal{G}})$ for which the steady states, $\theta^*_{\tilde{a}_n,\mathcal{G}}$, are stable or unstable.

cease to exist for $\mathcal{B} > \mathcal{B}^*_{2n,\mathcal{G}}$ (similarly for $\mathcal{B}^*_{2n+1,\mathcal{G}}$ and solutions of Type II). In Figure 7.13 we plot the critical values $\mathcal{B}^*_{i,\mathcal{G}}$ $i = \pm 2, 3, \ldots$ as a function of the pressure gradient. For example, if $\mathcal{G} \approx 15$, the critical value $\mathcal{B}^*_{-2,\mathcal{G}} \to \infty$ so that for $\mathcal{G} > 15$, the solution branches $\theta^*_{a_{-2},\mathcal{G}}$ and $\theta^*_{a_{-1},\mathcal{G}}$ do not coalesce and exist for all $\mathcal{B}$.

7.2 Time-dependent solutions

In this section, we study the time-dependent behavior of the system (6.20). We numerically compute the time-dependent solutions implementing a finite-difference method, with mesh resolution Δz =0.0125 and time step $\Delta t = 0.01$. As we have seen in Section 7.1, there are multiple static equilibria for a given pair $(\mathcal{G}, \mathcal{B})$ and it is of interest to investigate the steady-state selection, for different choices of the initial conditions. We perform a preliminary investigation of the parameter space by working with either constant

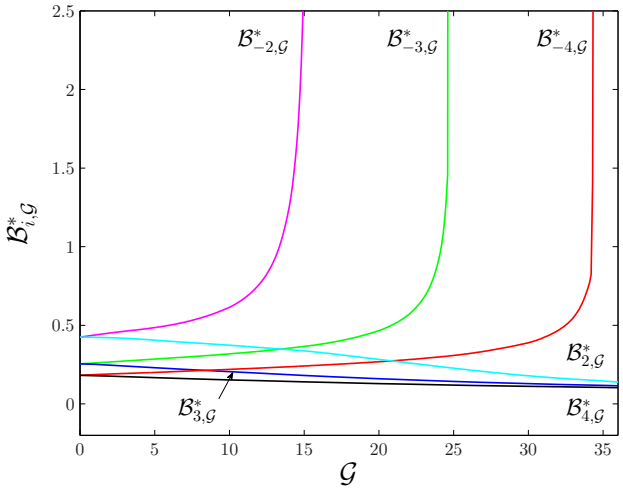

Figure 7.13: Evolution of the critical values $\mathcal{B}^*_{i,\mathcal{G}}$ as $\mathcal{G}$ increases.

or linear initial conditions. We conclude that the time-dependent system converges to:

$$\theta^*_{a_0,\mathcal{G}} \text{ if } \quad \Theta(z) = C, \tag{7.28}$$

$$\theta^*_{a_n,\mathcal{G}} \text{ if } \quad \Theta(z) = Cz, \tag{7.29}$$

$$\theta^*_{\tilde{a}_n,\mathcal{G}} \text{ if } \quad \Theta(z) = Cz + \frac{\pi}{2}, \tag{7.30}$$

where C is a constant. We note that the initial conditions in (7.28)-(7.30) do not satisfy the boundary conditions in (6.20) and later, we propose alternative initial conditions that respect these boundary conditions. In Figure 7.14 we use linear initial conditions (7.29) that have $C \in [-\frac{7\pi}{2}, \frac{7\pi}{2}]$, $\mathcal{G} = 2$, $\mathcal{B} = \frac{1}{10}$, and find that the steady state converges to different equilibria $\theta^*_{a_n,2}$, depending on the initial value C. We compute the corresponding winding numbers and use the winding number to label the static equilibria in Figure 7.14. Particularly, for any pair ($\mathcal{G}$,$\mathcal{B}$), we numerically find a critical value C^* such that if $C \in (C^* - \epsilon, C^* + \epsilon)$,

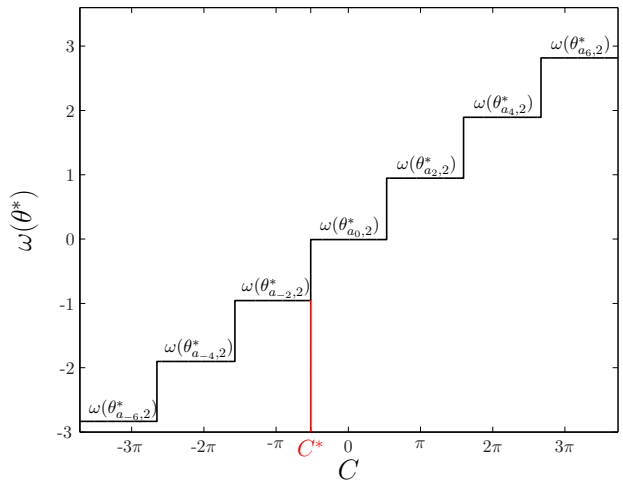

Figure 7.14: Winding number for the solution of the system (6.20) with $\mathcal{B} = \frac{1}{10}$, $\mathcal{G} = 2$, with different linear initial conditions $\Theta(z) = Cz$, $C \in [-7\frac{\pi}{2}, 7\frac{\pi}{2}]$. The critical value C^* is indicated on the x-axis.

with $\epsilon > 0$ sufficiently small, we have

$$\lim_{t\to\infty} \theta(t, z; Cz) = \begin{cases} \theta^*_{a_{-2},\mathcal{G}} & \text{if } C \in (C^* - \epsilon, C^*), \\ \theta^*_{a_0,\mathcal{G}} & \text{if } C \in [C^*, C^* + \epsilon). \end{cases} \tag{7.31}$$

Figure 7.15 plots the initial condition $\Theta(z) = C^* z$, where C^* is the critical value obtained with $\mathcal{G} = 2$

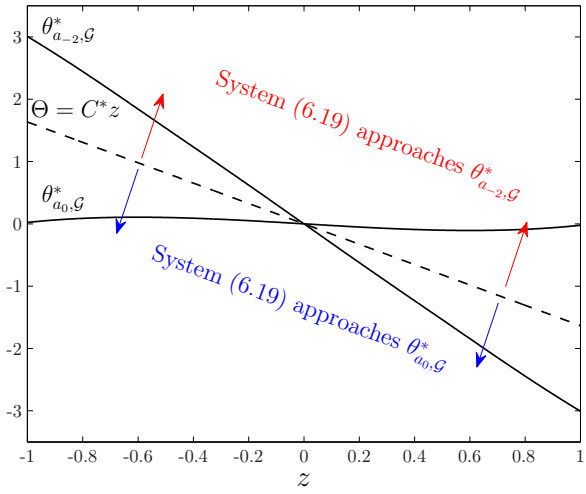

Figure 7.15: Solutions $\theta^*_{a_0,\mathcal{G}}$ and $\theta^*_{a_2,\mathcal{G}}$ obtained with $\mathcal{B} = \frac{1}{10}$ and $\mathcal{G} = 2$. The critical initial condition $\Theta(z) = C^* z$ is plotted with dashed line.

and $\mathcal{B} = \frac{1}{10}$. System (6.20) with initial condition $\Theta(z) = Cz$ approaches either $\theta^*_{a_0,2}$ or $\theta^*_{a_{-2},2}$ if $C \geq C^*$ or $C < C^*$, respectively.

Tuning the pressure gradient and the boundary conditions

The pressure gradient and boundary conditions have been assumed to be constants in our computations to this point. However, it is of experimental interest to consider situations where both the pressure gradient and boundary conditions are continuously tuned over a short period of time until they attain the desired state. We consider tuning the flow at a rate δ by applying

$$\mathcal{G}(t) = \begin{cases} 0 & \text{if } t \leq t_1, \\ \bar{\mathcal{G}} \tanh(\delta(t - t_1)) & \text{otherwise.} \end{cases} \tag{7.32}$$

Similarly, we apply time-dependent anchoring conditions of the form

$$\theta_z(1,t) = \begin{cases} C & \text{if } t \leq t_2 \\ C(1 - \tanh(\kappa(t - t_2))) & \\ \qquad - \dfrac{\sin(2\theta(1,t)) \tanh(\kappa(t - t_2))}{\mathcal{B}} & \text{otherwise,} \end{cases}$$

$$\theta_z(-1,t) = \begin{cases} C & \text{if } t \leq t_2 \\ C(1 - \tanh(\kappa(t - t_2))) & \\ \qquad + \dfrac{\sin(2\theta(1,t)) \tanh(\kappa(t - t_2))}{\mathcal{B}} & \text{otherwise,} \end{cases} \tag{7.33}$$

for some constant $\kappa > 0$. In particular, these conditions are satisfied by the initial (linear) condition $\Theta = Cz$ for $t \leq t_2$ and then, the anchoring is switched on with a tuning rate κ, to attain the required weak anchoring conditions at $z = \pm 1$.

We numerically study this modified dynamic system, using (7.32) and (7.33), and find that if $t_1 \leq t_2$, then the final steady state is identical to the steady state attained with constant values $\mathcal{G} = \bar{\mathcal{G}}$ and boundary conditions (6.20b)-(6.20c), for the parameter sweep that we performed. This indicates that if we

first apply a pressure gradient and then enforce strong anchoring, the system will always relax to the same equilibrium state, regardless of the time delay between application of the pressure gradient and anchoring.

On the other hand, if we apply the anchoring condition before the pressure gradient by choosing $t_1 > t_2$, then a different steady state can be attained, depending on the time delay and the respective rates. As an illustrative example, we find that if $\Theta = Cz$ with $C < C^*$ and $\mathcal{B} > \mathcal{B}^*_{-2}$, solutions of system (6.20) with (7.32)-(7.33) may approach the equilibrium solution, $\theta^*_{a_0,\bar{\mathcal{G}}}$, instead of the expected solution, $\theta^*_{a_{-2},\bar{\mathcal{G}}}$. This can be explained as follows: when $t_2 < t \leq t_1$, i.e., while $\mathcal{G} = 0$, the trivial solution $\theta^*_{a_0} = 0$ is the unique steady state and thus the system must approach this solution during the early stages. As a consequence, when the flow begins ($t > t_1$), the solution is already sufficiently close to $\theta^*_{a_0}$ and thus can no longer access the equilibrium state $\theta^*_{a_{-2},\bar{\mathcal{G}}}$, as it would do if $t_1 \leq t_2$. Hence, given model parameters $\bar{\mathcal{G}}$, $\mathcal{B}$, t_2, κ and δ, if the initial condition is $\Theta = Cz$, one can define a critical value $t_1^*(C)$ such that

$$\left\{ \begin{array}{ll} \lim\limits_{t\to\infty} \theta(t,z;Cz) = \theta^*_{a_{-2},\bar{\mathcal{G}}} & \text{if } t_1 < t_1^*(C) \\ \\ \lim\limits_{t\to\infty} \theta(t,z;Cz) = \theta^*_{a_0,\bar{\mathcal{G}}} & \text{if } t_1 \geq t_1^*(C). \end{array} \right\} \tag{7.34}$$

If C is such that $\lim_{t\to\infty} \theta(t,z;Cz) = \theta^*_{a_{-2},\bar{\mathcal{G}}}$ for all $t_1 > 0$, $t_1^*(C)$ is not defined.

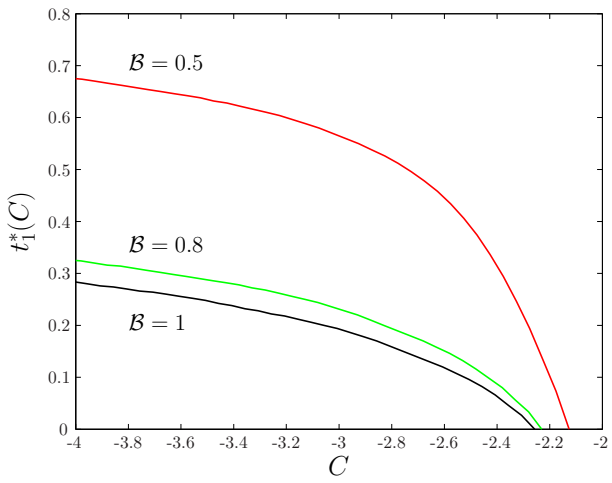

Figure 7.16: Critical values $t_1^*(C)$ obtained when solving the system (6.20),(7.32)-(7.33) with $\bar{\mathcal{G}} = 40$, $t_2 = 0$ and $\delta = \kappa = 5$. For $t_1 < t_1^*(C)$, the solution evolves to the steady state $\theta^*_{a_{-2},\bar{\mathcal{G}}}$; for $t_1 \geq t_1^*(C)$, the system evolves to the steady state $\theta^*_{a_0,\bar{\mathcal{G}}}$. Note that $t_1^* = 0$ when $C = C^*$ (see Definition (7.31)).

Figure 7.16 shows the dependence of the critical times $t_1^*(C)$ on C and $\mathcal{B}$. We observe that, as the inverse anchoring strength $\mathcal{B}$ increases, the critical time $t_1^*(C)$ decreases. This is expected since as $\mathcal{B}$ increases, the anchoring strength decreases and thus the system is able to reorient itself more easily.

Chapter 8

Conclusions and future work

In this part of the thesis, we have described, modeled and analyzed the behavior of nematic microfluidics. In Chapter 6, the dynamics of uniaxial nematic liquid crystals was characterized by the coupling of vectors $\boldsymbol{n}$ and $\boldsymbol{v}$, describing, respectively, the direction of molecular alignment of liquid crystals and the instantaneous motion of the fluid. Particularly, in Section 6.1 we presented a general description of the dynamic Leslie–Ericksen governing equations and weak anchoring boundary conditions. Then, in Section 6.2 we simplified the general Leslie–Ericksen model to describe the dynamics of a unidirectional nematic flow in a prototype microfluidic channel. These simplifications yield to a decoupled system of partial differential equations for the director field.

The asymptotic behavior of the simplified model was studied in Chapter 7. More precisely, in Section 7.1 we have computed the static equilibrium solutions, as a function of the pressure grandient $\mathcal{G}$ and the inverse anchoring strength $\mathcal{B}$, concluding that the system may be multistable for admissible pairs $(\mathcal{G}, \mathcal{B})$. As $\mathcal{B} \to 0$, one approaches the strong-anchoring limit and our equilibrium solutions correspond to the solutions presented in Anderson et al. [**?**]. In contrast with the conjectures presented in [**?**], our stability analysis suggests that solutions do not lose stability as $\mathcal{G}$ increases. Moreover, we have performed an asymptotic analysis in the limits $\mathcal{G} \to 0$ and $\mathcal{G} \to \infty$, with the latter regime yielding useful information about the boundary layers near channel surfaces, which are experimentally observed for strong-flow regimes in Sengupta et al. [**?**]. Section 7.2 is devoted to a numerical study of the dynamic Leslie–Ericksen model and its sensitivity to the initial condition. Working with a linear initial condition, we numerically found critical values that separate basins of attraction for the distinct steady states. Further, we have also studied the effect of varying the pressure gradient and anchoring conditions with time and how the rate of change can affect the critical initial conditions that lead to the selection of a particular steady state. This numerical experiment may guide future physical experiments on these lines if experimentalists can control fluid flow and anchoring conditions with time, so as to attain a desired state or at least control transient dynamics.

Throughout this part of the thesis we have performed an exhaustive exploration of the asymptotic behavior of nematic microfluidics, using a large variety of mathematical techniques in the process. Nevertheless, there are still some improvements that can be performed to capture nematic properties observed in practice. For example, the dynamic model proposed in Chapter 6 could be replaced by the fully coupled Leslie–Ericksen model, eliminating the hypothesis of symmetry in the flow profile and allowing transitions between the steady states (not captured by our model). Better improvements might be achieved if the Beris–Edwards model is used instead of Leslie–Ericksen model, since it catches variations in the degree of orientational order and topological defects, where the director cannot be defined.

Appendix A

A.1 Elementary inequalities

a. Young's Inequality with $\epsilon > 0$ [?].

$$ab \leq \epsilon a^2 + \frac{b^2}{4\epsilon} \qquad \forall a, b \in \mathbb{R}, \epsilon > 0. \tag{A.1}$$

b. Gronwall's Inequality (integral form) [?].
Let $\varepsilon(\cdot)$ and $\psi(\cdot)$ be nonnegative continuous functions on $I = [a, \infty)$, which satisfies for a.e.t the integral inequality

$$\varepsilon(t) \leq \int_0^t \varepsilon(s)\psi(s)\mathrm{d}s + c,$$

where c is a nonnegative constant. Then:

$$\varepsilon(t) \leq ce^{\int_a^t \psi(s)\mathrm{d}s} \qquad \forall t \in I. \tag{A.2}$$

c. Friedrich's Inequality [?, ?].
Let Ω be a bounded, connected Lipschitz domain in $\mathbb{R}^n$, $n \geq 2$. Then, given any set $E \subset \delta\Omega$ with $mes(E) > 0$, there exists a constant C which depends on n, E and Ω such that

$$\int_\Omega |u|^2\mathrm{d}x \leq C\Big(\int_\Omega |\nabla u|^2\mathrm{d}x + \int_E |u|^2\mathrm{d}S\Big) \qquad \forall u \in H^1(\Omega). \tag{A.3}$$

d. Trace Inequality [?].
If $\Omega \subset \mathbb{R}^n$ is open and Lipschitz and $\Gamma = \delta\Omega$, the trace operator $\gamma : H^1(\Omega) \to L^2(\Gamma)$ defined as $\gamma(u) = u|_\Gamma$ is well defined and continuous, i.e, there exists a constant $C_\mathrm{T} > 0$ such that

$$\|\gamma(u)\|_{L^2(\Gamma)} \leq C_\mathrm{T}\|u\|_{H^1(\Omega)}. \tag{A.4}$$

A.2 Ordinary differential equations

Definition A.2.1 (Absolutely Continuous Function)**.** *Let I be an interval in $\mathbb{R}$. A function $f : I \to \mathbb{R}$ is absolutely continuous on I if there corresponds for every $\epsilon > 0$ a $\delta > 0$ so that*

$$\sum_{i=1}^n |f(\beta_i)f(\alpha_i)| < \epsilon$$

for any n and any disjoint collection of segments (α_1, β_1), ..., (α_n, β_n) in I, whose lengths satisfy

$$\sum_{i=1}^n |\beta_i - \alpha_i| < \delta.$$

The collection of all absolutely continuous functions on I is denoted $AC(I)$.

Definition A.2.2. *Let I be an interval in $\mathbb{R}$, D be any subset of $\mathbb{R}^n$. The function $f : I \times D \to \mathbb{R}^n$ is said to satisfy the Carathéodory conditions on $I \times D$ if*

- *f is continuous with respect to x for a.e.$t \in I$,*
- *f is measurable with respect to t for each $x \in D$,*
- *There exists a Lebesgue integrable function $m : I \to \mathbb{R}$ such that*

$$\|f(t,x)\| \leq m(t) \qquad \text{for all } t \in I, x \in D.$$

Theorem A.2.3. *Let $J = [0,T]$, $R \subset \mathbb{R}^n$ a compact set, $G = J \times R$ and consider the following evolution problem*

$$\begin{aligned} x' &= f(t,x), \\ x(0) &= x_0. \end{aligned} \tag{A.5}$$

If the function $f : G \to \mathbb{R}^n$ satisfy the Carathéodory conditions, then there exists a solution $x \in AC([0,\bar{T}])^n$, where $0 < \bar{T} \leq T$. Moreover, if there exists a Lebesgue integrable function $k : J \to \mathbb{R}$ such that

$$\|f(t,x_1) - f(t,x_2)\| \leq k(t)\|x_1 - x_2\| \qquad \forall (t,x_1),(t,x_2) \in G,$$

then the solution is unique.

Proof. See Theorem 1 in Chapter 1 of [**?**]. □

Theorem A.2.4. *[Picard Lindelöf Theorem] Let $J = [0,T]$, $R \subset \mathbb{R}^n$ a compact set, $G = J \times R$ and consider the evolution problem* (A.5) *with $f \in \mathcal{C}(G, \mathbb{R}^n)$. If there exists a constant $k > 0$ such that*

$$\|f(t,x_1) - f(t,x_2)\| \leq k\|x_1 - x_2\| \qquad \forall (t,x_1),(t,x_2) \in G,$$

then there exists a unique solution $x \in \mathcal{C}^1([0,\bar{T}])^n$, where $0 < \bar{T} \leq T$.

Proof. See Theorem 2.2 in [**?**]. □

Theorem A.2.5. *Let f and $\frac{\partial f}{\partial x}$ continuous functions in $\mathbb{R}^n$ and $x(t)$ a solution of the evolution problem* (A.5) *defined on the interval (α,ω). If $\|x(t)\| \leq M$ for all $t \in [t_0,\omega)$, with $t_0 \in (\alpha,\omega)$, then $\omega = +\infty$.*

Proof. Theorem 3 in Chapter 1 of [**?**]. □

Theorem A.2.6 (Sturm's Theorem)**.** *Let p, q and r be continuous-real valued functions on $[a,b]$ such that p' and r'' exists and are continuous and such that p and r and everywhere positive for $a \leq t \leq b$. Let c_1, c_2, d_1, d_2 be real number such that c_1 and c_2 are not both 0 and d_1 and d_2 are not both 0. Finally, for each complex number λ, let (SL) be the following set of conditions on a function $u : [a,b] \to \mathbb{C}$ with two continuous derivatives:*

$$(p(t)u')'q(t)u + \lambda r(t)u = 0, \tag{SL1}$$

$$c_1 u(a) + c_2 u'(a) = 0 \tag{SL2}$$

$$d_1 u(b) + d_2 u'(b) = 0 \tag{SL3}$$

Then the system (SL) has a nonzero solution for a countably infinite set of values of λ.
If E denotes this set of values, then the members λ of E are all real, they have no limit point in $\mathbb{R}$, and the vector space of solutions of (SL) is 1-dimensional for each such λ. Let enumare E as λ_1, λ_2, ..., let $u = \phi_n$ be a nonzero solution of (SL) when $\lambda = \lambda_n$ and define $(f,g)_r = \int_a^b f(t)\bar{g}(t)r(t)\mathrm{d}t$ and $\|f\|_r = (\int_a^b |f(t)|^2 r(t)\mathrm{d}t)^{\frac{1}{2}}$ for continuous f and g, and normalize ϕ_n such that $\|\phi_n\|_r = 1$. Then $(\phi_n,\phi_m)_r = 0$ for $n \neq m$, and the functions ϕ_n satisfy the following completeness conditions:

(a) Any u having two continuous derivatives on $[a,b]$ and satisfying (SL2)-(SL3) *has the property that the series $\sum_{n=1}^{\infty}(u,\phi_n)_r\phi_n(t)$ converges absolutely uniformly to $u(t)$ on $[a,b]$.*

(b) The only continuous ϕ on $[a,b]$ with $(\phi,\phi_n)_r = 0$ for all n is $\phi = 0$.

(c) Any continuous ϕ on $[a,b]$ satisfies

$$\|\phi\|_r^2 = \sum_{n=1}^{\infty} |(\phi,\phi_n)_r|^2, \tag{A.6}$$

usually called Parseval's equality.

Proof. See Theorem 1.3 of [**?**]. □

Nonlinear Stability Analysis

We consider the nonlinear autonomous system

$$x' = F(x), \tag{A.7}$$

where $x : \mathbb{R} \to \mathbb{R}^n$ and $F : \mathbb{R}^n \to \mathbb{R}^n$ is a smooth function. We assume that the solution exist for every $t \geq 0$ and is unique when initial data is provided.

Definition A.2.7. *Given initial data $x(0) = x_0$, we define the flow of (A.7) as $\phi(t,\cdot) : \mathbb{R}^n \to \mathbb{R}^n$, $\phi(t,x_0) = x(t,x_0)$.*

Definition A.2.8. *A critical point x^* (also called an equilibrium, fixed, or stationary point) satisfies*

$$F(x^*) = 0.$$

We would like to analyze the behavior of system (A.7) in a neighborhood $U(x^*,\epsilon)$, $0 < |\epsilon| < 1$. In order to do that, we need to linearize system (A.7) by approximating the function $F(x)$ around the equilibrium point x^* by its tangent around that fixed point. Thus, using Taylor's expansion one has

$$F(x) \sim F(x^*) + DF(x^*)(x - x^*),$$

where $DF(x^*) = \frac{\mathrm{d}F}{\mathrm{d}x}$ is the Jacobian Matrix of function $F(x) = [F_1(x_1^*,\cdots,x_n^*),\cdots,F_n(x_1^*,\cdots,x_n^*)]^T$. Considering $z = x - x^*$ the linearization of (A.7) can be written as:

$$z' = DF(x^*)z, \qquad z \in U(0,\epsilon). \tag{A.8}$$

Thus, the flux on the linearized system around the equilibrium point x^* is obtained by the integration of (A.8), and is of the form

$$z(t) = (x_0 - x^*)e^{DF(x^*)t}. \tag{A.9}$$

Theorem A.2.9. *Suppose x^* is a critical point of the nonlinear system (A.7) and suppose the real part of the eigenvalues of DF (the linearization) are negative. Then the critical point is locally asymptotically stable.*

Proof. See Theorem 3.1 of [**?**]. □

Theorem A.2.10. *Suppose x^* is a critical point of the nonlinear system (A.7) and at least one eigenvalue of DF is positive. Then the critical point is unstable.*

Proof. See Theorem 3.2 of [**?**]. □

Theorem A.2.11 (Hartman-Grobman Theorem)**.** *Suppose x^* is a hyperbolic critical point (i.e., the real part of the eigenvalues of DF are not zero). Then the phase portrait of the linearization and the nonlinear equations are locally homeomorphic, i.e., there is an homomorphism $h : \mathbb{R}^n \to \mathbb{R}^n$ defined locally on a neighborhood U of x^* such that*

$$h \circ e^{tDF} = \phi(t, \cdot) \circ h,$$

where ϕ is the flux of system (A.7).

Proof. See Theorem 9.9 of [**?**]. □

Remark A.2.12. *If the critical point x^* has associated a zero eigenvalue, two different situations arise. If the other eigenvalue is positive, the critical point is unstable. If the other eigenvalue is negative, the linearization may not describe the nonlinear system.*

Definition A.2.13. *Given $x \in \mathbb{R}^n$, the set*

$$\gamma(x) = \{\phi(t, x) : t \in \mathbb{R}\}$$

is called orbit of x. Notice that if $y \in \gamma(x)$, then $y \in \phi(t, x)$ and hence $\gamma(x) = \gamma(y)$. Moreover

$$\gamma^+(x) = \{\phi(t, x) : t \in \mathbb{R}^+\}$$

is called the positive semiorbit of x, and the set

$$\gamma^-(x) = \{\phi(t, x) : t \in \mathbb{R}^-\}$$

is called the negative semiorbit of x.

Definition A.2.14. *Given $x \in \mathbb{R}^n$, the α-limit and the ω-limit sets of x (with respect to (A.7)) are defined respectively by*

$$\alpha(x) = \bigcap_{y \in \gamma(x)} \overline{\gamma^-(y)},$$

and

$$\omega(x) = \bigcap_{y \in \gamma(x)} \overline{\gamma^+(y)},$$

Particularly for the planar case, i.e., if we consider system (A.7) with $x \equiv (x, y) \in \mathbb{R}^2$ and $F \equiv (F_1, F_2) : \mathbb{R}^2 \to \mathbb{R}^2$, one has the two following theorems.

Theorem A.2.15 (Generalized Poincaré Bendixson Theorem)**.** *If the positive orbit $\gamma^+(x)$ in (A.7) is contained in a compact set K, where K only contains a finite number of critical points, then one of the following situations occur:*

- *$\omega(x)$ is a critical point.*
- *$\omega(x)$ is a periodic orbit.*
- *$\omega(x)$ is a connected set composed of a finite number of fixed points together with homoclinic and heteroclinic orbits connecting these fixed points.*

Proof. See Theorem 7.16 of [**?**]. □

Theorem A.2.16 (Dulac's Criterion)**.** *Let E be a simply connected region in the phase plane. If there exists a continuously differentiable function $\psi(x,y)$ such that*

$$\frac{\mathrm{d}}{\mathrm{d}x}(\psi(x,y)F_1(x,y)) + \frac{\mathrm{d}}{\mathrm{d}y}(\psi(x,y)F_2(x,y))$$

has constant sign in E, then the dynamical system

$$\begin{cases} x' = F_1(x,y) \\ y' = F_2(x,y) \end{cases}$$

has no closed orbits lying entirely in E.

Proof. See Theorem 1.8.2 of [**?**]. □

A.3 Partial differential equations

Theorem A.3.1 (Schauder Fixed Point Theorem)**.** *Assume X is a Banach space, $K \subset X$ is compact and convex, and assume also*

$$A : K \longrightarrow K$$

is continuous. Then A has a fixed point in K.

Proof. See Theorem 3 in Chapter 9.2 of [**?**]. □

Theorem A.3.2. *Let X a reflexive Banach space and $\{f_n\}_n \subset X'$ a bounded sequence, then there exists a subsequence $\{f_{n_k}\}_k$ that converges in the weak-$*$ topology to some $f \in X'$.*

Proof. See Theorem 3.18 of [**?**]. □

Theorem A.3.3. *Let $1 \leq p \leq \infty$. If $\{f_n\}_n \subset L^p(Q)$ and $f \in L^p(Q)$, such that $\|f_n - f\|_{L^p(Q)} \to 0$, then there exists a subsequence $\{f_{n_k}\}_k$ such that $f_{n_k} \to f$ almost everywhere in Q.*

Proof. See Theorem 4.9 of [**?**]. □

Theorem A.3.4. *If $\{f_n\}_n \subset X'$ converges to $f \in X'$ in the weak-$*$ topology, $\{x_n\}_n \subset X$, $x \in X$ such that $\|x_n - x\|_X \to 0$, then*

$$< f_n, x_n >_{X' \times X} \to < f, x >_{X' \times X} .$$

Proof. See the statement (iv) in Proposition 3.13 of [**?**]. □

Definition A.3.5. *Let V, H Hilbert spaces such that $V \subset H$, V is dense on H and V' is the dual of V. The space $W(0,T,V,V')$ is defined as*

$$W(0,T,V,V') = \{u | u \in L^2(0,T,V), \frac{\mathrm{d}u}{\mathrm{d}t} \in L^2(0,T,V')\},$$

and the norm

$$\|u\|_{W(0,T,V,V')} = \big(\int_0^T \|u(t)\|_V^2 \mathrm{d}t + \int_0^T \|\frac{\mathrm{d}u}{\mathrm{d}t}(t)\|_{V'}^2 \mathrm{d}t \big)^{\frac{1}{2}}.$$

Theorem A.3.6. $W(0,T,V,V') \subset C^0([0,T],H)$.

Proof. See Theorem 3.1 and Proposition 2.1 of [**?**]. □

Theorem A.3.7. *Let us consider the following evolution problem*

$$\begin{cases} \text{Find } u \in W(0,T,V,V') & \text{such that} \\ A(t)u + \frac{\mathrm{d}u}{\mathrm{d}t} = f, & \text{where } f \in L^2(0,T,V'), \\ y(0) = u_0, & \text{where } u_0 \in H. \end{cases} \tag{A.10}$$

If $a(t,\cdot,\cdot) =< A(t)\cdot,\cdot >_{V'\times V}$ *satisfyies the following conditions:*

$$\begin{cases} \forall\ u,v \in V & \text{the function } t \to a(t,u,v) \text{ is measurable and} \\ \exists\ c \in \mathbb{R}: \ |a(t,u,v)| \le c\|u\|_V\|v\|_V & \forall u,v \in V,\ a.e.t \in [0,T], \end{cases} \tag{A.11}$$

and there exists $\lambda, \alpha > 0$ *such that*

$$a(t,v,v) + \lambda\|v\|_H^2 \ge \alpha\|v\|_V^2 \qquad \forall v \in V,\ a.e.t \in [0,T], \tag{A.12}$$

then the problem (A.10) has a unique weak solution.

Proof. See Theorem 1.2 in Chapter III of [**?**]. □

Lemma A.3.8 (Aubin–Lions Compactness Lemma)**.** *Let* $X \subset B \subset Y$ *Banach spaces such that the inclusion* $X \subset B$ *is a compact embedding. Then, for any* $1 < p < \infty$, $1 \le q \le \infty$, *the space*

$$\{f : f \in L^p(0,T,X) \text{ and } \frac{\mathrm{d}f}{\mathrm{d}t} \in L^q(0,T,Y)\}$$

is compact embedded in $L^p(0,T,B)$.

Particularly, if $q = p = 2$, $X = H^1(\Omega)$ *and* $B = L^2(\Omega)$ *and* $Y = (H^1(\Omega))'$ *it follows that*

$$W(0,T,H^1(\Omega),(H^1(\Omega))') \subset L^2(0,T,L^2(\Omega)),$$

with compact embedding.

Proof. See Theorem 5.1 of [**?**]. □

Nonlinear stability analysis

Consider the nonlinear system defined on a Banach space X with norm $\|\cdot\|$

$$u_t = F(u), \tag{A.13}$$

where $F : \mathcal{D}(F) \subset X \to X$ is densely defined on X. We assume that the solution exist for all $t \ge 0$ and is unique when initial data u_0 is provided. Let u^* be an equilibrium of (A.13); that is, it satisfies $F(u^*) = 0$ in (A.13). The following definitions can be found in [**?**].

Definition A.3.9 (Stable Equilibrium)**.** *The equilibrium* u^* *is said to be stable if for every* $\epsilon > 0$, *there exists* $\delta > 0$ *such that*

$$\text{if } \|u_0 - u^*\| < \delta, \text{ then } \|u(t) - u^*\| < \epsilon \text{ for all } t \ge 0,$$

where u *is the solution of* (A.13).

Definition A.3.10 (Asymptotically Stable Equilibrium)**.** *The equilibrium* u^* *is said to be asymptotically stable if there exists* $\delta > 0$ *such that*

$$\text{if } \|u_0 - u^*\| < \delta, \text{ then } \lim_{t\to\infty} \|u(t) - u^*\| = 0,$$

where u *is the solution of* (A.13).

Definition A.3.11 (Unstable Equilibrium)**.** *The equilibrium* u^* *is said to be unstable if it is not stable.*

Bibliography

[1] E.L. Allgower and K. Georg. *Introduction to Numerical Continuation Methods*. Classics in Applied Mathematics. Society for Industrial and Applied Mathematics, 2003.

[2] T.G. Anderson, E. Mema, L. Kondic, and L.J. Cummings. Transitions in Poiseuille flow of nematic liquid crystal. *International Journal of Non-Linear Mechanics*, 75:15–21, 2015.

[3] J.F. Andrews. A mathematical model for the continuous culture of microorganisms utilizing inhibitory substrates. *Biotechnology and Bioengineering*, 10(6):707–723, 1968.

[4] J.L. Ansoni and P. Seleghim. Optimal industrial reactor design: development of a multiobjective optimization method based on a posteriori performance parameters calculated from CFD flow solutions. *Advances in Engineering Software*, 91(C):23–35, 2016.

[5] S.N. Antontsev, J.I. Díaz, and S. Shmarev. *Energy Methods for Free Boundary Problems: Applications to Nonlinear Pdes and Fluid Mechanics*. Progress in Nonlinear Differential Equations and Their Applications. Birkhäuser Boston, 2002.

[6] J. Antony. Aerodynamic design via control theory. *Journal of Scientific Computing*, 3(3):233–260, 1988.

[7] G.B. Arfken. *Mathematical Methods for Physicists*. Elsevier Science, 2013.

[8] R. Aris. Phenomena of multiplicity, stability and symmetry. *Annals of the New York Academy of Sciences*, 231(1):86–98, 1974.

[9] N.H. Asmar. *Partial Differential Equations with Fourier Series and Boundary Value Problems*. Pearson Prentice Hall, 2005.

[10] M. Avriel. *Nonlinear Programming: Analysis and Methods*. Dover Books on Computer Science Series. Dover Publications, 2003.

[11] J.E. Bailey and D.F. Ollis. *Biochemical Engineering Fundamentals*. Chemical engineering. McGraw-Hill, 1986.

[12] M. Ballyk, L. Dung, D.A. Jones, and H.L. Smith. Effects of random motility on microbial growth and competition in a flow reactor. *SIAM J. Appl. Math.*, 59(2):573–596, 1998.

[13] J.R. Banga, E.B. Canto, C.G. Moles, and A.A. Alonso. Dynamic optimization of bioreactors - a review. *Proceedings of the Indian Academy of Sciences*, 2003.

[14] G. Barbero and L.R. Evangelista. *Adsorption Phenomena and Anchoring Energy in Nematic Liquid Crystals*. Liquid Crystals Book Series. CRC Press, 2005.

[15] J.M. Bello, B. Ivorra, A.M. Ramos, A. Rapaport, and J. Harmand. Bioreactor shape optimisation. modeling, simulation, and shape optimization of a simple bioreactor for water treatment. In *Les STIC pour l'environnement 2011*, pages 125–141. Lavoisier, 2011.

[16] A.N. Beris and B.J. Edwards. *Thermodynamics of Flowing Systems: with Internal Microstructure*. Oxford Engineering Science Series. Oxford University Press, 1994.

[17] T.A. Bibila and D.K. Robinson. In pursuit of the optimal fed-batch process for monoclonal antibody production. *Biotechnology Progress*, 11(1):1–13, 1995.

[18] J.P. Bitog, I.-B. Lee, C.-G. Lee, K.-S. Kim, H.-S. Hwang, S.-W. Hong, I.-H. Seo, K.-S. Kwon, and E. Mostafa. Application of computational fluid dynamics for modeling and designing photobioreactors for microalgae production: A review. *Computers and Electronics in Agriculture*, 76(2):131–147, 2011.

[19] H. Brezis. *Functional Analysis, Sobolev Spaces and Partial Differential Equations*. Universitext. Springer, 2010.

[20] A.W. Bush and A.E. Cook. The effect of time delay and growth rate inhibition in the bacterial treatment of wastewater. *Journal of Theoretical Biology*, 63(2):385–395, 1976.

[21] G.J. Butler, S.B. Hsu, and P. Waltman. Coexistence of competing predators in a chemostat. *Journal of Mathematical Biology*, 17(2):133–151, 1983.

[22] G.J. Butler and G.S.K. Wolkowicz. A mathematical model of the chemostat with a general class of functions describing nutrient uptake. *SIAM Journal on Applied Mathematics*, 45(1):138–151, 1985.

[23] E.F. Campana, D. Peri, Y. Tahara, and F. Stern. Shape optimization in ship hydrodynamics using computational fluid dynamics. *Computer Methods in Applied Mechanics and Engineering*, 196(13):634–651, 2006.

[24] A.P. Carvalho, L.A. Meireles, and F.X. Malcata. Microalgal reactors: A review of enclosed system designs and performances. *Biotechnology Progress*, 22(6):1490–1506, 2006.

[25] J.A. Castellano. *Liquid Gold: The Story of Liquid Crystal Displays and the Creation of an Industry*. World Scientific, 2005.

[26] J. Chiou and F. Wang. Hybrid method of evolutionary algorithms for static and dynamic optimization problems with application to a fed-batch fermentation process. *Computers & Chemical Engineering*, 23(9):1277–1291, 1999.

[27] Y. Chisti. Biodiesel from microalgae. *Biotechnology Advances*, 25(3):294–306, 2007.

[28] T. Coenen, W.V. Moortel, F. Logist, J. Luyten, J.F.M. van Impe, and J. Degrève. Modeling and geometry optimization of photochemical reactors: Single- and multi-lamp reactors for UVH_2O_2 AOP systems. *Chemical Engineering Science*, 96:174–189, 2013.

[29] M. Crespo, I. Griffiths, A. Majumdar, and A.M. Ramos. Solution landscapes in nematic microfluidics. Submitted. Preprint: `https://arxiv.org/abs/1607.05054`, 2016.

[30] M. Crespo, B. Ivorra, and A.M. Ramos. Existence and uniqueness of solution of a continuous flow bioreactor model with two species. *RACSAM*, Serie A:1–21, 2015.

[31] M. Crespo, B. Ivorra, and A.M. Ramos. Asymptotic stability of a coupled advection-diffusion-reaction system arising in bioreactor processes. Submitted. Preprint: `http://eprints.ucm.es/39501`, 2016.

[32] M. Crespo, A.M. Ramos, B. Ivorra, and A. Rapaport. Modeling and optimization applied to the design of a continuous bioreactor. Submitted, 2016.

[33] M. Crespo, A.M. Ramos, B. Ivorra, and A. Rapaport. Modeling and optimization of activated sludge bioreactors for wastewater treatment taking into account spatial inhomogeneities. Submitted. Preprint: `https://hal.archives-ouvertes.fr/hal-01171033`, 2016.

[34] G. D'Ans, D. Gottlieb, and P. Kokotovic. Optimal control of bacterial growth. *Automatica*, 8:729–736, 1972.

[35] P.G. de Gennes and J. Prost. *The Physics of Liquid Crystals*. International Series of Monographs on Physics. Clarendon Press, 1995.

[36] W.R. Dean. The stream-line motion of fluid in a curved pipe (second paper). *The London, Edinburgh, and Dublin Philosophical Magazine and Journal of Science*, 5(30):673–695, 1928.

[37] K. Deb. *Multi-Objective Optimization using Evolutionary Algorithms*. Wiley Interscience Series in Systems and Optimization. Wiley, 2001.

[38] D. Dochain. *Automatic Control of Bioprocesses*. ISTE. Wiley, 2010.

[39] D. Dochain and P. Vanrolleghem. *Dynamical Modelling and Estimation in Wastewater Treatment Processes*. IWA Publishing, 2001.

[40] A.K. Dramé. A semilinear parabolic boundary-value problem in bioreactors theory. *Electronic Journal of Differential Equations*, 2004.

[41] A.K. Dramé, C. Lobry, J. Harmand, A. Rapaport, and F. Mazenc. Multiple stable equilibrium profiles in tubular bioreactors. *Mathematical and Computer Modelling*, 48(1112):1840–1853, 2008.

[42] M. El-Sayed, T. Sun, and J. Berry. Shape optimization with computational fluid dynamics. *Advances in Engineering Software*, 36(9):607–613, 2005.

[43] L.C. Evans. *Partial Differential Equations*. American Mathematical Society, 1998.

[44] G. Farin. *Curves and Surfaces for Computer-Aided Geometric Design: A Practical Guide*. Computer science and scientific computing. Elsevier Science, 2014.

[45] A.F. Filippov. *Differential Equations with Discontinuous Righthand Sides*. Mathematics and its Applications. Springer Science & Business Media, 1988.

[46] F.C. Frank. I. Liquid crystals. On the theory of liquid crystals. *Discussions of the Faraday Society*, 25:19–28, 1958.

[47] A. Friedman. *Partial Differential Equations of Parabolic Type*. Prentice Hall Inc, 1964.

[48] F.N. Fritsch and R.E. Carlson. Monotone piecewise cubic interpolation. *SIAM Journal on Numerical Analysis*, 17(2):238–246, 1980.

[49] P. Gajardo, J. Harmand, H.C. Ramírez, and A. Rapaport. Minimal time bioremediation of natural water resources. *Automatica*, 47(8):1764–1769, 2011.

[50] P. Gajardo, H. Ramírez, V. Riquelme, and A. Rapaport. Bioremediation of natural water resources via optimal control techniques. In *Biomat 2011 - International Symposium on Mathematical and Computational Biology*, pages 178–190. World Scientific, 2012.

[51] I.M. Gelfand and G.E. Shilov. *Generalized Functions: Properties and operations*. Academic Press, 1964.

[52] R. Glowinski. *Numerical Methods for Nonlinear Variational Problems*. Scientific Computation. Springer Berlin Heidelberg, 2013.

[53] D.E. Goldberg. *Genetic Algorithms in Search, Optimization, and Machine Learning.* Artificial Intelligence. Addison-Wesley, 1989.

[54] J.P. Grivet. Nonlinear population dynamics in the chemostat. *Computing in Science Engineering*, 3, 2001.

[55] C. Gu and P. Yeh. *Optics of Liquid Crystal Displays.* Wiley, 2009.

[56] J. Guckenheimer and P. Holmes. *Nonlinear Oscillations, Dynamical Systems and Bifurcations of Vector Fields*, volume 42 of *Applied Mathematical Sciences.* Springer, 1983.

[57] R.D. Gulati and E. van Donk. *Lakes in the Netherlands, their origin, eutrophication and restoration: state-of-the-art review*, pages 73–106. Springer Netherlands, 2002.

[58] S.E. Harding and P. Johnson. The brownian diffusion of dormant and germinating spores of bacillus megaterium. *Journal of Applied Bacteriology*, 60(3):227–232, 1986.

[59] J. Harmand and D. Dochain. The optimal design of two interconnected (bio)chemical reactors revisited. *Computers & Chemical Engineering*, 30(1):70–82, 2005.

[60] J. Harmand, A. Rapaport, and A. Trofino. Optimal design of interconnected bioreactors: New results. *AIChE Journal*, 49(6):1433–1450, 2003.

[61] D. Herbert, R. Elsworth, and R.C. Telling. The continuous culture of bacteria; a theoretical and experimental study. *Journal of general microbiology*, 1956.

[62] G.A. Hill and C.W. Robinson. Minimum tank volumes for CFST bioreactors in series. *The Canadian Journal of Chemical Engineering*, 67(5):818–824, 1989.

[63] M.J. Hirsch, P.M. Pardalos, and M. Resende. Speeding up continuous grasp. *Journal of Operational Research*, 2006.

[64] S.B. Hsu. Limiting behavior for competing species. *SIAM Journal on Applied Mathematics*, 34(4):760–763, 1978.

[65] S.B. Hsu, S. Hubbell, and P. Waltman. A mathematical theory for single-nutrient competition in continuous cultures of micro-organisms. *SIAM Journal on Applied Mathematics*, 32(2):366–383, 1977.

[66] J.A. Infante and J.M. Rey. *Métodos Numéricos. Teoría, problemas y prácticas con MATLAB.* Ediciones Pirámide. Grupo Anaya, 2015.

[67] S. Ishihara, M. Otsuji, and A. Mochizuki. Transient and steady state of mass-conserved reaction-diffusion systems. *Phys. Rev. E*, 75:015203, 2007.

[68] B. Ivorra, B. Mohammadi, and A.M. Ramos. A multi-layer line search method to improve the initialization of optimization algorithms. *European Journal of Operational Research*, 247(3):711–720, 2015.

[69] B. Ivorra, J.L. Redondo, J.G. Santiago, P.M. Ortigosa, and A.M. Ramos. Two- and three-dimensional modeling and optimization applied to the design of a fast hydrodynamic focusing microfluidic mixer for protein folding. *Physics of Fluids (1994-present)*, 25(3), 2013.

[70] A. Kanekanian. Fermentation microbiology and biotechnology (2007) - Edited by E.M.T. El-mansi, C.F.A. Bryce, A.L. Damain and A.R. Allman. *International Journal of Dairy Technology*, 62(2):284–285, 2009.

[71] H. Kawamoto. The history of liquid-crystal displays. *Proceedings of The IEEE*, 90:460–500, 2002.

[72] Y.K. Kim, B. Senyuk, and O.D. Lavrentovich. Molecular reorientation of a nematic liquid crystal by thermal expansion. *Nature Communications*, 3(1133), 2012.

[73] A.W. Knapp. *Advanced Real Analysis*. Cornerstones. Birkhäuser Boston, 2005.

[74] H.J. Kuiper. Invariant sets for nonlinear elliptic and parabolic systems. *Journal on Mathematical Analysis*, 11(6):1075–1103, 1980.

[75] C.-M. Kung and B.C. Baltzis. The growth of pure and simple microbial competitors in a moving distributed medium. *Mathematical Biosciences*, 111(2), 1992.

[76] O.A. Ladyzhenskaîa, V.A. Solonnikov, and N.N. Ural'tseva. *Linear and Quasi-linear Equations of Parabolic Type*. American Mathematical Society, translations of mathematical monographs. American Mathematical Society, 1968.

[77] L. Lanzani and Z.W. Shen. On the Robin boundary condition for Laplace's equation in Lipschitz domains. *Communications in Partial Differential Equations*, 29(1 & 2):91–109, 2004.

[78] D. Lauffenburger, R. Aris, and K.H. Keller. Effects of random motility on growth of bacterial populations. *Microbial Ecology*, 7(3):207–227, 1981.

[79] O.D. Lavrentovich. Transport of particles in liquid crystals. *Soft Matter*, 10:1264–1283, 2014.

[80] S. Lee. The Leslie coefficients for a polymer nematic liquid crystal. *The Journal of Chemical Physics*, 88(8):5196–5201, 1988.

[81] O. Lehmann. Über fliessende krystalle. *Z. phys. Chem*, 4:462–472, 1889.

[82] F. M. Leslie. Continuum theory for nematic liquid crystals. *Continuum Mechanics and Thermodynamics*, 4(3):167–175, 1992.

[83] F.M. Leslie. Some constitutive equations for liquid crystals. *Archive for Rational Mechanics and Analysis*, 28(4):265–283, 1968.

[84] R.J. LeVeque. *Finite Difference Methods for Ordinary and Partial Differential Equations: Steady-State and Time-Dependent Problems*. Society for Industrial and Applied Mathematics, 2007.

[85] B. Li. Global asymptotic behavior of the chemostat: General response functions and different removal rates. *SIAM J. Appl. Math.*, 59(2):411–422, 1998.

[86] G.M. Lieberman. Intermediate schauder theory for second order parabolic equations. iv. time irregularity and regularity. *Differential and Integral Equations*, 5(6):1219–1236, 1992.

[87] H.C. Lim and H.S. Shin. *Fed-Batch Cultures: Principles and Applications of Semi-Batch Bioreactors*. Cambridge Series in Chemical Engineering. Cambridge University Press, 2013.

[88] F.H. Lin and C. Liu. Nonparabolic dissipative systems modeling the flow of liquid crystals. *Communications on Pure and Applied Mathematics*, 48(5):501–537, 1995.

[89] F.H. Lin and C. Liu. Existence of solutions for the Ericksen–Leslie system. *Archive for Rational Mechanics and Analysis*, 154:135–156, 2000.

[90] J.L. Lions. Sur les problèmes mixtes pour certains systèmes paraboliques dans les ouverts non cylindriques. *Annales de l'institut Fourier*, 7:143–182, 1957.

[91] J.L. Lions. *Contrôle optimal de systèmes governés par des équations aux dérivées partiales*. Dunod, Paris, 1968.

[92] J.L. Lions. *Quelques méthodes de résolution des problèmes aux limites non linéaires*. Les Cours de référence. Dunod, 2002.

[93] J.L. Lions and E. Magenes. *Non-homogeneous Boundary value Problems and Applications. Volume I*. Springer-Verlag, 1972.

[94] W. Liu. *Elementary Feedback Stabilization of the Linear Reaction-Convection-Diffusion Equation and the Wave Equation*. Mathématiques et Applications. Springer Berlin Heidelberg, 2009.

[95] K.Ch.A.M. Luyben and J. Tramper. Optimal design for continuous stirred tank reactors in series using Michaelis Menten kinetics. *Biotechnology and Bioengineering*, 24(5):1217–1220, 1982.

[96] R.A.E. Mäkinen, J. Periaux, and J. Toivanen. Multidisciplinary shape optimization in aerodynamics and electromagnetics using genetic algorithms. *International Journal for Numerical Methods in Fluids*, 30(2):149–159, 1999.

[97] N.I. Marcos, M. Guay, D. Dochain, and T. Zhang. Adaptive extremum-seeking control of a continuous stirred tank bioreactor with Haldane's kinetics. *Journal of Process Control*, 14(3):317–328, 2004.

[98] G.B. Marin. Advances in Chemical Engineering: Multiscale analysis. *Advances in Chemical Engineering*, 2005.

[99] B. Massey and J. Ward-Smith. *Mechanics of Fluids (8th edn)*. Taylor & Francis, 2005.

[100] C.R. McGowin and D.D. Perlmutter. Tubular reactor steady state and stability characteristics. I. Effect of axial mixing. *AIChE Journal*, 17(4):831–837, 1971.

[101] N.D. Mermin. The topological theory of defects in ordered media. *Rev. Mod. Phys.*, 51:591–648, 1979.

[102] J. Monod. *Recherches sur la croissance des cultures bacteriannes*. Hermann, Paris, 1942.

[103] J. Monod. La technique de la culture continue: Théorie et applications. *Annales de l´Institut Pasteur*, 79:390–410, 1950.

[104] J. Moreno. Optimal time control of bioreactors for the wastewater treatment. *Optimal Control Applications and Methods*, 20(3):145–164, 1999.

[105] Y. Morita and T. Ogawa. Stability and bifurcation of nonconstant solutions to a reaction diffusion system with conservation of mass. *Nonlinearity*, 23(6):1387, 2010.

[106] F. Muyl, L. Dumas, and V. Herbert. Hybrid method for aerodynamic shape optimization in automotive industry. *Computers & Fluids*, 33(56):849–858, 2004.

[107] J.G. Na, Y. Chang, B. Chung, and H. Lim. Adaptive optimization of fed-batch culture of yeast by using genetic algorithms. *Bioprocess and Biosystems Engineering*, 24(5):299–308, 2002.

[108] J. Necas. *Les Méthodes Directes En Théorie Des Équations Elliptiques*. Academia, 1967.

[109] V. Nejati and K. Matsuuchi. Aerodynamics Design and Genetic Algorithms for Optimization of Airship Bodies. *JSME international journal. Ser. B, Fluids and thermal engineering*, 46(4):610–617, 2003.

[110] M.I. Nelson and H.S. Sidhu. Evaluating the performance of a cascade of two bioreactors. *Chemical Engineering Science*, 61(10):3159–3166, 2006.

[111] S.K. Nguang, L. Chen, and X.D. Chen. Optimisation of fed-batch culture of hybridoma cells using genetic algorithms. *ISA Transactions*, 40(4):381–389, 2001.

[112] R. Nogueira and L.F. Melo. Competition between nitrospira spp. and nitrobacter spp. in nitrite-oxidizing bioreactors. *Biotechnology and Bioengineering*, 95(1):169–175, 2006.

[113] A. Novick and L. Szilard. Description of the chemostat. *Science*, 112(2920):715–716, 1950.

[114] Chia Ven Pao and Wei Hua Ruan. Positive solutions of quasilinear parabolic systems with nonlinear boundary conditions. *Journal of Mathematical Analysis and Applications*, 333(1):472 – 499, 2007.

[115] C.V. Pao. Asymptotic stability of reaction-diffusion systems in chemical reactor and combustion theory. *Journal of Mathematical Analysis and Applications*, 82(2):503–526, 1981.

[116] C.V. Pao. *Nonlinear Parabolic and Elliptic Equations*. Fems Symposium. Springer US, 1992.

[117] O. Parodi. Stress tensor for a nematic liquid crystal. *J. Phys. France*, 31(7):581–584, 1970.

[118] V. Patil, K.-Q. Tran, and H.R. Giselrød. Towards sustainable production of biofuels from microalgae. *International Journal of Molecular Sciences*, 9(7):1188–1195, 2008.

[119] C.F. Pérez and J.M.V. Montaner. *Ecuaciones diferenciales*. Number 2 in Ciencia y técnica. Pirámide, 1996.

[120] A.J. Perumpanani, J.A. Sherratt, and P.K. Maini. Phase differences in reaction-diffusion-advection systems and applications to morphogenesis. *IMA Journal of Applied Mathematics*, 55:19–33, 1995.

[121] O. Pironneau. *Optimal Shape Design for Elliptic Systems*. Springer series in computational physics. Springer-Verlag, 1984.

[122] S.J. Pirt. *Principles of microbe and cell cultivation*. Halsted Press book. Wiley, 1975.

[123] C. Poloni, A. Giurgevich, L. Onesti, and V. Pediroda. Hybridization of a multi-objective genetic algorithm, a neural network and a classical optimizer for a complex design problem in fluid dynamics. *Computer Methods in Applied Mechanics and Engineering*, 186(24):403–420, 2000.

[124] L. Pramparo, J. Pruvost, F. Stüber, J. Font, A. Fortuny, A. Fabregat, P. Legentilhomme, J. Legrand, and C. Bengoa. Mixing and hydrodynamics investigation using CFD in a square-sectioned torus reactor in batch and continuous regimes. *Chemical Engineering Journal*, 137(2):386–395, 2008.

[125] Z. Qiu, K. Wang, and Y. Zou. The asymptotic behavior of flowreactor models with two nutrients. *Mathematical and Computer Modelling*, 40(56):465–479, 2004.

[126] H. Ramírez, A. Rapaport, and V. Riquelme. Minimal time bioremediation of water resources with two patches. In *SIAM Conference on Control & Applications CT15*, 2015.

[127] A.M. Ramos. *Introducción al Análisis Matemático del Método de Elementos Finitos*. Editorial Complutense, 2012.

[128] V.S.H. Rao and P. Raja Sekhara Rao. Basic chemostat model revisited. *Differential Equations and Dynamical Systems*, 17(1):3–16, 2009.

[129] A. Rapaport, I. Haidar, and J. Harmand. Global dynamics of the buffered chemostat for a general class of response functions. *Journal of Mathematical Biology*, 71(1):69–98, 2015.

[130] F. Reinitzer. Beiträge zur kenntniss des cholesterins. *Monatshefte für Chemie und verwandte Teile anderer Wissenschaften*, 9(1):421–441, 1888.

[131] F. Reinitzer. Contributions to the knowledge of cholesterol (translation of reference [**?**]). *Liquid Crystals*, 5(1):7–18, 1989.

[132] B.R. Reiter. Assessment of laboratory methods for quantifying aqueous bacterial diffusion. Master's thesis, University of Saskatchewan, 1999.

[133] A. Richmond, S. Boussiba, A. Vonshak, and R. Kopel. A new tubular reactor for mass production of microalgae outdoors. *Journal of Applied Phycology*, 5(3):327–332, 1993.

[134] M. Ronen, Y. Shabtai, and H. Guterman. Optimization of feeding profile for a fed-batch bioreactor by an evolutionary algorithm. *Journal of Biotechnology*, 97(3):253–263, 2002.

[135] J.A. Roubos, G. van Straten, and A.J.B. van Boxtel. An evolutionary strategy for fed-batch bioreactor optimization; concepts and performance. *Journal of Biotechnology*, 67:173–187, 1999.

[136] K.-Y. San and G. Stephanopoulos. Optimization of fed-batch penicillin fermentation: A case of singular optimal control with state constraints. *Biotechnology and Bioengineering*, 34(1):72–78, 1989.

[137] A. Sengupta, U. Tkalec, M. Ravnik, J.M. Yeomans, C. Bahr, and S. Herminghaus. Liquid Crystal Microfluidics for Tunable Flow Shaping. *Phys. Rev. Lett.*, 110, Jan 2013.

[138] L. Shangerganesh and K. Balachandran. Existence and uniqueness of solutions of predator-prey type model with mixed boundary conditions. *Acta Applicandae Mathematicae*, 116(1):71–86, 2011.

[139] R.R. Sharapov. *Genetic Algorithms: Basic Ideas, Variants and Analysis*. InTech, 2007.

[140] J. Siebert, S. Alonso, M. Bär, and E. Schöll. Dynamics of reaction-diffusion patterns controlled by asymmetric nonlocal coupling as a limiting case of differential advection. *Phys. Rev. E*, 89:052909, 2014.

[141] E. Sierra, F.G. Acién, J.M. Fernández, J.L. García, C. González, and E. Molina. Characterization of a flat plate photobioreactor for the production of microalgae. *Chemical Engineering Journal*, 138(13):136–147, 2008.

[142] V. Singh. *Environmental Hydrology*. Water Science and Technology Library. Springer Netherlands, 2013.

[143] I.Y. Smets, J.E. Claes, E.J. November, G.P. Bastin, and J.F. van Impe. Optimal adaptive control of (bio)chemical reactors: past, present and future. *Journal of Process Control*, 14(7):795–805, 2004.

[144] H. Smith and P. Waltman. *The theory of the Chemostat. In Cambridge studies in Mathematical biology*, volume 13. Cambridge: Cambridge University Press, 1995.

[145] M. Søndergaard, E. Jeppesen, T.L. Lauridsen, C. Skov, E.H. van Nes, R. Roijackers, E. Lammens, and R. Portielje. Lake restoration: successes, failures and long-term effects. *Journal of Applied Ecology*, 44(6):1095–1105, 2007.

[146] I.W. Stewart. *The Static and Dynamic Continuum Theory of Liquid Crystals: A Mathematical Introduction*. Liquid Crystals Book Series. Taylor & Francis, 2004.

[147] P.S. Stewart. Diffusion in biofilms. *Journal of Bacteriology*, 185(5):1485–1491, 2003.

[148] H.A. Stone, A.D. Stroock, and A. Ajdari. Engineering flows in small devices: microfluidics toward a lab-on-a-chip. *Annu. Rev. Fluid Mech.*, 36:381–411, 2004.

[149] K.R. Symon. *Mechanics*. Addison-Wesley World student series. Addison-Wesley Publishing Company, 1971.

[150] G. Teschl. *Ordinary Differential Equations and Dynamical Systems*. Graduate Studies in Mathematics. American Mathematical Society, 2012.

[151] M.R. Tredici and G.C. Zittelli. Efficiency of sunlight utilization: Tubular versus flat photobioreactors. *Biotechnology and Bioengineering*, 57(2):187–197, 1998.

[152] S.A. Vejtasa and R.A. Schmitz. An experimental study of steady state multiplicity and stability in an adiabatic stirred reactor. *AIChE Journal*, 16(3):410–419, 1970.

[153] R.T. Venterea and D.E. Rolston. Mechanistic modeling of nitrite accumulation and nitrogen oxide gas emissions during nitrification. *Journal of Environmental Quality*, 29(6):1741–1751, 2000.

[154] F.A. Verhulst. *Nonlinear Differential Equations and Dynamical Systems*. Hochschultext / Universitext. Springer-Verlag, 1996.

[155] H. Wang, T.X. Wu, S. Gauza, J.R. Wu, and S. Wu. A method to estimate the Leslie coefficients of liquid crystals based on MBBA data. *Liquid Crystals*, 33(1):91–98, 2006.

[156] T. Weise. *Global Optimization Algorithms - Theory and Application*. Self-Published, Second edition, 2009.

[157] C.Y. Wen and L.T. Fan. *Models for Flow Systems and Chemical Reactors*. Chemical Processing and Engineering. Dekker, 1975.

[158] G.M. Whitesides. The origins and the future of microfluidics. *Nature*, 442(7101):368–373, 2006.

[159] J.J. Winkin, D. Dochain, and P. Ligarius. Dynamical analysis of distributed parameter tubular reactors. *Automatica*, 36(3):349–361, 2000.

[160] H. Wu, X. Xu, and C. Liu. On the general Leslie–Ericksen system: Parodi's relation, well-posedness and stability. *Archive for Rational Mechanics and Analysis*, 208:59–107, 2013.

[161] J.-Y. Xia, S.-J. Wang, S.-L. Zhang, and J.-J. Zhong. Computational investigation of fluid dynamics in a recently developed centrifugal impeller bioreactor. *Biochemical Engineering Journal*, 38(3):406–413, 2008.

[162] G. Xu and S.-P. Yung. Lyapunov stability of abstract nonlinear dynamic system in Banach space. *IMA J. Math. Control & Information*, 20:105–127, 2003.

[163] K. Yamuna Rani and S.V. Ramachandra Rao. Control of fermenters – a review. *Bioprocess Engineering*, 21(1):77–88, 1999.